Dynamics of HIV treatment and social contagion

Dynamics of HIV treatment and social contagion

A DISSERTATION PRESENTED
BY
ALISON LYNN HILL
TO
THE COMMITTEE ON HIGHER DEGREES IN BIOPHYSICS

IN PARTIAL FULFILLMENT OF THE REQUIREMENTS
FOR THE DEGREE OF
DOCTOR OF PHILOSOPHY
IN THE SUBJECT OF
BIOPHYSICS

HARVARD UNIVERSITY
CAMBRIDGE, MASSACHUSETTS
APRIL 2013

Thesis advisor: Martin A. Nowak Alison Lynn Hill

Dynamics of HIV treatment and social contagion

Abstract

Modern-day management of infectious diseases is critically linked to the use of mathematical models to understand and predict dynamics at many levels, from the mechanisms of pathogenesis to the patterns of population-wide transmission and evolution. This thesis describes the development and application of mathematical techniques for HIV infection and dynamics on social networks. Treatment of HIV infection has improved dramatically in the past few decades but is still limited by the development of drug resistance and the inability of current therapies to completely eradicate the virus from an individual. We begin with a synthesis of the important evolutionary principles governing the HIV epidemic, emphasizing the role of modeling. We then describe a modeling framework to study the emergence of drug-resistant HIV within a patient. Our model integrates laboratory data and patient behavior, with the goal of predicting outcomes of clinical trials. Current results demonstrate how pharmacologic properties of antiretroviral drugs affect selection for drug resistance, and can explain drug-class-specific resistance risks. Thirdly, we describe models for a new class of drugs that aim to eliminate cells with latent viral infection. We provide estimates for the required efficacy of these drugs and describe the potential challenges of future clinical trials. Finally, models and mechanisms for understanding viral dynamics are increasingly finding applications outside traditional virology. They can be used to study the dynamics of behaviors, to help predict and intervene in their spread. We describe techniques for applying infectious disease models to social contagion, drawing on techniques for network epidemiology. We use this framework to interpret data on the interpersonal spread of health-related behaviors.

Contents

Acknowledgments

I have been privileged to have not only one, but three, incredibly supportive research advisors who contributed to the work presented here. My primary advisor, Martin Nowak, has supported me at the Program for Evolutionary Dynamics (PED) for the past four and a half years. I'm so grateful for the opportunity to work in this inspiring environment, and for the freedom I've been afforded in my research and extracurricular pursuits. I can't imagine many other professors who would be equally willing to have you drag them back into a former research field as to have you go to India for the summer on two weeks notice. I've learned a whole new way of thinking about science from Martin that will certainly influence the rest of my career.

During my first projects at PED I worked closely with Nicholas Christakis and he has continued to be a mentor ever since. Despite his hectic schedule he always gives his undivided attention and has provided thoughtful feedback and advice to me throughout my graduate studies. His enthusiasm is contagious and I hope to emulate his work-life-service balance someday.

The HIV work presented here was inspired and led by Bob Siliciano, who is truly a role model as a PI. We were immediately welcomed into his lab and have felt like part of the family ever since. Bob's unique knack for integrating biology and modeling, and his attention to detail in all aspects of our work have been the determining factors in the success of our collaboration. It has been an honor to have our work highlighted in his engaging conference presentations.

Jim Hogle has served as an advisor to me in many aspects of graduate life: as an academic advisor through the Biophysics Program, as a member of my qualifying exam and dissertation advisory committees, and as the Master of Dudley House where I worked as a fellow. His community-building skills are truly unparalleled and I have no doubt that my incredible experiences in all aspects of graduate school were, if not directly, at least indirectly due to his work.

Arup Chakraborty recently took over the leadership of the institute that houses my program at MIT, and has been a strong supporter of our students ever since. I am extremely grateful for his enthusiasm for my work and his willingness to fill in on my committee on short notice.

My HST academic advisors Lee Gehrke and Fred Bowman have always been a source of candid advice and a grounded perspective. Valerie Pronio Stelluto was an incredible leader during my clinical medicine terms and truly made the HST experience for me. During my research rotations in first year Ron Walsworth was the most supportive advisor possible.

Navigating through complicated inter-institutional academics and research appointments would have been a nightmare if not for the help of some amazing administrative staff: Michele Jakoulov from the Biophysics Program, May Huang and Michael Wojcik at PED, and Bonita Grant at Johns Hopkins. I rarely had to worry about the details of funding or scheduling and am eternally grateful for all of their help over the years.

Most importantly, I would like the thank the amazing lab mates I have worked side-by-side with during my PhD. I'm sure we have spent thousands of hours together in person and on email or Skype developing and debating every detail of our projects. I am sometimes shocked that we have never had a single fight and I can only attribute this to their infinite patience and dedication. Daniel and I worked in parallel on all the HIV projects, and I am certain the collaboration we've built would have never happened without him becoming interested in HIV. His big-picture vision, mathematical prowess and enviable writing and presentation style have contributed significantly to my development as a scientist. Ali was our guide into the Siliciano lab and the world of experimental virology, and the constant source of translation between the modeling and the data. We worked together tirelessly as a triad on the resistance paper. Ali's incredibly forward-thinking views on the field have created more projects than we'll ever have time to work on.

I first started working at PED as a disenchanted experimentalist on the recommendation of Dave Rand, and I think he was the single most important person in determining the course of my graduate career. We worked together closely on the social network projects, where I learned how his incredible positivity and interdisciplinary vision brings out the best everyone who works with him. I am very grateful for all the mentorship he's provided me over the years. All the other researchers who called PED their home over the years have made such a positive influence on my graduate study; thanks to Ivana, Corina, Stefany, Anna, Oliver, Peter, Ben, Feng, Erez, Michael, JB, Thomas, Jan, Nate, Jeff, Moshe, Jordi, Mattijs and everyone else. PED is truly a one-of-a-kind place.

1

Introduction

Effective public health systems require the ability to make rapid and reliable predictions about future trends in disease incidence and the benefit of potential interventions. In the absence of prior experience or the ability to do exhaustive randomized trials, models become necessary. In biomedical research and clinical medicine we search for mechanistic explanations to unify diverse observations. Quantitative theories can guide experimental design and interpretation. When the system of interest involves dynamic processes and interactions between many entities, mathematical models are needed to describe the behavior. This becomes readily apparent in the study of infectious diseases, where a parasite invades a host population that may respond with its own defense mechanisms. Mathematical models of infection dynamics are a well-established tool integrated into all levels of scientific understanding in this field, from the seasonal patterns of influenza spread to the origin of genetic variation in the human population.

In this thesis, we describe a sequence of studies modeling infection dynamics. We focus mainly on HIV treatment, with both traditional antiretroviral therapy and investigational latency reversing agents, and also consider the dynamics of social contagion. Each chapter is self-contained, and includes an introduction to and discussion of the particular study.

Here, we give a brief background to the topics considered.

1.1 Basic modeling framework

The common thread linking the chapters of this thesis, and a large body of work in this field, is the basic mathematical framework for modeling the dynamics of an infectious disease[10, 247]. We consider a population of hosts, where individuals may be infected with a parasite. Uninfected hosts, whose abundance is described with the state variable $x(t)$, have a death rate d_x and are maintained by an influx rate θ (which could be birth or migration, for example). Infected hosts are tracked with the variable $y(t)$. They have an increased death rate d_y. Contact between infected and uninfected hosts occurs at a rate proportional to both their prevalences, and with some probability leads to the uninfected host becoming infected. The overall infection rate is described by the transmissibility, β. This system can be described by the system of first-order ordinary differential equations:

$$\begin{aligned} \frac{dx}{dt} &= \theta - \beta xy - d_x x \\ \frac{dy}{dt} &= \beta xy - d_y y \end{aligned} \tag{1.1}$$

Despite its simplicity, this model captures the most important properties of infectious diseases dynamics. This system of equations yields two regimes of qualitatively different behavior. If the disease transmissibility is high enough, if it is not too deadly, and if the host population is large enough, an epidemic will occur. Starting with a small number of infected hosts, the prevalence of the infection will rapidly increase, following a characteristic epidemic curve. A substantial fraction of the population will eventually be infected. However, if these conditions are not met, the disease will quickly die out before many more hosts are infected. The quantity that determines which regime the system is in is called the *basic reproductive ratio*[10]. It describes the average number of new infections

caused by a single infected individual introduced into a population of uninfected hosts. Mathematically, the basic reproductive ratio for this model is

$$R_0 = \frac{\theta\beta}{d_x d_y} \tag{1.2}$$

which can be justified as follows. The average lifetime of an infected host is $1/d_y$. During this lifetime, the rate at which an individual contacts and infects others is βx^*, where x^* is the abundance of uninfected hosts before the epidemic, which is θ/d_x (we assume a large population, this is roughly unchanged by the presence of a single infected individual). R_0 is a critical concept for infectious diseases because it quantitatively defines the goal of all treatment and control strategies - to alter the parameters of the disease such that $R_0 < 1$, so as to prevent or stop an epidemic. Mathematically, R_0 corresponds to a transcritical bifurcation between two uniquely stable equilibria.

This model is but one simple example of an entire class of models used to study infectious processes. Hosts may represent individual organisms, such as humans[222], animals[109], or crop plants, and the infection may be caused by any type of microorganism. Many models include the possibility for hosts to recover or become immune, and often more finely divide hosts into clinical stages of infection. The common *SIS* or *SIR* models of epidemiology are examples [10]. Alternatively, the host population could represent cells in the body that are infected with a virus. Model extensions may explicitly track virus levels, allow for infection of different cell types, or describe an immune response mounted against the infection. Such scenarios often fall under the umbrella of *viral dynamics* models [247]. More broadly considered, a modeled 'infection' could describe the state of knowing a particular piece of information, displaying a particular behavior, or possessing any other quality that is transmitted between individuals by any number of processes[95, 117]. The model may track multiple infectious agents, if there are competing infections in a single host population[313], or if the infectious agent may evolve over the course of the infection [295]. While differential equations are a popular

tool for infectious disease modeling, in some situations it is more appropriate to use a stochastic process to track the infection[51].

1.2 Applications to HIV

The human immunodeficiency virus (HIV) is the infectious agent that causes acquired immune deficiency syndrome (AIDS), and currently infects an estimated 34 individuals worldwide[255]. Since the identification of the syndrome in the 1980's, over 25 have died from the disease [234]. The virus infects cells of the immune system and is dominantly found in $CD4^{+}$T lymphocytes. During early infection with HIV, individuals may experience the nonspecific symptoms of acute viremia, but then often remain symptom-free for years before the onset of disease. AIDS occurs when the virus has degraded the immune system to the extent that it is unable to fend off infections from virulent opportunistic parasites. HIV generates enormous diversity both within an individual[317] and on the global scale[150], due to large population sizes of the virus and error-prone viral replication[212]. This affords the virus nearly unlimited potential to rapidly evolve to avoid immunological responses and treatment efforts[144].

Mathematical models of infection dynamics have complimented experimental and clinical work on HIV since the early stages of the virus's discovery (reviewed in [247]). At the within-host level, models have helped explain the virus's escape from the immune system and the progression to AIDS [248], the immunological mechanisms of viral control [185], the rate of cell turnover [364], the properties of long-lived infected cells [269], the viral tropism switch [285], and the effects of drug treatment [47] At the population level, infection dynamics models have lead to advances such as evaluations of treatments [43, 126] and preventative measures [237, 342], forecasts for the history and course of the epidemic [335], an understanding of the role of contact patterns [157], and predictions of the evolutionary optimal virulence [323]. We begin this report, in Chapter 2, wtih a synthesis of the important evolutionary factors governing the HIV epidemic, and include

the contributions of mathematical modeling and population genetics to the understanding of the disease.

The life-expectancy of patients with HIV, and the course of the epidemic in many parts of the world, has been dramatically improved by the introduction of antiretroviral drugs used in combination therapy[259]. These drugs can stop viral replication, leading to restored immune function, and preventing both progression to AIDS and disease transmission. There are currently 8 million individuals worldwide receiving antiretroviral treatment [254]. However, the virus's capacity for adaptation can also lead to the development of drug resistant strains that compromise treatment. When single antiretroviral agents were used, resistant virus appeared within weeks of treatment, and while combinations of drugs from different classes can reduce and delay the emergence of resistance, it is still a common occurrence[158]. While not yet at the same crisis levels as the problem of antibiotic resistance, antiretroviral resistance is an important clinical concern and is likely to increase in prevalence as treatment scale-up programs continue around the globe[42].

Another limitation of current antiretroviral drugs is their inability to cure an infected individual[326]. Drugs must be taken continuously for a lifetime, which exacerbates the logistic issues of supplying expensive drugs reliably in the developing world, and further increases the opportunity for drug resistance to develop[132]. This limitation arises from the ability of HIV to establish a type of 'latent' infection[110]. After the virus enters host $CD4^+$T-cells, its genetic material integrates into the host cell genome. As a natural part of their life-cycle, a small fraction $CD4^+$T-cells revert to a long-lived resting state, where they form the basis of immunological memory. If a cell with integrated HIV DNA reverts, the virus remains archived in the cell despite anitretroviral treatment, and can restart infection whenever the cell reactivates, which may be months to years later[89, 298]. This virus population is called the *latent reservoir*. A large research effort is currently dedicated to understanding the details of latency and identifying compounds that can prematurely

reactivate latent HIV from memory cells[98]. The hope is for these compounds to be given along with current antiretroviral drugs, to flush out the latent reservoir and eradicate the infection from the treated individual, allowing drugs to be discontinued without risk of a resurgence of the infection.

In this report we present research findings related to these two shortcomings of current HIV treatment. The development of drug resistance follows distinct patterns among different classes of antiretroviral drugs, and the relationship between a patient's adherence to treatment and the probability of resistance is often non-intuitive. In Chapters 3 and 4 we develop a mathematical viral dynamics model that integrates laboratory data and patient behavior, and culminates in attempting to realistically simulate clinical trials. Our current results demonstrate how pharmacodynamics and pharmacokinetics of antiretroviral drugs affect the generation and selection of resistance mutations. We can explain class-specific resistance-adherence relationships, and the puzzling finding that patients may fail treatment with the protease-inhibitor drug class without developing resistance.

Our second focus concerns the new class of drugs called *latency reversing agents* that are being investigated to eliminate the reservoir of latent virus. While it is generally accepted to be infeasible for a drug to clear every single cell from this reservoir, an acceptably safe number for the post-treatment cell count is unknown and of great importance to the field. In Chapters 5 and 6 we compile clinical and laboratory data and derive estimates for the size, composition, and dynamics of the HIV latent reservoir, allowing us to compare the stochastic rates of cell death, reactivation, and viral replication. We use these measurements in a viral dynamics model to calculate likelihood and timing of virologic rebound following treatment interruption, for a given drug-induced reduction in the number of latently infected cells. Our results suggest that LRA may need to reduce the reservoir by 99.9-99.999% to prevent relapse in most patients, and that patients may rebound without warning even after many years of treatment cessation. We suggest that large interpatient variability and particular unknown parameters will complicate the

interpretation of clinical trials.

1.3 Applications to social dynamics

Health depends not only on biological processes but on the interplay of human behavior. People often choose what preventative measures or treatments they use, and may be influenced in these decisions by others. Just as a physical contact networks determine the transmission patterns of a microbial infection, social networks - formed from direct interpersonal interactions or a form of media - can direct the transmission of ideas and behaviors.

Analyzing the influence of contagion in these systems and predicting future prevalence levels have become popular research questions, and mathematical models of infection dynamics have been adapted for these systems. These models may take the form of traditional epidemiological equations, with additional terms for the role of behavioral decisions (reviewed in [117]). Individuals may base decisions on globally available information (for example, CDC warnings) or their own local experience (for example, sick coworkers). The information content may be a direct property of the epidemic (like the current prevalence) or relatively independent (like the decision to vaccinate). In response to information, individuals may alter disease parameters (like decreasing transmission rate by improved hygiene or increasing recovery rate by treatment), directly alter their state (vaccination causes a susceptible individual to become immune), or alter the contact network through which the disease spreads. All of these responses can later the course of an epidemic in ways that could not be predicted by simple equations ignoring human behavior.

Beyond simply influencing the spread of microbial infections, behaviors themselves may obey infection dynamics. Individuals may receive information from their contacts, imitate the actions of those they observe, or be unknowingly influenced. These processes are termed generally termed *social contagion*, and are well established to occur in many systems. Drug use[69], mental health states[31, 55, 111], and health care[61, 231] are

examples of behaviors found to spread between individuals [333]. The adoption of new technologies and opinions about vaccination can be observed as they spread through social networks [13, 303, 350]. Understanding these dynamics is crucially important, either to predict how they will affect health outcomes (for example, see [302]), or to devise ways to use social contagion to actually target interventions [353].

In the final sections of this thesis (Chapters 7 and 8) we present two closely related papers that focus on modeling the spread of behaviors between individuals in a social network. We designed a modeling framework based on traditional infectious disease epidemiology to analyze and interpret findings for social contagion, and applied it to the spread of emotions and weight levels in the Framingham Heart Study Network. We highlight the importance of characterizing the particular dynamic of social influence for a given system, based on the availability of longitudinal data. We present methods for interpreting the importance of contagion and for understanding mechanisms behind changes in incidence over time. We don't attempt to determine the mechanisms of spread, but rather focus on properties of the contagious process. Our analysis can be applied to many other systems involving complex network structures and social influence.

2

Evolutionary dynamics of HIV at multiple spatial and temporal scales

2.1 Abstract

Infectious diseases remain a formidable challenge to human health, and understanding pathogen evolution is crucial to designing effective therapeutics and control strategies. Here, we review important evolutionary aspects of HIV infection, highlighting the concept of selection at multiple spatial and temporal scales. At the smallest scale, a single cell may be infected by multiple virions competing for intracellular resources. Recombination and phenotypic mixing introduce novel evolutionary dynamics. As the virus spreads between cells in an infected individual, it continually evolves to circumvent the immune system. We discuss evolutionary mechanisms of HIV pathogenesis and progression to AIDS. Viral spread throughout the human population can lead to changes in virulence and the transmission of immune-evading variation. HIV emerged as a human pathogen due to selection occurring between different species, adapting from related viruses of primates. HIV also evolves resistance to antiretroviral drugs within a single infected host, and we

explore the possibility for the spread of these strains between hosts, leading to a drug resistant epidemic. We investigate the role of latency, drug-protected compartments and direct cell-to-cell transmission on viral evolution. The introduction of an HIV vaccine may select for viral variants that escape vaccine control, both within an individual and throughout the population. Due to the strong selective pressure exerted by HIV-induced morbidity and mortality in many parts of the world, the human population itself may be co-evolving in response to the HIV pandemic. Throughout the paper, we focus on trade-offs between costs and benefits that constrain viral evolution and accentuate how selection pressures differ at different levels of selection.

2.2 Introduction

Over the course of the 20th century, human lifespans increased dramatically in many parts of the world. This reduction in mortality is largely attributed to a reduced burden of infectious diseases, due to improved nutrition and sanitation, and the introduction of both antibiotics and vaccines. We were so confident of our domination over the microbial world that in the mid-20th century it was common to surmise the end of infectious diseases as a significant health issue [107, 274, 337]. This sentiment turned out to be especially ill timed, as the last few decades saw the emergence of many novel and extremely dangerous pathogens, including Ebola, SARS, Lyme disease, Legionella, and drug-resistant malaria and tuberculosis. Perhaps no disease shattered this view as much as the outbreak of the human immunodeficiency virus (HIV), and the acquired immune deficiency syndrome (AIDS) that it causes. Reaching 34 million currently infected worldwide[255], a prevalence of 0.3% in the US [60], and near 100% untreated fatality rate, the HIV pandemic exemplifies humanity's continued vulnerability to pathogens and highlights how much we have yet to learn about infectious diseases.

Evolution has been used to understand human disease processes from allergy to cancer to cystic fibrosis, reviving the field of evolutionary medicine[340, 348]. Nowhere is the

connection between evolution and medicine more evident than in the field of infectious diseases. Although we have recently added vaccines and chemotherapy to our arsenal of defenses against microorganisms, augmenting the protection offered by our innate and adaptive immune responses, it is now accepted that the rapid rate of pathogen evolution ensures infectious diseases will inevitably remain important health concerns. Therefore, understanding the evolutionary processes relevant to infectious diseases is absolutely necessary to prevent, control, treat and ultimately, minimize the damage to human health due to pathogens.

HIV infection is a particularly well-suited example to highlight the medical relevance of evolutionary dynamics occurring simultaneously on multiple spatial and temporal scales (Figure 2.1), including the evolution of the virus within an individual and at the global level, as well as the co-evolution between HIV and the human population. HIV originated from a cross-species transmission of simian immunodeficiency virus (SIV), and it eventually evolved adaptations facilitating productive infection in, and transmission between, human hosts. At the individual level, the virus evolves in response to a dynamic, variably hostile environment presented by the immune system and drug treatment. At the population level, HIV likely evolves to evade immune control, optimizing virulence levels, and possibly transmitting drug resistance. Creation of a vaccine is hindered by rapid and unpredictable evolution of the virus, and if introduced, may further drive viral evolution, potentially causing resistance to the vaccination. Due to the strong selective pressure exerted by HIV-induced morbidity and mortality in many parts of the world, evolution of human populations in response to the virus is likely.

In this review, we will summarize the range of evolutionary processes important to HIV, and highlight how understanding them can help guide prevention, control and treatment of AIDS. We first summarize the natural history of the epidemic and the host-driven selective pressures that the virus faces regardless of treatment. We then consider the effect of medical interventions on viral evolution, focusing on recent efforts to

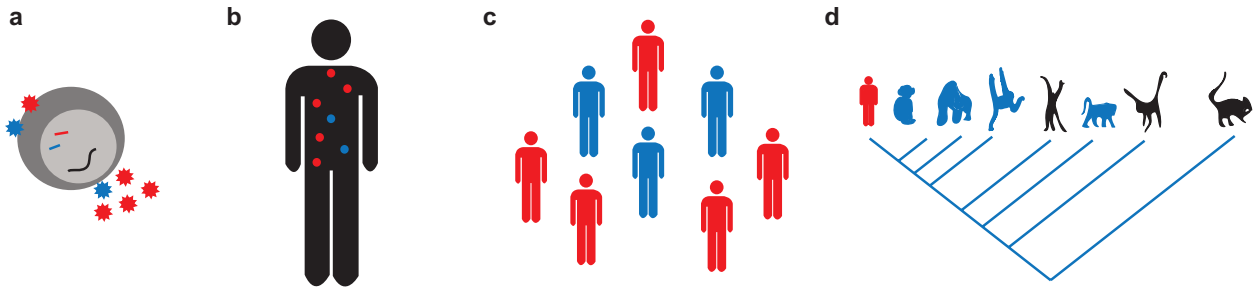

Figure 2.1: HIV evolution occurs on multiple spatial and temporal scales. a) Multiple virions may infect a single cell, competing for cellular resources controlling viral replication. Budding virions may contain RNA, structural proteins and enzymes from various genetic backgrounds. b) During infection of a single individual, HIV diversifies into multiple strains that compete to infect $CD4^+$T cells and evade immune responses and drug treatment. c) As HIV spreads through the human population it may adapt, becoming more or less virulent and accumulating mutations selected by immune responses or even widespread drug use. d) HIV arose from a cross-species transmission of simian immunodeficiency virus (SIV), known to infect many primate groups. Primate phylogeny, from left to right: humans, chimpanzees, gorillas, orangutans, gibbons, old world monkeys, new world monkeys, prosimians.

understand and quantify the mechanisms that can render treatment ineffective.

2.3 Natural history of the HIV pandemic

2.3.1 High retroviral mutation rate facilitates rapid evolution

Evolution requires the generation of variation through mutation. The capacity for HIV to evolve exceeds that of many other pathogens, due in part to the high mutation rate of retroviruses. At 3×10^{-5} substitutions per base per replication cycle [212] and a genome size of 9800 base pairs, one in every three replication events is expected to create a mutated genome. This puts the virus very near the error catastrophe threshold: at mutation rates higher than approximately one per genome per replication cycle, it is not possible for a genome to accumulate and maintain beneficial alleles, and a lineage risks extinction [54, 103, 150, 241](Section 3.1.8 of [150]). While the high mutation rate of retroviruses is usually explained by the fact that their virally encoded reverse transcriptase lacks error-correcting domains found in other organisms, it is currently unknown how much of this mutation rate is due to HIV reverse transcriptase and how much is due to host cell

RNA polymerase, since experiments to date cannot separate out these two steps. High mutation rates are expected to be favored more often in heterogeneous or rapidly changing environments than in stable ones [167], and due to the chronic nature of HIV infection and its ability to reach many tissues, it is possible that its high mutation rate has been favored by natural selection. Recent theoretical modeling work demonstrates that host-pathogen co-evolution may also generate selective pressure for high pathogen mutation rates, even in a static, homogeneous environment [167, 233]. Interestingly, mutation in HIV seems to be strongly skewed towards adenosines, much more than is represented by the adenosine bias in its sequence composition [3, 296]. The high mutation rate of HIV leads to tremendous variation in a given viral population; with up to 10% sequence variation between strains within an individual and up to 50% between different types circulating over the globe (Figure 7.10 Section 7.2 of [18, 150]).

Humans and other primates actually have an innate defense targeted towards the high mutation rate of retroviruses. The APOBEC3G enzyme edits the viral cDNA during reverse transcription, likely as part of a host defense mechanism. HIV encodes a protein Vif that facilitates polyubiquitylation and subsequent proteasomal degradation of APOBEC3G, but in the absence of Vif, the enzyme causes sufficient mutation to scramble the viral genome, triggering an "error catastrophe" and preventing productive infection [65, 133, 195].

In addition to mutation, the potential of the virus to recombine during replication is high, as reverse transcriptase typically jumps templates about 10 times per genome[199]. If two distinct viral strains infect the same cell (the likely frequency of such an event is discussed in a later section on within-cell competition), then each one may contribute to one of the two RNA copies in budding virus. When this virion infects a new cell, recombination between the two parental genomes may then occur. Many strains of HIV currently circulating the globe appear to be recombinant forms of divergent virus strains[346].

2.3.2 The emergence of HIV

As HIV spreads between individuals in a population, selection occurs on traits that maximize its transmission. HIV is a zoonotic disease, meaning it had its origins in a closely related infection of animals; in this case, non-human primates. Analysis of molecular phylogenies has traced the origin of HIV-1 (for example, see Section 7.2 in [150]), the viral strain responsible for the largest global epidemic, to the simian immunodeficiency virus infecting chimpanzees (SIVcpz) [173]. Similar cross-species jumps have happened with other primate species: a smaller epidemic of HIV restricted mainly to western Africa is caused by HIV-2, with origins in the virus of sooty mangabeys (SIVsmm) [305].

Adaptation of any disease to a new species proceeds through five phases (adapted from Chapters 12 & 16 of [340]): Firstly, there must be contact between the animal reservoir and humans that allows transfer of the pathogen. For SIV, this is hypothesized to have occurred through hunting for and preparing primate bushmeat. The second phase of adaptation - the ability to produce a productive infection in the new human host - is calculated to have occurred at the turn of the 20th century near Kinshasa in the present day Democratic Republic of Congo[376]. However, both these first and second phases have occurred more than once: humans in some central African regions may have antibodies to multiple simian viruses[374] (suggesting primary transmissions may be frequent), and the ancestry of HIV-1 subtypes implies distinct human-chimpanzees zoonoses (Section 7.2 in [150]). SIV infection of humans is not able to generate high viral loads needed for transmission. The third phase is for the disease to become transmittable between humans. However, to cause an epidemic, the pathogen must be suitably adapted to the new host so that every infected individual passes the disease on average to at least one other individual[10, 218]. HIV has been in this fourth phase of emergence for the past three decades. This phase may be facilitated by viral adaptations, or, by changes in the host population that increase transmission[336], such as higher population density and increase in behaviors that facilitate transmission. The later is believed to be an important factor for

HIV, potentially explaining the delay between the evolution of HIV's ability to productively infect humans, and the beginning of the global epidemic.

Determining the origins of HIV is not just for scientific and historical interest - hopes are that it could be key to determining how to control the disease. SIV infections are common in many species of primates, and related CD4-tropic lentiviruses are found in many other mammals, with current evidence pointing to a lentiviral origin over 7 million years ago [171]. Most SIV infections in their native hosts do not lead to AIDS-like immunodeficiency illness. Viral loads may be sustained at very high levels, but $CD4^+$T cell levels remain high. These findings have strongly suggested that HIV pathogenesis is driven by more than direct killing of target cells by the virus [329] Chronic immune activation is emerging as a potential mechanism for HIV pathogenesis; in natural SIV infection, immune activation is only transient [105]. In SIV infections, there are also strong cellular immune responses that seem to recognize highly conserved regions of the viral genome [125, 307]. The recency of successful immune control and avirulence of SIV in natural host populations is a topic of debate. Rapid host virus-coevolution towards reduced pathogenicity would result in a selective sweep, which would likely be detected by molecular phylogenetic methods as a relative absence of lineages that coalesce prior to the emergence of avirulence [149, 368]. A recent study suggests that the most recent intraspecies common ancestors of SIV in sooty mangabeys and chimpanzees, respectively, existed just 200 and 500 years ago, consistent with very recent evolution of an avirulent infection in both viral strains [368]. Biogeographical evidence gathered from comparisons of island and mainland viral strains in west Central Africa, however, suggests that SIV evolution proceeds at a rate two orders of magnitude slower than HIV evolution, implying a corresponding increase in the time since a common ancestor [377]. Further supporting this analysis, phylogenetic reconstruction that is unconstrained by geological or historical evidence may systematically underestimate branch lengths when lineages are subject to strong purifying selection, as is generally the case for RNA viruses [367].

While viruses represent only about 15% of all human pathogens, the majority of emerging diseases are RNA viruses, with high mutation rates (Chapter 16 of [340]). Emerging diseases tend to have reservoirs in animals, and they tend to be adapted to a broad range of hosts prior to arrival in humans. By examining likely patterns of cross-species transmission in HIV/SIV and other widespread RNA viruses [149], we may uncover clues that allow us to identify pathogens at risk for jumping the species barrier into humans.

Frequent viral recombination presents a major obstacle to an accurate understanding of HIV origins. Indeed, the entire scheme of classifying the main group of HIV-1 into nine subtypes has recently been called into question by evidence that subtype G may actually have resulted from recombination between subtypes A and J[2]. The occurrence of recombination, which requires infection of a cell by two strains and so should grow roughly as the square of viral load, may mirror the situation in some bacterial species, in which the frequency of horizontal gene transfer depends on population density[85]. The recent growth and success of "species tree" approaches in molecular systematics provides a powerful method for disentangling the discordant evolutionary histories of multiple loci that are brought together by recombination (reviewed in [101]). Though useful in metazoic taxa, these approaches have not been applied to virus evolution; they require the partitioning of the genome into discrete loci, with recombination occurring between, but not within, loci [75, 101]. The frequency of recombination in HIV may be prohibitively high, and therefore the "effective locus size" prohibitively small, in order to import these methods wholesale to the study of its evolutionary history.

2.3.3 Is HIV evolving to be less virulent?

The fifth and final phase of emergence of a new infectious disease is adaptation of the pathogen to optimize transmission between hosts, and the switch from an epidemic phase (rapidly increasing prevalence) to an endemic one. Although disease prevalence may remain

approximately constant in this phase, the system is by no means static - both pathogen and host populations can evolve continually to circumvent each other, in an evolutionary arms race (also known as "Red Queen" race)[352]. The infectivity of a strain is defined as the rate of infection of susceptible individuals, and the virulence is usually defined as the increased death rate that infected individuals suffer due to the virus. At first glance, it seems that it would be optimal for a disease to evolve to both maximize its infectivity and minimize its virulence in a host, the latter allowing the host to live longer and infect more people. However, there are often trade-offs between these two parameters that complicate the optimization of transmission - for example, high numbers of pathogens within a host may be necessary for infectivity but may contribute to virulence [217]. As well, there are clear conflicts between the role of within-host evolution and population level evolution on virulence-related traits. Competition within a host selects for the fastest replicating strain, which could be more virulent, while at the population level an intermediate replication rate that maximizes transmission may be favored [220, 246]. Even within a host there is selection to control the death rate of infected cells to maximize transmission between cells. Bottlenecks that occur at transmission may to some extent "reset" viral evolution between hosts [18], with the result being that within-host selection may have little effect on the long-term, population level evolution of HIV. However, recent studies have shown that in the case of HIV, there is heritable variation in virulence (measured by viral load) between 20-60%(reviewed in [232]). There is no clear consensus as to whether HIV is evolving at a population level to become less virulent (summarized in [18, 323]), although a recent meta-analysis has concluded that virulence has actually increased over the past three decades [141]. A recent paper modeling the evolution of HIV virulence based on known viral load-transmission rate and viral load-mortality relations concluded that HIV has already reached the optimal virulence to maximize transmission between hosts [323].

2.3.4 Does competition within a single cell drive evolution?

In HIV infection there is potential for multiple genetically distinct virions to infect a single cell [94]. This results in a new level of selection for the virus which we call within-cell (as opposed to within-host and population level), which introduces novel viral dynamics. Firstly, competition for resources related to viral replication within the cell can select for an increased production rate of virions and hence greater cytopathicity [372]. Secondly, when multiple virions infect the same cell, the new virions created will have a mix of genetic material from both strains and structural proteins and enzymes (determining "phenotype") also from both strains. This is termed phenotypic mixing [370]. As a result, deleterious mutations may persist at a higher frequency than expected by mutation-selection balance, since they can be shielded by the wildtype phenotype [240, 370]. Virions carry two strands of RNA genome, which may be from different strains. When this virion infects a new cell, these genomes may recombine, as reverse transcriptase often jumps between RNA strands[199]. Recombination alters the spread of viral genotypes maintained by mutation and changes the error catastrophe threshold [44]. Together, the effects of co-infection have been shown in models to accelerate the rate of CTL escape [230] but may either promote or hinder the development of drug resistance, depending on whether multiple mutations display synergistic or antagonistic epistasis [50]. Importantly, a pre-requisite for these dynamics to affect the genetic composition of the population is the existence of a significant number of cells co-infected with genetically distinct virions. Some studies claim that co-infection with genetically distinct virions happens quite frequently in the lymph tissue [166], but much lower rates (1-10%) have been found in the peripheral blood [163] and have been estimated from effective recombination rates measured from patient sequence data [30, 235].

2.3.5 HIV pathogenesis involves immune-directed evolution

Despite three decades of research on HIV, its mechanism of pathogenesis is still not entirely clear. Evolutionary processes are implicated to a large extent in the hypothesized mechanisms of disease progression [247, 248, 250, 306]. It is well understood that over the course of a single infection, HIV continually evolves to circumvent host defenses. HIV infects $CD4^+$T lymphocytes, also known as helper T cells, using the receptors that they uniquely express to gain access to the cell. After initial HIV infection, patients experience very high viral loads and occasionally the flu-like symptoms of acute viremia, after which viral load declines to a comparatively low level called the "set point", where it may remain for many years. This decline occurs both due to the limitation of uninfected target $CD4^+$T cells [272] and by the appearance of cellular immune responses against HIV [331].

Immune control of HIV is largely due to $CD48^+$T cells [203, 359, 373](also called "killer" T cells or cytotoxic T lymphocytes (CTLs)), though antibodies [365] and innate immunity [62] also play a roll. Small virus-derived peptides called epitopes are presented on the surface of infected cells by the HLA class 1 molecules, which then allows CTLs to recognize and kill these cells. Throughout the course of chronic infection, which may last from a few years to a decade, viral diversity and fitness gradually increase [18, 49, 189]. Antigenic diversity also increases, as HIV continuously generates escape mutations in CTL epitopes, preventing them from being presented or recognized [8, 49, 124, 250, 273]. About 2/3 of mutations acquired over the course of HIV infection have been attributed to CTL selection pressure [7]. These mutants are subsequently selected and may grow to a high frequency. The immune response is further weakened by the fact that HIV is infecting and destroying cells involved in immune control.

While evolution is typically thought of as an open-ended process that may follow many paths, certain aspects of HIV evolution are very predictable. For a given HLA allele present in an individual, certain escape mutations in epitope regions are highly consistent between patients [53, 57]. Another predictable evolutionary event is a switch in the virus's

machinery for entering its target cells (reviewed in [200, 285]). HIV enters cells by binding to the $CD4^+$cell surface receptor, but also requires a co-receptor. Early in infection, the viral population seems to be composed of strains that preferentially use the CCR5 co-receptor, termed "R5" virus. Later on in infection, about 50% of patients experience a switch in the tropism of the dominant virus population to an "X4" virus that instead uses another co-receptor, CXCR4, for entry. The factors determining this switch are not completely understood. It seems that R5 viruses have a selective advantage early in infection and dominate the viral population after sexual, mother-to-child, or direct blood-to-blood transmission, though individuals homozygous for the $\Delta ccr5$ mutation can be infected with X4 virus [322]. Later in infection, selection pressure seems to change to favor X4 virus. This is hypothesized to be a result of the change in the population composition of T cells over the course of chronic infection. The X4 virus seems to be more susceptible to antiviral immunity but able to infect a broader range of target cells, including resting T cells, and so as immune function declines, it may outcompete R5 viruses. The reason only 50% of patients experience this switch is unclear, though could be a result of the chance accumulation of multiple mutations required to make the tropism switch. Patients with X4 virus tend to experience more rapid decline in $CD4^+$T cells, and so this phenotype switch may be facilitated by immune deficiency but then lead to accelerating deficiency. The co-receptor switch is less common in treated patients [197].

Mathematical models have demonstrated that the accumulation of escape mutations can explain the clinical course of HIV infection [167, 248, 286](Figure 2.2). Viral diversity increases as HIV progressively escapes CTL responses, resulting in higher viral load, and due to HIV-induced damage of $CD4^+$T cell populations, a progressively weaker immune response. There is an asymmetry in the HIV-T cell interaction, since any strain of HIV can infect and damage any $CD4^+$T cell, but each CTL can only target the HIV strain it is specific for. Eventually infection reaches a point where the immune response is unable to control the variable strains of HIV, and viral loads rapidly increase as $CD4^+$T cell levels

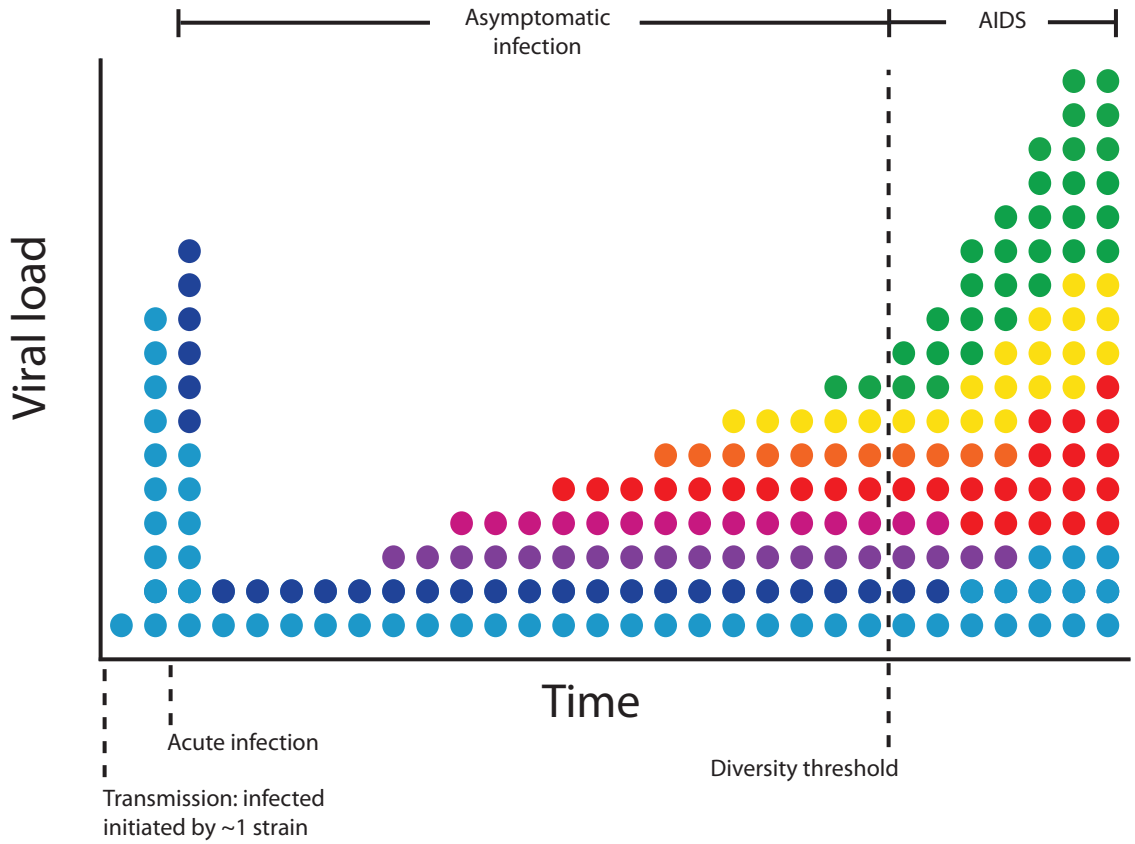

Figure 2.2: Hypothetical evolutionary mechanism for HIV pathogenesis. Colors schematically represent diversity of viral strains. Bottlenecks during transmission lead to acute infection growing from approximately a single viral strain. Viral loads peak and decline rapidly during acute infection, with diversity remaining low. During asymptomatic infection, which may last from months to decades, viral loads remain near a lower set point. Diversity gradually increases, potentially as mutants that escape cytotoxic T cells are generated. At a certain point helper ($CD4^+$T cells) reach a critically low level, due to direct and indirect effects of HIV, leading to rapid rise in viral load and progression to the clinical symptoms of AIDS. Mathematical models suggest that crossing a diversity threshold could cause progression to disease. At the final stages of disease, diversity begins to decrease, possibly due to reduced selection pressure from a failing immune system. Figure adapted from [18, 174, 196, 242, 317]

fall. This is called the "diversity threshold", and could explain the onset of the clinical symptoms of immune deficiency, called AIDS. This theory highlights that the two specific features of HIV, which make it especially harmful to the host, are the fact that its target cells are involved in orchestrating the immune response, and its high rate of evolution in a single infected host.

Despite its elegance, the evolutionary model for HIV pathogenesis may not be the whole story. Various lines of evidence suggest that CTL responses are important for viral control, including the observation that the selective advantage of escape mutations correlates with rate of disease progression (specifically, the portion of this rate that is statistically associated with particular HLA alleles)[20]. However, it has been observed that only a small fraction of $CD4^+$T cells are infected with HIV, making it difficult to explain how either direct viral killing or CTL killing, for which death rates have been measured, could be responsible for such a large decline in their numbers. During infection, there is a large increase in the death rate of uninfected (termed "bystander") $CD4^+$T cells. Multiple, though not mutually exclusive, mechanisms have been proposed to explain this observation, including 1) direct cytotoxicity of free-floating HIV proteins on uninfected cells, 2) an increase in apoptotic signals, or 3) an increase in the fraction of activated, short-lived T cells due to HIV-induced immune activation [5, 84, 200]. While the importance of each of these mechanisms remains to be determined, it is interesting to note that models for many potential pathogenic processes have found that the extremely slow decline of $CD4^+$T cells is difficult to explain by any process that does not, at some level, involve gradual evolution and an accompanying change in the balance between the virus and host defenses [382]. However, evolution could be either viral or related to somatic evolution of T cells: an increased turnover rate of cells could lead to the accumulation of deleterious mutations and eventual senescence of immune cells [118]. The ability of HIV to induce immune activation may itself be subject to selection. The direction and strength of selection depend on the trade-off between creating more target cells and increased virulence. However, the ability

to cause immune activation is only under selection if it preferentially changes the fitness of a particular viral genotype, that is, if it is local. The ability to cause systemic immune activation affecting all viral genotypes is a selectively neutral trait [28].

Clues to the virus's mechanism of harm can be deduced from a rare group of patients who become infected with HIV, but maintain lifelong low viral loads and do not seem to progress to AIDS[92]. Existence of these "elite controllers" suggests that immune control of the virus is possible in humans, though how this control works is still under investigation. This sub-population of individuals is enriched for certain HLA alleles, and their CTL responses tend to have higher HLA avidity, proliferate more, kill better, and preferentially recognize epitopes from the HIV capsid protein Gag (reviewed in [186]). Immune activation levels remain relatively low in elite controllers. Despite very low viral loads, they do seem to experience ongoing viral replication, and even continual evolution, including escape mutations [251]. How then, do they avoid increasing viral loads and decreasing immune function? When HIV mutates to avoid immune recognition, these mutations often harm native functions of the virus, leading to a fitness cost (defined as a reduction in replication rate as compared to a wildtype virus in a laboratory environment, free of immune response). The selective advantage of an escape mutant depends on a trade-off between the benefit attained from escaping CTL killing and the fitness cost of the mutation, and it in elite controllers the cost of escape may be so great and the advantage so low that viral loads remain approximately constant [226, 227, 251, 378]. The "diversity threshold" model of HIV pathogenesis mentioned earlier does include specific parameter regimes where indefinite control of the virus occurs[244], but it has yet to be determined if these parameter regimes are quantitatively consistent with elite controllers.

The ability of HIV to rapidly escape from immune control has important implications for vaccine development. There are currently effective vaccines for many diseases, including measles, smallpox and polio. For each of these diseases, a single natural infection provides lasting immunity. Vaccine-induced immunity is similarly effective. In contrast, individuals

infected with HIV can be superinfected with other strains and effective immune control is rarely achieved. Designing an HIV vaccine requires first determining the unknown correlates of immune control. Such a vaccine will have to elicit immune responses to an extremely diverse viral population. All currently used protective vaccines elicit antibodies, which until recently were believed to be generally ineffective in controlling HIV, leading to much focus on CTL-based vaccines [261]. However, recent years have seen advances in the characterization of "elite neutralizers," individuals capable of naturally controlling HIV infection with potent broadly neutralizing antibody responses, which has renewed confidence in the future of antibody-based vaccines (reviewed in [184]). This strategy is complicated by the finding that elite neutralizers can produce these antibodies only after extensive somatic mutation of B cells, suggesting that a vaccine may have to elicit the "ancestral" antibodies and then direct evolution through particular affinity maturation pathways. Studying the mechanisms of immune control in elite controllers and elite neutralizers will likely continue to be an important step in research towards a vaccine [39].

HIV's ability to evade immune responses also emphasizes the importance of trade-offs in evolution [160]. Overall, HIV and other lentiviruses have evolved an infection strategy that evades many defenses of the immune response, allowing the virus to persist and establish a chronic infection lasting many years. One of the particular adaptations enabling this strategy is the arrangement of the cell-binding proteins in the viral envelope. These proteins are placed so that conserved regions are inaccessible to antibody recognition, explaining the scarcity of broadly neutralizing antibodies against HIV. However, as a result, HIV's ability to infect cells is compromised. In immune-free cell culture, strains quickly evolve which have higher replication rates but are more susceptible to antibodies. Other viruses infecting humans take a different strategy; replicating very quickly and relying on most transmission to occur before the host mounts an immune response, which will then likely clear the infection. This trade-off between the "acute infector" and "persistor" viral lifecycle strategies is reminiscent of life history theory [338, 339], which

posits that trade-offs constrain fertility and that organisms respond to dynamic environments with a variety of reproductive strategies, e.g., producing few offspring and investing heavily in each, or producing many offspring each with a low chance of survival.

2.3.6 Is HIV evolving at the population level response to human immune control?

There is evidence that HIV may be evolving at the population level, evading immune responses characteristic of specific human sub-populations. Escape mutations prevent the virus from being recognized by a certain individual host's immune response, and when the virus is transmitted to another host, they may revert back to wildtype [198] or be maintained [124]. Studies have shown that in various populations, the prevalence of escape mutations in particular epitopes was highly correlated with the prevalence of the HLA allele presenting that epitope, even when only individuals without the allele were considered. Particular escape mutants also appeared to be increasing in prevalence over time [114, 172]. It has been suggested that in populations where there are HLA alleles common to many individuals, CTL escape mutations may be retained upon transmission and contribute to increasing virulence of the epidemic, while in populations with high HLA diversity (many African populations), it is more likely for virulence to decrease [18].

2.3.7 Host-pathogen co-evolution: Are humans evolving in response to HIV?

We have so far discussed evolution of HIV in response to selection pressure imposed by host immune defenses and by potential vaccines. It is however also possible that the human population may be evolving in responding to the virus. Given the high prevalence of HIV in certain regions, and the severe decrease in reproductive success incurred by untreated HIV-positive individuals, a strong selective pressure for protective alleles is expected and changes in allele frequency should be apparent in several generations. Since severe disease burdens have only existed for 1-2 generations so far, these changes may not yet be

detectable.

Studies have identified various sources of natural genetic variation to HIV infection in humans [108, 139, 228]. Heterozygosity at the HLA loci, and certain HLA alleles, especially at the HLA-B locus, are strongly related to slower disease progression. Two cellular proteins involved in innate antiviral immunity show strong signatures of positive selection in human populations, and polymorphisms have been implicated in differential susceptibility to HIV infection. TRIM5α interferes with the uncoating of the viral capsid upon entry into a host cell, and APOBEC3G, as discussed earlier, can edit viral cDNA during reverse transcription, leading to hypermutation of viral genomes. Variation in cytokine loci are also implicated in HIV control. About 1% of the European population is homozygous for a 32 base pair deletion in the CCR5 gene ($\Delta ccr5$), rendering them resistant to infection by HIV, which requires the CCR5 protein as a co-receptor during initial infection. To the extent that these polymorphisms are prevalent in regions with a high burden of HIV-induced mortality, their frequency may change in response to the epidemic.

2.4 HIV evolution in response to medical interventions

2.4.1 How might an HIV vaccine drive population level virulence?

Attempts to make a vaccine against HIV have so far been unsuccessful, largely due to the enormous genetic variation of HIV, both within an individual, starting early in infection, and worldwide. Due to the fact that HIV is only rarely controlled by antibodies, which are induced by most vaccines to date, and that the virus quickly establishes long-lived reservoirs in latently infected cells, it has been suggested that a potential vaccine may not be able to prevent infection, but may instead only lead to a reduced viral load set-point [26]. Theory suggests that vaccines that completely prevent infection could lead to reduced virulence, either by directly targeting virulence factors (as is the case with the diphtheria vaccines), or, by reducing co-infection and hence the strength of within-host competition,

which often selects for high replication rates and high virulence[119, 246]. The latter effect is likely to be relevant in certain high-risk populations where infection with multiple strains is common, though in general multiple infections are a rare occurrence [355]. However, "leaky" vaccines that allow some infection but reduce host death rate, like that proposed for HIV, can alter the virulence-infectivity trade-off, making increased virulence less costly (less chance of host death) and more beneficial (to achieve high transmission in face of reduced pathogen titers), and therefore lead to evolution of increased virulence [119]. Virus may also escape vaccine control, similar to escape to naturally occurring immune responses, with unknown consequences for virulence.

2.4.2 HIV evolves resistance to antiretroviral drugs

In the developed world, deaths from AIDS have decreased dramatically since the introduction of highly active antiretroviral therapy (HAART) in the late 1990's [259]. By targeting multiple HIV proteins with drug combinations at high doses, HAART minimizes the likelihood of developing resistance. However, these drugs remain prohibitively expensive and inaccessible to most HIV infected individuals, and suboptimal adherence and drug resistance remain a problem worldwide. At first we consider the case of resistance evolving de novo, in an individual initially infected with drug-sensitive HIV; later we consider the less frequent case where resistance is transmitted.

Like the host immune response, antiretroviral drug treatment provides a strong selective pressure on the virus, and over the course of a single individual's infection, HIV can evolve drug resistance. Unlike the immune response in a typical individual, drug treatment easily results in a negative growth rate for the virus, limiting ongoing viral replication and slowing the rate of evolution. Resistance mutations can arise from one of three sources [296]. Firstly, if treatment does not completely suppress all viral replication, new mutations may arise during treatment from the residual viral replication. This likelihood of generating resistance depends on the strength of the drug, measured by the

fraction of viral replication events prevented by the drug at a given concentration. Secondly, viral loads are generally quite high when treatment starts, and mutations may pre-exist in the viral population with some low frequency termed mutation-selection balance [47, 288], which is determined by the mutation rate and the fitness cost of the mutation in the absence of treatment. Thirdly, occasionally HIV-infected $CD4^+$T cells revert to a resting state, bringing with them integrated HIV in their genome. These cells comprise the latent reservoir and may remain in a resting state for many years, unaffected by drug treatment, which only inhibits active viral replication. Cells in the latent reservoir harbor a representative sample of viral genomes that have existed in the plasma over the course of infection. Mutation frequencies in the reservoir are likewise determined by mutation-selection balance, and resting cells may re-activate randomly at any point during drug treatment, reseeding the infection with both wildtype and mutant viruses.

In order for clinical drug resistance to emerge, resistant viral strains must be selected for. Viral fitness is determined by drug concentration, and typically follows a sigmoidal dose-response curve with a variable IC_{50} and slope [319]. Mutant viruses have altered dose-response curves and benefit from having a higher IC_{50} or lower slope. Resistant mutants also tend to carry a fitness cost, meaning that in the absence of the drug, their fitness is lower than the wildtype virus [304]. As a result there is only a certain range of intermediate drug concentrations, termed the mutant selection window (MSW), where any particular mutant is selected over the wildtype (Figure 2.3a). At lower concentrations, the wildtype is favored, and at higher concentrations, even mutant fitness is so low that the growth rate is negative. No HIV mutants have been characterized that lack susceptibility to any drug concentration, though many may only be controlled with concentrations that are not clinically achievable due to toxicity [304]. Even when concentrations fall within the MSW, the favored mutant may still be lost to random drift, with a probability depending on the population dynamics of the infection. Heterogeneity and fluctuations in the host environment during treatment generally increase drift, making a favored mutant less likely

to establish a persistent lineage (see Box 1).

Drug concentrations within the MSW may inhibit wildtype growth but select for resistance. Drug concentrations are not constant in a given individual, but fluctuate due to the dose taken, the drug bioavailability and half-life, and the patient's adherence to medication (Figure 2.3b). Consequently, selection pressures also fluctuate (Figure 2.3c). Drug concentrations that are high, yet still within the MSW, may slow the rate of emergence of resistance, since ongoing viral replication is greatly reduced and resistant mutants can only arise if they are pre-existing (either in the actively infected cells or in the latent reservoir).

Keeping drug levels above the MSW is required to guarantee the resistant mutant won't be selected for. If these concentrations are clinically possible, then this particular mutant alone is not an insurmountable threat, since if it arose, it could be eradicated by ensuring that drug concentrations exceed the MSW for sufficient time. However, clinically relevant resistance may require more than a single mutation. If a single resistance mutation arises, it may facilitate the emergence of stronger, untreatable strains with multiple mutations (Fig 2.3g), or with compensatory mutations, which reduce the fitness cost of the first mutation. It is possible that these strains will then be untreatable at maximum clinical drug concentrations, in which case they will lead to treatment failure.

Most current first-line antiretroviral regimens include a drug that can reduce viral replication by at least five orders of magnitude, even at minimum clinical plasma concentrations [319, 320], and so it is likely that multiple factors acting in concert are typically required to provoke treatment failure. Three main environmental factors can conspire to enable viral replication despite ongoing treatment. First, drug concentrations may temporarily drop, either when the concentration reaches a minimum prior to a scheduled dose or when the patient fails to adhere to the regimen. Certain drugs, notably the protease inhibitors, have very sharp dose-response curves, meaning that despite having the benefit of requiring lower concentrations to achieve the same inhibition, have the

Figure 2.3 ***(following page)*:** Drug-dependent fitness landscape for the antiretroviral drug efavirenz derived using measured pharamacodynamic and pharmacokinetic parameters for wildtype and the K103N drug resistant strain. Viral growth rate is positive only when $R_0 > 1$ (above grey dotted line) a) Fitness of wildtype and resistant strains follow dose-response curves, resulting in a *mutant selection window* where resistant strains are selected. We compare a single mutant (K103N) to two hypothetical double mutants by adding either a second equivalent resistant mutation (further increases IC_{50} and decreases slope) or a compensatory mutation (changes fitness cost only). b) Drug concentrations decay over time according to drug half-life. c) Relative fitnesses of wildtype and resistant strains consequently change over time as drug decays d) In the CSF, reduced drug penetration results in concentrations reduced to 0.5%, allowing viral replication at higher systemic drug levels. e) Assuming about 10% of cells are susceptible to direct cell-to-cell transmission, which typically occurs with around 100 virions and is sustainable with a single virion. f) Combining the effects of (d) and (e). g) At the maximum clinical drug concentration (immediately following a dose), only the doubly resistant mutant can grow. h) At intermediate concentrations, the single resistant mutant can grow, facilitating evolution of the compensated mutation or the untreatable doubly resistant mutant. i) Without treatment, the wildtype is favored. While the doubly resistant mutant can step-wise revert to wildtype, the compensated mutant is less likely to do so due to the presence of a fitness valley at either of the intermediate single mutants. See Appendix (§2.5) for methods.

Figure 2.3: (continued)

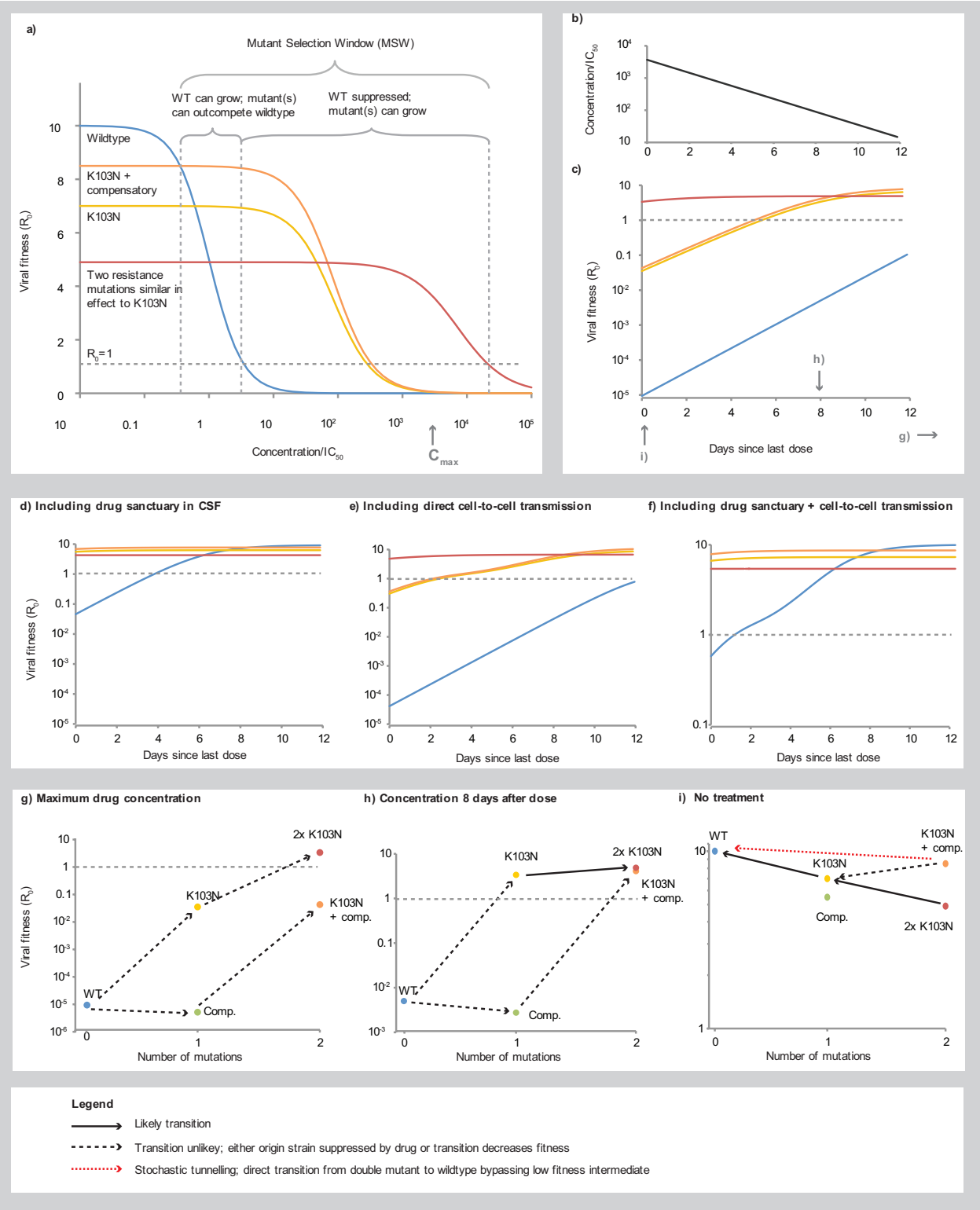

disadvantage that a small decline in drug concentration can lead to a large drop in viral suppression [319]. Secondly, replication rates are increased in tissues such as lymph nodes that are densely populated with target cells. In particular, multiple infections per cell (for example, by local spread of virus or direct cell-to-cell transmission via virological synapses) may occur in such tissues[127, 162], although the evidence for a high multiplicity of infection in vivo is limited [163, 166]. The presence of even a small collection of cells vulnerable to this mode of transmission may suffice to dampen a drug regimen's inhibitory effect by an order of magnitude [324] (Figure 2.3e,f).

Finally, drug concentrations in certain anatomical compartments may be a small fraction of plasma levels. The concentration of efavirenz in the CNS, for instance, is typically only 0.5% of the plasma level [36] (Figure 2.3d, f). Infected monocytes may introduce the virus to the CNS or other drug refuge, thereby initiating a locally blooming infection, despite successful viral suppression elsewhere in the host [36, 38, 83]. For example, on the basis of a simple calculation using dose-response curves measured in vitro, we estimate that wildtype (drug-susceptible) virus can generate a self-sustaining infection in the CNS if target cells are also capable of direct cell-to-cell transmission [324], in the presence of efavirenz therapy just below the clinical minimum drug concentration (Figure 2.3d). A single missed or delayed dose would allow concentrations to dip below this minimum level, allowing the infection to grow locally. If a resistance mutation occurs every 104 replication events, then a transient growth in viral load to detectable levels ($\approx$ 50 copies/ml, or 25 virions/ml) confined to the CNS ($\approx$ 200 ml), experiencing daily turnover [214], should generate a resistant mutant every other day. This explains why resistant strains may evolve in vulnerable anatomical compartments even while plasma viral load is suppressed, potentially leading to therapy failure[102, 332]. Equations and parameters for generating Figure 2.3 are given in the Appendix (§2.5).

Drugs that inhibit binding of HIV to host cells (entry or fusion inhibitors) are currently in various stages of development. Like antiretrovirals that act at other phases of the viral

lifecycle, these drugs come with a risk for the development of resistance; but they may also have other consequences for disease progression. Models have shown that drugs that inhibit the CCR5 co-receptor (for example, FDA-approved Maraviroc) could facilitate the switch to more pathogenic X4 variants, while anti-CXCR4 drugs may have the added benefit of decreasing selection pressure for X4 strains [285, 366].

The risk of resistance can be reduced with higher drug concentrations and by ensuring that drugs penetrate all tissue compartments; combination therapy plays a crucial role. When multiple drugs with different sites of action are used, the virus may need mutations that reduce susceptibility to all drugs in order for treatment failure to occur. Since multiple independent mutation events are relatively unlikely to occur on the same viral genome, it is generally more difficult for the virus to become fully resistant to combination therapy than to single therapy.

Predicting drug resistance should be an important consideration when designing dosing regimes for antiretroviral drugs, and would ideally be done as a part of the drug design process. Laboratory assays can characterize costs and benefits of mutant strains in the presence of drugs[304]; however, mutations are typically chosen for study only after they are observed in patients failing therapy. Bioinformatic techniques are needed to predict sites where resistance-conferring mutations may occur and how multiple mutations interact[33, 34, 193]. High-throughput implementations of known techniques for creating and testing mutant strains could help prevent the emergence of resistance and aid in design of "resistance-proof" drug regimens.

There are a few novel ideas for drug treatments that act in a very different way from current antiretrovirals, which reduce viral infectivity; instead, they aim to alter HIV's intrinsic mutation rate. Drugs have been proposed which increase the mutation rate beyond the error catastrophe discussed previously, besetting the viral genome with unsustainable levels of deleterious mutational load (reviewed in Section 4.3 of [150]). An example is inhibitors of the viral protein Vif, which prevents the cellular APOBEC3G

enzyme from hypermutating HIV cDNA during reverse transcription. A mutagenic drug (ribavirin) that acts with a different mechanism already exists for the hepatitis C, foot and mouth disease, and respiratory syncytial virus [82]. It is also possible that drugs that decrease the mutation rate may be useful, since much of HIV's proposed pathogenesis is due to its high mutation rate. It has also been hypothesized that drugs could be used in concert with natural immune control to create an evolutionary trap for HIV: if drugs are designed such that any potential resistance mutations are potent CTL-eliciting epitopes, than the virus would be unable to escape both methods of control simultaneously [385].

2.4.3 Could HIV become a drug-resistant epidemic?

It is generally assumed that individuals are infected with drug-sensitive virus, and that suboptimal treatment (i.e. monotherapy) or poor adherence leads to the de novo generation and selection of resistant mutants within that individual, as described earlier. Recent data, however, suggests a significant minority of cases where individuals are infected with a resistant strain. Worldwide, the detection of transmitted drug resistance in treatment-naive individuals is becoming increasingly worrisome. Between 10-25% of individuals in high-risk groups in the US and Europe are infected with virus harboring mutations associated with resistance to one or more antiretroviral drug [275, 354]. Surprisingly, drug resistance is transmitted not only from treated individuals, but may be transmitted directly between untreated individuals[153]. Transmitted drug resistance occurs much more frequently in regions where antiretroviral use is more prevalent. As drugs become more readily available globally, will the HIV epidemic become untreatable?

Widespread transmission of drug resistance requires both the generation of resistance within infected individuals, as well as the maintenance of these mutations upon transmission to uninfected individuals. Traditionally, it was believed that the fitness cost of resistance mutations, resulting in them having a lower fitness that wildtype strains in untreated individuals, made persistence of resistance unlikely (Fig 2.3a/i). Often, reversion

of resistance mutations is observed when studying transmission pairs. However, reversion to wildtype is observed to occur much more slowly than the initial take-over by a resistant mutant [206], sometimes taking years due to smaller relative difference in fitness in the absence of drugs that in their presence (see Figure 2.3g-i). In other cases, resistance may persist. This occurs when the fitness of resistance mutations is offset by the accumulation of compensatory mutations, which have been identified for many resistance mutations. Even if these compensatory mutations are unable to fully offset the cost, reversion may be very unlikely to occur if intermediate mutational steps leading back to the wildtype are less fit than the original (multi-step) mutant[131, 275, 310](Fig 2.3i). When this occurs, resistance is no longer reversible, and persistence of resistant strains in untreated individuals will occur, compromising their likelihood of treatment success when they begin antiretroviral therapy.

Transmitted drug resistance is just beginning to be studied in the context of HIV. The finding that overall, lower viral loads are not observed with transmitted drug resistance [134] suggests that the mutations are not costly, and it was also shown that transmitted resistance impairs treatment responses [371]. A recent modeling study for the spread of drug resistance in San Francisco, where prevalence of transmitted resistance is among the highest in the world, suggested that the most important determinants of spread are the relative fitnesses of the wildtype and resistant strain, especially during the asymptomatic (i.e. early, untreated) stage of infection [335].

Many other diseases have already established widespread, costly, and often deadly drug-resistant epidemics: examining them may help assess the threat of spread of drug resistant HIV (reviewed in [340, 384](Chapter 10 of [340]). Antibiotic resistant bacterial epidemics, such as methicillin resistant Staphylococcus aureus (MRSA) and vancomycin resistant Enterococcus (VRE), are facilitated in hospital settings by widespread antibiotic use and easy transfer between high densities of often immunocompromised patients. Bacteria may acquire drug resistant genes on plasmids through horizontal gene transfer

with unrelated bacterial species. Since many antibiotics were derived from naturally occurring compounds, resistance genes may pre-exist in certain environmental bacteria[6]. Widespread use of antibiotics in livestock exacerbates this problem. Multiple factors contribute to the persistence of resistance genes even when bacteria infect untreated individuals. When carried on small plasmids or linked (on plasmids) to beneficial genes, there may be little fitness cost incurred for carrying the resistance gene. Plasmids may potentially carry resistance genes to multiple drugs. Drug resistant infections may be more or less virulent than susceptible ones, due to either linked virulence factors or fitness costs to resistance, and studies have found that both scenarios occur[78]. The multidrug resistant tuberculosis (MDR-TB) epidemic in the developed world first emerged in immunocompromised individuals, particularly AIDS patients[100], and has been suggested-though not consistently demonstrated-to be less virulent and transmissible [79]. It is clear that persistence of HIV drug resistance is not influenced by many of these factors facilitating antibiotic resistance.

Examining the potential for transmitted drug resistance from an evolutionary point of view suggests that it will likely be easier to prevent such an epidemic from occurring, than to control it once it emerges. Worldwide, there have been multiple population level attempts to reduce the prevalence of drug resistant infections by lowering sub-therapeutic use of antibiotics (for example, in agriculture, or in mild infections of humans): they have shown very little success. Predicting resistance during drug development will be an important step. Improving patient adherence to drugs is extremely important. Most currently HAART regimes involve drug combinations that suppress viral replication to such an extent that clinical resistance is extremely unlikely, and the strongest predictor of resistance is patient adherence, which currently averages around 70% [24]. While using antiretroviral treatment as a preventative measure against HIV infection in high risk groups (called pre-exposure prophylaxis, or PrEP) may reduce the number of new infections, in some cases it could increase the percent of infections that are drug resistant

[342]. A similar effect could potentially occur for "test-and-treat" strategies, which aim scale-up diagnostic tests in underserved areas and to start antiretroviral treatment as soon as individuals are diagnosed with HIV [42].

2.4.4 Box 1: Population size and emergence of drug-resistant mutation from the latent reservoir

Several studies have estimated the *effective population size* (denoted N_e) of the HIV infection at various stages of the infection. This quantity is used to describe the strength of random genetic drift [135], and so it is important for understanding the likelihood that a favored drug resistance mutation will by lost by chance [188, 268]. Since effective population size is an abstract concept defined in the context of particular mathematical models, the appropriate definition to use depends on the particular biological question being asked. To demonstrate this point, we explore a general mathematical description of emergence of drug resistance from the latent reservoir. Though simple, this framework can be used to understand clinical data on the frequency of treatment failure due to drug resistance [268].

While a patient is on suppressive HAART, the rate at which a drug-resistant mutation from the latent reservoir becomes active and generates a persistent resistant strain is

$$r_{DRM} = aP_{mutant}P_{survive} \tag{2.1}$$

where a is the rate at which infected cells exit the latent reservoir, P_{mutant} is the probability that a randomly selected latently infected cell carries a resistance mutation, and $P_{survive}$ is the probability that a resistance mutation, once in the actively replicating population, survives drift and establishes a persistent lineage during drug treatment.

A patient on fully suppressive HAART still has approximately 3000 cells in the actively infected population [93, 147, 296], all of which come from the latent reservoir. Since these cells have a lifespan of approximately one day [214], a can be estimated to be 3000 cells per

day.

If the latent reservoir is seeded by a pre-treatment population that has reached mutation-selection balance, then P_{mutant} can be estimated as u/s, where u is the rate at which a resistance mutation occurs during replication, and s is the selective disadvantage (fitness cost) of the mutation in the absence of treatment. The value of u for a single-nucleotide replacement varies from 2×10^{-7} to 6×10^{-5}, with a genome-wide average of 3×10^{-5} [3, 296]. The value of s also varies widely, from 0.05 to 0.9 [296, 304]. Note that, while u/s represents an average value, stochastic effects can cause P_{mutant} to vary over time and among patients, even taking zero values for many patients. In particular, a smaller pre-treatment effective population size would lead to a more dispersed P_{mutant} distribution.

The probability $P_{survive}$ depends on the population dynamics during treatment. Assuming that the wildtype (drug-susceptible) virus cannot replicate during treatment, only the description of mutant replication matters for calculating $P_{survive}$. The viral fitness, defined as the basic reproductive ratio R_0, is the expected number of offspring cells generated by a single mutant-infected cell during its lifetime[247]. For this simple model, we assume that R_0 is constant (that is, fluctuations in drug concentration are negligible). If this value is not too much greater than 1, then a second-order approximation can be used to estimate survival probability [106, 268]:

$$P_{survive} \approx \frac{2(R_0 - 1)}{\sigma^2} \tag{2.2}$$

where σ^2 is the variance in expected number of offspring for the drug-resistant mutant during treatment. This parameter is higher for "winner-take-all" types of infection dynamics. In the limit that $\sigma^2 \to 0$, $P_{survive}$ approaches either 0 or 1, and this approximation does not hold. To see more concretely how σ^2 relates to a possible scenario involving reproductive skew: if a single infected cell may either die or give rise to k many offspring cells in a single timestep, then $\sigma^2 = R_0(k - R_0)$.

Combining the three factors, the rate at which drug-resistance emerges is

$$r_{DRM} \approx \frac{2au(R_0 - 1)}{s\sigma^2}. \tag{2.3}$$

Note that this rate does *not* depend upon the infection population size, except insofar as the parameter a depends on the size of the latent reservoir. Estimates of the pre-treatment N_e [52, 297] are not relevant to understanding the expected value of r_{DRM}, though they can explain inter-patient variation in this rate.

The composite quantity a/σ^2 may be thought of as an ersatz "effective reservoir exit rate" analogous to an effective population size. It is, roughly, the number of cells activating from the latent reservoir each day that are relevant to the future infection dynamics during treatment. Using resistance data from a 3-year clinical study to parameterize the expression for r_{DRM} [213], a study estimated a/σ^2 to be only 5 cells per day [268], which (using $a = 3000$) implies an enormous variance $a/\sigma^2 \approx 600$. This result could be achieved, e.g., with $R_0 \approx 2$ and reproductive skew (as defined above) of $k \approx 300$. In that case, the vast majority of resistant mutants do not reproduce, but 0.7% give rise to 300 or more offspring. This extreme state of affairs is plausible if the host environment is heterogeneous, and in addition to being resistant, an infected cell must find itself in a replication-permissive locale in order to have any offspring at all. Three important sources of this heterogeneity are discussed in the main text: temporal variation in drug concentrations, spatial variation in drug concentrations, and spatial variation in target cell density.

2.5 Appendix

2.5.1 Deriving viral fitness values for Figure 2.3

Wildtype viral fitness (described by the basic reproductive ratio, R_0) varies with drug concentration according to a dose-response curve, with $R_0(D) = R_0(0)/(1 + (D/IC_{50})^m)$. Drug resistant virus sustains a fitness cost s and obeys an altered dose response curve with

altered IC_{50} and slope given by

$$R_{mut} = \frac{R_0(1-s)}{1+\left(\frac{D}{\rho IC_{50}}\right)^{m(1+\sigma)}} \tag{2.4}$$

After a single dose of drug is taken, drug concentration falls exponentially over time with a rate determined by the half-life T: $D(t) = C_{max}2^{t/T}$. In the CSF, if drug levels are only a fraction α of the plasma level, then viral fitness here is given by $R_{CSF}(D) = R_0(\alpha D)$. If a fraction f of infectable cells are susceptible to a direct cell-to-cell (or other high multiplicity-of-infection) process, in which MOI infectious units enter a cell at once when the drug is absent, then viral fitness is given by:

$$R_{c2c}(D) = (1-f)R_0(D) + fR_0(0)\frac{1-e^{-MOIR_0(D)/R_0(0)}}{1-e^{-MOI}} \tag{2.5}$$

If direct cell-to-cell transmission can occur in the CSF, then viral fitness is then given by $R_{c2c-CSF}(D) = R_{c2c}(\alpha D)$.

Parameters were used for the drug efavirenz (an NNRTI) and the K103N mutation: $R_0(0) = 10$, $IC_50 = 0.0035\mu M$, slope$(m) = 1.69$, $C_{max} = 12.9\mu M$, half-life $(T) = 35.8$ hours, $\rho = 85$, σ = -0.17, $s = 0.3$ [296, 304, 319] . For the hypothetical double mutant, $\rho \to \rho^2$, $(1+\sigma) \to (1+\sigma)^2$ and $(1-s) \to (1-s)^2$. For the hypothetical compensatory mutation alone, $s = 0.45$ and $\rho = 1$ and $\sigma = 0$. For the compensatory mutation along with K103N, $s = 0.15$, $\rho = 85$ and σ = - 0.17. We assumed that in the CSF, the drug concentration was reduced to a fraction $\alpha = 0.5\%$ of plasma values [36] and that f= 10% of cells were susceptible to direct cell-to-cell infection with an $MOI = 100$ [324].

2.6 Acknowledgements

We are grateful for support from the National Science Foundation/National Institutes of Health joint program in mathematical biology (M.A.N., A.L.H.), the Bill & Melinda Gates

Foundation (M.A.N., A.L.H.), a National Science Foundation Graduate Research Fellowship (D.I.S.R.), the John Templeton Foundation (M.A.N.), and J. Epstein (M.A.N.). We thank Pleuni Pennings, Alal Eran, Alireza Rabi, and two anonymous reviewers for helpful comments with the manuscript.

2.7 Manuscript Information

2.7.1 Previously published as

A related version of this manuscript appeared in [144]:

A. L. Hill, D. I. S. Rosenbloom, and M. A. Nowak. Evolutionary dynamics of HIV at multiple spatial and temporal scales. *Journal of Molecular Medicine*, 90(5):543–561, May 2012. ISSN 0946-2716. doi: 10.1007/s00109-012-0892-1. URL http://www.springerlink.com/content/l4511r1091r86672/abstract/

2.7.2 The author's contribution

Conducted the literature review and wrote the paper: ALH. Contributed sections on evolution of mutation rates, ancestry of HIV and SIV, recombination, effective population size, and cell-to-cell transmission: DISR. Designed and analyzed the models: ALH DISR. Conceived of the paper: ALH MAN.

3

Antretroviral dynamics determines HIV evolution and predicts treatment outcomes

3.1 Abstract

Despite the high inhibition of viral replication achieved by current anti-HIV drugs, many patients fail treatment, often with emergence of drug-resistant virus. Clinical observations show that the relationship between adherence and likelihood of resistance differs dramatically among drug classes. We developed a mathematical model that explains these observations and predicts treatment outcomes. Our model incorporates drug properties, fitness differences between susceptible and resistant strains, mutations and adherence. We show that antiviral activity falls quickly for drugs with sharp dose-response curves and short half-lives, such as boosted protease inhibitors, limiting the time during which resistance can be selected for. We find that poor adherence to such drugs causes treatment failure via growth of susceptible virus, explaining puzzling clinical observations. Furthermore, our model predicts that certain single-pill combination therapies can prevent resistance regardless of patient adherence. Our approach represents a first step for

simulating clinical trials of untested anti-HIV regimens and may help in the selection of new drug regimens for investigation.

3.2 Introduction

The prognosis of HIV infection has dramatically improved since the introduction of highly active antiretroviral therapy (HAART), which, when successful, can bring viral loads below the detection limit, improve immune function and prevent progression to AIDS[260]. Although a complete understanding of how virologic, pharmacologic and host factors interact to determine therapeutic outcome is still lacking, it is clear that a major obstacle to successful treatment is suboptimal drug adherence. Non-adherence can lead to virologic failure and the emergence of drug resistance[121, 132, 210, 357].

Because of their high antiviral activity, protease inhibitors are crucial in HIV-1 treatment and are used in three of the five recommended initial regimens and many salvage regimens[253]. Clinical trials have shown that for many drug combinations involving protease inhibitors, treatment failure occurs without resistance mutations in the viral gene encoding protease[19, 137, 278, 343], though mutations conferring resistance to other drugs in the regimen are often found. It is generally believed that combination therapy works because it is unlikely that multiple mutations conferring resistance to all drugs in the combination will appear in the same viral genome. Thus, failure without protease inhibitor resistance is puzzling, because it seems to contradict this fundamental explanation for the success of HAART. It is commonly believed that protease inhibitors have a higher 'barrier to resistance' than other drugs, meaning that clinically significant protease inhibitor resistance requires the accumulation of multiple mutations in the protease gene[80]. Protease inhibitor resistance also typically occurs at a narrower range of adherence levels than resistance to other drug classes[121, 177]. Although these concepts are suggestive, no theory has been developed to explain why patients fail protease inhibitor-based regimens without protease inhibitor resistance.

A resistance mutation may exist before treatment in the latent or active viral populations or may arise during treatment[239]. Drug resistance develops clinically if the mutant strain is selected for over the wild-type strain. Selection depends on the fitness costs and benefits of the mutation, as well as on drug levels, which vary with the dosing interval, the drug half-life and the patient's adherence. Here we use a modeling approach to integrate these factors, enabling us to determine when a resistance mutation will be selected and to predict the outcome of therapy with different drugs. Our results explain the unique adherence-resistance relationship for protease inhibitors and show why patients fail protease inhibitor-based therapy without protease inhibitor resistance.

3.3 Results

3.3.1 Defining the mutant selection window

Antiretroviral drugs reduce viral fitness in a dose-dependent manner (Fig. 3.1a). Viral fitness can be summarized as a single parameter, the basic reproductive ratio R_0, which encompasses all phases of the viral life-cycle [247] (Supplementary Methods, §4.1). The Hill dose-response curve describes the relationship between drug concentration and R_0:

$$R_0 = \frac{R_{00}}{1 + \left(\frac{D}{IC_{50}}\right)^m} \tag{3.1}$$

Here D is drug concentration, IC_{50} is the concentration at which 50% inhibition occurs, and m is a parameter determining steepness of the curve [66, 319]. The numerator R_{00} is baseline fitness in the absence of treatment.

A drug-resistant mutant is any viral variant that is less inhibited than the wild type for some drug concentration, described by the altered dose-response curve that determines

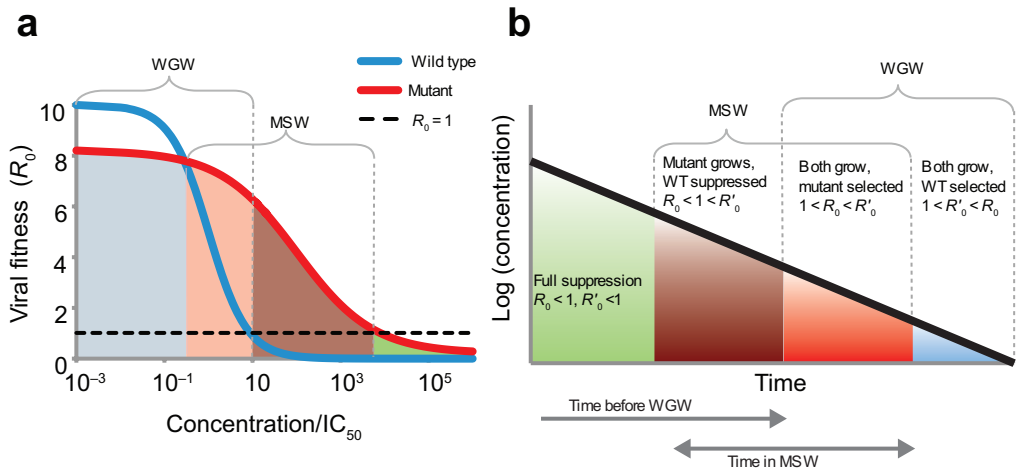

Figure 3.1: Drug concentrations determine the relative fitness of the wild-type virus and a resistant mutant. (a) The fitness of the wild-type virus (R_0, blue line) decreases with increasing drug concentration (here shown normalized by wild-type IC_{50}), following equation (1). A drug-resistant strain (R'_0, red line) is less fit than the wild type at low concentrations but more fit at higher concentrations, owing to an increased IC_{50} or a reduced slope. The MSW is the range of concentrations where a resistant mutant, if present, will grow faster than the wild type and still has $R'_0 > 1$. The WGW is the range of low concentrations where the wild type has $R_0 > 1$, leading to treatment failure without the need for resistance. For drug concentrations in the overlapping range of these windows, virologic failure can occur even without resistance but will be hastened by the appearance of a faster-growing mutant. (b) As drug concentrations decay after the last dose is taken, the viral fitness passes through four different selection ranges. Depending on the drug, dose level and mutation, not all of these ranges may exist. The time spent in each selection window is also determined by the drug half-life. WT, wild type.

viral fitness R_0':

$$R_0' = \frac{R_{00}(1-s)}{1+\left(\frac{D}{\rho IC_{50}}\right)^{m(1+\sigma)}} \tag{3.2}$$

Mutations have a fitness cost, meaning that the drug-free fitness of the mutant virus is reduced by a fraction s ($0 < s < 1$). In the presence of the drug, the mutation confers a benefit, multiplying the IC_{50} by a factor ρ (the fold change in IC_{50}, $\rho > 1$). Many mutations also reduce the slope (m) of the dose-response curve by a fraction $\sigma < 0$ [304].

Virologic failure occurs when treatment fails to prevent the growth of virus to high levels. A viral strain grows when $R_0 > 1$. The strain with highest R_0 outcompetes others[247]. The range of drug concentrations where a resistant mutant can cause virologic failure is called the mutant selection window (MSW)[96, 97]. Above the MSW, even replication of the mutant is suppressed ($R_0'(D) < 1$), although toxicity may prevent these drug concentrations from being achieved clinically. We here define the wild-type growth window (WGW), where drug concentrations are so low that wild-type virus is not adequately suppressed and failure can occur even without resistance ($R_0(D) > 1$).

3.3.2 The MSW explains therapy outcome patterns

To predict how well each drug suppresses growth of resistant and susceptible strains, we computed the time during a treatment interruption that a patient spends in the MSW and WGW. During treatment interruption, both R_0 and R_0' increase. Up to four selection ranges can be identified (Fig. 3.1b). Using pharmacokinetic and pharmacodynamic data[304, 319](Suppl. Table 4.1), we determined the time spent in these ranges for 66 drug-mutation pairs (Fig. 3.2a) on the basis of their specific dose-response curves (Fig. 3.2b-e). For each pair, we determined how soon after the most recent dose the mutant or wild-type virus starts to grow. This quantity is shorter than the expected time until virologic failure, which requires plasma HIV RNA to reach detectable levels and may also

depend on the time until mutant virus appears. We examined here only single-point mutations that are fully characterized by their effect on the dose-response curve (Eq. (3.2), Supplementary Tables 2-3). For this reason, we caution that our results may be over-optimistic, as virus with multiple resistance mutations often appears during infection. Use of our results for clinical recommendations is therefore premature. Below, we discuss extending the model to multiple mutations.

Successful treatment must both minimize the time spent in the MSW and delay entry into the WGW. These two goals are in tension, as shortening the time spent in the MSW (for example, by decreasing drug half-life) can also hasten entry into the WGW (Fig. 3.1b). Results from our model (Fig. 3.2a) suggest that non-nucleoside reverse-transcriptase inhibitors (NNRTIs) are protected against failure via wild-type virus due to their long half-lives but are vulnerable to mutation due to the time spent in the MSW. Protease inhibitors are at the opposite end of the spectrum, with little time spent in the MSW but rapid entry into the WGW. This behavior is caused by high slope parameters (extreme sensitivity to changes in concentration) and short half-lives. These results explain the unique trade-off presented by protease inhibitor therapy: greater protection against the evolution of resistance but vulnerability to wild-type-based virologic failure after short treatment interruptions. This feature is depicted schematically by plotting the drugs along a single axis, which measures the relative risk of mutant growth versus wild-type growth, independent of the overall risk of virologic failure (Fig. 3.2f and Suppl. Methods 4.1).

3.3.3 Simulation of clinical outcomes

Whereas the MSW and WGW concepts describe instantaneous growth of mutant and wild-type virus for a given drug concentration, virologic failure depends on sustained growth and, therefore, drug concentrations over time. To explain clinical observations

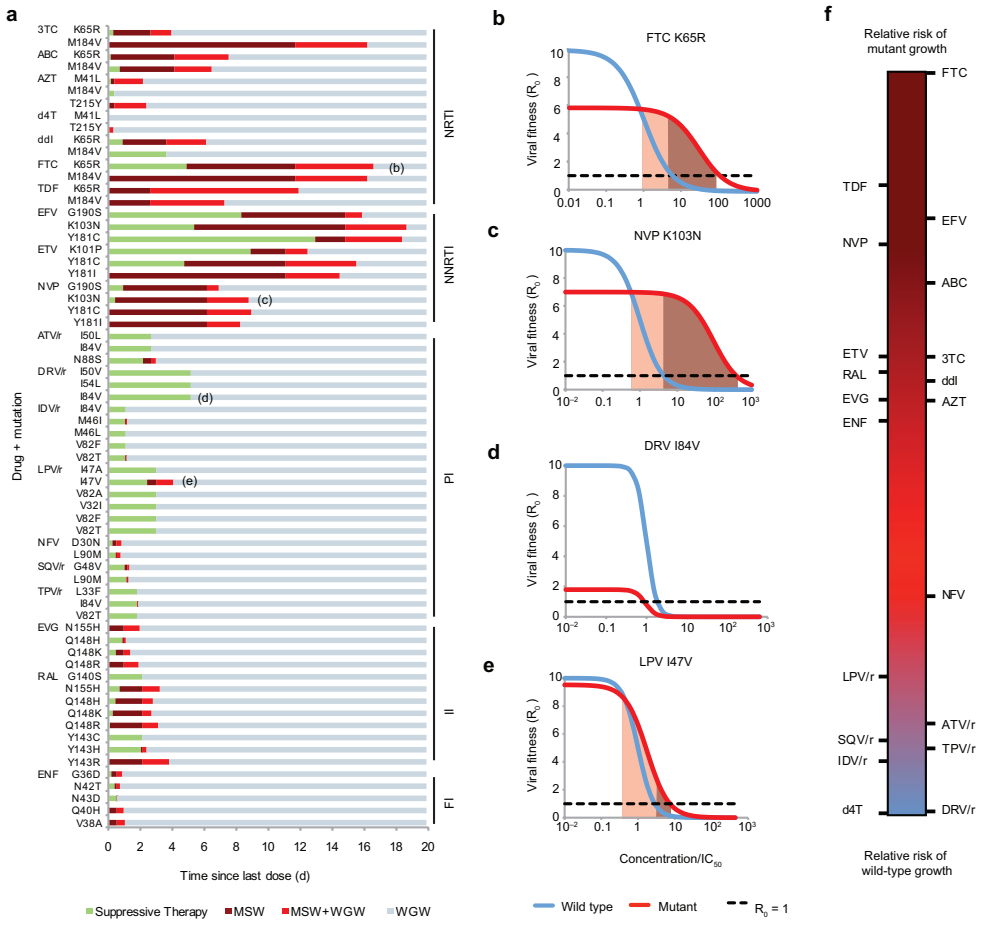

Figure 3.2: Selection windows can be calculated for particular drug-mutation pairs. (a) The distance to the right along each horizontal bar is the time since the last dose, and the color corresponds to the selection window during that time interval (described in Fig. 3.1b). (b-e) Examples of dose-response curves (showing drug concentration normalized by wild-type IC_{50}) for drug-mutation combinations indicated in a. Shading indicates the MSW. If the cost of a mutation is too high or its benefit (ρ or σ) too low, it is possible that the MSW does not exist. (f) Rank of each drug for relative risk of wild-type versus mutant virus growth, independent of the overall risk of therapy failure. For each drug, we show a 'synthetic', worst-case, single-nucleotide mutation (Suppl. Methods,§4.1, and Suppl. Fig. 4.12). PI, protease inhibitors; FI, fusion inhibitors; II, integrase inhibitors; ABC, abacavir; FTC, emtricitabine; ATV, atazanavir; TPV, tipranavir; EVG, elvitegravir; ENF, enfuvirtide. Protease inhibitors are often boosted (co-formulated) with ritonovir (/r), which interferes with breakdown in the liver and increases half-life.

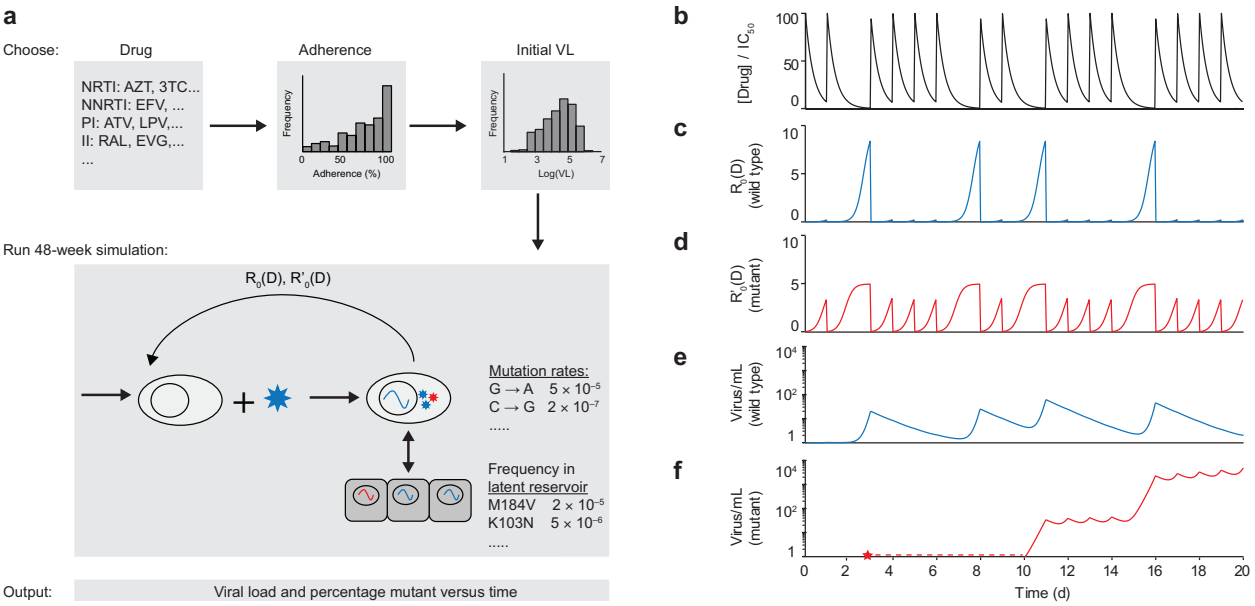

Figure 3.3: Schematic of algorithm for simulating viral dynamics in a patient undergoing treatment. (a) A single simulated patient takes a particular drug (or drug combination) with a designated adherence level, starting with an initial viral load (VL). Over a 48-week clinical trial, drug levels fluctuate and viral load levels are simulated according to a viral dynamics model. (b) Drug levels fluctuate according to patient s dosing pattern and pharmacokinetics (dose size, half-life, bioavailability); gaps show missed doses (figure shows single drug). (c) Wild-type viral fitness (R_0) fluctuates in response to drug concentration depending on the dose-response curve. (d) Fitness of drug-resistant strain (R_0') depends on an altered dose-response curve; at high drug concentrations, mutant fitness exceeds that of the wild type. (e) Wild-type viral load depends on viral dynamics equations, which account for active replication, exit from the latent reservoir and competition between strains. (f) A mutant virus may appear (red star) but be below the threshold for detection (dotted red line) before eventually leading to virologic failure.

across drug classes and adherence levels, we developed a stochastic model of viral evolution (Fig. 3.3 and Methods). Our model builds on the large body of previous work modeling HIV therapy [247, 294, 334, 358, 379] by integrating new data on class-specific drug properties[319] and realistic costs and benefits of mutations[304]. We also modified past approaches by allowing drug concentrations, and hence R_0, to fluctuate, rather than taking time-averages.

We first simulated 48-week trials of single agents in a cohort of patients. The results are presented in two ways: as outcome versus patient adherence at the trial endpoint (Fig. 3.4a) and as outcome versus time for a distribution of patient adherence levels (Fig. 3.4b,c).

Consistent with a previous meta-analysis of combination therapy clinical trials[23], our

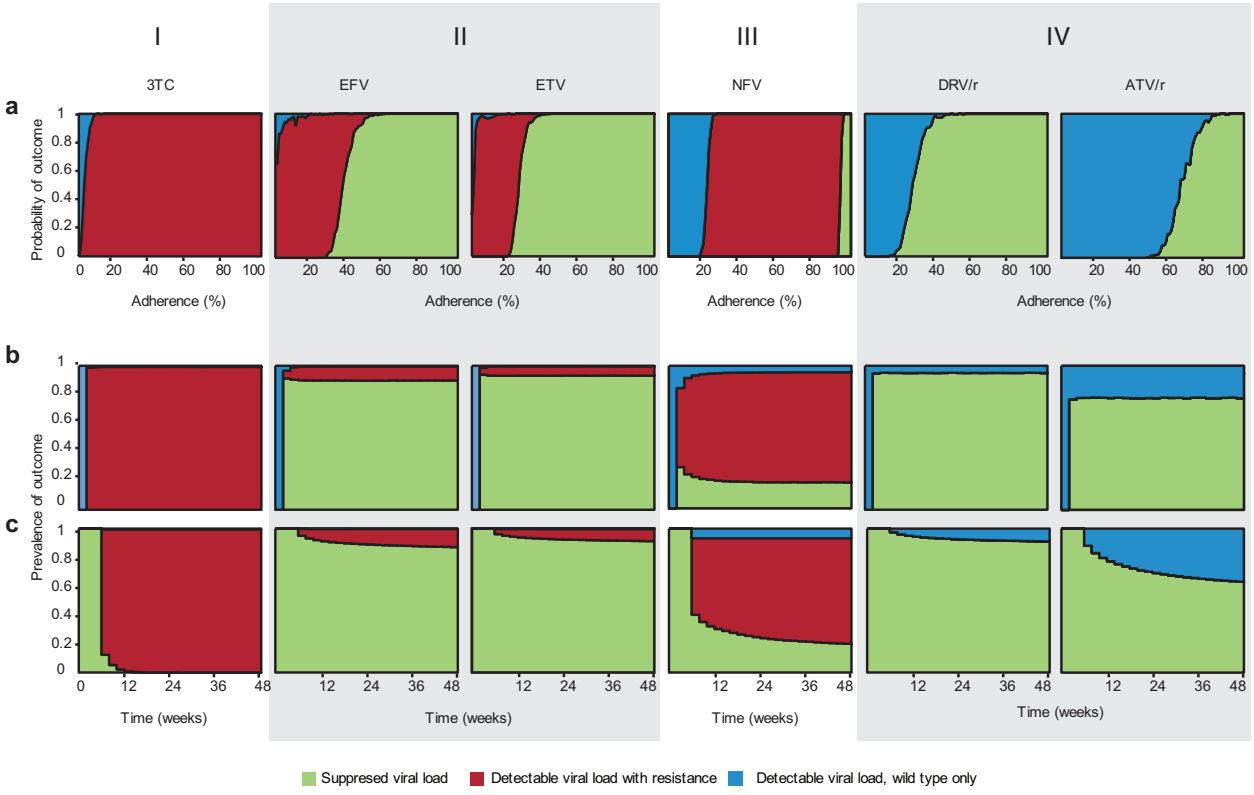

Figure 3.4: Outcomes for simulated patients in a clinical trial. (a-c) The height of the area shaded indicates probability of the corresponding outcome at a given adherence level (a) or time point (b,c). (a) Adherence is defined as the fraction of scheduled doses taken. These are maintenance trials (see Methods). (b,c) Measurements are taken every 2 weeks for simulated patients with a distribution of adherence levels (Suppl. Methods 4.1 and Suppl. Fig. 4.13b). (b) Suppression trials (see Methods). (c) Maintenance trials. (1) 3TC therapy (pattern includes AZT, ABC, d4T, ENF, EVG, FTC, NVP, RAL, TDF). (2) EFV and ETV therapy. (3) NFV therapy (pattern includes ddI). (4) DRV/r and ATV/r therapy (pattern includes ATV, TPV/r; variation on this pattern described in the Results includes LPV/r, SQV, SQV/r IDV, IDV/r).

model predicts that the level of adherence necessary for mutant virologic failure differs by drug class (Fig. 3.5). Specifically, for the NNRTIs efavirenz (EFV) and etravirine (ETV), the risk of mutant virologic failure is greatest at low adherence levels; for unboosted protease inhibitors, the risk peaks at a higher adherence level and remains substantial up to 100% adherence; for boosted protease inhibitors (paired with ritonavir to increase half-life), resistance occurs infrequently and at intermediate adherence levels. Researchers have previously argued that drug half-life and fitness costs of mutations are key factors explaining these general trends[121, 177]. By incorporating these factors as parameters, our model formalizes this argument.

In examining simulations of each drug individually (Suppl. Figs. 4.1-4.6), we found four qualitative patterns of outcome, which correspond closely-but not exactly-to drug class (Fig. 3.4).

For most nucleoside reverse-transcriptase inhibitors (NRTIs), the integrase inhibitors, the fusion inhibitor, and the NNRTI nevirapine (NVP), even perfect adherence led to mutant virologic failure in all simulated patients. As adherence declined, some wild-type virologic failure occurred. Virologic failure and resistance occurred soon after the trials started. These results are consistent with the notion that monotherapy often leads to rapid evolution of resistance.

For most protease inhibitors and the NNRTIs EFV and ETV, however, perfect adherence resulted in treatment success in simulations. Control of viral replication has been observed in a substantial fraction of patients in protease inhibitor monotherapy trials[270], but similar trials with EFV and ETV have not been carried out. In simulations, declining adherence affected performance of these two drug classes differently.

For the NNRTIs EFV and ETV, there was a large range of low-to-intermediate adherence for which mutant virologic failure was likely. Below this range, wild-type virologic failure became increasingly likely, whereas above this range the simulated patients succeeded. The size of this range is explained by the low fitness costs of drug-resistant

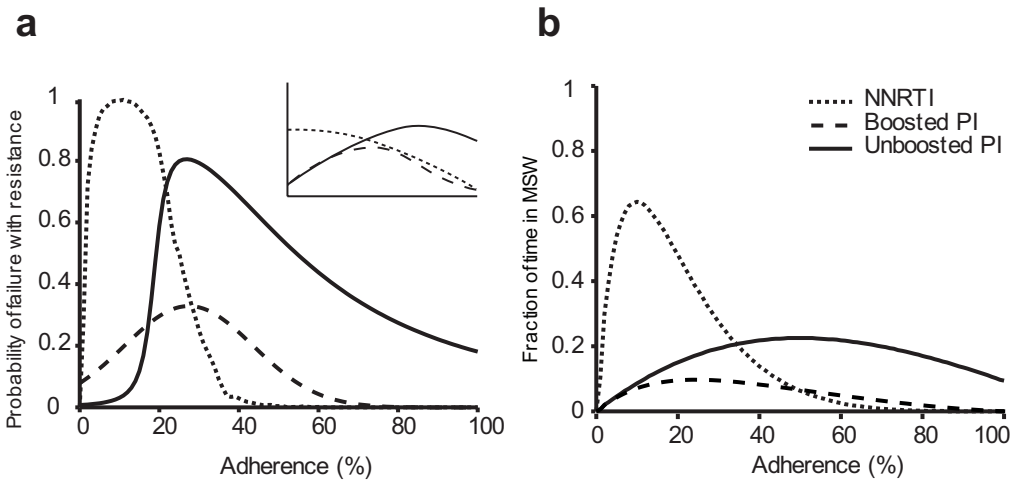

Figure 3.5: Our calculated adherence-resistance relations are in agreement with those observed in clinical trials. (a) Adherence versus simulated probability of resistance in a 48-week suppression trial for a protease inhibitor, a boosted protease inhibitor and an NNRTI. The inset shows a qualitative summary of results from a meta-analysis of clinical trials[23], which agrees with our simulations. (b) Adherence versus fraction of time spent in the MSW for the same drugs. Adherence-resistance trends demonstrate that time in MSW is a good proxy for the risk of mutant-based virologic failure. For both plots, curves were generated by averaging over all boosted protease inhibitors, all unboosted protease inhibitors, and the NNRTIs EFV and ETV. Protease inhibitor curves in a were fitted to skewed-T distributions to smooth step-like behavior. NVP, which was excluded from this figure, shows a different pattern from the other two NNRTIs; specifically, mutant virologic failure can occur even for perfect adherence (Suppl. Figs. 4.1 and 4.2).

mutations and long half-lives of NNRTIs, which allowed the patient to remain within the MSW for a substantial duration (suggested in [25]).

The protease inhibitor nelfinavir (NFV) and the NRTI didanosine (ddI) showed a large range of intermediate adherence leading to mutant virologic failure. Near-perfect adherence was required for treatment success. Under most clinical settings (adherence $< 95\%$), our model predicts that these drugs perform similarly to monotherapy with other NRTIs, typically leading to mutant virologic failure.

For many protease inhibitors, a decline from perfect adherence led abruptly from success to wild-type virologic failure, with little or no intermediate range for mutant virologic failure. This result explains the outcomes of clinical studies, which have shown that virologic failure in many boosted protease inhibitor-based regimens (including

monotherapy) does not require the evolution of resistance[19, 137, 343]. Variations on this pattern exist for some protease inhibitors: simulations of lopinavir (LPV/r), saquinavir (SQV, SQV/r), and indinavir (IDV, IDV/r) showed mutant virologic failure at low and moderate adherence levels, mainly for trials where initial viral load was high. Still, like all the protease inhibitors simulated except NFV, as adherence declined from the successful range, the first failing outcome observed was wild-type virologic failure (Suppl. Figs. 4.1 and 4.2).

We also examined the sensitivity of our results to changes in the baseline viral fitness, R_{00} (Suppl. Figs. 4.8 and 4.9). As the intracellular half-lives of several NRTIs are not definitively established, we tested a range of half-lives for lamivudine (3TC), azidothymidine (AZT), stavudine (d4T), ddI and tenofovir disoproxil fumarate (TDF) (Supplementary Fig. 10). Against a strain with higher R_{00}, higher adherence levels were required for treatment success, and there was a wider range of adherence levels for which mutant virologic failure occurred. The effect of increasing half-life was drug-dependent, but for most NRTIs simulated, it increased the likelihood of mutant virologic failure.

3.3.4 Explaining outcomes of combination therapy

Equipped with a model of drug interaction, we were able to extend the simulations to combination therapy (Suppl. Methods,§4.1 and Suppl. Fig. 4.11). For proof of concept, we use a two-drug combination of the boosted protease inhibitor darunavir (DRV/r) with the integrase inhibitor raltegravir (RAL). The combined effect of these two drugs is given by a Bliss-independent[41] interaction pattern[159], which describes drugs acting on different targets, therefore reducing viral replication multiplicatively. In a recent DRV/r-RAL clinical trial[343], patients experiencing virologic failure had their plasma viral population genotyped. Although 17% of patients tested positive for RAL-resistance mutations in the gene encoding integrase, no patients tested positive for DRV resistance in the gene encoding protease[343]. Our simulation is consistent with this study: treatment failure

occurred without DRV resistance (Fig. 3.6a).

RAL-resistant mutants were selected for only when the concentration of DRV/r was low and the concentration of RAL was moderate to high (Suppl. Fig. 4.11). This state of effective monotherapy ([25]) can occur if the drugs are administered as separate pills. If, however, dual therapy were administered as a combination pill, then the two concentrations would rise and fall roughly together, reducing the chance that they reach the discordant levels that select for resistance. Simulation of dual therapy as a single combination pill verified this hypothesis. However, this protection from resistance came at a cost: higher adherence was required to prevent wild-type virologic failure. For example, to ensure a 95% chance of success in the simulation, a patient taking separate pills must be 25% adherent to each pill (Fig. 3.6b), but 35% adherent to a combination pill (Fig. 3.6c). We expect this trend to apply to other drug combinations.

3.4 Discussion

Recent efforts to quantify pharmacodynamics [304, 319, 321], combined with insights into patients drug-taking behavior[24], have enabled us to develop what is to our knowledge the first explanatory model of virologic failure in agreement with clinical trials. All parameters in our model have direct physical interpretations, and their values were taken directly, or derived from, previous literature. The model was not fit or trained to match clinical data. Despite our model s simplicity, it can explain the clinically observed drug-class-specific relationship between adherence and outcome[23] (Fig. 3.5). Even without full viral dynamic simulations, a straightforward analysis of the mutant selection window can explain why certain drugs are more likely to select for resistance (Figs. 3.2f and 3.5b).

In addition, we address a long-standing mystery of antiretroviral therapy. Even when failure of protease inhibitor-based regimens is documented, mutations that confer resistance to the protease inhibitor appear infrequently[19, 137, 278, 343]. Although it is possible that mutations may occur outside the protease-encoding gene[87, 130, 238, 265]

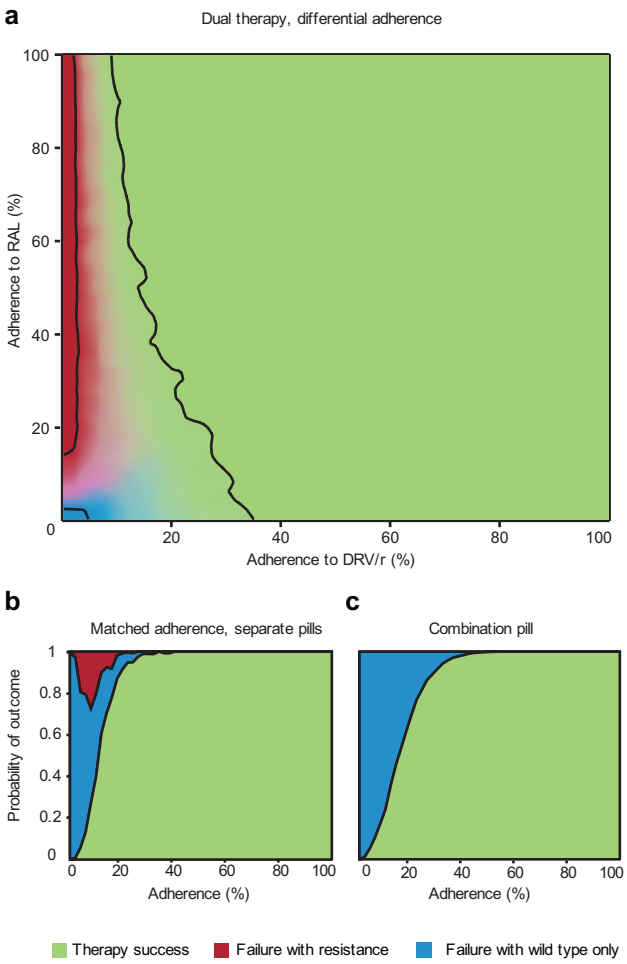

Figure 3.6: Outcomes of DRV/r plus RAL dual suppression therapy simulations, considering resistant mutants for both drugs. (a) Each drug is taken independently, and adherence may differ between them. The brightness of each color at a particular point indicates the probability of the corresponding outcome, with the black contours showing where each outcome occurs 95% of the time. Success depends largely on adherence to DRV/r (success is almost certain if adherence is >50%), whereas the type of failure is determined by adherence to RAL (resistance is almost certain if adherence is >30%). All failure via resistance is due to RAL mutant-based virologic failure. DRV mutant-based virologic failure (virologic failure) never occurs in the simulations. (b,c) Drugs are taken with equal average adherence. The height of the area shaded indicates probability of the corresponding outcome at that adherence level. (b) Drugs are taken as separate pills. Average adherence is the same, but pills are taken independently. (c) Drugs are packaged as a combination pill and are always taken together. Mutant virologic failure occurs only when the two drugs are given in separate pills; combination pills eliminate mutant virologic failure but increase the adherence required for near-certain success.

and escape routine detection, our model provides a more straightforward explanation: due to the sharp slope of protease inhibitor dose-response curves[319], even relatively strong protease inhibitor resistance mutations are selected only in a narrow range of drug concentrations. Moreover, as protease inhibitor concentrations decay rapidly compared to other drugs, they traverse this narrow range quickly, leaving little time for a resistant strain to grow before wild-type-based virologic failure. We predict that patients who fail protease inhibitor therapy with wild-type virus should be able to re-suppress the virus if the same drug is taken with improved adherence. A previous study[177] observed this outcome in patients who failed LPV/r without detectable resistance. Even with protease inhibitors that are more susceptible to resistance, only wild-type virus is detectable when adherence dips below the level guaranteeing success, providing an antiresistance 'buffer' that may warn clinicians of resistance risk. NFV is the sole exception to this pattern, owing to its having the lowest slope and second-highest IC_{50} of the protease inhibitors and consistent with its documented vulnerability to resistance[177].

The tradeoff between protection from resistant and susceptible strains occurs not only between drug classes but also between different formulations of the same drugs. We predict that a new combination pill containing DRV/r and RAL would not lead to resistance, even though the current separate-pill formulation does. This result suggests that some combination pills may be 'resistance proof', but their known benefit of increasing patient adherence must be weighed against the fact that they require higher adherence to prevent wild-type-based virologic failure. This tradeoff results from the possibility that a patient who is prescribed multiple pills may at times take only some of them[120], providing partial protection from the virus but allowing entry into a 'zone of monotherapy'[25] that can select for resistance.

We can extend our model to a broader range of combination therapies once interactions between drugs[159] are characterized; these interactions affect the evolution of resistance[223]. Our monotherapy results are a first step for examining how

pharmacokinetics and pharmacodynamics determine treatment outcomes. These results can inform innovations in lower-cost maintenance therapy among highly adherent patients, for whom monotherapy shows promise but also poses resistance risks[270]. Specifically, on the basis of our simulations, we propose that EFV and ETV monotherapy may be promising avenues for further study, despite the disheartening performance of monotherapy with the first approved NNRTI, NVP[64], and the ambiguous performance of ETV-based HAART for patients with resistance to the NRTI backbone[300].

Simulations that start with a high viral load (suppression phase) and simulations that start with an undetectable viral load (maintenance phase) generally showed similar outcomes; however, for several drugs, failure with resistance was more likely during the suppression phase. Such differences are often attributed to the presence of preexisting mutants when viral load is high[47, 165, 262, 330]. However, in our model, frequent reactivation from the latent reservoir provides a sufficient source of mutants during both phases (Suppl. Tables 4.4 and 4.5), and ongoing replication is an additional common cause of resistance (Suppl. Figs. 4.6 and 4.7). The key difference between the two phases is in how virologic failure is defined. As patients remained in suppression simulations until the predefined endpoint, wild-type growth sometimes preceded (and contributed to) growth of the mutant. More frequent measurement of viral load in maintenance simulations improved the chance that virologic failure was diagnosed before resistance reached detectable levels, consistent with clinical meta-analysis[129]. Also consistent with clinical observations[148], continuation of maintenance trials after rebound allowed the possibility of re-suppression, but it sometimes led to emergence of resistance (Suppl. Fig. 4.5).

It is difficult to quantitatively compare our simulations to clinical trials, as adherence is rarely precisely known. We suspect that our results are biased toward success for several reasons. First, we considered only single-point mutations, but strains with multiple mutations may lead to failure at higher adherence levels. Second, we considered neither correlations between consecutive missed doses nor variations in the time of day when a

dose is taken, both factors that lead to longer treatment interruptions and increase the chance of virologic failure [170, 207, 263, 264, 358]. Third, as is common in models of viral dynamics, we assumed that the virus population is homogeneous and well mixed. Actual infections may include subpopulations that grow faster (higher R_0, for example, owing to cell-to-cell transmission[324]) or that reside in tissues that drugs do not fully penetrate[178, 308, 356]. For example, the concentration of EFV in the cerebrospinal fluid is only 0.5% of plasma concentrations[36]. As our predictions rely on plasma drug concentrations, they may be optimistic in the case of EFV (see [144] for further discussion). In the absence of strong evidence for these effects, suboptimal adherence is the most likely cause of treatment failure. Given the above limitations, our modeling results should not be taken as clinical recommendations at this stage.

Patients experiencing virologic failure may not respond to a similar regimen in the future[145, 204, 263], but the precise reasons for this are not clear. The simplest explanation is that growth of a resistant strain during prior treatment makes it more likely this strain will exist in the future[46]. This explanation assumes that, in the absence of prior growth, most resistant mutants are relatively rare. If the diversity (effective population size) of the latent reservoir is not severely depleted over time, then our calculations contradict this assumption for single mutations: even in the absence of prior treatment, a majority of mutations exit the reservoir every few weeks. Resistance is then available to be selected regardless of prior growth. The occurrence of multiple mutations within the same viral genome is unlikely, however, without prior growth. To explain generally how prior virologic failure undermines future treatment, we need to model the long-term accumulation of multistep mutations in the viral population[249, 317]. To build such models, it will be important to understand interactions between mutations (including compensatory mutations[144]) and account for recombination[235].

We have emphasized here the variable nature of anti-HIV drug resistance. Common practice classifies a genotype as resistant if it is associated with virologic failure in a

meta-analysis of clinical outcomes; otherwise it is sensitive. This categorization is misleading: a mutation's ability to promote viral growth depends on all of the drugs in a regimen, adherence and the other mutations present. As standards of care evolve and study populations change, a mutation may gain or lose resistant status as a result of shifts in these confounding variables. Our model provides a rigorous alternative for evaluating resistance, by using mechanistic parameters to predict clinical outcomes. Our framework can help researchers prioritize drugs for clinical trials and select regimens for personalized HIV treatment.

3.5 Methods

3.5.1 Pharmacokinetics, pharmacodynamics and the mutant selection window

Viral fitness followed equation (3.1) with parameters R_{00}, IC_{50} and m. Fitness of resistant mutants followed equation (3.2) with parameters s, ρ and σ. (Suppl. Tables 4.1-4.3). Relative wild-type and mutant viral fitness values $R_0(D)/R_{00}$ and $R'_0(D)/R_{00}$ were measured using *in vitro* assays and were fit to Hill curves to determine the parameters IC_{50}, m, σ, ρ and s; these values were reported previously[304, 319]. We estimated absolute *in vivo* viral fitness in the absence of drugs (R_{00}) using measurements from previous studies (Suppl. Methods, §4.1). We modeled drug concentration as instantaneously increasing after a dose to the steady-state peak concentration (C_{max}) and then decaying exponentially (with half-life $T_{1/2}$) to the trough concentration (C_{min}) before the subsequent dose. When doses were missed (representing suboptimal adherence), the concentration continued to decay, and a subsequent dose increased the concentration by $\Delta C = C_{max} - C_{min}$.

We determined the bounds of the MSW by solving for D in $R_0(D) = R'_0(D)$ and $R'_0(D) = 1$. We determined the upper bound of the WGW by solving $R_0(D) = 1$. We computed the time after a single dose when a particular concentration D was reached by

solving for t in $D = C_{max}2^{-t/T_{1/2}}$.

The MSW concept as applied here to antiretroviral therapy was adapted from the extensive literature on antibiotic resistance. Both *in vitro* and *in vivo*, drug concentrations that fluctuate within the MSW lead to the development of resistance, but those outside it do not (reviewed in [97]). Although some studies of antibiotic-resistant *Escherichia coli* have found no upper limit to the MSW[383], no such results are known for antiretroviral resistance. The definition of the MSW most commonly used in antibiotic work is slightly different from the one we use, with the lower limit defined as $R_0(D) = 1$ because of experimental constraints[96]. We have chosen to modify this definition, as selection for the mutant can occur even at lower drug concentrations where $R_0(D) > 1$ [128]. The MSW and WGW can be described for each drug during combination therapy (Suppl. Methods, §4.1).

3.5.2 Simulation of the viral dynamics model.

Our model for HIV dynamics during antiretroviral drug treatment uses equations common in the literature[247]. These equations track the number of uninfected $CD4^+$cells, amount of free virus and number of infected $CD4^+$cells. A constant number of uninfected cells are produced each day, and they die at a constant rate. Cells are infected at a rate proportional to the number of uninfected cells, the amount of virus, and the viral fitness. Virion production from infected cells is described by the burst rate, and virions are cleared at a constant rate. Infected cells have a higher death rate than uninfected cells. Additionally, we include a population of long-lived infected cells in the latent reservoir, which activate at a constant daily rate regardless of viral fitness. Because we are interested only in viral dynamics during treatment and at the initial stages of failure, we have ignored the effects of the immune response. Viral fitness, and hence the rate of infection of new $CD4^+$cells, is determined by the baseline R_0 and the drug concentration. All equations and parameters are given in the Supplementary Methods (§4.1) and Supplementary Table 4.6. In the Supplementary Methods, we also derive a simplified form of HIV dynamics that

requires fewer parameters and only one state variable per viral strain; we used this simplified model to design our simulations. More detailed models that explicitly track multiple stages of the viral life cycle may more accurately reflect some short-term dynamics, such as lags in viral growth during acute infection or lags in viral decay during the early days of treatment[289, 312]. Summarizing viral fitness by a single parameter (R_0) smoothes out these dynamics.

There may be multiple strains of virus (wild-type and mutants) and consequently multiple types of infected cells. Even in the absence of drug, mutations will arise due to random errors in replication, though they will be selected against due to their fitness cost (s). Each mutation appears at a rate u that depends on the particular nucleotide changes required to effect the desired amino acid substitution (Supplementary Tables 4.2, 4.3, 4.7). The balance between these two processes results in all mutations being present in the population at an expected low level u/s, called mutation-selection equilibrium[247, 288]. We assume that the plasma virus population reaches this equilibrium in each patient before treatment (that is, that sufficient time has passed between initial infection and treatment initiation and that no prior treatment has selected for resistance to the particular drug being studied) and that the population in the latent reservoir is representative of the plasma population (Supplementary Tables 4.4 and 4.5). *De novo* mutations occur with a probability u during replication.

We used stochastic simulations to study the dynamics of the system described. Many mutations have been characterized for each drug, and to model a realistic worst-case scenario we considered a single synthetic mutant defined as having the highest benefits (ρ, negative σ), lowest cost (s), highest mutation rate and highest equilibrium frequency (due to mutation-selection balance) of all the single-nucleotide mutants known for that drug. Each monotherapy simulation therefore tracked only two strains, wild-type and mutant. For dual therapy, we considered three strains: wild-type, resistant to drug 1, and resistant to drug 2. Simulations modeled 48-week trials, using discrete time-steps of $\Delta t = 30$ min.

All simulations were done in Matlab R2010b. The full details of the algorithm for simulating a single patient are given in the Supplementary Methods(§4.1).

In maintenance trials, patients began with full viral suppression (2 RNA copies per ml, c ml^{-1}) and underwent monotherapy for 48 weeks or until virologic failure, whichever occurs first. Virologic failure is defined as 'confirmed rebound': two consecutive weekly measurements (starting at week 5) with viral load above 200 c ml^{-1}. In suppression trials, patients began with a realistic distribution of treatment-naive viral loads (between 3,000 and 10^6 c ml^{-1}) (Supplementary Fig. 4.13a) and underwent monotherapy for a full 48 weeks. We tracked measurements every 2 weeks. Virologic failure is defined as a viral load above 50 c ml^{-1}at week 48. In both types of trials, virologic failure is classified as with resistance if at least 20% of the viral population at the time of detection is mutant.

We simulated imperfect adherence by allowing each dose to be missed with a constant probability given by the expected adherence level parameter. In reporting outcomes versus time, we simulated patients with a distribution of adherence levels taken from a study using unannounced pill counts[24]. For simulations with two drugs, the value of adherence may be different for each drug, allowing for differential adherence, which has been observed in many studies[120]. Even when adherence to the two drugs has the same average value, the drugs can be simulated as two separate pills (allowing each pill to be taken or forgotten independently) or as a single combination pill (causing the two drug concentrations to rise and fall in lockstep).

3.6 Acknowledgements

We thank T. Antal, I. Božić, F. Fu, M. Sampah,and L. Shen for discussion during the conception of this work, and we thank J. Gallant, J.-B. Michel, P. Pennings, and three anonymous reviewers for their comments on the manuscript. We thank D. Bangsberg of Massachusetts General Hospital for supplying adherence data from the REACH study (supported by US National Institutes of Health grant R01 MH54907). Simulations were

run on the Odyssey cluster supported by the Research Computing Group of Harvard University. We are grateful for support from the US National Institutes of Health (R01 AI081600 (R.F.S., S.A.R.), R01 GM078986 (M.A.N., A.L.H.)), the Bill & Melinda Gates Foundation (M.A.N., A.L.H.), a Cancer Research Institute Fellowship (S.A.R.), a US National Science Foundation Graduate Research Fellowship (D.I.S.R.), the Howard Hughes Medical Institute (R.F.S., S.A.R.), a Canadian Natural Sciences and Engineering Research Council Post-Graduate Scholarship (A.L.H.), the John Templeton Foundation (M.A.N.) and J. Epstein (M.A.N.).

3.7 Manuscript Information

3.7.1 Previously published as

This manuscript appeared in [296]:

D. I. S. Rosenbloom, A. L. Hill, S. A. Rabi, R. F. Siliciano, and M. A. Nowak. Antiretroviral dynamics determines HIV evolution and predicts therapy outcome. *Nature Medicine*, 18(9):1378–1385, 2012. ISSN 1078-8956. doi: 10.1038/nm.2892. URL http://www.nature.com/nm/journal/v18/n9/full/nm.2892.html

3.7.2 The author's contribution

The first three authors contributed equally to this work. Designed and analyzed the model: ALH, DISR, SAR. Wrote the paper: ALH, DISR, SAR. Conceived of the study: ALH, DISR, SAR, RFS, MAN.

4

Supplementary Information: Antiretroviral dynamics determines HIV evolution and predicts therapy outcome

4.1 Supplementary Methods

4.1.1 Viral dynamics model

The following system of equations models the dynamics of multiple strains ($i = 1, 2, \ldots, n$) of HIV in a patient:

$$\begin{aligned} \dot{x} &= \lambda - \sum_{i=1}^{n} \beta_i x v_i - d_x x \\ \dot{y_i} &= \beta_i x v_i + A_i - d_y y_i \\ \dot{v_i} &= k_i y_i - d_v v_i \end{aligned} \tag{4.1}$$

where state variables x, y_i, and v_i are the number of infectable CD4$^+$T-cells, the

number of actively infected cells of strain i, and the number of free virus particles of strain i, respectively. The number of latently infected cells is considered to be constant, as it doesn't decay significantly over the course of a clinical trial, and so latently infected cells of strain i activate at a constant rate A_i. Active cells produce virus at rate k_i and die at rate d_y, and virus is cleared at rate d_v. The infectivity parameter β_i determines the rate at which virus of strain i infects susceptible host cells. Host cell dynamics are determined by production rate λ and death rate d_x.

When $A_i = 0$ for a strain i, this model reduces to the traditional viral dynamics model[247]. For that model we can describe the *basic reproductive ratio*, which is defined as the number of new infections generated by a lone infected cell before it dies. Strain i will only have a positive growth rate and be capable of sustaining an infection if its basic reproductive ratio, $R_{0i} := \lambda\beta_i k_i / (d_x d_y d_v)$, is greater than 1. In the model we present here the latent reservoir provides a constant source of virus (A_i), which removes the threshold criteria for R_0, although this value still describes viral fitness and the amount of ongoing viral replication.

For a single strain, the unique non-negative steady-state solution to our model is

$$y_1 = \frac{\lambda}{2d_y R_{01}}\left[R_{01}\left(\frac{A_1}{\lambda}+1\right) - 1 + \sqrt{R_{01}^2\left(\frac{A_1}{\lambda}+1\right)^2 + 2R_{01}\left(\frac{A_1}{\lambda}-1\right)+1}\right] \tag{4.2}$$

In our model, for $R_{0i} > 1$, strain i grows to a high steady state that depends on availability of host cells and the abundance of other strains. There are several limiting cases that can be derived from equation (4.2). In the absence of other strains (or if $R_{0j} \ll 1$ for all $j \neq i$), and for small reactivation $A_i \ll \lambda$, strain i grows to the steady state $y_i \approx \tilde{Y}_i := \lambda\left(R_{0i} - 1\right) / \left(d_y R_{0i}\right)$. The value $\tilde{Y}_i$ is the setpoint viral load that is maintained by replication alone, without additional contribution from the latent reservoir. The residual active infection maintained by the latent reservoir in complete absence of viral

replication ($R_{0i} = 0$) is $\tilde{y}_{0i} := A_i/d_y$. For positive $R_{0i} < 1$, strain i reaches a low steady state $y_i \approx \tilde{y}_i := \tilde{y}_{0i}/(1 - R_{0i})$. Since anti-HIV drugs act by decreasing β_i and k_i, the value of R_{0i} is understood to depend on the current drug concentration(s).

To eliminate some of the model parameters and smooth the high-frequency fluctuations that may have little clinical impact over the course of a drug trial, we study a simplified version of the model in equation (4.1). We assume that v_i and x are at equilibrium relative to y_i. This allows us to derive a reduced n-dimensional model:

$$\dot{y}_i = A_i + d_y y_i \left[\frac{\lambda R_{0i}}{\lambda + \sum_{j=1}^{n} R_{0j} d_y y_j} - 1 \right] \tag{4.3}$$

When the total infection is small, the summation term vanishes, and $\dot{y}_i \approx A_i + d_y y_i (R_{0i} - 1)$. For $R_{0i} \ll 1$, nearly all of strain i is produced by exit from the reservoir; y_i therefore approaches a value near $\tilde{y}_{0i}$. As the total infection grows (assuming $R_{0i} > 1$ for one or more i), the fractional term approaches 1, describing saturation of the limiting resource, at which point new infection events are balanced precisely by death of infected cells and y_i approaches a value near $\tilde{Y}_i$. This reduced model has identical steady state values of virus and CD4$^+$cells as the full model, but smooths out fluctuations in infection size caused by the dynamics of total CD4$^+$cells. Because we focus on initial virologic failure, which occurs at relatively low viral loads, the fluctuations in CD4$^+$cell levels are minor, and the approximation captures the full dynamics (equation (4.1)) well.

We can account for mutation by including the mutation rate matrix Q, where Q_{ij} describes the probability that an infected cell of type j gives rise to one of type i:

$$\dot{y}_i = A_i + \frac{\lambda d_y \sum_{j=1}^{n} y_j R_{0j} Q_{ij}}{\lambda + \sum_{j=1}^{n} R_{0j} d_y y_j} - d_y y_i \tag{4.4}$$

4.1.2 Model parameters

The value of R_{0i} at each point in time depends on the baseline basic reproductive ratio ($R_{00} = 10$, see below), the current drug concentration(s), and parameters describing resistance of the strain, as described by equations 1 and 2 in the main text. The death rate of actively infected cells, d_y, is 1 per day [214]. Supplementary Table 4.6 summarizes the parameters used in the model.

4.1.2.1 Basic reproductive ratio

The basic reproductive ratio (R_0) combines various components of viral fitness into a single number. $R_0 > 1$ is required for the virus to have a positive growth rate and sustain an infection. The baseline R_0, which we denote R_{00}, is defined in the absence of drug and has been estimated in past studies by measuring the increase in viral load during the early days of acute infection or during planned treatment interruption. During the acute phase, before the CTL response develops, typical values for R_{00} are 10-20[205, 289]. After this initial phase, R_{00} declines to 2-5, with some outliers as high as 6-11 [89, 116, 154, 190, 279]. Based on these findings, we chose a value of R_{00}=10 to present our results. We also checked sensitivity to this parameter by using larger and smaller R_{00} values (Figures 4.8 -4.9).

We can also double-check that our value of R_{00} from the literature is consistent with an independent set of measurements. The growth rate of a mutant strain in the absence of drug is $R_{00} * (1 - s)$ (see equation 1 in the main text), where s is the reduction in the replication capacity of the mutant virus. If $R_{00} * (1 - s) > 1$, then a mutant strain will expand in the absence of drug. If this condition fails, then the mutant strain would never be detected at high abundance (ignoring secondary or compensatory mutations). Since all the resistance mutations that we study do occur clinically, we expect that $R_{00} > 1/(1 - s)$ should almost always hold. 95% of the mutations studied have $s < 0.9$, for which the positive growth condition is satisfied for the value $R_{00} = 10$.

To maintain consistency with the chosen value $R_{00} = 10$, we capped the cost of

mutations used in the viral dynamics simulation at $s = 0.9$, guaranteeing that no mutant's baseline R_0 would be less than 1. Values of s that are negative are also inappropriate for our model, as they imply that the resistant mutant is more fit than the wild type even in the absence of the drug, causing the mutant to be prevalent at baseline. Measurements of s that were close to 0 or negative were assumed to be caused by experimental error, and so we set these values to $s = 0.05$ to represent a small cost to these mutations.

4.1.2.2 Latent reservoir exit rate

Based on the following argument, we estimate the total reservoir exit rate $\sum_i A_i$ to be 3000 cells per day. The exit rate for a particular mutant strain is determined by multiplying by the equilibrium frequency of pre-existing mutants, u/s. (Our simulation treats each exit as an independent event; use of this modeling approach implicitly assumes that the reservoir was seeded by a large, diverse population, and that its diversity, or effective population size, is maintained over time.) Viral loads of around 2 RNA copies per mL are maintained in patients on maximally suppressive HAART [93]. The rate of exit from the reservoir must be enough to account for this residual viral load, since ongoing replication is negligible. This viral load corresponds to $\approx 3 \times 10^3$ plasma virions (for a 70 kg person with 3L plasma). It has been shown, for a wide range of viral loads, that the total number of infected cells in a patient is roughly equal to the number of plasma virions [147]. The infection size $\sum y_i \approx \left(\sum A_i\right)/d_y$ is therefore 3×10^3, implying a total reservoir exit rate of 3000 cells per day.

Alternately, we can estimate the number of infected cells by noting that total viral production (burst from infected cells) must balance total viral clearance (breakdown of free virus in lymphatic tissue). Using parameters previously established[91], free virus in lymph tissues is 100 times as abundant as virus in the extracellular fluid, and so would be about 1.5×10^6 virions (based on 15L ECF) for this example. This paper also determined that the ratio of viral burst size to viral clearance rate is typically 500 virions per cell (e.g., $k_i =$

10,000 virions per day per cell; $d_v = 20$ per day). These figures again imply an infection size of 3000 cells.

Our calculations also agree with the results of a model which examined the many years-long decay of the latent reservoir in HAART patients [311]. Although this model used different sources for parameter values, it is consistent with an exit rate of 3000 cells per day, as long as the reservoir is not significantly depleted.

4.1.2.3 Host cell production rate

For a single wild-type strain in the absence of drug, the model (equation (4.3)) provides $\lambda = \tilde{Y} d_y R_{00} / (R_{00} - 1)$, where $\tilde{Y}$ is the total number of infected cells at infection setpoint. As established above, this value is approximately equal to the number of plasma virions at setpoint. We considered setpoint viral loads from 3000 to 10^6 RNA copies per ml plasma, or 4.5×10^6 to 1.5×10^9 total plasma virions. These values give a range of 5×10^6 to 1.7×10^9 cells per day for λ.

4.1.2.4 Resistance mutation rates

The mutation rate matrix entry Q_{ij} describes the probability that strain j reproduces to create strain i. We include only single step mutations from the wild type ($j = 1$) to another strain i (at rate u_i) and ignore back-mutation. Therefore $Q_{i1} = u_i$ for $i > 1$, $Q_{1,1} = 1 - \sum_{k=2}^{n} u_k$, $Q_{ii} = 1$ for $i > 1$ and $Q_{ij} = 0$ for all other entries.

The overall mutation rate for HIV is 3×10^{-5} per base per replication cycle [212], and recent work has shown that the rate varies considerably depending on the specific base changes involved. The nucleotide mutation matrix used in this study was derived by normalizing mutation accumulation data from a study of HIV replication of lacZα reporter sequence [3]. The normalized data was then rescaled to convert from the lacZα base composition to the HIV consensus sequence base composition [191]. Specifically:

1. Define the variables:

- $u = 3 \times 10^{-5}$ is the average per-site mutation rate of HIV.
- s_{xy} is the total number of single-nucleotide substitutions from base x to base y, combining data from both the forward and reverse orientations of lacZα in Table 3A of Abram et al. [3].
- s_{x*} is the total number of single-nucleotide substitutions from base x to any other base.
- S is the total number of single-nucleotide substitutions overall.
- n_x and n'_x are the abundance of base x in the reporter sequence and in the HIV consensus sequence, respectively. N and N' are the lengths of the two sequences, respectively.
  - $n_T = 37$, $n_C = 56$, $n_A = 36$, $n_G = 45$; $N = 174$
  - $n'_T = 2163$, $n'_C = 1772$, $n'_A = 3411$, $n'_G = 2373$; $N' = 9719$

2. Calculate the relative mutability of each base x in the reporter sequence, $r_x = (s_{x*}/n_x) \,/\, (S/N)$. A value $r_x > 1$ indicates that base x is more mutable than the average, while $r_x < 1$ indicates the opposite.

3. The per-site mutation rates from all bases x, denoted u_{x*}, are assumed to be proportional to the relative mutabilities r_x. To compute the values u_{x*}, scale the relative mutabilities so that the sum $n'_T u_{T*} + n'_C u_{C*} + n'_A u_{A*} + n'_G u_{G*}$ equals $N'u$, the genomic mutation rate of HIV (about 0.3 substitutions per replication). The correct scaling factor is $u_{x*}/r_x = N'u \,/\, (\sum r_x n'_x)$.

4. To determine the individual rates u_{xy}, partition each value u_{x*} proportional to the substitutions counted in the reported sequence; that is, $u_{xy} = u_{x*}\,(s_{xy}/s_{x*})$.

Supplementary Table 4.7 gives the resulting per-site probability (u_{xy}) for each nucleotide substitution in a single round of viral replication.

Mutation rates were calculated only for those amino acid substitutions which could be achieved via a single nucleotide change. All drugs studied had at least one such substitution that conferred resistance. For each possible starting codon, the rate of substitution equals the sum of all rates of nucleotide substitutions that achieve the desired amino acid change. The mutation rate u then equals the average of rates for all possible starting codons, weighted by the probability of finding that codon (based on the HIV consensus sequence base composition) (used in Supplementary Tables 4.4, 4.5).

4.1.3 Simulation algorithm

We used stochastic simulations to study the dynamics of the system described in equation (4.3) with mutation. Multiple mutations have been characterized for each drug, and to model a realistic worst-case scenario, we considered a single "synthetic" mutant defined as having the highest benefits (ρ, negative σ), lowest cost (s), and highest mutation rate of all the single-nucleotide mutants known for that drug. Each monotherapy simulation therefore tracked only two strains, wild type y_1 and mutant y_2. Simulations modeled 48-week trials, using discrete timesteps of $\Delta t = 30$ minutes. All simulations were done in Matlab R2010b. The following steps describe the simulation for a single patient on monotherapy, with expected adherence value α:

1. Draw from the viral load setpoint distribution in Figure 4.13a. This setpoint is used to determine the value of the λ parameter, assuming that the patient has 3 L plasma.

    - In the suppression phase of therapy, the initial infection size is the setpoint, rounded to the nearest integer number of cells.
    - In the maintenance phase of therapy, the initial infection size is the fully-suppressed infection size $\sum y_i \approx \left(\sum A_i\right)/d_y = 2$ c.ml^{-1}(RNA copies per ml).

2. Assign each infected cell to the mutant population (y_2) with probability u/s; otherwise the cell is in the wild-type population (y_1).

3. Identify all scheduled doses for the entire trial. All scheduled doses are evenly spaced, with the first dose occurring at the beginning of the trial. The patient takes each scheduled dose with probability α.

    - Exception: in the maintenance phase, the patient is always assumed to take the first scheduled dose.

4. Calculate the drug concentration every timestep, as described in §3.5.

    - In the suppression phase, the initial drug concentration is zero.
    - In the maintenance phase, the initial drug concentration is C_{max}.

5. Calculate the basic reproductive ratios for the wild type and the mutant every timestep, as described in equations 1 and 2 of the main text and the §3.5.

6. For each timestep:

    (a) The number of infected cells of strain i to exit the reservoir is drawn from a Poisson distribution with mean value $A_i \Delta t$.

    (b) The number of newly infected cells generated by strain i is drawn from a Poisson distribution with mean value $d_y y_i \Delta t \left[\frac{\lambda R_{0i}}{\lambda + \sum_{j=1}^{n} R_{0j} d_y y_j} \right]$.

    (c) Each cell newly infected by the wild type enters the mutant population with probability u; otherwise it remains wild type. Cells infected by the mutant do not back-mutate.

    (d) Each infected cell dies with probability $1 - \exp(-d_y \Delta t)$.

7. Determining outcome at 48 weeks:

- In the suppression phase, the patient's status is observed at the end of the 48-week trial. If viral load is below 50 c.ml^{-1}, the trial is declared successful; otherwise virologic failure occurs.
- In the maintenance phase, the patient's status is observed each week for 48 weeks, beginning at Week 5. If any two consecutive observations show a viral load of at least 200 c.ml^{-1}, virologic failure occurs; otherwise the trial succeeds.
- A failed trial is considered a mutant-based failure if at least 20% of the viral population is mutant; otherwise it is considered a wild type-based failure.

8. Determining outcome over time:

    - Patient's status was evaluated every 2 weeks, for 48 weeks.
    - In the suppression phase, if viral load is below 50 c.ml^{-1} at the evaluation, the patient is classified as having "suppressed viral load;" otherwise the patient has "detectable viral load."
    - In the maintenance phase, the patient's viral load is measured each week for 48 weeks, beginning at Week 5. If any two consecutive measurements at or before the evaluation show a viral load of at least 200 c.ml^{-1}, the patient is declared to have "detectable viral load," and is then removed from the trial, retaining this classification for all future time-points. Otherwise, the patient is declared to have "suppressed viral load."
    - In the maintenance phase allowing recovery, the patient's viral load is measured as in the maintenance phase above. If viral load is at least 200 c.ml^{-1} both at the evaluation and at the immediately preceding measurement, the patient is declared to have "detectable viral load." Patients who were previously "detectable" remain in the trial and may re-suppress.
    - A measurement of "detectable viral load" is considered "via resistance" if at

least 20% of the viral population is mutant; otherwise it is considered to be "via wild type."

By using a well-mixed population and by assuming that the processes of reservoir exit, replication, and death are Poisson, this method implicitly sets the effective population size of the infection equal to the census size of infected cells. Population structure, selection on linked loci, and variations in burst size among infected cells are all mechanisms that could increase variance in viral offspring number, decreasing the effective population size [4, 113]. Estimating the relevant population size to use for a model of drug resistance is difficult, as most approaches define an effective population size only for neutral loci. Simply "plugging in" a population size derived from a model without selection would be misleading in this context [187], and in lieu of a more informed value, we simply use the census size. This approach likely overestimates probabilities of mutant emergence and underestimates variability among patients [144, 267].

For dual therapy, we consider three strains: wild type, resistant to Drug 1, resistant to Drug 2. The two drugs can be simulated as two separate pills (allowing each pill to be taken or forgotten independently) or as a single combination pill (forcing the two drug concentrations to rise and fall in lockstep). In the case of two separate pills, the value of α may be different for each drug, allowing for "differential adherence" – which has been observed in some studies [120].

4.1.4 Graphing outcome versus adherence

For each monotherapy, 25,250 patients were simulated, with expected adherence α ranging from 0 to 1 (roughly equal numbers of patients were simulated for each 1% increment, including 50 patients with $\alpha = 0$ and 50 patients with $\alpha = 1$). The x-axis measures the *ex post* adherence for patients — that is, the actual percentage of doses taken, which may differ from the expectation α. Results were plotted for overlapping 2% windows, centered every 1% between 0 and 1, as well as for the points 0 and 1 themselves.

Analysis of dual therapy with a combination pill was similar to that of monotherapy, but with 126,250 patients (including 250 patients with $\alpha = 0$ and 250 patients with $\alpha = 1$).

For dual therapy with separate pills, 169,000 patients were simulated, with expected adherences α_1, α_2 ranging from 0 to 1 (roughly equal numbers of patients were simulated for each 4% × 4% increment, including 25,000 patients on the border of the distribution where at least one α_i is equal to 0 or 1.) As with monotherapy, the axes measure *ex post* adherence. Results were plotted for overlapping 4% × 4% windows, centered every 2% between 0 and 1; points plotted on the border of the distribution show patients with at least one α_i exactly equal to 0 or 1.

Note that, for maintenance therapy, the axes do not include zero, as each patient is guaranteed to take the first dose (adherence is never zero).

4.1.5 Graphing outcome over time

Analysis was performed separately for each overlapping 2% adherence window, centered every 1% between 0 and 1, as well as for the points 0 and 1 themselves. The resulting graph shows a weighted average of these results, using the adherence distribution in Figure 4.13. Measurements were taken every two weeks, and the graphs show the proportion of the population with each outcome. As there is no censoring of data, the analysis is equivalent to the Kaplan-Meier method [168].

4.1.6 MSW for combination therapy

For calculations involving combination therapy (limited to two drugs in this paper), viral fitness is influenced by the dose-response curves of all drugs. DRV and RAL belong to different classes and have been shown to reduce fitness in a multiplicative (Bliss-independent) fashion, which is often expected for drugs acting on different targets [41, 159]. The equation describing viral fitness with two Bliss-independent drugs is given by:

$$R_0\left(D_1, D_2\right) = \frac{R_{00}}{\left(1 + \left(\frac{D_1}{IC_{50,1}}\right)^{m_1}\right)\left(1 + \left(\frac{D_2}{IC_{50,2}}\right)^{m_2}\right)} \tag{4.5}$$

where D_1, D_2 are the concentrations of each drug in the relevant compartment, $IC_{50,1}, IC_{50,2}$ are the concentrations at which 50% inhibition occurs, and m_1, m_2 are the slope parameters. The numerator R_{00} is the baseline basic reproductive ratio in the absence of drug treatment. Mutations that confer resistance to a given drug change the IC_{50}, slope and drug-free fitness similarly to the way described in equation 2 (main text).

For a two-drug combination where we assume that a viral strain may only be resistant to a single drug, there are now eight potential selection windows. Drug levels may be high enough for guaranteed treatment success; in the MSW for one or both drugs; in the overlapping region for one or both of the MSWs and the WGW, or strictly in the WGW. Figure 4.11 shows the possible windows for the RAL+DRV/r combination.

4.1.7 Derivation of Fig. 3.2f: comparing risk of wild type-based and mutant-based VF from selection window data

Figure 3.2f in the main text ranks drugs by the relative risk of mutant versus wild-type failure, regardless of the total risk of failure, based on the time spent in each selection window. The ranks are plotted along a line with values ranging from -1 (DRV/r and d4T, highest relative risk of wild-type failure) to 1 (FTC, the highest relative risk of mutant failure). This plot was constructed based on the data in Figure 3.2a in the main text. To

devise this scale, we let

$$\begin{aligned} x &= \text{time until entry into MSW (days) / time until entry into WGW (days)} \\ &= \text{ length of green bar / length of green + dark red bars,} \\ y &= \text{time spent in MSW (days)} \\ &= \text{length of both red bars.} \end{aligned} \tag{4.6}$$

If the drug immediately enters the WGW at day 0, or if it skips the MSW completely, then x is defined to be 1.

Then the scale value to be plotted, a, is calculated as

$$a = \frac{y}{y_{max}} - x \tag{4.7}$$

where $y_{max} \approx 16.5$ days, the maximum time that a drug spends in the MSW (obtained for FTC). Since both x and y/y_{max} range between 0 and 1, the scale ranges between -1 (failure via wild type only) and 1 (largest relative risk of resistance).

In this formula, x is a proxy for the rapidity of wild type-caused virologic failure ("wild-type risk") relative to mutant-caused virologic failure ("mutant risk"). When x is small, the MSW window is reached long before the WGW, meaning that "mutant risk" is high and "wild-type risk" is low. When x is high, the WGW is reached soon after the MSW, or without ever entering the MSW, and so "wild-type risk" is high and "mutant risk" is low. While x considers how quickly the infection can start to grow, it does not consider the length of time in the MSW. Even if the MSW begins as soon as a dose is taken (so that $x = 0$), one still needs to consider for how long the mutant strain is selected over the wild-type to determine whether mutant-based or wild type-based virologic failure is more likely to occur. Figure 4.12 shows a scatter plot of y versus x.

4.2 Supplementary Tables

Table 4.1: Pharmacokinetic and pharmacodynamic parameters for anti-HIV drugs used in the study[304]

Class	Drug	IC_{50} (μMol)	slope	C_{max} (μMol)	half-life (hrs)	dosing (d^{-1})
NRTI	3TC	0.0298	1.15	15.3	10.0	2
	ABC	0.0381	0.93	10.5	21.0	2
	AZT	0.1823	0.85	4.5	8.5	2
	d4T	0.5524	1.13	2.3	3.5	2
	ddI	0.1795	1.07	39.4	18.0	1
	FTC	0.0079	1.20	7.3	39.0	1
	TDF	0.0561	0.97	1.1	60.0	1
NNRTI	EFV	0.0035	1.69	12.9	35.8	1
	ETV	0.0050	1.75	1.6	41	2
	NVP	0.0490	1.49	25.2	21.5	1
PI	ATV	0.0150	2.90	3.3	6.5	1
	ATV/r	0.0150	2.90	6.3	8.6	1
	DRV/r	0.0265	3.55	14.8	15.0	2
	IDV	0.0550	4.5	10.9	1.8	3
	IDV/r	0.0550	4.5	12.5	3.5	2
	LPV/r	0.0380	2.1	15.6	9.9	2
	NFV	0.2360	1.88	5.1	4.0	3
	SQV	0.0550	3.74	3.1	4.3	3
	SQV/r	0.0550	3.74	7.9	4.3	2
	TPV/r	0.2500	2.55	77.6	6.0	2
II	EVG	0.0280	0.94	1.7	8.6	1
	RAL	0.0150	1.03	4.0	10.0	2
FI	ENF	0.0349	1.60	1.1	3.8	2

Table 4.2: Parameters for all single-point mutations considered in the study[304]

Class	Mutation	Cost (s)	u	Drug	ρ	σ
NRTI	K65R	0.41	1.1×10^{-5}	3TC	61	-0.19
				ABC	47	0.01
				ddI	20	-0.09
				FTC	29	-0.04
				TDF	43	0.00
	M184V	0.46	1.1×10^{-5}	3TC	963	-0.58
				ABC	9.5	-0.44
				AZT	0.28	-0.03
				ddI	9.5	-0.21
				FTC	1186	-0.49
				TDF	3.0	-0.27
	M41L	0.17	1.3×10^{-6}	AZT	2.2	0.07
				d4T	1.0	0.07
	T215Y	0.05	*	AZT	3.1	-0.34
				d4T	1.08	-0.12
NNRTI	G190S	0.79	2.2×10^{-5}	EFV	70	-0.40
				NVP	237	-0.34
	K101P	0.7	*	ETV	5.00	-0.27
	K103N	0.3	1.5×10^{-6}	EFV	85	-0.17
				NVP	94	-0.15
	Y181C	0.26	1.1×10^{-5}	EFV	2.6	-0.11
				ETV	11	-0.26
				NVP	234	-0.40
	Y181I	0.44	*	ETV	100	-0.37
				NVP	1309	-0.50

* Indicates mutation that requires two nucleotide changes;
mutation rate depends on prevalence of intermediate states.

Table 4.3: Parameters for all single-point mutations considered in the study (Cont'd)[304]

Class	Mutation	Cost (s)	u	Drug	ρ	σ
PI	D30N	0.27	5.5×10^{-5}	NFV	2.3	-0.29
	G48V	0.45	8.5×10^{-7}	SQV	2.0	-0.23
	I47A	0.9	*	LPV	5.8	-0.40
	I47V	0.05	1.1×10^{-5}	LPV	1.8	-0.29
	I50L	0.75	9.0×10^{-7}	ATV	1.2	-0.34
	I50V	0.93	1.1×10^{-5}	DRV	0.68	-0.07
	I54L	0.05	9.0×10^{-7}	DRV	0.98	-0.01
	I84V	0.82	1.1×10^{-5}	ATV	0.60	-0.34
				DRV	0.94	-0.01
				IDV	0.73	-0.39
				TPV	0.26	-0.39
	L33F	0.49	6.3×10^{-6}	TPV	1.4	0.02
	L90M	0.30	3.2×10^{-6}	NFV	1.5	0.01
				SQV	1.1	-0.28
	M46I	0.05	5.6×10^{-5}	IDV	1.0	-0.29
	M46L	0.05	1.3×10^{-6}	IDV	0.76	-0.24
	N88S	0.55	1.1×10^{-5}	ATV	3.1	-0.31
	V32I	0.09	4.1×10^{-5}	LPV	0.53	-0.16
	V82A	0.59	1.1×10^{-5}	LPV	1.03	-0.33
	V82F	0.79	3.4×10^{-7}	IDV	0.89	-0.58
				LPV	1.45	-0.44
	V82T	0.22	*	IDV	0.98	-0.34
				LPV	0.87	-0.17
				TPV	0.68	-0.20
II	G140S	0.71	2.2×10^{-5}	RAL	2.1	0.03
	N155H	0.55	5.3×10^{-7}	EVG	20	0.00
				RAL	27	0.02
	Q148H	0.73	2.0×10^{-6}	EVG	6.8	-0.04
				RAL	86	0.06
	Q148K	0.76	6.5×10^{-6}	EVG	19	0.03
				RAL	128	-0.06
	Q148R	0.61	1.1×10^{-5}	EVG	68	0.06
				RAL	90	0.04
	Y143C	0.74	1.1×10^{-5}	RAL	3.6	0.06
	Y143H	0.55	1.1×10^{-5}	RAL	2.7	-0.04
	Y143R	0.32	*	RAL	75	-0.01
FI	G36D	0.12	2.2×10^{-5}	ENF	1.7	-0.45
	N42T	0.54	5.3×10^{-7}	ENF	2.9	-0.13
	N43D	0.88	1.1×10^{-5}	ENF	13	-0.06
	Q40H	0.26	1.5×10^{-6}	ENF	12	-0.31
	V38A	0.17	1.1×10^{-5}	ENF	11	-0.32

* Indicates mutation that requires two nucleotide changes;
mutation rate depends on prevalence of intermediate states.

Table 4.4: Parameters for pre-existing frequency of mutations and exit rate from the latent reservoir. See §3.5 and §4.1 for explanations.

class	mutation	equilibrium frequency	reservoir exit (days)
NRTI	K65R	2.7×10^{-5}	12
	M184V	2.4×10^{-5}	14
	M41L	7.8×10^{-6}	43
	T215Y	*	*
NNRTI	G190S	2.8×10^{-5}	12
	K101P	*	*
	K103N	4.9×10^{-6}	68
	Y181C	4.3×10^{-5}	8
	Y181I	*	*
PI	D30N	2.0×10^{-4}	2
	G48V	1.9×10^{-6}	177
	I47A	*	*
	I47V	2.2×10^{-4}	2
	I50L	1.2×10^{-6}	279
	I50V	1.2×10^{-5}	28
	I54L	1.8×10^{-5}	19
	I84V	1.4×10^{-5}	25
	L33F	1.3×10^{-5}	26
	L90M	1.1×10^{-5}	31
	M46I	1.1×10^{-3}	< 0.5
	M46L	2.6×10^{-5}	13
	N88S	2.0×10^{-5}	17
	V32I	4.6×10^{-4}	1
	V82A	1.9×10^{-5}	18
	V82F	4.3×10^{-7}	769
	V82T	*	*
II	G140S	3.1×10^{-5}	11
	N155H	9.6×10^{-7}	349
	Q148H	2.0×10^{-6}	166
	Q148K	8.5×10^{-6}	39
	Q148R	1.8×10^{-5}	18
	Y143C	1.5×10^{-5}	22
	Y143H	2.0×10^{-5}	17
	Y143R	*	*
FI	G36D	1.8×10^{-4}	2
	N42T	9.8×10^{-7}	342
	N43D	1.3×10^{-5}	27
	Q40H	5.6×10^{-6}	59
	V38A	6.5×10^{-5}	5

* Indicates mutation that requires two nucleotide changes;
equilibrium frequency depends on prevalence of intermediate states.

Table 4.5: Parameters for pre-existing frequency and exit rate from the latent reservoir for best "synthetic" mutation for each drug. See §3.5 and §4.1 for explanations.

class	drug	equilibrium frequency	reservoir exit (days)
NRTI	AZT	2.4×10^{-5}	14
	d4T	7.8×10^{-6}	43
	3TC	2.7×10^{-5}	12
	FTC	2.7×10^{-5}	12
	ABC	2.7×10^{-5}	12
	ddI	2.7×10^{-5}	12
	TDF	2.7×10^{-5}	12
NNRTI	EFV	4.3×10^{-5}	8
	NVP	4.3×10^{-5}	8
	ETV	4.3×10^{-5}	8
PI	DRV	1.8×10^{-5}	19
	NFV	2.0×10^{-4}	2
	SQV	1.1×10^{-5}	31
	LPV	4.6×10^{-4}	1
	ATV	2.0×10^{-5}	17
	IDV	1.1×10^{-3}	< 0.5
	TPV	1.4×10^{-5}	25
II	RAL	3.1×10^{-5}	11
	EVG	1.8×10^{-5}	18
FI	ENF	1.8×10^{-4}	2

Table 4.6: Viral dynamics parameters in the absence of drug therapy

	Parameter	Value	Units	Reference
R_{00}	Baseline basic reproduction ratio	10	(unitless)	See text
d_y	Death rate of actively infected cells	1	d^{-1}	[214]
v_0	Residual plasma viral load maintained by activation from latent reservoir, absent viral replication	2	RNA copies per ml plasma	[93]
A	Latent reservoir exit rate	3000	cells.d^{-1}	Based on v_0, see text

Table 4.7: Nucleotide substitution rate parameters for HIV. Each entry gives the per-site transition probability from row base to column base in one round of viral replication. For derivation and source see Section 4.1.2.4. The extraordinary skew of this matrix (the largest entry, G-to-A mutation, is more than 300 times the smallest, C-to-G mutation) reflects the base composition of the genome, particularly the bias towards A. Values less than 10^{-6} are particularly uncertain, as they were computed from fewer than 5 substitution observations each.

	U	C	A	G
U		1.1×10^{-5}	1.3×10^{-5}	3.6×10^{-6}
C	2.4×10^{-5}		6.5×10^{-6}	1.7×10^{-7}
A	7.9×10^{-7}	5.3×10^{-7}		1.1×10^{-5}
G	8.5×10^{-7}	8.5×10^{-7}	5.5×10^{-5}	

4.3 Supplementary Figures

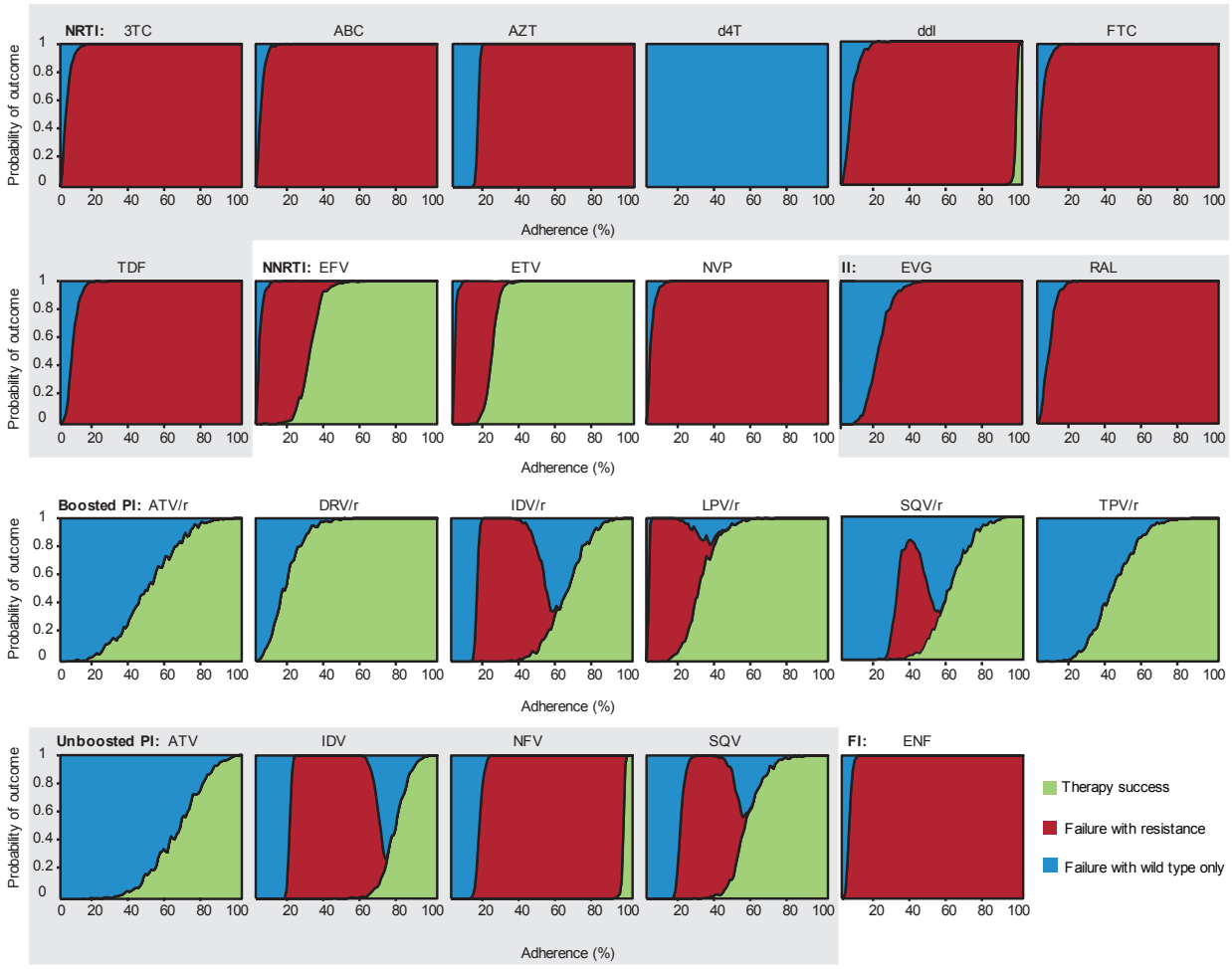

Figure 4.1: Simulated clinical outcomes versus adherence for all drugs. In "Suppression" trials, patients begin with a realistic distribution of treatment-naive viral loads (between 3000 and 10^6 c.ml^{-1}) and undergo monotherapy for a full 48 weeks. Virologic failure (VF) is defined as a viral load above 50 c.ml^{-1}at Week 48. VF is classified as "via resistance" if at least 20% of the viral population at the time of detection is mutant. Adherence (x-axis) is measured as the fraction of scheduled doses taken. The height of the area shaded indicates probability of the corresponding outcome at that adherence level. 3TC, lamivudine; ABC, abacavir; AZT, zidovudine; d4T, stavudine; ddI, didanosine, FTC, emtricitabine; TDF, tenofovir disoproxil fumarate; EFV, efavirenz; ETV, etravirine; NVP, nevirapine; ATV, atazanavir; DRV, darunavir; IDV, indinavir; LPV, lopinavir; NFV, nelfinavir; SQV, saquinavir; TPV, tipranavir; EVG, elvitegravir; RAL, raltegravir; ENF, enfuvirtide.

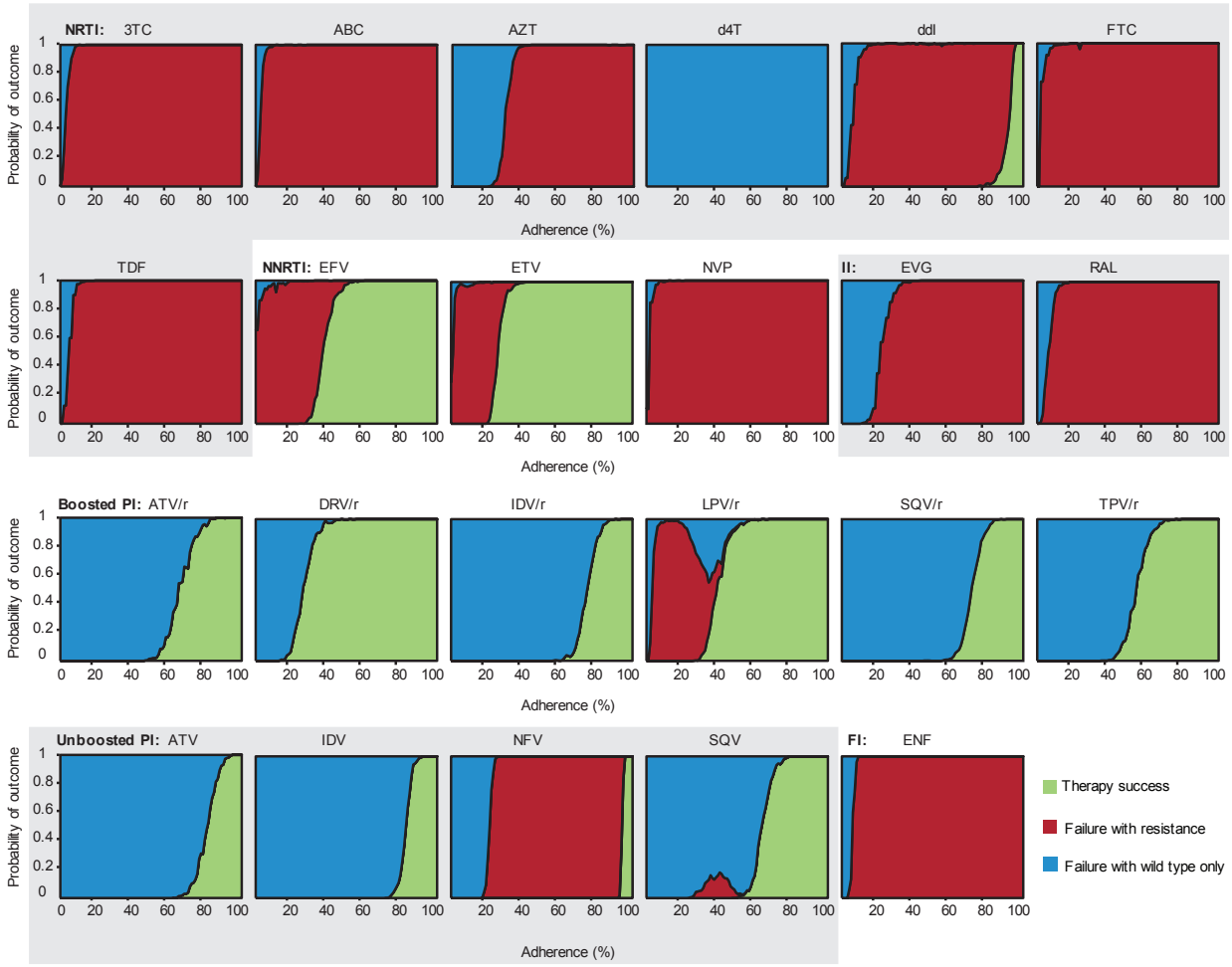

Figure 4.2: Simulated clinical outcomes versus adherence for all drugs. In "Maintenance" trials, patients begin with full viral suppression and undergo monotherapy for 48 weeks or until virologic failure (VF), whichever occurs first. VF is defined as "confirmed rebound": two consecutive weekly measurements (starting at week 5) with viral load above 200 c.ml^{-1}. VF is classified as "via resistance" if at least 20% of the viral population at the time of detection is mutant. Adherence (x-axis) is measured as the fraction of scheduled doses taken. The height of the area shaded indicates probability of the corresponding outcome at that adherence level.

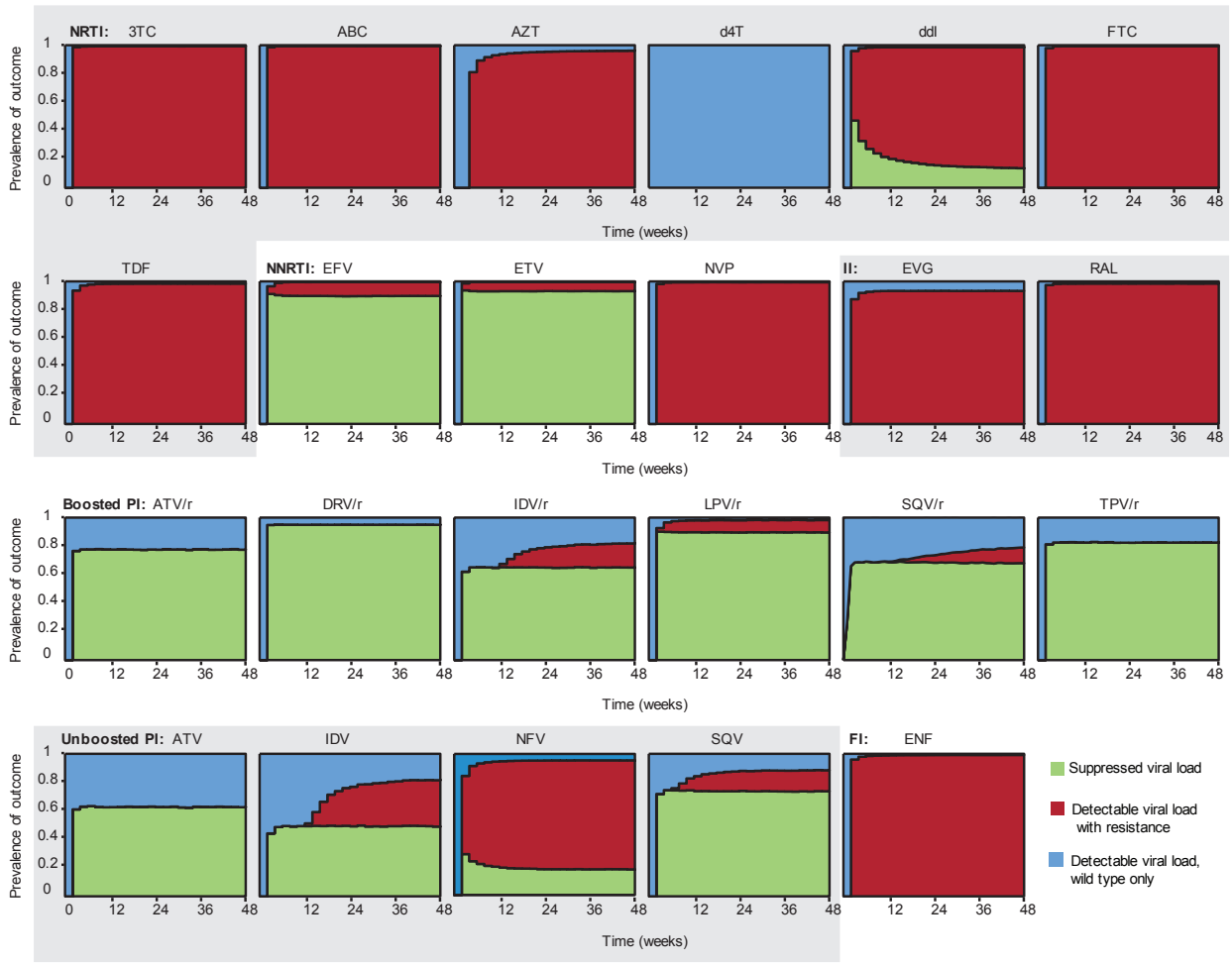

Figure 4.3: Simulated clinical outcomes versus time for all drugs. In "Suppression" trials, patients begin with a realistic distribution of treatment-naive viral loads (between 3000 and 10^6 c.ml^{-1}) and undergo monotherapy for a variable time (x-axis). "Detectable viral load" is defined as above 50 c.ml^{-1}and is classified as "via resistance" if at least 20% of the viral population at the time of detection is mutant. The height of the area shaded indicates prevalence of the corresponding outcome at that time. Patients have a realistic distribution of adherence levels with an average of 70%.

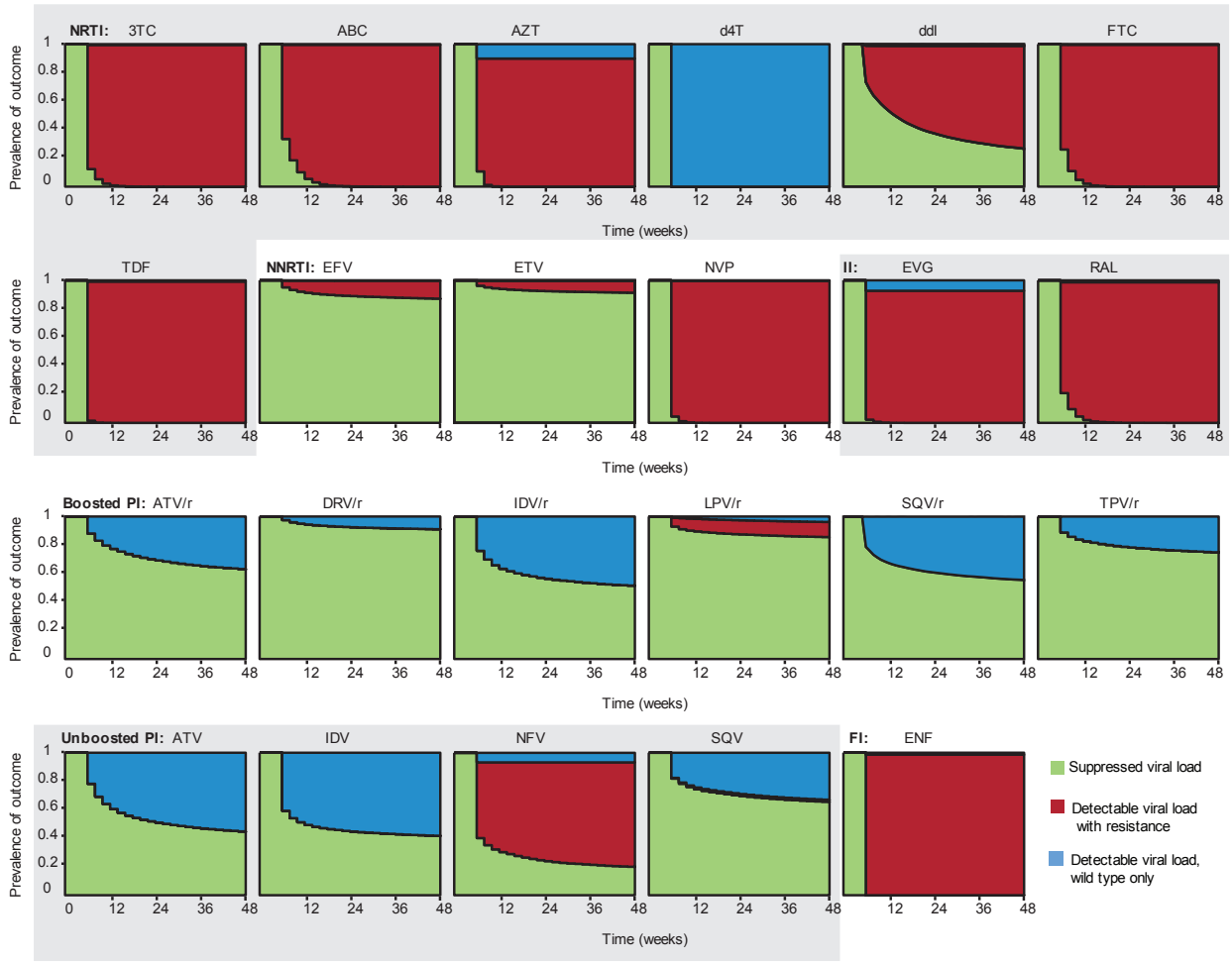

Figure 4.4: Simulated clinical outcomes versus time for all drugs. In "Maintenance" trials, patients begin the trial with full viral suppression and undergo monotherapy for a variable amount of time (x-axis) or until "detectable viral load" is observed, whichever occurs first. "Detectable viral load" is defined as "confirmed rebound": two consecutive weekly measurements (starting at Week 5) above 200 c.ml^{-1}. It is classified as "via resistance" if at least 20% of the viral population at the time of detection is mutant. The height of the area shaded indicates prevalence of the corresponding outcome at that time. Patients have a realistic distribution of adherence levels with an average of 70%.

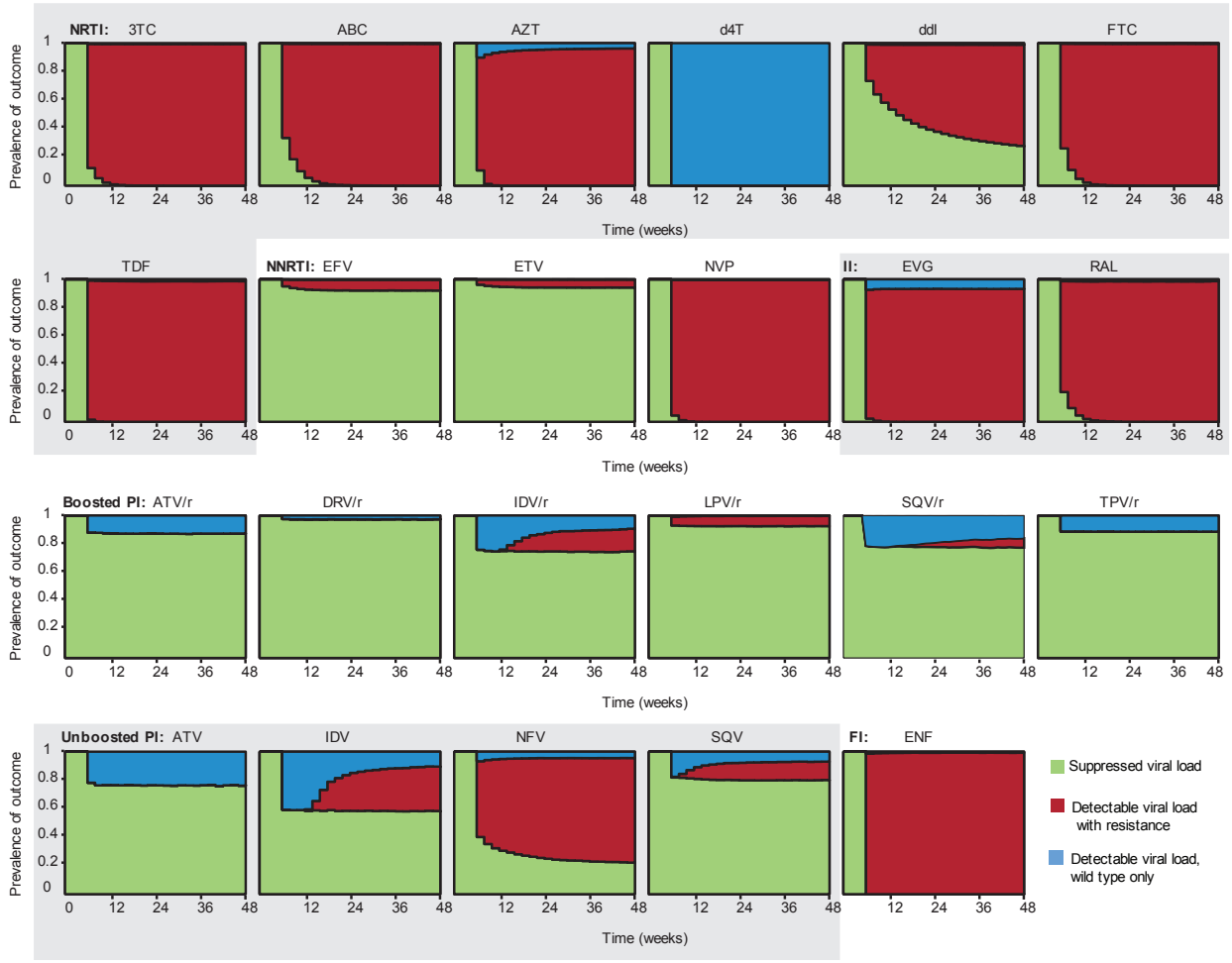

Figure 4.5: Simulated clinical outcomes versus time for all drugs. In "Maintenance with recovery" trials, patients begin the trial with full viral suppression and undergo monotherapy for a variable amount of time (x-axis). "Detectable viral load" is defined as "confirmed rebound": two consecutive weekly measurements (starting at Week 5) with viral load above 200 c.ml^{-1}. It is classified as "via resistance" if at least 20% of the viral population at the time of detection is mutant. We allow recovery, meaning that patients stay in the trial to see if they will re-suppress, instead of being removed immediately like in regular "Maintenance" trials. The height of the area shaded indicates prevalence of the corresponding outcome at that time-point. Patients have a realistic distribution of adherence levels with an average of 70%.

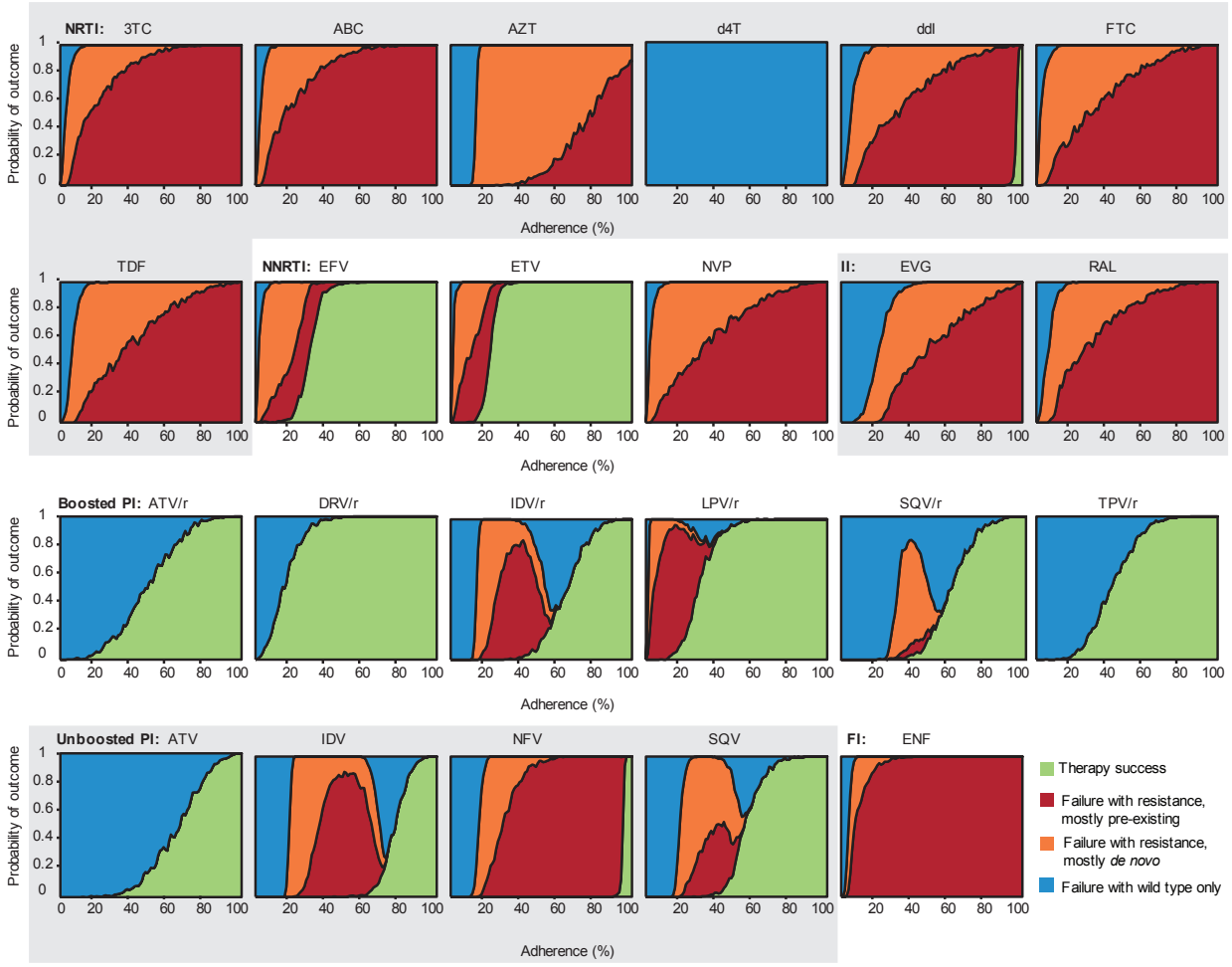

Figure 4.6: Simulated clinical outcomes versus adherence for all drugs, distinguishing pre-existing from *de novo* mutations. In the "Suppression" trials shown, patients begin with a realistic distribution of treatment-naive viral loads (between 3000 and 10^6 c.ml^{-1}) and undergo monotherapy for a full 48 weeks. Virologic failure (VF) is defined as a viral load above 50 c.ml^{-1}at Week 48. VF is classified as "via resistance" if at least 20% of the viral population at the time of detection is mutant. Resistance is classified as *de novo* if the majority of mutants at the time of failure descended from a mutation event that occurred during replication since the start of the trial. Otherwise, resistance is classified as "pre-existing," which includes mutants arising from both the pre-treatment plasma population and the latent reservoir. Adherence (x-axis) is measured as the fraction of scheduled doses taken. The height of the area shaded indicates probability of the corresponding outcome at that adherence level.

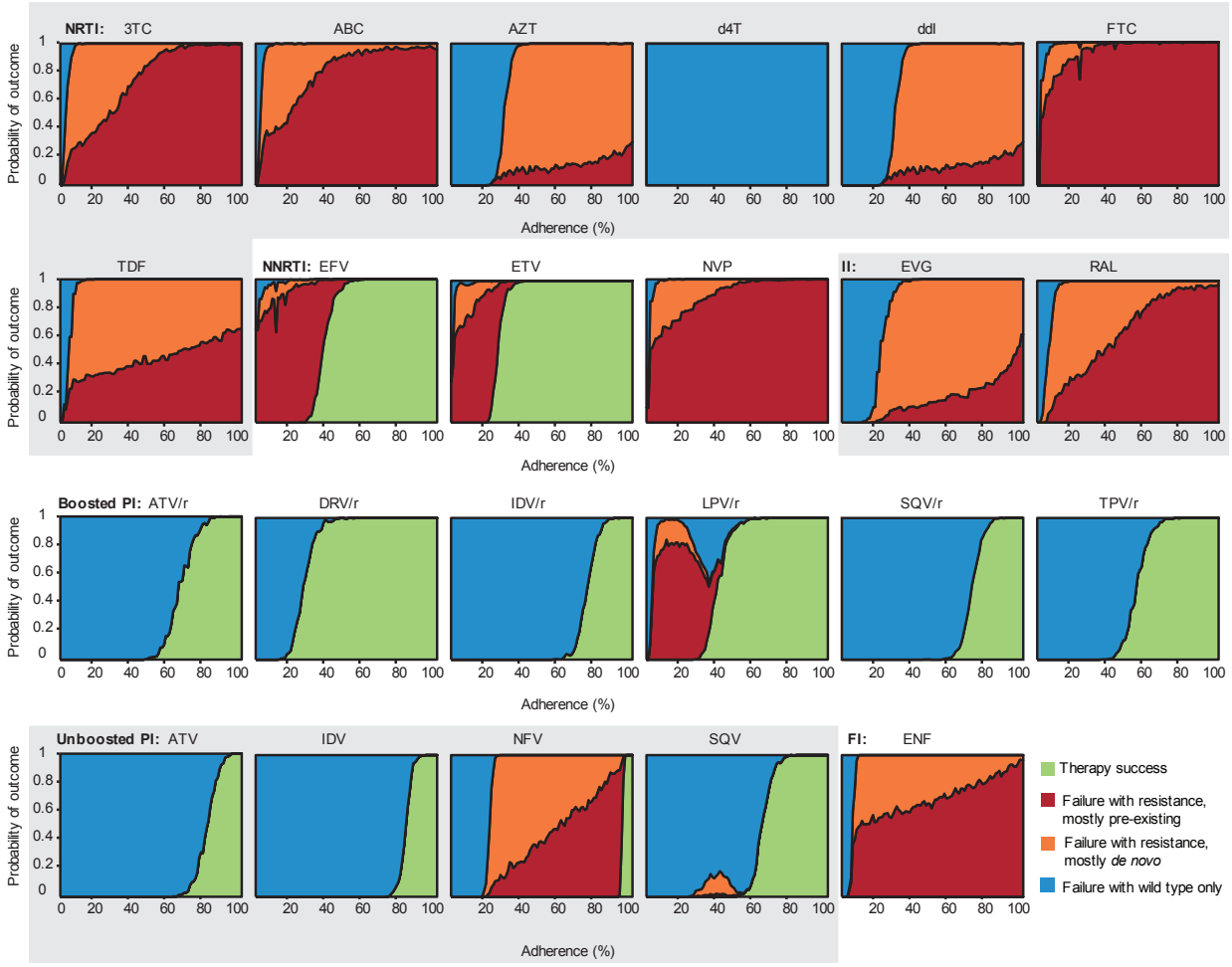

Figure 4.7: Simulated clinical outcomes versus adherence for all drugs, distinguishing pre-existing from *de novo* mutations. In the "Maintenance" trials shown, patients begin with full viral suppression and undergo monotherapy for 48 weeks or until virologic failure (VF), whichever occurs first. VF is defined as "confirmed rebound": two consecutive weekly measurements (starting at Week 5) with viral load above 200 c.ml^{-1}. VF is classified as "via resistance" if at least 20% of the viral population at the time of detection is mutant. Resistance is classified as *de novo* if the majority of mutants at the time of failure descended from a mutation event that occurred during replication since the start of the trial. Otherwise, resistance is classified as "pre-existing," which includes mutants arising from both the pre-treatment plasma population and the latent reservoir. Adherence (x-axis) is measured as the fraction of scheduled doses taken. The height of the area shaded indicates probability of the corresponding outcome at that adherence level.

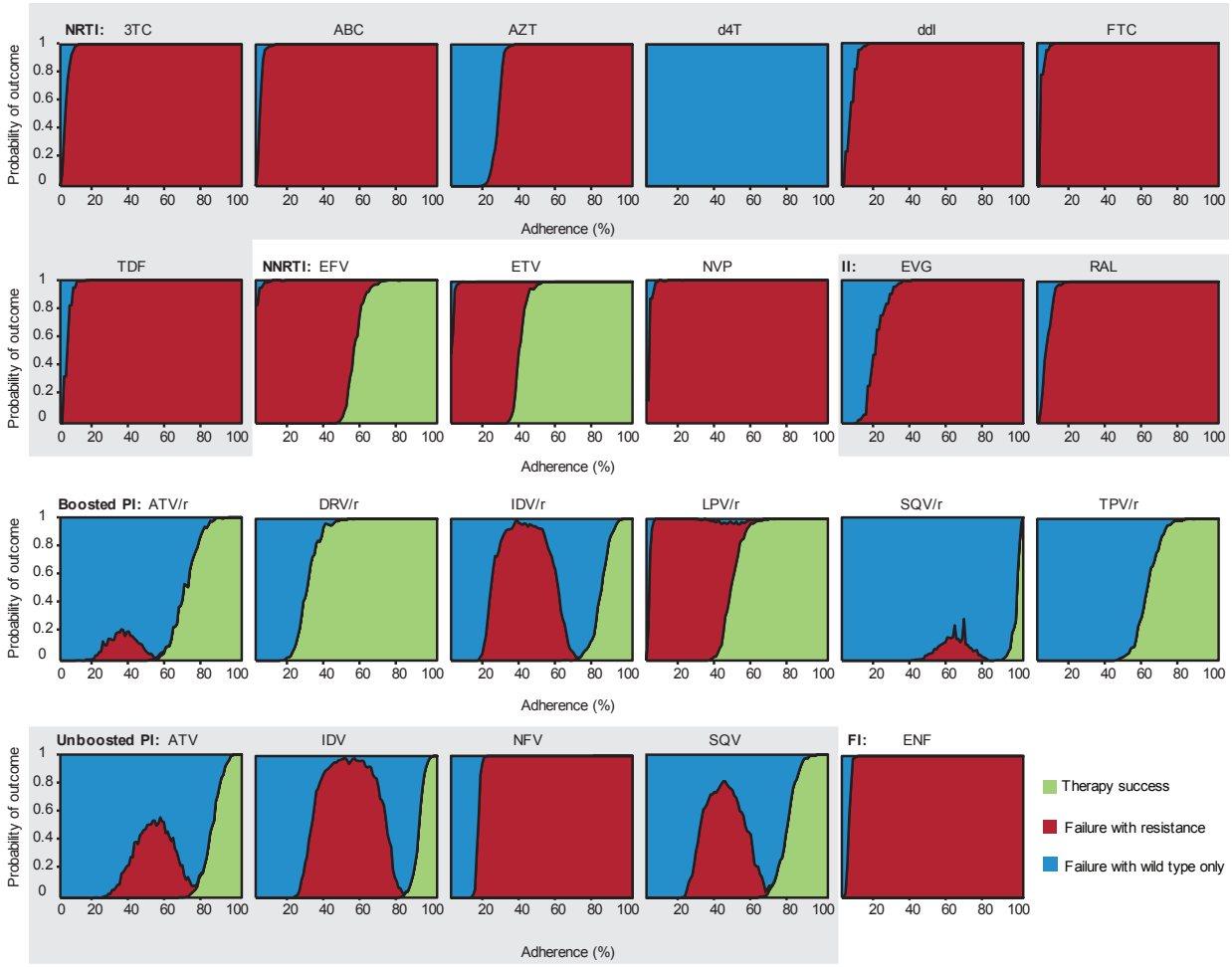

Figure 4.8: Simulated clinical outcomes versus adherence for all drugs, R_{00}=20. Results are shown for "Maintenance" trials only. In the "Maintenance" trials shown, patients begin with full viral suppression and undergo monotherapy for 48 weeks or until virologic failure (VF), whichever occurs first. VF is defined as "confirmed rebound": two consecutive weekly measurements (starting at Week 5) with viral load above 200 c.ml^{-1}. VF is classified as "via resistance" if at least 20% of the viral population at the time of detection is mutant. Adherence (x-axis) is measured as the fraction of scheduled doses taken. The height of the area shaded indicates probability of the corresponding outcome at that adherence level. As compared to R_{00}=10, increasing R_{00} to 20 leads to higher adherence levels being required for treatment success, and it extends the range of adherence levels (in both directions) for which resistant strains can cause failure. Mutant VF becomes a possible outcome for the PIs ATV, ATV/r, IDV, IDV/r, and SQV/r, and treatment success cannot occur at any adherence level for ddI and NFV.

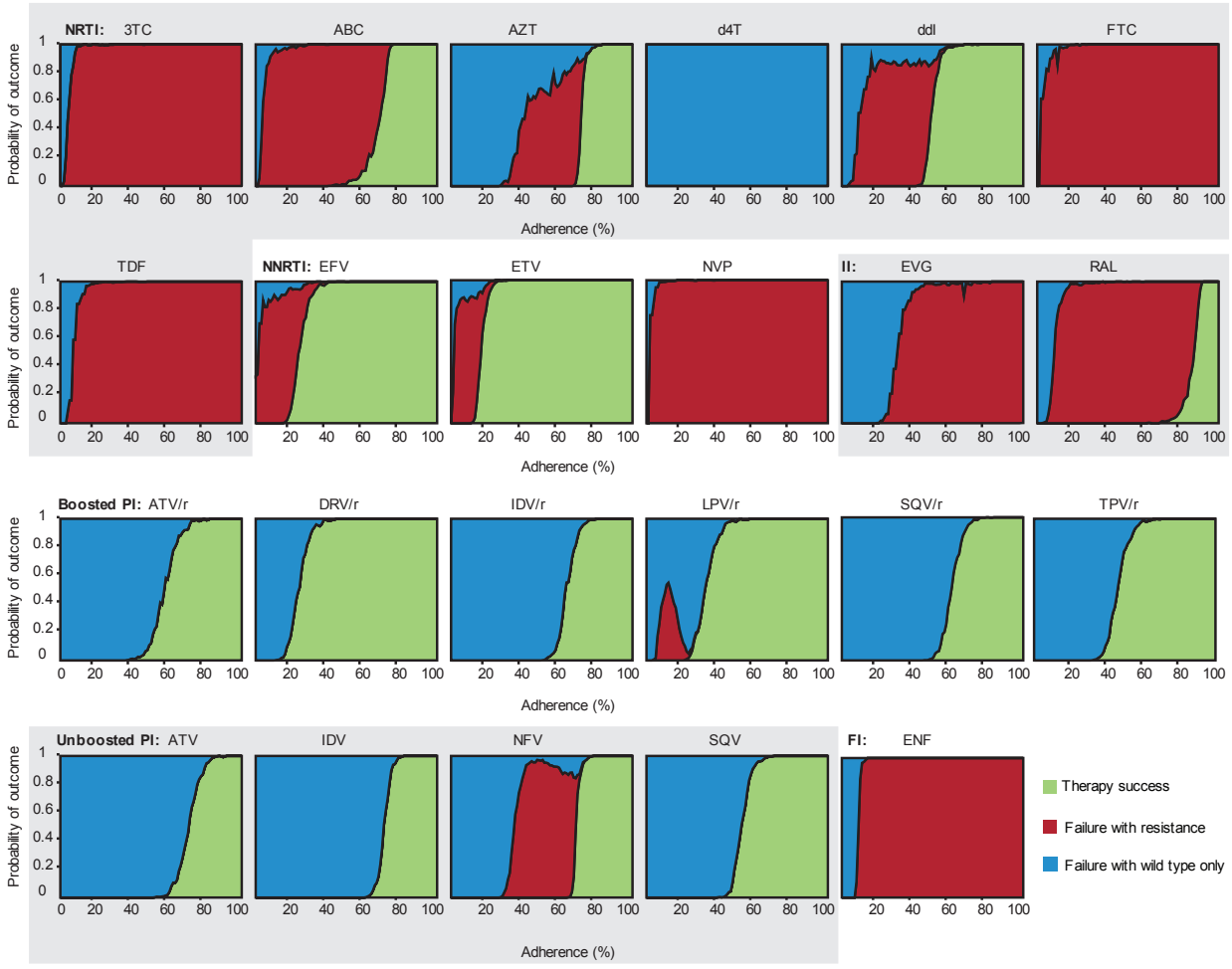

Figure 4.9: Simulated clinical outcomes versus adherence for all drugs, R_{00}=5. Results are shown for "Maintenance" trials only. In the "Maintenance" trials shown, patients begin with full viral suppression and undergo monotherapy for 48 weeks or until virologic failure (VF), whichever occurs first. VF is defined as "confirmed rebound": two consecutive weekly measurements (starting at Week 5) with viral load above 200 c.ml^{-1}. VF is classified as "via resistance" if at least 20% of the viral population at the time of detection is mutant. Adherence (x-axis) is measured as the fraction of scheduled doses taken. The height of the area shaded indicates probability of the corresponding outcome at that adherence level. As compared to R_{00}=10, decreasing R_{00} to 5 leads to lower adherence levels being required for treatment success, and it reduces the range of adherence levels for which resistant strains can cause failure. A range of high adherence levels appears where there is treatment success for ABC and AZT, and near-perfect adherence is no longer required for ddI and NFV success. Mutant VF no longer occurs for SQV, and for AZT and ddI, wild-type failure may be the first outcome to occur as adherence levels decrease from the successful range.

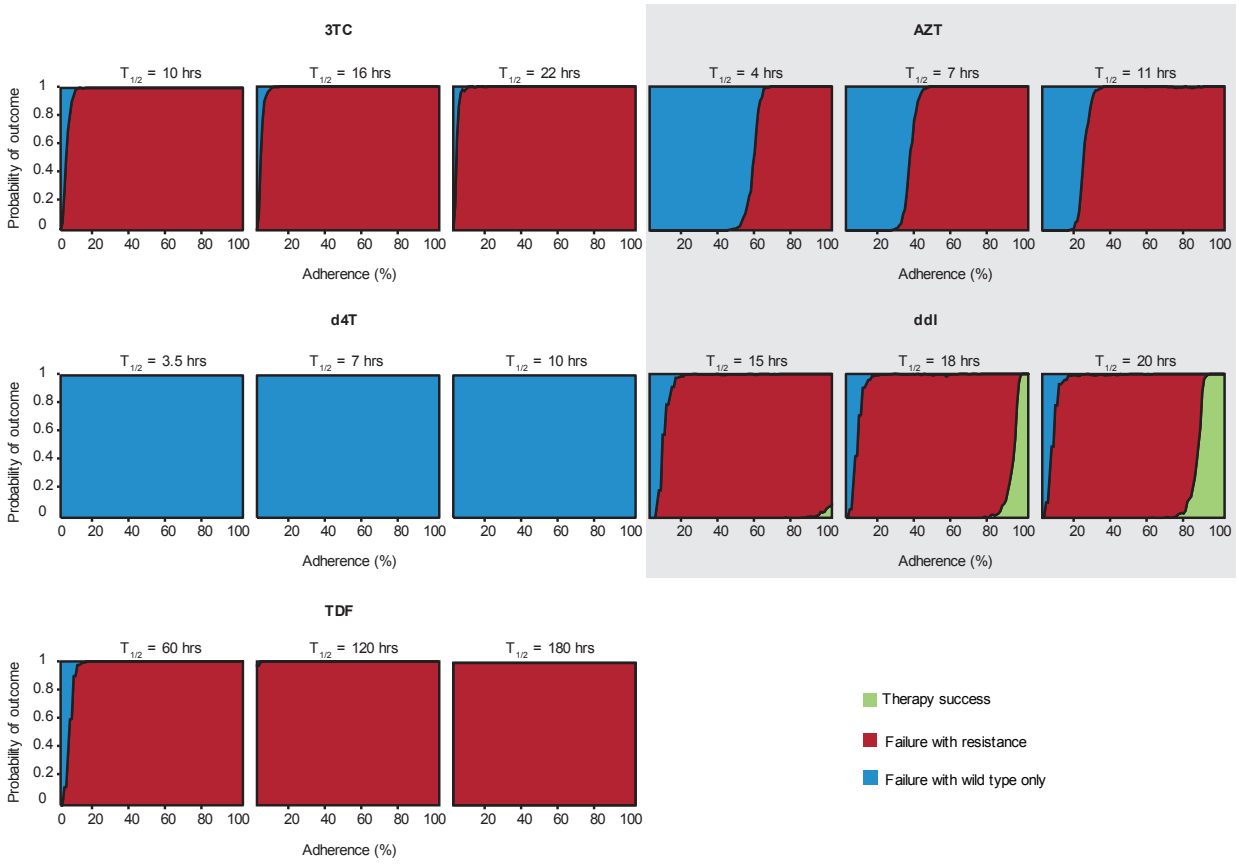

Figure 4.10: Simulated clinical outcomes versus adherence for NRTIs with large inter-experimental variation in half-life. The ranges included were {10, 16, 22} for 3TC, {4, 8.5, 11} for AZT, {3.5, 7, 10} for d4T, {15, 18, 20} for ddI, and {60, 120, 180} for TDF. Results are shown for "Maintenance" trials only. In the "Maintenance" trials shown, patients begin with full viral suppression and undergo monotherapy for 48 weeks or until virologic failure (VF), whichever occurs first. VF is defined as "confirmed rebound": two consecutive weekly measurements (starting at Week 5) with viral load above 200 c.ml^{-1}. VF is classified as "via resistance" if at least 20% of the viral population at the time of detection is mutant. Adherence (x-axis) is measured as the fraction of scheduled doses taken. The height of the area shaded indicates probability of the corresponding outcome at that adherence level. Compared to the half-lives used throughout the rest of the paper (see Table 4.1), the results barely change for 3TC or d4T. For AZT, varying the half-life changes the adherence level where wild-type failure becomes more likely than mutant failure. For ddI, the adherence level where treatment success occurs shifts. For higher TDF half-lives, mutant VF becomes the only outcome, with the exception of rare ($< 3\%$) wild-type failure at the lowest adherence levels for $t_{1/2} = 120$ hours.

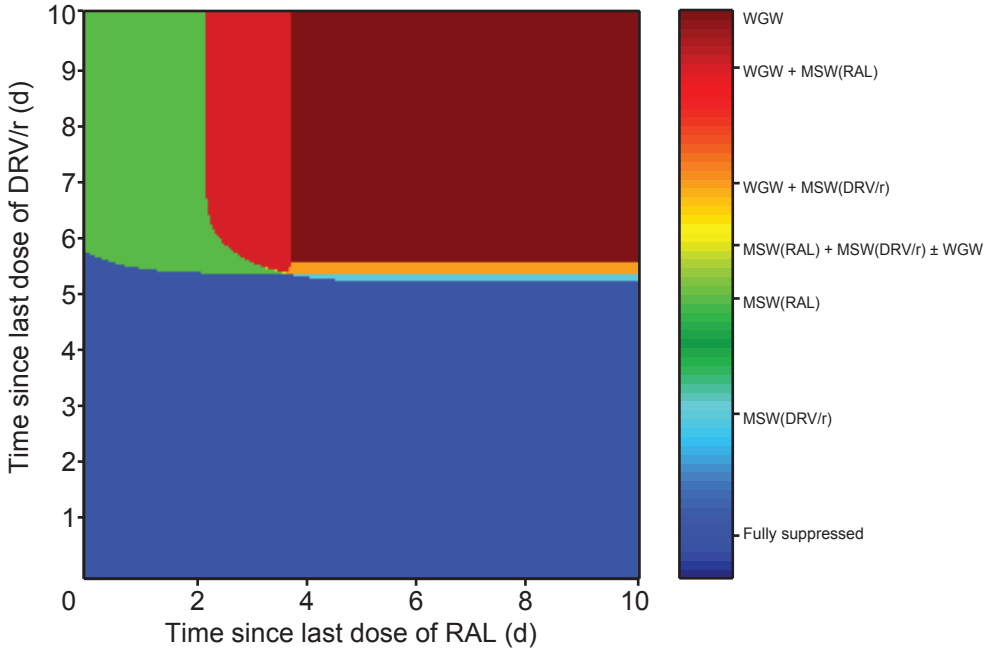

Figure 4.11: Selection regimes for DRV/r-RAL two-drug therapy. Depending on the length of a treatment interruption to one or both drugs, treatment may be fully suppressive or select for the wild-type strain, a mutant resistant to DRV, a mutant resistant to RAL, or combinations of these strains. The yellow region, where the MSW for both drugs overlap, is barely visible, and it is located where the other MSW regions meet, near the center of the graph.

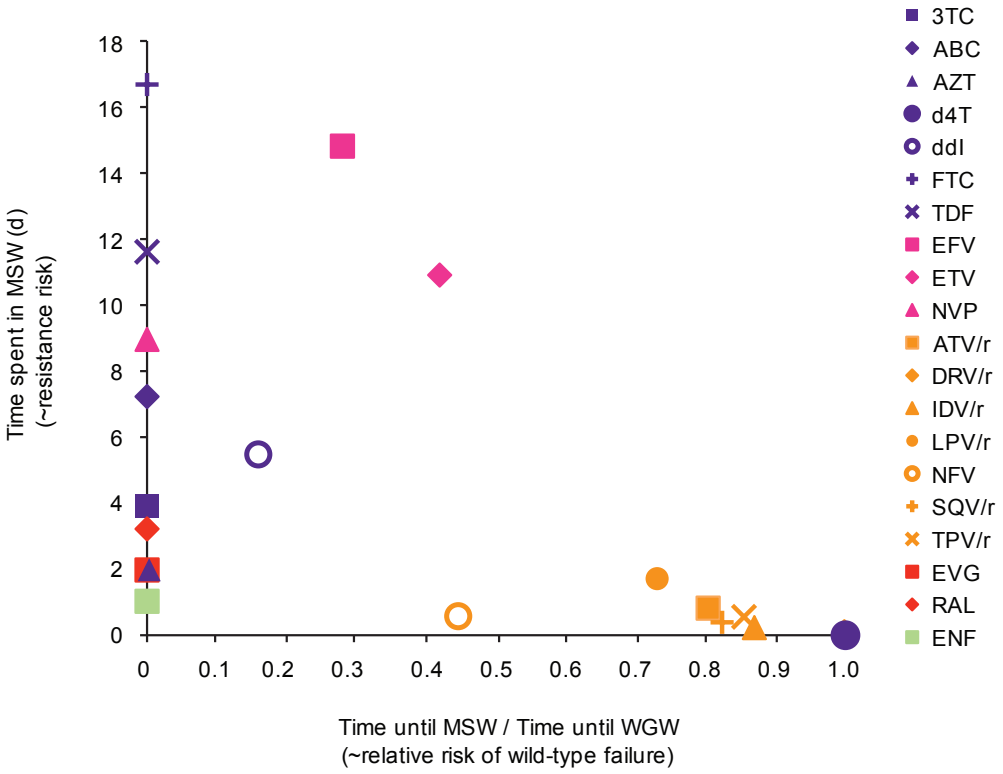

Figure 4.12: Relative risk of wild type- vs. mutant-caused virologic failure for anti-HIV drugs, considering the best "synthetic" mutation defined in Section 4.1.3. Two metrics can be used to compare the risk of resistance to the likelihood of wild-type growth, shown on both axes. The x-axis measures the time until a patient interrupting treatment reaches the MSW, divided by the time until that patient reaches the WGW. The y-axis measures the number of days that a patient spends in the MSW during a treatment interruption. Drugs tend to cluster near the endpoints of the x-axis: most NRTIs, the IIs, and the FI are on the left, meaning that the patient enters the MSW immediately or soon after interruption, and most PIs are on the right, meaning that the patient waits relatively long to enter the MSW. Section 4.1.7 further describes the two metrics and explains how they were used in Figure 3.2f in the main text to rank the drugs by relative risk of mutant-based versus wild type-based VF. Note that the symbol for DRV/r is obscured behind the symbol for d4T at $(1, 0)$.

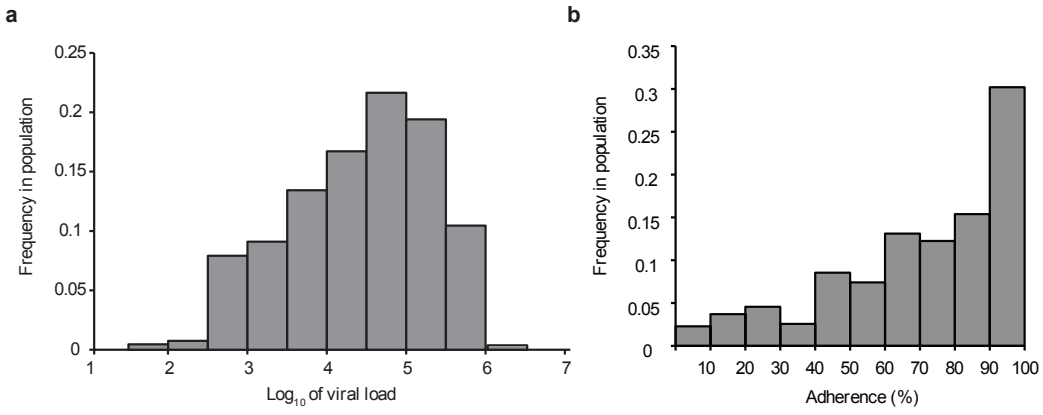

Figure 4.13: Distribution of a) viral load setpoints[180] (data available at www.hiv.lanl.gov/content/immunology) and b) adherence levels [24] used in simulations.

5

Predicting the outcome of treatments to eradicate the HIV-1 latent reservoir

5.1 Abstract

Highly active antiretroviral therapy (HAART) controls HIV-1 replication but cannot eradicate the infection due to a reservoir of latent virus present in resting memory $CD4^+$T cells. Latency reversing agents (LRAs) that reactivate latent HIV-1, rendering the infected cells susceptible to viral cytopathic effects and host cytolytic T lymphocytes, offer hope of a cure. Here we use a stochastic model of infection dynamics to interpret measurements of reservoir composition obtained by both PCR and co-culture experiments, and we calculate the degree of reservoir reduction needed to prevent viral rebound during long periods of HAART interruption. Our findings suggest that reduction of 1,000- to 20,000-fold is required to let a majority of patients interrupt HAART for one year without rebound and that viral rebound may occur suddenly after multiple years of successful interruption. We predict that large variation in rebound times following LRA therapy will complicate interpretation of clinical trials.

5.2 Introduction

The latent reservoir (LR) for HIV-1 is a population of long-lived resting memory $CD4^+T$ cells with HIV-1 DNA integrated into their genomes [71, 72]. After the reservoir is established during acute infection [74], it increases to $10^5 - 10^7$ cells and then remains stable. As only actively replicating virus is targeted by current anti-HIV drugs, latently infected cells persist even after years of effective treatment [73, 110, 327, 375]. Cellular activation leads to virus production and, if treatment is interrupted, a rapid increase in viremia is observed within weeks of discontinuation of therapy. This dynamic prevents cure of HIV-1 by HAART alone and thus necessitates lifelong adherence to HAART. Drugs that specifically target LR cells for rapid activation may reduce the size of the LR [67, 98]. Collectively called *latency reversing agents* (LRA), this class includes the histone deacetylase inhibitors such as vorinostat [14, 16] and valproic acid [15, 328], the alcoholism drug disulfiram [380], protein kinase C activators prostratin [37] and bryostatin [221, 280], and quinoline derivatives [381]. The hope is that following treatment with these drugs, patients might be able to discontinue HAART with minimal risk of viral rebound. While the discovery of LRAs is now the subject of an intense research effort, it is unclear how much the LR must be reduced to enable patients to discontinue HAART safely. Mathematical models of treatment dynamics are urgently needed to inform clinical trial design, interpret outcomes, and guide further drug discovery.

Mathematical models have been instrumental in understanding the dynamics of HIV-1 infection, including the LR. Multi-compartment models of HIV-1 infection have successfully been used to describe the phases of viral decay after initiation of HAART [181, 247, 269], the role of ongoing replication in slowing the rate of LR decay [311], and the appearance of viral "blips" during treatment [81, 292, 293]. Recent studies have considered the role of the LR in the development of drug resistance to HAART[296]. However, no model has been developed to study the effect of treatment with LRAs. Here we build and analyze such a

model to predict how *in vitro* drug efficacy translates to patient outcomes, measured as the length of time following discontinuation of HAART before viral rebound occurs.

5.3 Methods

We consider proposed therapy protocols for latency reversing agents (LRAs) that administer the treatment while a patient is on fully suppressive HAART [98]. It is believed that LRA therapy will reactivate transcription at the HIV-1 LTR, leading to production of cytotoxic viral products and cell death. While plasma HIV-1 levels may increase during this phase, strict adherence to HAART is expected to prevent new cellular infections. After a period of treatment with both LRAs and HAART, both therapies would be interrupted. Here we provide a model of the viral infection immediately after this therapy ends (Fig. 5.1(A)). Our goal is to estimate the probability of cure, or, barring that best-case outcome, to estimate the distribution of times until virologic rebound, in terms of parameters describing the underlying infection dynamic and the LRA therapy.

The model tracks two cell types: productively infected active $CD4^+$ T cells, and latently infected resting $CD4^+$ T cells. Cells carrying nonviable HIV-1 provirus (which may vastly outnumber cells carrying replication-competent proviruses) are excluded from these two quantities. The level of plasma virus is not tracked explicitly, but is assumed to be proportional to the productively infected cells. Four types of events can occur in this model, which is described formally as a two-type branching process (Fig. 5.1(C)). A latently infected cell can either activate at rate a, or die at rate d_z. An actively infected cell can either produce a burst of virions at rate b, resulting in the infection of c other cells, after which it dies, or it can die without producing virions (at rate d). The number of cells infected after each burst event is a Poisson random variable with mean and variance λ (Fig. 5.1(D)). Details of the model are described in Suppl. Methods. §6.1.3.

The total death rate of productively infected cells ($d_y = b + d$) has been well characterized to be 1 day^{-1} from treatment initiation studies. The rate of reactivation of

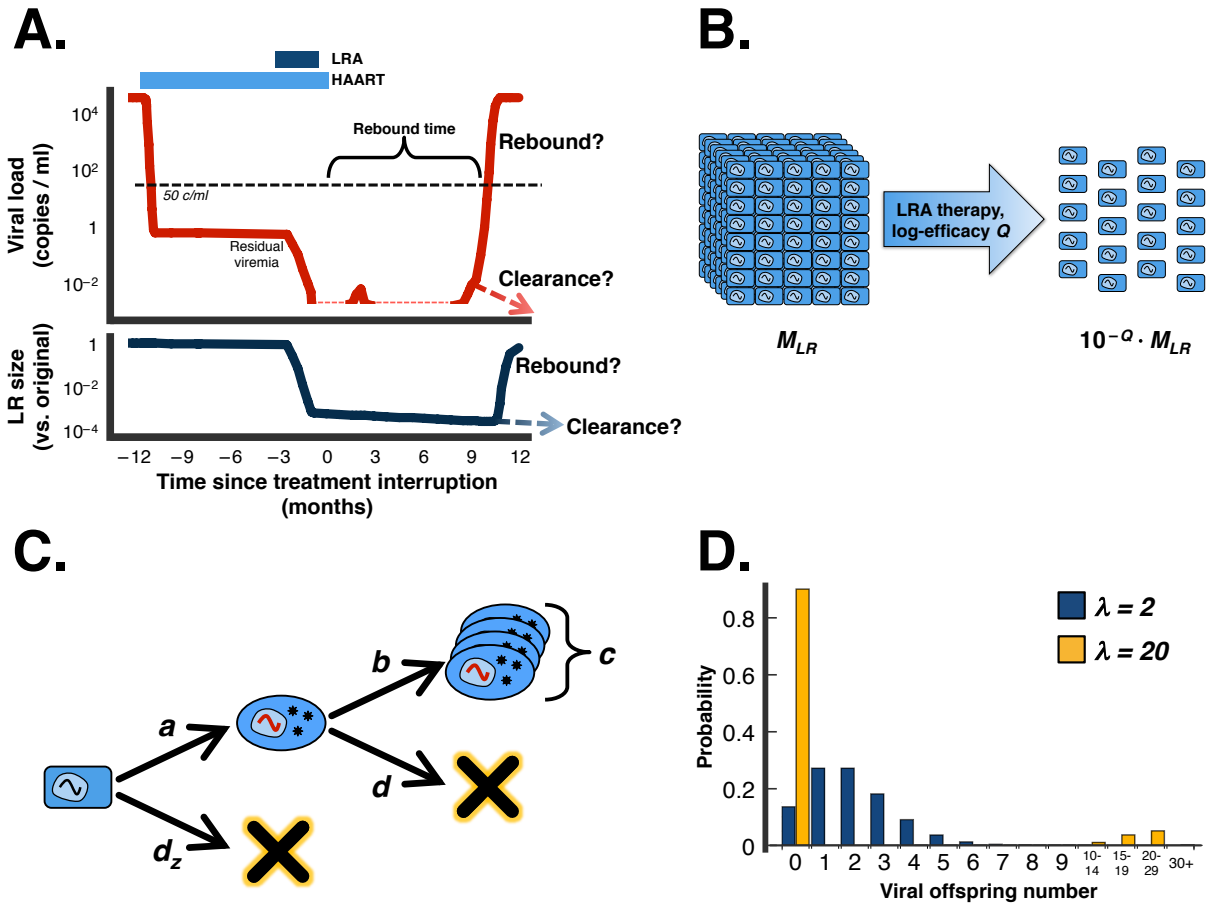

Figure 5.1: Schematic of LRA therapy and stochastic model of rebound following therapy. A) Proposed treatment protocol, illustrating possible viral load and size of latent reservoir before and after LRA therapy. When HAART is started, viral load decreases rapidly and may fall below the limit of detection. The latent reservoir is established early in infection (not shown) and decays very slowly over time. When LRA is administered (either continuously, as shown, or in intervals), the latent reservoir declines. Depending on the efficacy of LRA therapy, the infection may be cleared, or viremia may eventually rebound. B) LRA efficacy is defined by the parameter Q, the number of $\log_{10}$-reductions in LR size. C) Stochastic model of viral dynamics following LRA therapy, tracking both latently (rectangles) and actively (ovals) infected cells. Each arrow represents a type of event that occurs in the model and its rate, described in the text. D) The expected number of "offspring" for each productively infected cell is the basic reproductive ratio $R_0 = 2$. The "infectivity variance" parameter λ determines variance of the offspring distribution. The offspring distribution conditional on event b occurring is given by a Poisson: $P(c) = \lambda^c e^{-\lambda}/c!$

cells from the latent reservoir can be estimated based on the size and composition of the LR (Fig. 5.2) and the level of residual plasma virus for patients on fully suppressive HAART ($\approx$ 2 copies HIV-1 RNA per milliliter plasma, c ml^{-1}). We estimate a to be 7×10^{-5} day^{-1} and consider values in the range 10^{-5} to 3×10^{-3}. The death rate of latently infected cells is estimated from studies of the rate of decay of the LR to be $d_z = 4.6 \times 10^{-4}$ day^{-1} (corresponding to a 44 month half-life). We also present results for two extremes: a half-life of only 6 months, and, $d_z = 0$. The basic reproductive ratio for this model, defined as the expected number of new infected cells that a single actively infected cell produces, is $R_0 = \lambda b/(b + d)$. The average R_0 value is estimated from time-to-rebound in HAART-interruption studies to be $R_0 = 2$ (which is lower than the values estimated for acute infection). R_0 does not uniquely determine the dynamics of the stochastic model because b and λ cannot be simultaneously identified. Holding R_0 constant, the parameter λ controls the strength of random drift in the infection: for high λ, reproduction resembles a "jackpot" event where a few infected cells give rise to many new infection events, while many other infected cells die before infecting additional cells. Here we vary λ in the range 2 – 50. Justifications for these parameter estimates are provided in Suppl. Methods. §6.1.2.

The initial conditions depend upon the number of latently infected cells that survive LRA therapy. This quantity is defined by the latent reservoir size prior to LRA therapy and the log-efficacy of LRA therapy (Fig.5.1(B)). The model aims to determine whether or not this population of cells will escape drift and restart the infection before all the cells die. These results are independent of the details of how the drug is administered or the mechanism of action. As the model does not provide for any limitation of growth as the infection becomes large, it is valid only for the initial stages of viral rebound. Since clinical viral rebound thresholds (viral load above 50 – 200 c ml^{-1}) are well below carrying capacity (typical setpoint viral load of 10^4 – 10^6 c ml^{-1}), this model suffices to analyze the probability and timing of rebound following LRA therapy and HAART interruption.

5.4 Results

We used several experimental findings to estimate the size range of the LR, which we define as the number of resting CD4$^+$T cells with integrated HIV that are capable of producing infectious virus upon reactivation (Fig. 5.2). We considered three cases for the LR size distribution among patients. Limiting dilution co-culture assays [325] are currently the gold standard for LR size measurement. In case (i), we assume all patients have a reservoir size equal to the average measured in these assays ($\approx 1 \times 10^{-6}$ cells), and in case (ii) we incorporate inter-patient variability in assay results [104]. PCR measurements detect cells with HIV-1 DNA at a higher frequency than co-culture assays, but much of this virus may be defective. Full genome clonal sequencing of provirus from cells not induced in co-culture identifies a portion with all open reading frames intact [146]. In case (iii), we include these cells in the LR. For all cases we assume a total resting CD4$^+$cell count of 10^{12}. The resulting distributions are shown in Fig. 5.3(A). Formal definition of each distribution is provided in Suppl. Methods. §6.1.1.2

The best-case outcome of LRA therapy, barring complete eradication of the reservoir, is that none of the surviving latently infected cells activate and lead to a resurgent infection. In this case, we say that LRA has cleared the infection. We used the model to predict the relationship between LRA log-efficacy (denoted Q) and clearance probability (Suppl. Methods §6.1.3.2.1). Fig. 5.3(B) shows results for the three possible reservoir distributions (i) – (iii) described above.In cases (i) and (ii), where the average pretreatment reservoir size is 10^6, the reservoir must be reduced by three to five orders of magnitude before half of patients clear the infection. Including inter-patient variability only causes the clearance probability to increase more gradually with Q. If co-culture does not detect all cells in the latent reservoir (case iii), then Q of four to six is required for 50% clearance. In all three cases, the clearance probability decreases with reservoir half-life. Clearance probability also increases with infectivity variance λ, as this parameter controls the

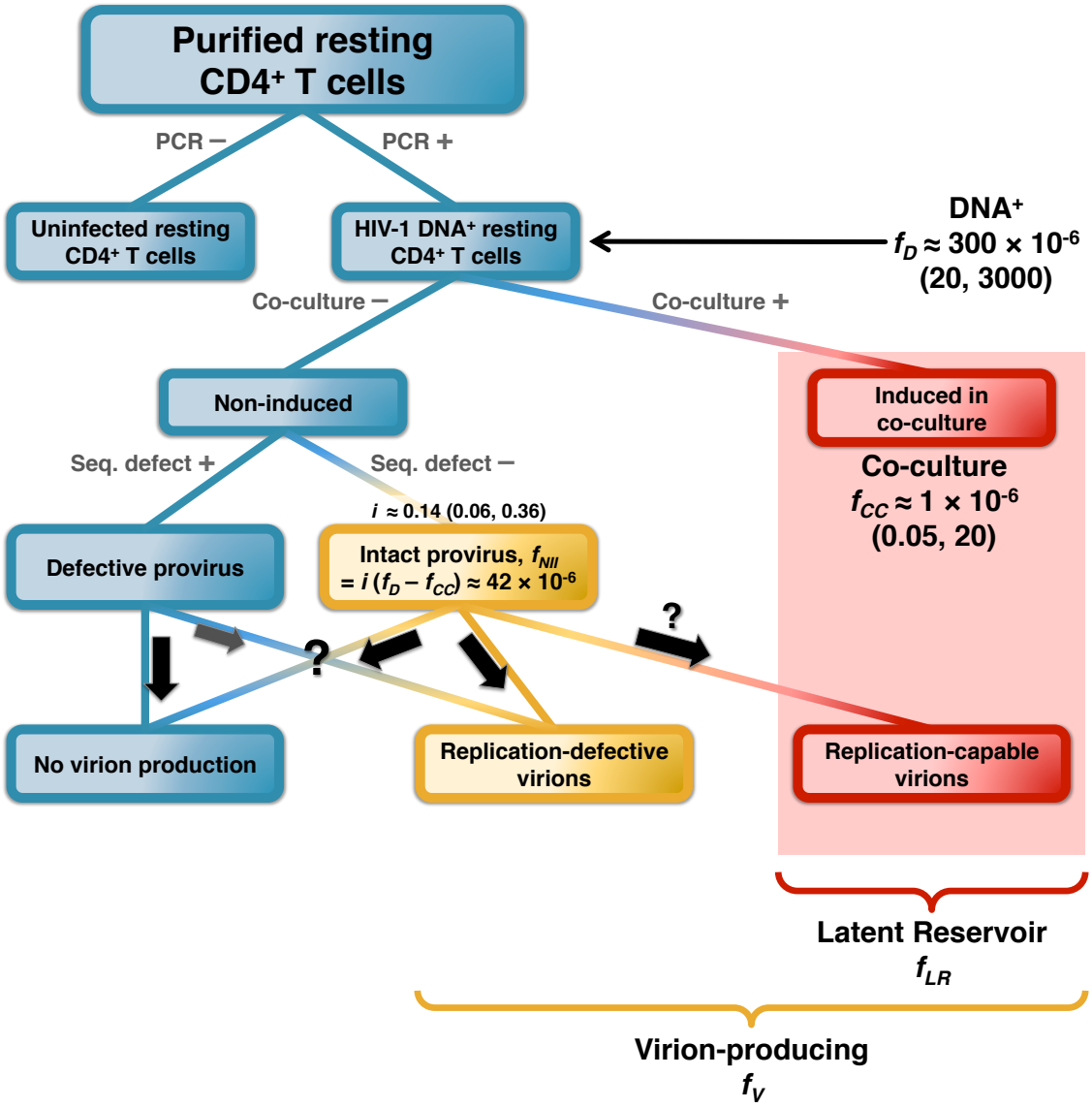

Figure 5.2: Experimental scheme for classifying resting CD4$^+$ T cells based on HIV-1 infection and viral production, using data from [104, 146]. Scheme starts at the top, with purified resting CD4$^+$ T cells, and proceeds downward through the experimental analyses listed. The f variables represent fractions of this resting CD4$^+$T cell pool with the characteristics listed. "PCR": Digital droplet PCR identified cells containing HIV-1 DNA, nearly all of which is expected to be integrated. "Co-culture": PHA was used to induce viral replication in latently infected cells. "Seq. defect": Non-induced cells were analyzed for genetic defects preventing production of replication-competent virus. A fraction i of these non-induced cells had no observable defects (all open reading frames intact); this fraction constitutes f_{NII} of all resting CD4$^+$T cells. Question marks indicate that it was not possible to determine by this analysis what fraction of cells would produce replication-competent virus *in vivo*, due to integration site effects and undetectable sequence defects. Even defective provirus may be able to produce defective virions that contribute to residual viremia (gray arrow). The latent reservoir (shaded box) consists of induced and replication-capable non-induced cells. Values shown are averages and ranges of ≈ 30 patients.

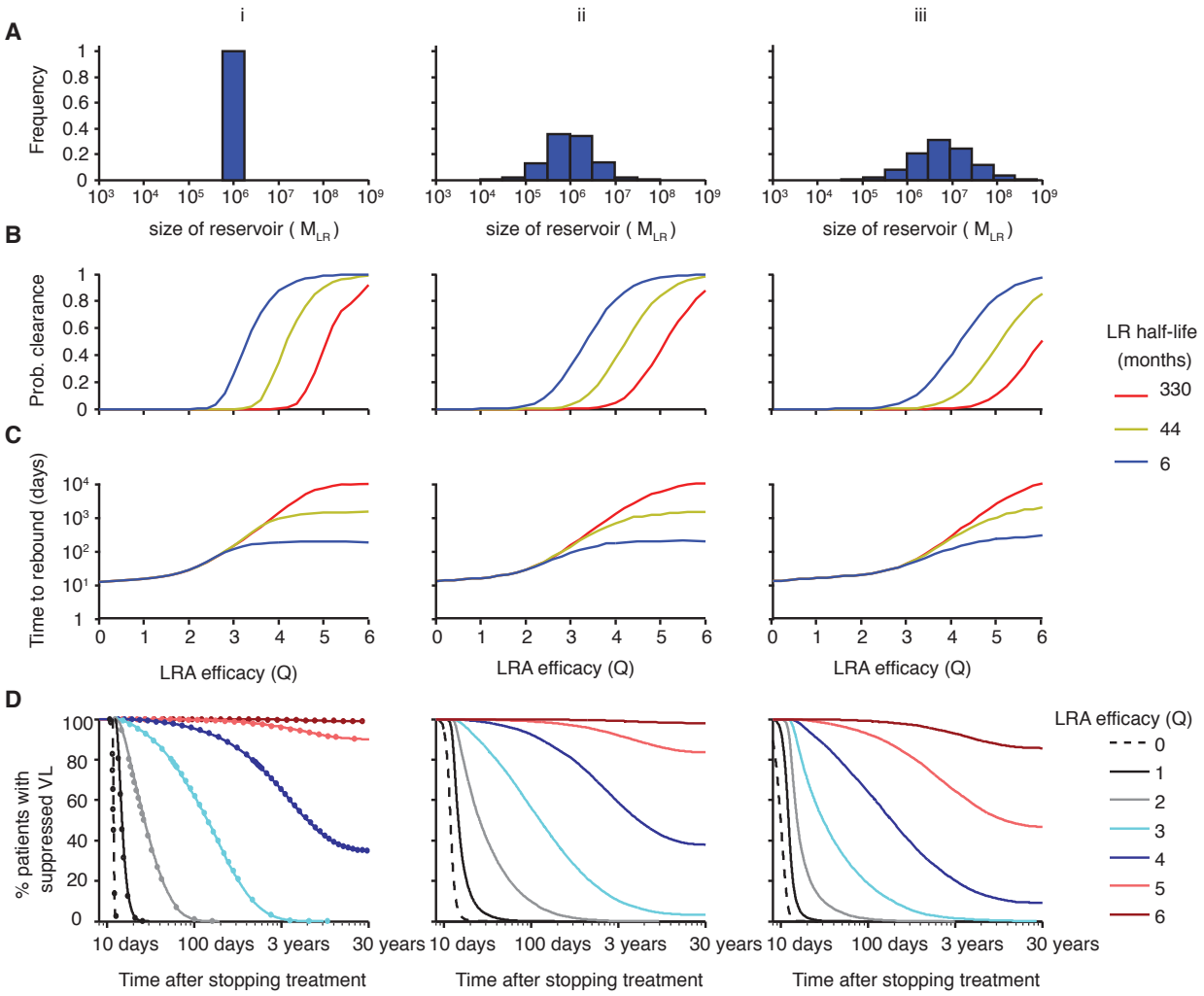

Figure 5.3: Clearance probabilities and rebound times following LRA therapy predicted from model. A) Three cases for the population-level distribution of LR size (Suppl. Methods §6.1.1.2). Case i) All patients have the same latent reservoir size, $M_{LR} = 10^6$, estimated from the geometric mean number of cells that are capable of producing infection in laboratory co-culture assays. Case ii) Latent reservoir size is distributed according to variation observed in co-culture assays, with geometric mean 10^6. Case iii) The latent reservoir includes many cells that fail to be detected in co-culture but have intact viral genomes. B) Probability that the reservoir is cleared by LRA. Clearance occurs if all cells in the reservoir die before a reactivating lineage leads to viral rebound. C) Median viral rebound times, among patients who do not clear the infection. D) Survival curves for patients following LRA therapy. The percentage of patients who have not yet experienced viral rebound is plotted as a function of the time after interruption of LRA therapy and HAART. Curve color indicates the efficacy of LRA in reducing the size of the LR ($Q = 0$ to 6, see legend). Results are shown for a half-life of 44 months; other half-lives are shown in Fig. 6.6 Solid lines represent simulations, and open circles represent approximations from a branching process calculation(Suppl. Methods §6.1.3.2.2),[81]). All simulations included $10^4 - 10^5$ patients and used parameters $a = 7 \times 10^{-7}$, $\lambda = 20$ and $R_0 = 2$.

likelihood of viral lineage extinction by drift (Fig. 6.4B).

If LRA therapy fails to clear the infection, the next-best outcome is substantial extension of the time until virologic rebound, defined as a viral load of 200 c ml^{-1}(§6.1.2.2). We computed the relationship between efficacy of LRA therapy and the median time until rebound, among the patients who do not clear the infection (Fig. 5.3(C)). For an LR size of 10^6 (case i), only modest increases in median rebound time are predicted for up to 100-fold reductions in the size of the reservoir ($Q \leq 2$). In this range, the rebound time is independent of latent cell lifespan, and it is driven mainly by the reactivation rate and the viral reproductive ratio. The curve inflects upward at $Q = 2$ (on a log scale) and reaches a ceiling as clearance of the infection becomes the dominant outcome (Fig. 5.3(C)(i)). If cells in the reservoir are extremely long-lived, it is possible for rebound to occur even after decades of apparent cure. If the LR size is larger (case iii), then the median rebound time curve is shifted rightwards, requiring higher LRA efficacy for the same outcomes (Fig. 5.3(C)(iii)). In all three cases, the inflection point decreases in λ. In case (i), this point varies between $Q = 1.5$ (for $\lambda = 50$) and $Q = 3$ (for $\lambda = 2$). Accordingly, the median rebound time increases in λ (Fig. 6.4C).

The upward inflection observed in median rebound time results from an important change in the forces governing viral dynamics. If the reservoir is large enough (low Q), a surplus of cell activation occurs such that the dominant component of rebound time is the time that it takes for virus from one of the many activated cells to grow exponentially to rebound levels; the system is in a *growth-limited regime*. If the reservoir is small (high Q), the expected waiting time until activation of the first cell fated to establish a rebounding lineage is the dominant component of rebound time; the system is in an *activation-limited regime*. Since this waiting time is roughly exponentially distributed, times to rebound in this regime can vary widely among patients. The "threshold Q" defining the boundary of these two regimes matches the value where upward inflections are observed (Fig. 6.5(A)).

The scope of predicted interpatient variability in outcomes can be seen in survival

curves, plotting the fraction of simulated patients maintaining virologic suppression over time (Fig. 5.3D). For small reductions in LR size ($Q \leq 2$) patients uniformly rebound within a few months, since rebound dynamics are not in the activation-limited regime (Fig. 5.3(D)(i)). If LRA therapy manages to decrease the reservoir size 1,000-fold ($Q = 3$), then about 20% of patients remain rebound-free for at least a year. Higher Q leads to clearance in many patients, though rebound can still occur after a decade without viremia. Interpatient variation in LR size makes it more likely to observe long periods without rebound (Fig. 5.3(A)(ii)). Rebound delays of over three years are achieved for 10% of simulated patients at $Q = 3$, versus only 1% in case (i). The fortunate few who completely clear the infection started with an LR smaller than the average size of 10^6 prior to treatment. Survival curves decline more rapidly if the average LR size is larger (case iii) or if λ is lower (Fig. 6.7), indiciating a less beneficial outcome for LRA therapy.

For all three reservoir size distributions considered, rebound may occur even after long periods of virologic suppression. Taking case (ii) for example, among the patients without rebound at six months post-therapy, 71%, 38%, or 11% suffer rebound in the following six months, for efficacies $Q = 2$, $Q = 3$, or $Q = 4$, respectively (Fig. 5.3(A)(ii)).

To set goals for treatment efficacy, we calculate three "target values" of Q, assuming a pretreatment reservoir size of 10^6. One month is near the upper limit of rebound times without LRA therapy, and we first calculate define the log-efficacy for which 50% of patients exceed this limit (Fig. 5.4(A)). This value is insensitive to the estimate for reservoir half-life and increases logarithmically with the activation rate. For a broad range of activation rates, a 1.5- to 3-log reduction is needed for a one-month delay. We next calculate the target efficacy for one-year delays (Fig. 5.4(B)). Using estimated parameter values, this goal requires a 3-log reduction in reservoir size. This value is only mildly sensitive to reservoir half-life (declining only for very short half-lives, at which reservoir clearance is likely) and also scales logarithmically with activation rate. If activation exceeds the estimated rate, then the target Q is closer to 4.5 – a 30,000-fold reduction.

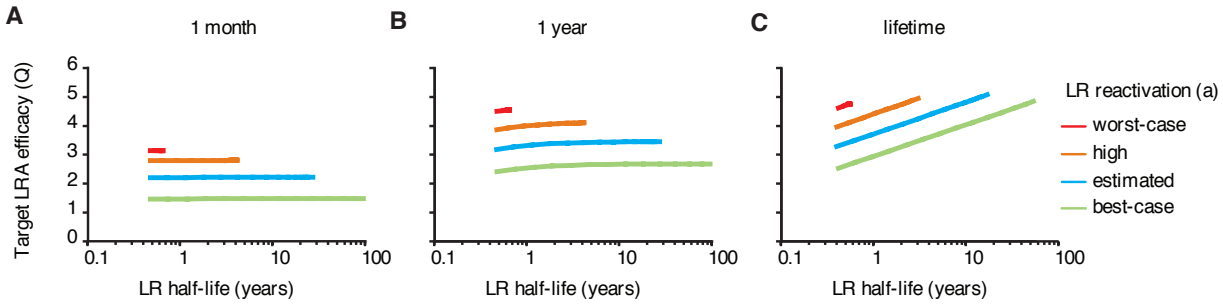

Figure 5.4: Efficacies required for successful LRA therapy. Target LRA efficacy values based on three different treatment goals are plotted versus reservoir half-life ($\frac{\ln(2)}{a+d_z}$) and the reservoir reactivation rate (a). A) The target efficacy Q at which at least 50% of patients still have suppressed viral load one month after treatment interruption. B) The target efficacy Q at which at least 50% of patients still have suppressed viral load one year after treatment interruption. C) The target efficacy Q at which at least 50% of patients have eradicated the reservoir without experiencing viral rebound. Because some patients may go for a year without rebound but then rebound later, the target Q for one year off therapy is always less than that for a lifetime off therapy. Results were calculated from the branching process description of the stochastic process, which agrees with simulation (Suppl. Methods §6.1.3.2.2). All calculations used $\lambda = 20$ and varied R_0 to ensure baseline rebound time was constant (12 days). Worst-case: $a = 3 \times 10^{-3}, R_0 = 1.43$, high: $a = 4.6 \times 10^{-4}, R_0 = 1.7$, estimated: $a = 7 \times 10^{-5}, R_0 = 2$, best-case: $a = 10^{-5}, R_0 = 2.21$.

Finally, since the ultimate goal of LRA therapy is to clear the reservoir completely, we determine the log-efficacy for which at least half of patients clear the infection (Fig. 5.4(C)). This value consistently exceeds the more modest one-year target and scales logarithmically with the product of activation rate and half-life. Parameter scaling relationships follow from a generating function analysis of the branching process, described in the Suppl. Methods §6.1.3.2.1, §6.1.3.2.3. All target Q values also scale with the reservoir: a 1-log increase in reservoir size would necessitate a unit increase in Q.

We evaluated the robustness of our conclusions to simultaneous changes in latent cell activation and death rates, pretreatment reservoir size distributions, and infectivity variance. For a worst-case analysis, the latent cell death rate was set to zero (such that the reservoir decays only via activation), the pretreatment reservoir size distribution was set to that of case (iii), and infectivity variance was set to a low value. The resulting target Q for a one-month delay increased by 2, and the clearance target Q increased by 3 versus baseline (Fig. 6.8(i) versus (iii)). For a best-case analysis, the latent cell activation rate was set to 7 times lower than baseline and the death rate was increased to yield a reservoir half-life of only six months, the pretreatment reservoir size distribution was set to that of case (i), and infectivity variance was set to a high value. The results were similar to that of the baseline case, but with Q shifted upwards by 1, and with a lower ceiling rebound time (200 days versus over 1,000 days) (Fig. 6.8(i) versus (iii)).

Throughout our analysis, we have characterized LRA drug efficacy by the log-reduction in reservoir size following therapy, which may not be observable. Laboratory studies of cellular models of latency may estimate Q, but their relevance *in vivo* remains unknown. It may not be possible to measure Q values above 1 by quantifying reservoir size following LRA therapy, as current co-culture assays cannot detect reservoirs smaller than about 10^5 cells [104]. Since current approaches to LRA therapy seek to reduce reservoir size by inducing activation of latently infected cells, Q may be estimated by measuring the dynamics of viral load during simultaneous HAART/LRA therapy (Suppl.

Methods §6.1.5). Since the effect of LRA therapy on resting $CD4^+$ T cell phenotype is not fully characterized [315, 316], there is considerable uncertainty in this relationship; nonetheless a sharp, transient peak viral load of at least several hundred c ml^{-1} is expected for highly effective therapy ($Q \geq 2$) (Table **??**).

5.5 Discussion

Our model is the first to describe the action of investigational latency reversing agents and set quantitative goals for LRA therapy, offering guidance for the design and testing of treatment protocols. There is currently little understanding of the degree of reservoir activation required to provide meaningful benefit. We analyzed experimental findings regarding reservoir size and composition to describe three plausible settings for LRA therapy (Fig. 5.3A). In each setting, our model translates a reactivation measure of therapy efficacy (parameter Q), which may be estimated *in vitro*, to a prediction of clinical benefits.

For a wide range of parameters, we find that LRAs must reduce the reservoir by at least 1.5–3 orders of magnitude to see a meaningful increase in the time to virologic rebound after HAART interruption (upward inflection in Fig. 5.3C and Fig. 6.4C), and that 3–5 orders of magnitude are needed for half of patients to clear the infection (Fig. 5.4C and Fig. 6.5). Standard deviations in rebound times of many months are expected to be the norm for successful therapy, owing to variation in pretreatment reservoir size and roughly exponentially-distributed reactivation times after effective LRA therapy brings the infection to an activation-limited regime. While the required LRA efficacy for these beneficial outcomes is almost certainly beyond the reach of current drugs, our results do permit some optimism: reactivation of all cells in the reservoir is unlikely to be necessary for complete reservoir clearance and safe cessation of HAART. This is due to the reasonably high probability that a cell in the LR will either die before reactivating or, following activation, fail to produce a chain of infection events leading to rebound. On a more cautionary note, the wide distribution in reactivation times implies that continual monitoring of patients is

essential, as rebound is possible even after long periods of viral suppression.

Clinical and laboratory findings constrain the basic reproductive ratio R_0 and active cell death rate d_y in a relatively narrow range. The rebound population size, while it may vary by over order of magnitude, has little effect on model outcomes, especially in the activation-limited regime. Remaining parameters — pretreatment reservoir size, latent cell half-life $\frac{\ln(2)}{a+d_z}$, latent cell activation rate a, and infectivity variance λ — have profound impacts on treatment outcome, and they are not well-established to within an order of magnitude. While LR size is generally estimated at 10^6, recent studies have shown that even co-culture assays — recognized as the gold standard for latency measurement — may drastically underestimate reservoir size (Fig. 5.3(A)(ii) versus 5.3(A)(iii)). We accounted for these studies to show that this underestimate may cause expectations of LRA therapy outcomes to be unduly optimistic (Figs. 5.3(B,C)(ii) and 5.3(ii) versus Figs. 5.3(B,C)(iii) and 5.3(iii)). Considering both variation in pretreatment reservoir size and latent cell half-lives, the log-reduction needed to delay rebound for one year in half of patients is ≈ 3 to ≈ 4.3 — a reduction of 1,000- to 20,000-fold (Fig. 6.6(C)(ii) vs. (A)(iii)). When broad variation in a and λ is also considered, the range expands to ≈ 2 to ≈ 5.2 (Fig. 6.8(C)(ii) vs. (C)(iii)).

Our analysis characterizing the required efficacy of LRA therapy does not rely on the specific mechanism of action of these drugs, only the amount by which they reduce the reservoir. We have assumed that the reservoir is a homogeneous population without variation in activation and death rates. The presence of reservoir compartments with different drug penetrations does not alter our results, as they are stated in terms of total reservoir reduction. If, however, these compartments vary in activation or death rates, or if viral dynamics of activated cells depends on their source compartment, then our model may need to be modified. In the absence of clear consensus on compartments constituting the LR, we have considered the simplest scenario with fewest assumptions, which may be able to fit future LRA therapy outcomes.

To date, laboratory and clinical studies of investigational LRAs have generally found weak potential for reservoir reduction, with $Q < 1$ [15, 76, 380]. We predict that much higher efficacy will be required for any hope of eradication. While we have focused on the role of LRA therapy in reducing the reservoir size, our main findings may also serve to interpret viral eradication or delays in rebound caused by early treatment initiation [40, 271, 341] or stem cell transplantation [140, 152], both of which also reduce the LR size.

5.6 Acknowledgments

The authors thank Ya-Chi Ho and Alireza Rabi for helpful discussions.

5.7 Manuscript Information

5.7.1 The author's contribution

The authors for this paper are Alison Hill, Daniel Rosenbloom, Feng Fu, Martin Nowak, and Robert Siliciano. The first two authors contributed equally to this work. Designed and analyzed the model: ALH, DISR. Calculated the branding process approximation: FF. Wrote the paper: ALH, DISR. Conceived of the study: ALH, DISR, MAN, RFS.

6

Supplementary Information: Predicting the outcome of treatments to eradicate the HIV-1 latent reservoir

6.1 Supplementary Methods

6.1.1 Characterizing the latent reservoir

This section details the calculations summarized in Fig. 5.2.

6.1.1.1 Components of the latent reservoir

Let M be the total number of resting CD4$^+$T cells in an individual. The fraction of these cells containing HIV-1 DNA, written f_D, is measured using PCR on purified resting CD4$^+$T cells [104]. The total number of resting CD4$^+$T cells with HIV-1 DNA is $M_D = f_D M$.

Many of these cells may not be capable of producing infectious virions upon reactivation. Limiting-dilution co-culture assays [325] measure the fraction f_{CC} of resting CD4$^+$T cells that produce replication-competent virus following cellular activation. The

total number of these cells is $M_{CC} = f_{CC}M$.

Experiments show that f_D exceeds f_{CC} by more than two orders of magnitude, but the reasons for this discrepancy are unclear. Some portion of cells with HIV-1 DNA may harbor defective provirus that cannot produce viral proteins. Others may contain intact provirus, but evade co-culture detection for other reasons. These two scenarios can be distinguished by full genome clonal sequencing of integrated provirus, from which defects preventing viral replication may be identified [146]. Among those cells infected with provirus but undetected in co-culture, let i be the fraction that nonetheless are shown by sequencing to have all open reading frames intact. Then f_{NII}, defined as the frequency of non-induced, intact provirus-containing cells, is $f_{NII} = i\,(f_D - f_{CC})$.

The quantity of interest for our model is the number of resting $CD4^+$T cells harboring proviral DNA capable of causing infection of other cells. This latent reservoir contains M_{LR} cells, or a fraction f_{LR} of M. At minimum, it includes those cells tested positive by co-culture, and at maximum, it includes all cells containing intact proviruses. It is likely to be less than the upper bound, since even cells with intact provirus may be incapable of re-starting infection due to integration into a transcriptionally silent site, or due to other defects that escaped detection.

6.1.1.2 Size of the latent resevoir and interpatient variability

The size and composition of the latent reservoir can vary significantly between patients. This variation is relevant to variation in rebound time. Based on results in [104, 146], we can calculate the average parameters and estimate the population level distributions:

Table 6.1: Estimated population level distributions of measures of latent reservoir size

Quantity	Average	Distribution
f_D	300×10^{-6}	$LogNormal(-3.5, 0.5)$
f_{CC}	10^{-6}	$LogNormal(-6, 0.5)$
i	0.14	$LogNormal(-0.85, 0.2)$

The distributions were estimated by assuming the ranges observed in these study of approximately 30 patients represent the center 95% of the distribution (ie 2 standard deviations). We examinine three different cases for inter-patient variability:

Case 1: All patients have the same LR size, which equals the average value measured in co-culture assays ($f_{LR} = f_{CC}$).

Case 2: The fraction f_{CC} varies among patients as in the table above, and $f_{LR} = f_{CC}$ for each patient.

Case 3: The fractions f_D, f_{CC}, and i are sampled from the above distributions, subject to the constraint $f_{CC} \leq f_D$. Then f_{NII} is computed. The value $\log(f_{LR})$ is then sampled uniformly from the interval $[\log(f_{CC}), \log(f_{NII})]$.

Inter-patient variability in outcomes is lowest for Case 1 and highest for Case 3. Throughout this paper, we assume the only parameters that vary between patients are those related the composition of the reservoir.

6.1.1.3 Estimating the number of virion-producing cells

The value f_V is defined as the fraction of resting memory $CD4^+T$ cells that are capable of producing virions that are detected in viral load assays, regardless of whether these virions are infectious. This value is used to calibrate the reactivation rate a from observed residual viral load values (Eq. (6.2), below). While $f_{LR} \leq f_V \leq f_D$, we cannot establish the relationship between f_V and f_{NII}, as some cells in f_{NII} may harbor transcriptionally silenced provirus, and conversely some cells in f_V may harbor provirus with detectable defects. As an intermediate estimate we assume $f_V = f_{CC} + f_{NII} = 43 \times 10^{-6}$, though we also consider the two extreme values in the best and worst case scenarios discussed in the main text.

6.1.2 Estimating viral dynamics parameters

Death rate of actively infected cells d_y

The parameter d_y has been measured in many treatment initiation studies to be 1 day^{-1} [214]. In the stochastic model we constrain $b + d = d_y = 1\text{day}^{-1}$.

6.1.2.1 Activation rate of latently infected cells a

Parameter a is estimated from observed viremia during fully supressive HAART treatment ($R_0 = 0$). Among patients, residual viral load is highly correlated to LR size [17]. Since reservoir decay is slow compared to the dynamics of actively infected cells, the residual viral load reaches a quasi-steady-state relative to the size of the latent reservoir (Section 6.1.3.2). At this level, the number of actively infected cells is

$$y_0 \approx \frac{az_0}{d_y} \tag{6.1}$$

Here z_0 is the number of cells in the LR capable of causing productive infection at the time HAART is interrupted, which is equal to $f_{LR}M$, as described in Section 6.1.1, above.

The value y_0 may be estimated from residual viral load measurements. Let σ be the proportionality constant such that v_0 (residual number of *infectious* virions during HAART) equals σy_0. Since viral load measurements do not distinguish between infectious and noninfectious particles, the only quantity that may be ascertained is the total number of virions w_0, which exceeds v_0. Assuming that infectiousness of the released virion affects neither viral burst rate nor decay rate, the same proportionality constant σ applies to the number of cells capable of producing (infectious or noninfectious) virions, written $\hat{y}_0$, resulting in the relationship $w_0 = \sigma\hat{y}_0$. Since $\hat{y}_0 \approx af_V M/d_y$, the value of a equals:

$$a = \frac{d_y w_0}{\sigma f_V M} \tag{6.2}$$

A reasonable estimate for the proportionality constant is $\sigma = 1$, as discussed in Suppl. Materials of [296]. We use $w_0 = 2$ HIV-1 RNA copies per milliliter plasma, c ml^{-1}, corresponding to 3,000 plasma virions for a 70 kg person with 3L plasma, and we use $M = 10^{12}$. Based on the observed averages $f_D = 3 \times 10^{-4}$, $f_{CC} = 10^{-6}$, and $i = 0.14$, we estimate $f_V = 4.3 \times 10^{-5}$ and $a = 7 \times 10^{-5}$ day^{-1}. This activation rate is below previous estimates [311] [287], which would predict a higher residual viral load than observed for patients on fully suppressive HAART. However, because the size and composition of the LR are still a matter of debate, we consider a range of values. For a worst-case scenario of high activation rate, we suppose that only cells testing positive in co-culture contribute to residual viremia ($f_V = f_{CC} = 10^{-6}$ and $a = 3 \times 10^{-3}$). For a best-case scenario of low activation rate, we suppose that residual viremia is seeded from all cells harboring HIV-1 DNA ($f_V = f_D = 3 \times 10^{-4}$ and $a = 10^{-5}$). Results for these scenarios are shown in Figs. 5.4 and 6.8.

6.1.2.2 Viral rebound threshold n

A viral rebound threshold of 200 c ml^{-1} corresponds to 3×10^5 plasma virions (for a 70 kg person with 3 L plasma). Using the estimate $\sigma \approx 1$ above, the number of actively infected cells at rebound is $n \approx 3 \times 10^5$. Model results are not sensitive to this value, as rebound probability depends on the logarithm of n (Section 6.1.3, below).

6.1.2.3 Death rate of latently infected cells d_z

Resting memory CD4$^+$T cells die at a rate d_z, which may be estimated from studies measuring the total decay rate of the reservoir, $a + d_z$. Given a mean half-life of 44

months [327], we estimate d_z to be

$$\begin{aligned} d_z &= \frac{ln(2)}{1320 \text{ days}} - a \\ &\approx 4.6 \times 10^{-4} \text{day}^{-1} \end{aligned} \tag{6.3}$$

This parameter is varied to explore a range of half-lives in Figs. 5.3, 5.4, 6.6.

6.1.2.4 Viral fitness R_0

The combined viral fitness parameter R_0 can be estimated from rebound times measured in HAART-interruption studies [88, 298]. The average rebound time in these studies is twelve days, which consists of both the time needed for drug levels to decay such that the infection can grow and the subsequent time needed for exponential viral growth to rebound levels computed in Equation (6.23). For estimating the drug decay time, we used the method of [159, 319] with a typical regimen of AZT, 3TC, and SQV. For Equation (6.23), we used a rebound factor (described in Section 6.1.4) of $r = 4{,}300$, based on residual viral load $w_0 = 2$ c ml^{-1}, *infectious* residual viral load $v_0 = w_0 \frac{f_{CC}}{f_V} = 0.0465$ c mL^{-1} (using average values of f_{CC} and f_V in Section 6.1.1, above), and detection at 200 c ml^{-1}. We compute a value of $R_0 = 2$, at which it takes about four days for drug levels to decay and another eight for viral growth to rebound levels.

6.1.2.5 Infectivity variance λ

Based on the rate at which patients fail therapy due to drug resistance, a previous study estimated the rate at which cells that are fated to establish a lineage activate from the latent reservoir to be about 4 per day, in the absence of treatment [268]. This estimate is highly uncertain, as it is sensitive to measured mutation rates and fitness costs of resistance mutations.

Using our baseline values of $a = 7 \times 10^{-5}$ and $M_{LR} = 10^6$, the number of cells

activating per day is 70. An extinction probability of $h_1 = 1 - 4/70 = 0.94$ (defined in Equation (6.8)) would make our baseline values consistent with the above estimate. Using $R_0 = 2$, the implied λ to obtain this lineage extinction probability is 28. To account for uncertainty, we consider λ between 2 and 50.

6.1.2.6 Birth and death parameters b and d

R_0 and d_y do not uniquely determine the dynamics of the stochastic model because b and λ cannot be simultaneously identified. After choosing a value for λ between 2 and 50, the parameter b is calculated using the relationship $R_0 = b\lambda/d_y$. The parameter d is then obtained from the relationship $b + d = d_y$.

6.1.3 Stochastic model of viral dynamics

6.1.3.1 Stochastic process

The stochastic model of viral dynamics described in the text can be formally represented as the reactions below:

$$\begin{aligned} &Z \rightarrow Y ... \text{ rate constant: } a \\ &Z \rightarrow 0 ... \text{ rate constant: } d_z \\ &Y \rightarrow cY ... \text{ rate constant: } b * p_\lambda(c) \\ &Y \rightarrow 0 ... \text{ rate constant: } d \end{aligned} \tag{6.4}$$

In this notation Y and Z are individual actively or latently infected cells, respectively, and the arrows represent events that lead one type of cell to become the other type. We assume that an actively infected cell can either die (at rate d) or produce a burst of virions (at rate b) that results in the infection of c other cells, where c is Poisson-distributed random variable with parameter λ, $p_\lambda(c) = \frac{\exp(-\lambda)\lambda^c}{c!}$. After a burst event, the original cell

dies. Since each birth event causes the death of the parent cell, the total death rate is $d_y := b + d$. This model describes a two-type branching process. The reproductive ratio for this model is $R_0 = \frac{b\lambda}{b+d}$, where $\lambda \geq R_0$. We do not explicitly track free virus, but assume it is at a level proportional to the number of infected cells. This assumption is valid because the rates governing the production of virus from infected cells and the clearance rate of free virus are much higher than other rates, allowing a separation of time scales. Because we are not interested in blips or other intraday viral dynamics, this assumption does not influence our results. A method for calculating the proportionality between free virus and infected cells is provided in Section 6.1.2, above.

6.1.3.2 Generating function analysis of the model

Let

$$\begin{aligned} f_1(\xi, \zeta, t) &= E\left[\xi^{y(t)}\zeta^{z(t)} \mid y(0) = 1 \;\&\; z(0) = 0\right], \\ f_2(\xi, \zeta, t) &= E\left[\xi^{y(t)}\zeta^{z(t)} \mid y(0) = 0 \;\&\; z(0) = 1\right] \end{aligned} \tag{6.5}$$

be the basic generating functions for the stochastic process, starting with one active cell and starting with one latent cell, repsectively. Dummy variables ξ and ζ correspond to active and latent cells, respectively. The backward Kolmogorov equations [169] can be represented by the system of coupled ordinary differential equations

$$\begin{aligned} \frac{\partial f_1}{\partial t} &= b\left(\exp\left[\lambda\left(f_1 - 1\right)\right] - f_1\right) + d\left(1 - f_1\right), \\ \frac{\partial f_2}{\partial t} &= a\left(f_1 - f_0\right) + d_z\left(1 - f_0\right), \end{aligned} \tag{6.6}$$

with boundary conditions $f_1(\xi, \zeta, 0) = \xi$ and $f_2(\xi, \zeta, 0) = \zeta$. The birth term $\exp\left(\lambda\left(f_1 - 1\right)\right)$ follows from the Poisson-distributed offspring distribution with parameter λ.

After LRA therapy, the initial reservoir size is z_0. The residual viremia y_0 is determined by activation-death equilibrium during HAART, and so it is Poisson-distributed with mean

$\frac{az_0}{d_y}$. The probability generating function corresponding to this initial condition is then

$$g_{z_0}(\xi,\zeta,t) = f_2(\xi,\zeta,t)^{z_0} \exp\left[\frac{az_0}{d_y}\left(f_1(\xi,\zeta,t)-1\right)\right]. \tag{6.7}$$

If the initial reservoir size is heterogeneous, then the relevant generating function is given by the sum $\sum_{z_0} p_{z_0} g_{z_0}(\xi,\zeta,t)$, where p_{z_0} is the probability that a patient has z_0 latently infected cells following LRA therapy.

6.1.3.2.1 Probability that LRA therapy clears the infection The fixed points of the differential equations (6.6) give the ultimate extinction probabilities h_1 and h_2, starting with a single active cell and a single latent cell, respectively. The probability h_1 is the smallest root of the equation

$$b\left(h_1 - \exp\left[-\lambda\left(1-h_1\right)\right]\right) = d\left(1-h_1\right), \tag{6.8}$$

and the probability h_2 of extinction starting from one latent cell follows,

$$h_2 = \frac{d_z}{a+d_z} + \frac{a}{a+d_z}h_1. \tag{6.9}$$

Using the above initial condition (y_0, z_0), the clearance probability P_{clr} is determined by substituting these fixed points into the generating function g_{z_0}:

$$P_{clr} = h_2^{z_0} \exp\left[-\frac{az_0}{d_y}\left(1-h_1\right)\right]. \tag{6.10}$$

Define $\epsilon = \frac{a(1-h_1)}{a+d_z}$, the probability that a latently infected cell is fated to activate and establish a rebounding lineage (assuming no interference from any prior rebounding

lineage). If this probability is small, then clearance probability is approximately

$$\begin{aligned} P_{clr} &\approx e^{-\frac{\epsilon z_0 (a+d_z+d_y)}{d_y}} \\ &\approx e^{-\epsilon z_0}, \end{aligned} \tag{6.11}$$

where the second approximation follows from the fact that active cell dynamics are faster than latent cell dynamics, $d_y ga + d_z$. The key parameter determining clearance probability is therefore ϵz_0, the expected number of latent cells fated to activate and establish a rebounding lineage.

The observation in the main text that the target value of Q (Fig. 5.4A) scales logarithmically with the product of a and reservoir half-life follows from this computation, since reservoir half-life is $\frac{\ln(2)}{a+d_z}$, and $Q \propto \log\left(\frac{1}{z_0}\right)$.

6.1.3.2.2 Approximation of rebound probability with simplified birth process

By approximating the Poisson birth event with a simpler process where only two new infections result per birth, closed forms for the generating functions can be derived, allowing easier computation of rebound probabilities. In this approximation, active cells die at "effective death rate" d_e and give rise to two new active cells at "effective birth rate" b_e. Latent cell dynamics are the same as in the full model. The two parameters are chosen to have the same extinction probability as in the original model,

$$\frac{d_e}{b_e} = h_1, \tag{6.12}$$

and the same expected growth rate (and thus the same R_0)

$$b_e - d_e = b(\lambda - 1) - d. \tag{6.13}$$

The differential equation for active cells, analogous to the first line of (6.6), is then

$$\frac{\partial f_1}{\partial t} = b\left(f_1^2 - f_1\right) + d\left(1 - f_1\right), \tag{6.14}$$

while the differential equation for latent cells is the same as in (6.6). The basic generating functions for this simplified process can be solved in closed form,

$$\begin{aligned} f_1(\xi,\zeta,t) &= \frac{b_e\xi - d_e + d_e(1-\xi)\exp\left[(b_e-d_e)\,t\right]}{b_e\xi - d_e + b_e(1-\xi)\exp\left[(b_e-d_e)\,t\right]}, \\ f_2(\xi,\zeta,t) &= \frac{1}{\exp\left[a+d_z\right]t}\left[\zeta\int_0^t \exp\left[a+d_z\right]\tau\left(d_z + a f_1(\xi,\zeta,\tau)\right)d\tau\right], \end{aligned} \tag{6.15}$$

for the supercritical case $b_e > d_e$.

The generating function $g_{z_0}(\xi,\zeta,t)$ for the process starting at the initial condition described above is again defined as in Eq. (6.7), now using the new functions f_1, f_2. The probability that there are y active cells at time t, written $P(y,t)$, is equal to the coefficient of ξ^y in the Taylor expansion of $g(\xi,\zeta,t)$ around $\xi = 0$, $\zeta = 1$. Repeated differentiation is computationally costly and subject to compounded rounding errors, and Cauchy's integral formula provides an effective alternative. Following [81], the probability that there are more than n active cells at time t equals

$$P(>n,t) = 1 - \frac{1}{\pi}\int_0^\pi \mathrm{Re}\left[g_{z_0}(e^{i\theta},1,t)\frac{1-e^{-i(n+1)\theta}}{1-e^{-i\theta}}\right]d\theta. \tag{6.16}$$

Let $f(\theta)$ be the real integrand in this equation, which presents damped oscillations of period $\frac{2\pi}{n+1}$, where $f\left(\frac{2k\pi}{n+1}\right) = 0$ for integers $1 \le k \le \frac{n+1}{2}$. We treat each half-period separately, defining a sequence of approximations a_k $(k = 0, 1, \ldots, n)$ where $a_k \approx \int_{k\frac{\pi}{n+1}}^{(k+1)\frac{\pi}{n+1}} f(\theta)d\theta$. Each a_k $(k > 0)$ is defined by a trapezoidal rule, splitting the interval $\left[k\frac{\pi}{n+1}, (k+1)\frac{\pi}{n+1}\right]$ into 150 equal-width segments. Since a sharp peak appears at $\theta = 0$ for certain parameter values, the value a_0 is defined using a global adaptive

numerical integration routine (quadgk in Matlab R2012b).

Not every a_k must be computed to approximate the integral. In Section 6.1.3.4.1 below, we describe an efficient method for selecting a small fraction of the a_k for computation, yielding a several hundred-fold speedup. This method is more reliable for this integral than the Euler summation approach presented in [1].

6.1.3.2.3 Estimating "target Q" for 50% probability of rebound A rough estimate of the initial reservoir size z_0 such that half of patients have rebounded at time t can be obtained directly from the generating function $g_{z_0}(\xi, \zeta, t)$ above. We used this rough estimate as an initial guess for the search algorithm described in Section 6.1.3.4.4 below to identify the target Q values in Fig. 5.4B,C.

The probability that there are no actively infected cells at time t is $g_{z_0}(0, 1, t)$. If sufficient time has passed to allow for substantial exponential growth (i.e., $e^{(b_e-d_e)t}g1$), then the integral in Eq. (6.15) is dominated by values at large τ, and so the fraction within the integral may be treated as a constant, $\frac{ad_e}{b_e}$. The probability is then

$$P(0,t) = g_{z_0}(0,1,t) \approx \exp\left[-\frac{az_0\,(1-h_1)}{d_y\,(1-h_1e^{-rt})}\right]\left[1-\frac{a}{a+d_z}\,(1-h_1)\left(1-e^{-(a+d_z)t}\right)\right]^{z_0}, \tag{6.17}$$

where the abbreviation $r = b_e - d_e$ is shorthand for the expected growth rate. If, furthermore, not so much time has passed that the reservoir may be depleted in many patients, then $\left(1-e^{-(a+d_z)t}\right) \ll 1$ and the expression can be approximated:

$$P(0,t) \approx \exp\left[-az_0\,(1-h_1)\left(t+\frac{1}{d_y}\right)\right]. \tag{6.18}$$

Note that d_z has dropped out of this estimate; the rate at which active cells become present is roughly $az_0\,(1-h_1)$.

To account for growth to the rebound threshold n, we can use a point estimate for the rebound time based on deterministic exponential growth starting at one active cell,

$t_{\text{grow}} \approx \frac{\ln(n)}{r}$. The rebound estimate then becomes

$$P(> n, t) \approx 1 - \exp\left[-az_0\,(1 - h_1)\left(t - \frac{\ln(n)}{r} + \frac{1}{d_y}\right)\right]. \tag{6.19}$$

The required initial reservoir size — and the corresponding target Q — can then be solved for, using $P(> n, t) = 1/2$ and the desired value of t. It follows from this computation that the required z_0 scales inversely with a. Since $Q \propto \log\left(\frac{1}{z_0}\right)$, the target Q scales logarithmically with a and is relatively insensitive to d_z, as observed in the main text.

6.1.3.3 Simulation of the model

We use the Gillespie algorithm to track the number of latently and actively infected cells in a continuous time stochastic process. We start with an intial number of latent cells $z_0 = 10^{-Q} M_{LR}$ and an initial number of actively infected cells y_0 chosen from a Poisson distribution with parameter $a\,10^{-Q} M_{LR}/d_y$, where M_{LR} is the pretreatment latent reservoir size (described in Section 6.1.1). The simulation proceeds until the number of actively infected cells reaches the threshold for clinical detection given by a viral load of 200 c ml^{-1} (equivalent to $y = 3 \times 10^5$ cells total). Because stochastic effects are important only for small y, we switch to a faster deterministic calculation when y reaches a level where the probability of extinction is very low. This switch occurs when the probability that no active cell currently alive establishes a growing infection, h_1^y, declines below 10^{-4}. For each Q value we perform 10^4 simulations.

6.1.3.4 Additional numerical methods

6.1.3.4.1 Approximation of the integral in Eq. (6.16) The sum $\sum_{k=0}^{n} a_k$ described following Eq. (6.16), above, was approximated using the following algorithm:

1. Compute a_k for $k = 0$ to $k = \text{InitialBlockSize} - 1$. Store the sum of these values as S.

2. Set NextK = InitialBlockSize. Set BlockSize = MinBlockSize. Set NumToCompute = MinNumToCompute.

3. While NextK $< n$, do:

   (a) Initialize A = 0, B = 0.

   (b) Split the block containing the values a_k from $k =$ NextK to $k =$ NextK + BlockSize − 1 into three sections:

      i. FirstPart contains a_k for k from NextK to NextK + NumToCompute − 1;

      ii. LastPart contains a_k for k NextK + BlockSize − NumToCompute to NextK + BlockSize − 1;

      iii. MiddlePart contains all a_k in between. *These values of a_k are not computed.*

   (c) Compute an UpperEstimate for the sum $\sum_{k=\text{NextK}}^{\text{NextK+BlockSize}-1} a_k$ by adding together all a_k in FirstPart and LastPart, and then approximating the value of each a_k in MiddlePart as the average of the *final two values* in FirstPart.

   (d) Compute a LowerEstimate for the sum similarly, except now approximating the value of each a_k in MiddlePart as the average of the *first two values* in LastPart. Since the sequence a_k decreases in an alternating manner, LowerEstimate < UpperEstimate.

   (e) If LowerEstimate and UpperEstimate are too far apart (see Notes below), increase NumToCompute by 2 and return to Step 3b. Otherwise, add the average of the two estimates to S and continue.

   (f) If NumToCompute = MinNumToCompute (indicating that the error between upper and lower estimates was never so far apart as to require increasing NumToCompute), increment A by 1; otherwise increment B by 1.

(g) Set NextK = NextK + BlockSize − 1. Reset NumToCompute to MinNumToCompute.

(h) If A ≥ 2B + NumRecentBlocks, then increase BlockSize by a multiplicative factor of BlockIncreaseFactor, rounding to the nearest even integer. Reset A = 0, B = 0.

6.1.3.4.2 Notes. LowerEstimate and UpperEstimate are required to have a difference of less than $\frac{2\pi}{n} \times 10^{-5}$ (ensuring a total error in S of under 10^{-5}), and a log-ratio of less than 0.04. The parameter BlockIncreaseFactor is itself adaptive, increasing by $0.4/(1 + 0.5 * (\text{BlockIncreaseFactor} - 1)$ immediately after Step 3h if B = 0; but decreasing by 0.4 (never dropping below 1.05) if B ≥ 1.

6.1.3.4.3 Parameters used. InitialBlockSize = 200. MinBlockSize = 40. MinNumToCompute = 6. BlockIncreaseFactor = 1.15. NumRecentBlocks = 6.

6.1.3.4.4 Binary search for Q for 50% probability of rebound The estimate in Section 6.1.3.2.3 is used as an initial guess for the post-therapy reservoir size z_0 that would produce a 50% chance of rebound. Survival probability P_{surv} was computed for this initial guess, using the method of Section 6.1.3.2.2. While P_{surv} was not within 10^{-4} of 0.5, a new guess for z_0 was made using a bisection method: If P_{surv} is too low (high), but a previously computed value was too high (low), then linear interpolation was used between the current and previous values to select a new z_0 that is estimated to have $P_{\text{surv}} = 0.5$. If P_{surv} is too low (high), but *no* previously computed value was too high (low), then the guess for z_0 was divided (multiplied) by 10. For all results reported, between 3 and 8 iterations were required to obtain the desired P_{surv}. Results were then converted to Q values for a given pre-treatment reservoir size.

6.1.4 Deterministic model of viral dynamics

A deterministic model was used for two purposes: to provide an estimate of R_0 (described in Section 6.1.2, above) and to estimate the threshold Q separating the growth-limited and activation-limited regimes. The threshold value is defined as that which equalizes the deterministic rebound time and the expected waiting time until activation of the first cell fated to establish.

6.1.4.1 Model definition

A complete model of viral dynamics including the latent reservoir is shown in the flow diagram of Fig. 6.1. All variables respresent total amounts present in the body. State variables x, y, v, and z are the number of infectable CD4$^+$T cells, the number of productively infected cells, the number of free virus particles, and the number of latently infected cells, respectively. Productively infected cells produce virus at rate k, die at rate d_y, and transition into latency at a rate γ. Virus is cleared at rate d_v. The infectivity parameter β determines the rate at which virus infects susceptible host cells. Host cell dynamics are determined by production rate θ and death rate d_x. Latently infected cells reactivate at a rate a and die at a rate d_z. When population sizes are large, this model can be described with a set of differential equations [181, 247, 269, 311]:

$$\begin{aligned}
\dot{x} &= \theta - \beta x v - d_x x \\
\dot{y} &= \beta x v - d_y y + a z - \gamma y \\
\dot{v} &= k y - d_v v \\
\dot{z} &= \gamma y - a z - d_z z
\end{aligned} \tag{6.20}$$

Here we make a number of simplifying assumptions valid for understanding dynamics leading to rebound. Because the terms k and d_v are an order of magnitude larger than other rates in the system, we can apply a separation of timescales and assume that free

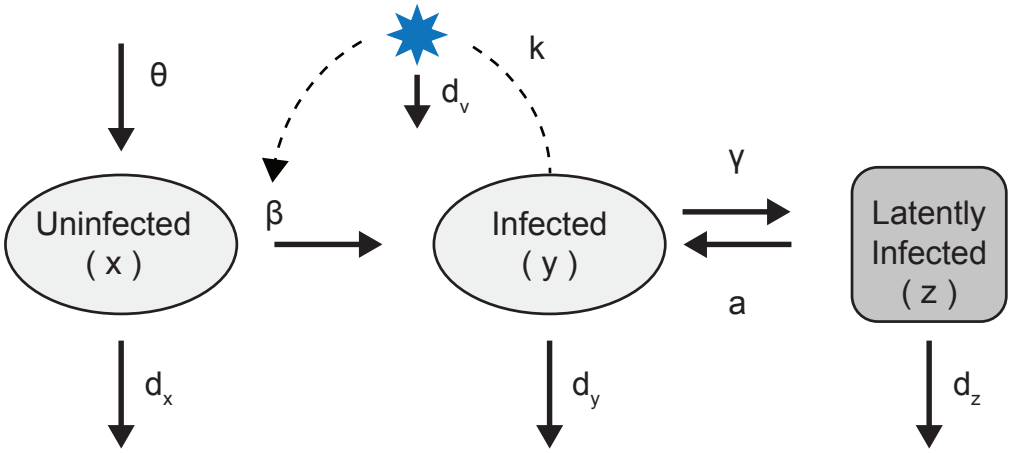

Figure 6.1: Schematic of the deterministic viral dynamics model including the latent reservoir. State variables x, y, v, and z are the number of infectable CD4$^+$T cells, the number of productively infected cells, the number of free virus particles, and the number of latently infected cells, respectively. Productively infected cells produce virus at rate k, die at rate d_y, and transition into latency at a rate γ. Virus is cleared at rate d_v. The infectivity parameter β determines the rate at which virus infects susceptible host cells. Host cell dynamics are determined by production rate θ and death rate d_x. Latently infected cells reactivate at a rate a and die at a rate d_z.

virus particle levels change so quickly that they track infected cell levels. Formally, this is accomplished by setting $\dot{v} = 0$, leading to $v = ky/d_v$ and only three differential equations. For viral loads at or below rebound levels, uninfected CD4$^+$T cells do not become limited and can be assumed to remain at their pre-infection/post-long-term-HAART steady-state level of $x = \theta/d_x$, and hence $\dot{x} = 0$. Moreover, at low viral loads, new influx into the latent reservoir can be ignored ($\gamma \approx 0$).

These assumptions lead to the reduced set of equations:

$$\begin{aligned} \dot{y} &= az + (R_0 - 1)\, d_y y \\ \dot{z} &= -\,(a + d_z)\, z, \end{aligned} \tag{6.21}$$

where R_0 is the combined viral fitness parameter $(\theta k \beta) \,/\, (d_v d_x d_y)$ describing the expected number of secondary infected cells produced by a single infected cell introduced to an uninfected host. As in the stochastic model described in Section 6.1.3, the initial conditions

(y_0, z_0) are such that z_0 is the reservoir size following LRA therapy, and — assuming that latent cell dynamics are much slower than active cell dynamics ($a + d_z \ll d_y$) — the residual active infection is $y_0 \approx az_0/d_y$.

6.1.4.2 Calculating rebound time from the deterministic model

Following HAART interruption (with or without LRA therapy), the number of infected cells (and thus viral load) grows according to Equation (6.21) with latent cells at a transiently constant value z_0. Let $y_r = ry_0$ be the infection size at which rebound is detected (e.g., ≈ 200 c ml^{-1}). The parameter r is the "rebound factor", the amount by which the infection must grow in order for rebound to be detected.

This equation can be solved exactly:

$$y(t) = y_0 \frac{R_0 e^{d_y(R_0-1)t} - 1}{R_0 - 1}, \tag{6.22}$$

giving the time to rebound as

$$t_0 = \frac{\ln\left(\frac{1+r(R_0-1)}{R_0}\right)}{d_y(R_0-1)}. \tag{6.23}$$

This equation is appropriate when cells exit the reservoir frequently (i.e. without highly effective LRA therapy). Incorporating reservoir decay negligibly changes the results because $a + d_z \ll 1$. In Section 6.1.2 above, this equation was used to calibrate R_0 based on observed rebound time t_0.

Following LRA therapy, the size of the reservoir is reduced to $10^{-Q}M_{LR}$. Let $q = 10^{-Q}$. Since the residual active infection y_0 also scales by q, the rebound factor increases to r/q. The time to rebound is now increased to

$$t_1 = \frac{\ln\left(\frac{1+(r/q)(R_0-1)}{R_0}\right)}{d_y(R_0-1)} \tag{6.24}$$

Eradication therapy therefore extends the rebound time by an amount Δt:

$$\begin{aligned}\Delta t &= t_1 - t_0 \\ &= \frac{1}{d_y(R_0-1)} \ln\left(\frac{1+(r/q)(R_0-1)}{1+r(R_0-1)}\right) \\ &\approx \frac{\ln(1/q)}{d_y(R_0-1)}\end{aligned} \tag{6.25}$$

where the approximation is valid for $r(R_0-1) >> 1$. This order relationship is very likely to hold as the rebound factor is ≈ 100 or more. The only way for the relationship to fail would be for R_0 to be in a very narrow range just above 1.

6.1.4.3 Above a threshold Q, the deterministic model disagrees with the stochastic model

Under the deterministic model, rebound time increases only logarithmically with the decrease in LR size. The stochastic model agrees with this relationship only in the *growth-limited regime*, where activation of fated-to-rebound cells is common. At higher Q, the waiting time until this activation occurs exceeds the deterministic growth time; in this *activation-limited regime*, the stochastic model predicts rebound times well in excess of those predicted by the deterministic model (Fig. 6.2). As a rough estimate, the waiting time in the stochastic model is $\frac{1}{a(1-h_1)z_0}$, where h_1 is the probability that a reactivating lineage goes extinct (defined in Equation (6.8)). The threshold drug efficacy Q_T defines the boundary between the two regimes. It can be estimated by solving numerically for the log-efficacy that sets deterministic growth time from Equation (6.24) equal to the stochastic waiting time:

$$\frac{\ln\left(\frac{1+r\,10^{Q_T}(R_0-1)}{R_0}\right)}{d_y(R_0-1)} = \frac{1}{a\,(1-h_1)\,M_{LR}\,10^{-Q_T}}. \tag{6.26}$$

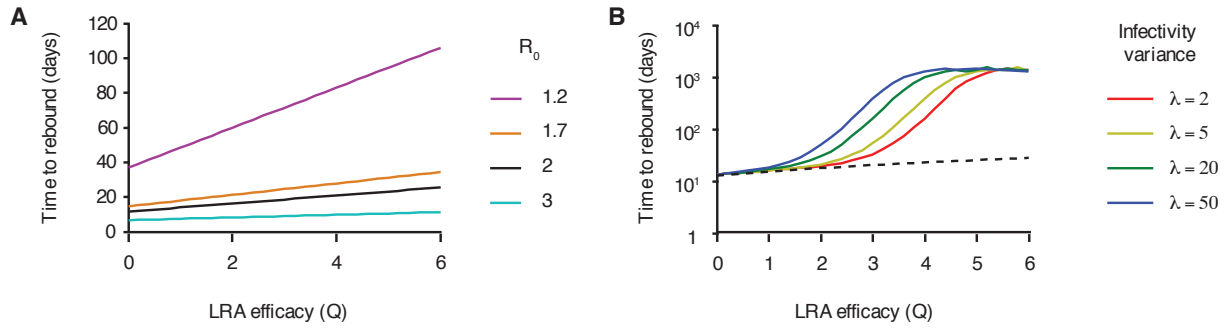

Figure 6.2: A fully deterministic model is a poor predictor of rebound times. A) Equation (6.25) was used to calculate the time to rebound for a given LRA drug efficacy, Q. The deterministic model assumes that LRA reduces the size of the reservoir and hence the residual viral load by Q orders of magnitude and then tracks the time for the viral population to grow to 200 c ml^{-1}. B) Rebound times calculated from the deterministic model for $R_0 = 2$ are compared to median rebound times calculated from the stochatic process. The models agree only for small Q. The Q values where the models diverge corresponds to the transition between the *growth-limited regime* and the *activation limited regime*.

This threshold can be observed in the upward inflection in the rebound time curves in Figs. 5.3C and 6.2 occurring at $Q \approx 1 - 2$.

Fig. 6.5 shows that Q_T increases with pretreatment reservoir size M_{LR} and decreases with variance parameter λ, since higher values of λ increase the extinction probability h_1. For pretreatment reservoir size $M_{LR} = 10^6$, reduction of approximately 30- to 1,000-fold is required to reach the activation-limited regime, in which substantial increases in rebound time may be achieved.

6.1.5 Viremia during adminstration of LRA therapy

If LRA therapy reduces reservoir size by inducing activation of latently infected cells, then an increase in viral load during therapy can be expected. The precise dynamics of viral load during LRA therapy depend on the efficacy and duration of therapy. To model these dynamics, we assume LRA therapy is administered continuously for a period of time τ (ignoring pharmacokinetics) and increases the reactivation rate of latently infected cells. During this time HAART is co-administered, and we assume no new infections can occur.

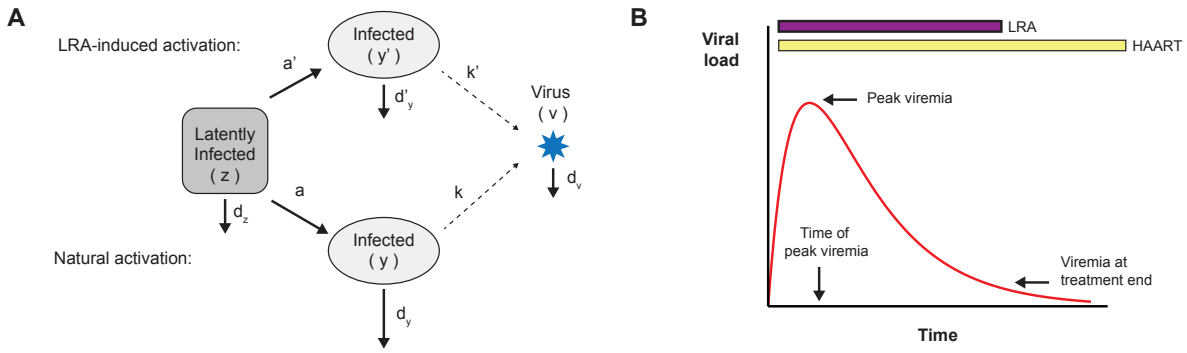

Figure 6.3: Schematic of viral dynamics during LRA therapy. (A) The model tracks latently infected cells, actively infected cells, and free virus, distinguishing between cells in which HIV-1 transcription is reactivated by LRA (y') or naturally (y). (B) Illustration of typical viral load dynamics during course of LRA therapy. LRA therapy increases the reactivation rate of cells from the LR, causing residual viral load to increase. The timing and magnitude of this peak allow for an estimation of the efficacy Q. We assume that HAART is administered for a short while beyond the end point of LRA therapy, preventing the reactivated cells from starting new infections. All symbols are defined in the text.

Since transcription at the HIV-1 LTR may be reactivated in resting CD4$^+$ T cells while the cell otherwise retains a resting phenotype, cellular functions in these LRA-activated cells may proceed at a slower rate [315]. We therefore track those cells reactivated by LRA separately from those reactivated normally by antigenic stimulus.

The model we use to consider this scenario is shown schematically in Fig. 6.3A and described formally in the next section. Since our goal is to track viral load during a period when HAART is administered, we consider all cells capable of producing virions, regardless of replication capability. As this collection of resting cells likely exceeds the LR by an order of magnitude or more (f_V versus f_{LR}, Fig. 5.2), and since therapy increases activation rate, large numbers of cells can be assumed to activate daily, and a deterministic model similar to the one presented in Section 6.1.4, above, suffices. Latent cells (z) die at a rate d_z and can be reactivated naturally (a) or by LRA-induced mechanisms (a'). Naturally reactivated cells (y) die at rate d_y, and LRA-reactivated cells (y') die at rate d'_y (which may be lower than d_y) [315]. Free virus is produced at a rate k from naturally reactivated cells and a rate k' from LRA-reactivated cells. Since induced cells may have smaller burst sizes [316], k'

may be less than k.

We use this model to relate change in residual viremia over time to the log-efficacy of LRA therapy, Q. Define $\alpha_z = a + a' + d_z$, the total rate at which z decays during treatment. Assuming that this decay affects latent cells regardless of whether the proviral sequence is able to replicate, the fraction of the latent reservoir that remains after treatment duration τ is $q = e^{-\alpha_z \tau}$. Log-efficacy of therapy is $Q = log_{10}(q)$, resulting in the relationship $\alpha_z = \ln(10) \cdot Q/\tau$. Viral load approximately follows a biexponential curve, generally reaching a peak quickly (time determined by the faster of the two rates α_z and d'_y) and then decaying slowly (at the slower of the two rates) (Fig. 6.3B).

The height of this peak and the time after treatment initiation at which it occurs are

$$\begin{aligned} v(t_{max}) &\approx w_0 \frac{k'}{k} \frac{a'}{a} \frac{d_y}{d'_y} \\ &\approx w_0 \frac{k'}{k} \frac{d_y}{d'_y} \frac{ln(10) * Q}{a\tau}, \end{aligned} \tag{6.27}$$

$$t_{max} = \frac{ln(d'_y) - ln(\alpha_z)}{d'_y - \alpha_z}, \tag{6.28}$$

where $w_0 \approx 2$ c ml^{-1} is the residual viral load (not necessarily infectious) before LRA therapy. This peak is reached before treatment ends if $\tau > 1/d'_y$ and $Q > \frac{1}{\ln(10)} \approx 0.43$. Derivations for these results are provided in the next section, and examples for selected treatment parameters are provied in Table ??. Even mildly effective therapy ($Q = 1$) can result in large increases in residual viremia from the baseline level, appearing after a few days of treatment. Viremia is lower if the same reservoir reduction Q is achieved over a longer treatment time τ. Viremia is also decreased if LRA-induced cells have a lower burst rate than normally activated cells ($k'/k < 1$). If LRA-induced cells have a longer lifespan ($d_y/d'_y > 1$), then peak viremia increases but is delayed.

In vivo estimates of LRA therapy efficacy may be obtained from measurement of viral load during therapy. Highly effective therapy is predicted to result in large, observable

Table 6.2: The timing and size of peak viremia, as well as viremia at treatment end, depend on the efficacy and duration of LRA therapy, the change in burst size, and the change in infected cell lifespan. Therapy protocol is described in the text and illustrated in Fig. 6.3. Time to peak viremia was calculated using Eq. 6.28. Peak viremia was calculated using Eq. 6.34, of which Eq. 6.27 is an approximation. Symbol definitions are provided in the text. Parameters used: $a = 7 \times 10^{-5}$ day^{-1}, $d_z = 4.6 \times 10^{-4}$ day^{-1}, $z_0 = M_v = 43 \times 10^6$ cells, $d_y = 1$ day^{-1}, and $w_0 = 2$ c ml^{-1} (implying $\frac{k}{d_v} = \frac{1}{1500}$ c ml^{-1} cell^{-1}).

Log-efficacy LRA (Q)	Treatment time (τ) (days)	Fold increase in burst size (k'/k)	Fold increase in lifespan (d_y/d'_y)	Time to peak (days)	Peak viremia (c ml^{-1})	Viremia at treatment end (c ml^{-1})
1	15	1	1	2	3×10^3	500
1	60	1	1	3	10^3	100
1	180	1	1	4	300	30
1	180	0.1	1	4	30	4
2	15	1	1	2	5×10^3	100
2	16	1	1	2	5×10^3	100
2	180	1	1	4	700	7
4	15	1	1	1	8×10^3	5
4	15	1	10	4	2×10^4	8×10^3
4	15	0.1	1	1	800	< 2
4	15	0.1	10	4	2×10^3	800
4	60	1	1	2	3×10^3	< 2
4	180	1	1	3	10^3	< 2

increases in residual viremia during continuous administration (Table ??). It is important to note that this conclusion applies only to forms of LRA that reactivate latently infected cells without damaging viral production in these cells.

6.1.5.1 Detailed calculations

We extend Equations 6.20 and 6.21, tracking latently infected cells z, productively infected cells reactivated naturally y, productively infected cells reactivated by LRA therapy y', and

free virus v:

$$\begin{aligned}
\dot{z} &= -(a+a')z - d_z z \\
\dot{y} &= az - d_y y \\
\dot{y'} &= a'z - d'_y y' \\
\dot{v} &= ky + k'y' - d_v v
\end{aligned} \tag{6.29}$$

These equations incorporate the simplifying assumptions that fully effective HAART yields $R_0 = 0$, that uninfected CD4$^+$T cells do not become limited and remain at their pre-infection/post-long-term-HAART steady state level, and that new influx into the LR can be ignored.

Using the separation of timescale for virus dynamics (v) and the initial conditions $z(0) = z_0$, $y(0) = az_0/d_y$, $y'(0) = 0$, these equations can be solved:

$$\begin{aligned}
z(t) &= z_0 e^{-\alpha_z t} \\
y(t) &= \frac{az_0}{d_y - \alpha_z}(e^{-\alpha_z t} - e^{-d_y t}) + \frac{az_0}{d_y} e^{-d_y t} \\
y'(t) &= \frac{a'z_0}{d'_y - \alpha_z}(e^{-\alpha_z t} - e^{-d'_y t}) \\
v(t) &= \frac{ky(t) + k'y'(t)}{d_v},
\end{aligned} \tag{6.30}$$

where $\alpha_z = a + a' + d_z$. Note that the timescale separation for $v(t)$ is based on the assumption that k, k', and d_v greatly exceed other rates, which may be violated if LRA-reactivated cells have much smaller burst rate k' and/or much higher death rate d'_y than normally reactivated cells. In general this approximation may only slightly overestimate viremia on the first day after LRA is started.

The amount by which LRA therapy increases the reactivation rate (a') can be related to the fraction to which the reservoir is reduced (q), or equivalently, to the log-efficacy

$Q = log_{10}(q)$, after a treatment time τ:

$$\begin{aligned} z(\tau) &= z_0 e^{-\alpha_z \tau} \\ &= q z_0, \end{aligned} \tag{6.31}$$

and so the reactivation rate is:

$$\begin{aligned} \alpha_z &= \frac{-ln(q)}{\tau} - (a + d_z) \\ &= \frac{ln(10) \cdot Q}{\tau} \end{aligned} \tag{6.32}$$

Note that some natural activation and cell death contribute to Q, so that the absence of treatment does not correspond to $Q = 0$ but to $Q = log_{10}(e)(a + d_z)\tau$, which is generally small.

From these equations, we can determine the expected changes in residual viral load over time during LRA therapy. The contribution to residual viremia from naturally activating cells (initially $w_0 = 2$ c ml^{-1}) only decreases during treatment, as the reservoir is depleted. If any increases in observable residual viremia occur in response to LRAs, it will come from compartment y' activated by the drug. This contribution follows a biexponential curve, increasing to peak value quickly (at roughly the smaller of the two times $1/d'_y$, $1/\alpha_z$ days), then decaying more gradually to zero (at the smaller of the two rates d'_y, α_z per day).

We can calculate precisely the time of the peak in residual viremia due to contributions from newly reactivated cells :

$$t_{max} = \frac{ln(d'_y) - ln(\alpha_z)}{d'_y - \alpha_z}. \tag{6.33}$$

The viral load at this peak is:

$$\begin{aligned} v(t_{max}) &= \frac{k'a'z_0}{d_v d'_y} u^{\frac{u}{1-u}} \\ &= \frac{k'a'}{d_v a}\frac{d_y}{d'_y} y_0 u^{\frac{u}{1-u}} \\ &= w_0 \frac{k'}{k}\frac{a'}{a}\frac{d_y}{d'_y} u^{\frac{u}{1-u}} \\ &\approx w_0 \frac{k'}{k}\frac{a'}{a}\frac{d_y}{d'_y} \\ &\approx w_0 \frac{k'}{k}\frac{d_y}{d'_y}\frac{ln(10)\cdot Q}{a\tau}, \end{aligned} \tag{6.34}$$

where $w_0 = ky_0/d_v$ is the residual viral load before LRA therapy and $u = \alpha_z/d'_y$. The first approximation holds when u is small (if Q/τ is small compared to d'_y), and the second holds when $a + d_z \ll a'$ (Q/τ is large compared to $a + d_z$). The peak viral load occurs during treatment when $t_{max} < \tau$, which holds if and only if both $\tau d'_y > 1$ and $\ln(10) \cdot Q > \tau d'_y$, which places requirements on both treatment time ($\tau > 1/d'_y$) and treatment strength ($Q > \frac{1}{\ln(10)} \approx 0.43$). When LRA is started, viral load approaches the peak linearly with an initial slope of $a'z_0$. Viremia at the end of treatment can be found by substituting in τ for t in Eq. (6.30).

6.2 Supplementary Figures

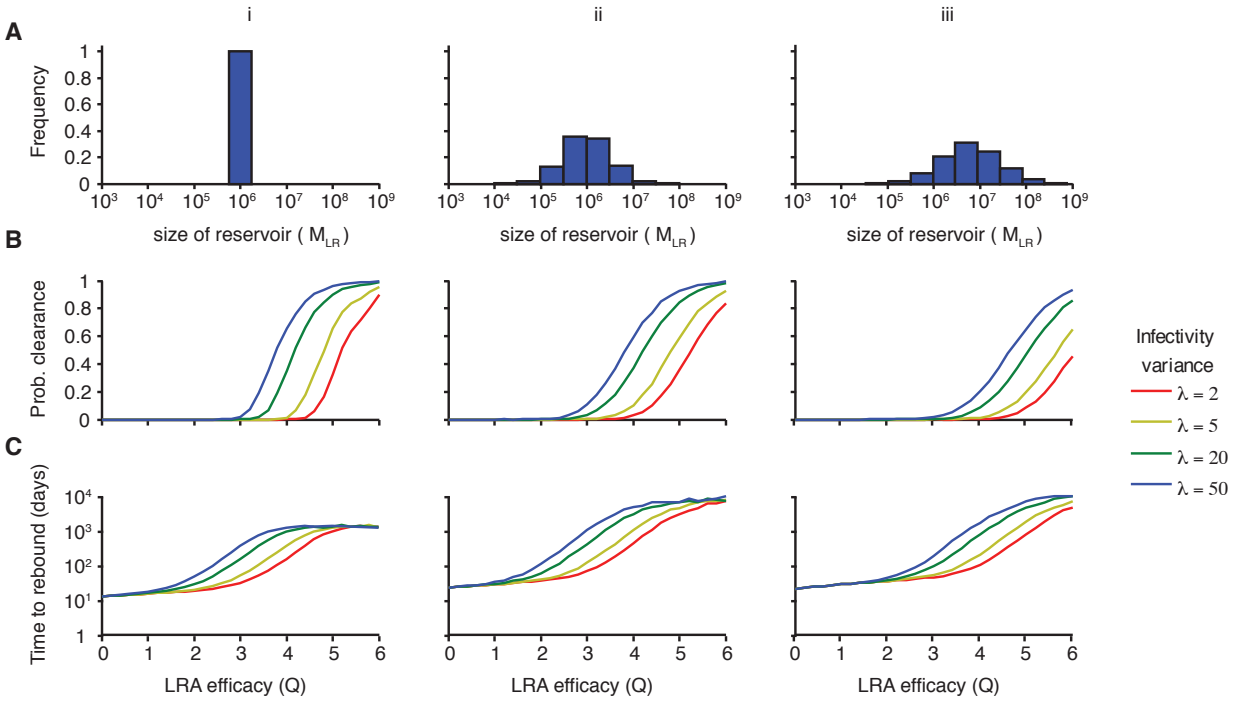

Figure 6.4: Clearance probabilities and rebound times following LRA therapy predicted from model, versus infectivity variance λ. A) Three cases for the population-level distribution of LR size (see Section 6.1.1). Case i) All patients have the same latent reservoir size, $M_{LR} = 10^6$, estimated from the geometric mean number of cells that are capable of producing infection in laboratory co-culture assays. Case ii) Latent reservoir size is distributed according to variation observed in co-culture assays, with geometric mean 10^6. Case iii) The latent reservoir includes many cells that fail to be detected in co-culture but have intact viral genomes. B) Probability that the reservoir is cleared by LRA. Clearance occurs if all cells in the reservoir die before a re-activating lineage leads to viral rebound. C) Median viral rebound times, among patients who do not have clearance. Each point shows the average of $10^4 - 10^5$ simulated patients. D) Survival curves for patients following LRA therapy. The percentage of patients who have not yet experienced viral rebound is plotted as a function of the time after LRA therapy and interruption of HAART. Curves are colored based on the efficacy of LRA in reducing the size of the LR ($Q = 0$ to 6, see legend). Results are shown for $10^4 - 10^5$ patients, a half-life of 44 months, $R_0 = 2$, and $a = 7 \times 10^{-5}$ day^{-1}.

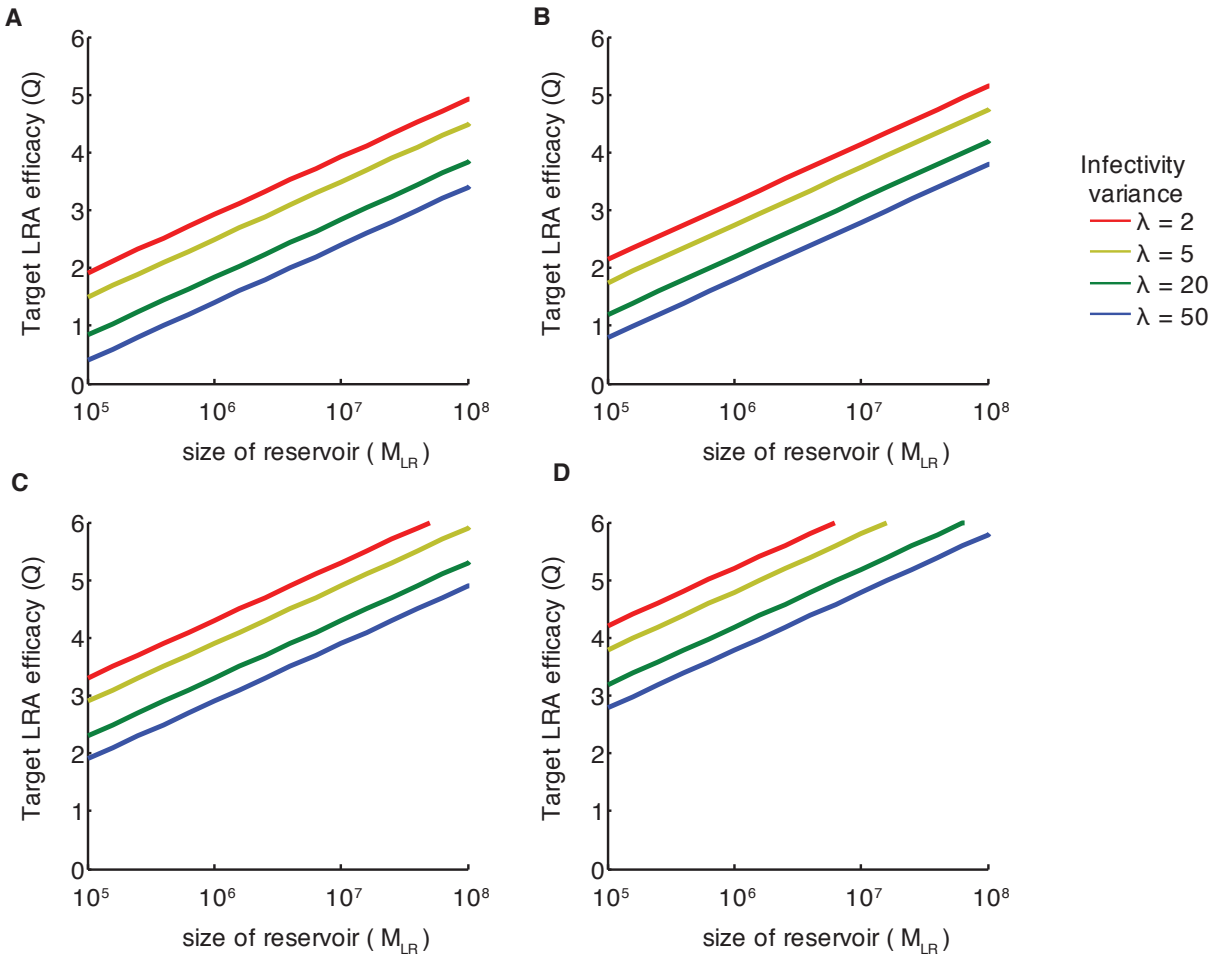

Figure 6.5: LRA therapy efficacies required for different goals, plotted versus reservoir size M_{LR} for different infectivity variances λ. A) The threshold Q that takes the patient into the activation-limited regime, where stochastic waiting time contributes substantially to rebound time (defined in Sec. 6.1.4.3). B) The target efficacy Q at which at least 50% of patients still have suppressed viral load one month after treatment interruption. C) The target efficacy Q at which at least 50% of patients still have suppressed viral load one year after treatment interruption. D) The target efficacy Q at which at least 50% of patients have eradicated the reservoir without experiencing viral rebound. Because some patients may go for a year without rebound but then rebound later, the target Q for one year off therapy is always less than that for a lifetime off therapy. Results are shown for $10^4 - 10^5$ patients, a half-life of 44 months, $R_0 = 2$, and $a = 7 \times 10^{-5}$ day^{-1}.

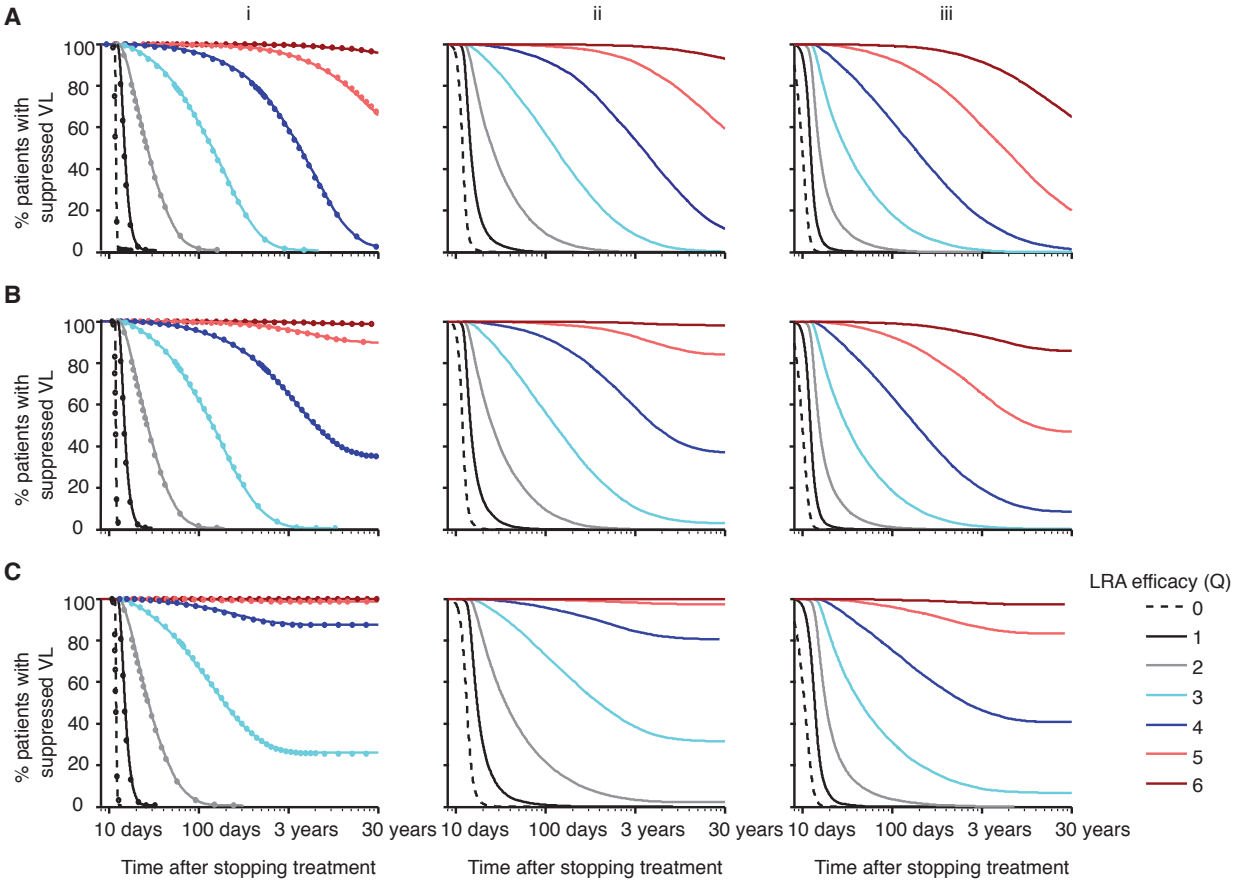

Figure 6.6: Survival curves for patients following LRA therapy depend on the size of the latent reservoir and the reservoir half-life (varying d_z).The percentage of patients who have not yet experienced viral rebound (viral load > 200 c ml^{-1}) is plotted as a function of the time after LRA therapy and interruption of HAART. Curves are colored based on the efficacy of LRA in reducing the size of the LR ($Q = 0$ to 6, see legend). A) $d_z = 0$ day^{-1}, half-life is 330 months (27 years). B) $d_z = 4.6 \times 10^{-4}$ day^{-1}, half-life is 44 months. C) $d_z = 4 \times 10^{-3}$ day^{-1}, half-life is 6 months. Decreasing the LR half-life (increasing d_z) makes survival times longer and clearance more likely. Including interpatient variation (ii) makes the survival curves fall off more gradually, while allowing for higher reservoir sizes (iii) increases the required drug efficacy. Solid lines represent simulations, and open circles represent approximations from a branching process calculation (Section 6.1.3.2.2). Results are shown for $10^4 - 10^5$ patients, $\lambda = 20$, $R_0 = 2$, and $a = 7 \times 10^{-5}$ day^{-1}

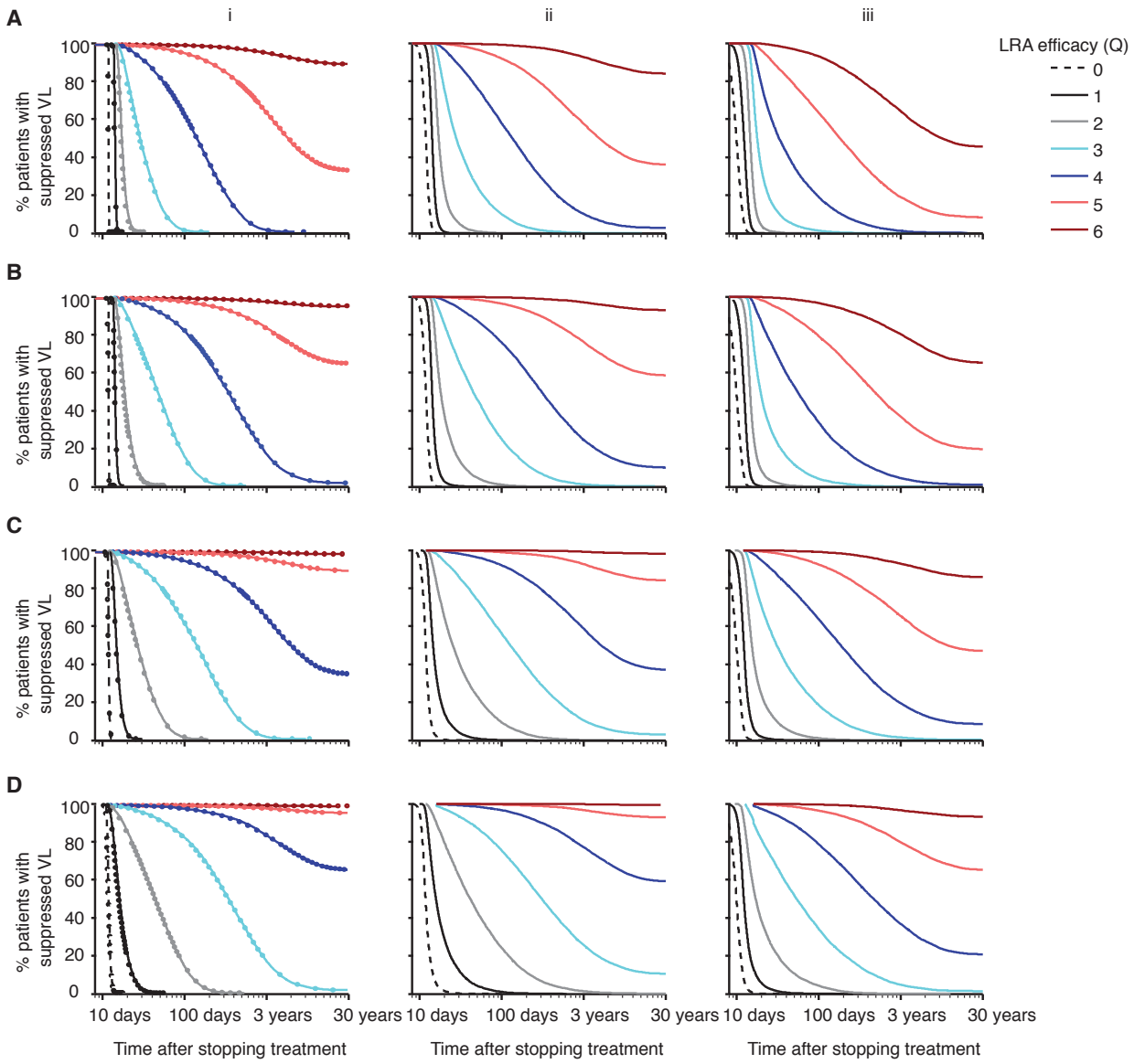

Figure 6.7: Survival curves for patients following LRA therapy depend on the size of the latent reservoir and the infectivity variance λ. The percentage of patients who have not yet experienced viral rebound (viral load $>$ 200 c ml^{-1}) is plotted as a function of the time after LRA therapy and interruption of HAART. Curves are colored based on the efficacy of LRA in reducing the size of the LR ($Q = 0$ to 6, see legend). Increasing the infectivity variance λ makes survival times longer and clearance more likely. Including interpatient variation (ii) makes the survival curves fall off more gradually, while allowing for higher reservoir sizes (iii) increases the required drug efficacy. Solid lines represent simulations, and open circles represent approximations from a branching process calculation (Section 6.1.3.2.2). Results are shown for a half-life of 44 months, $R_0 = 2$, and $a = 7 \times 10^{-5}$ day^{-1}.

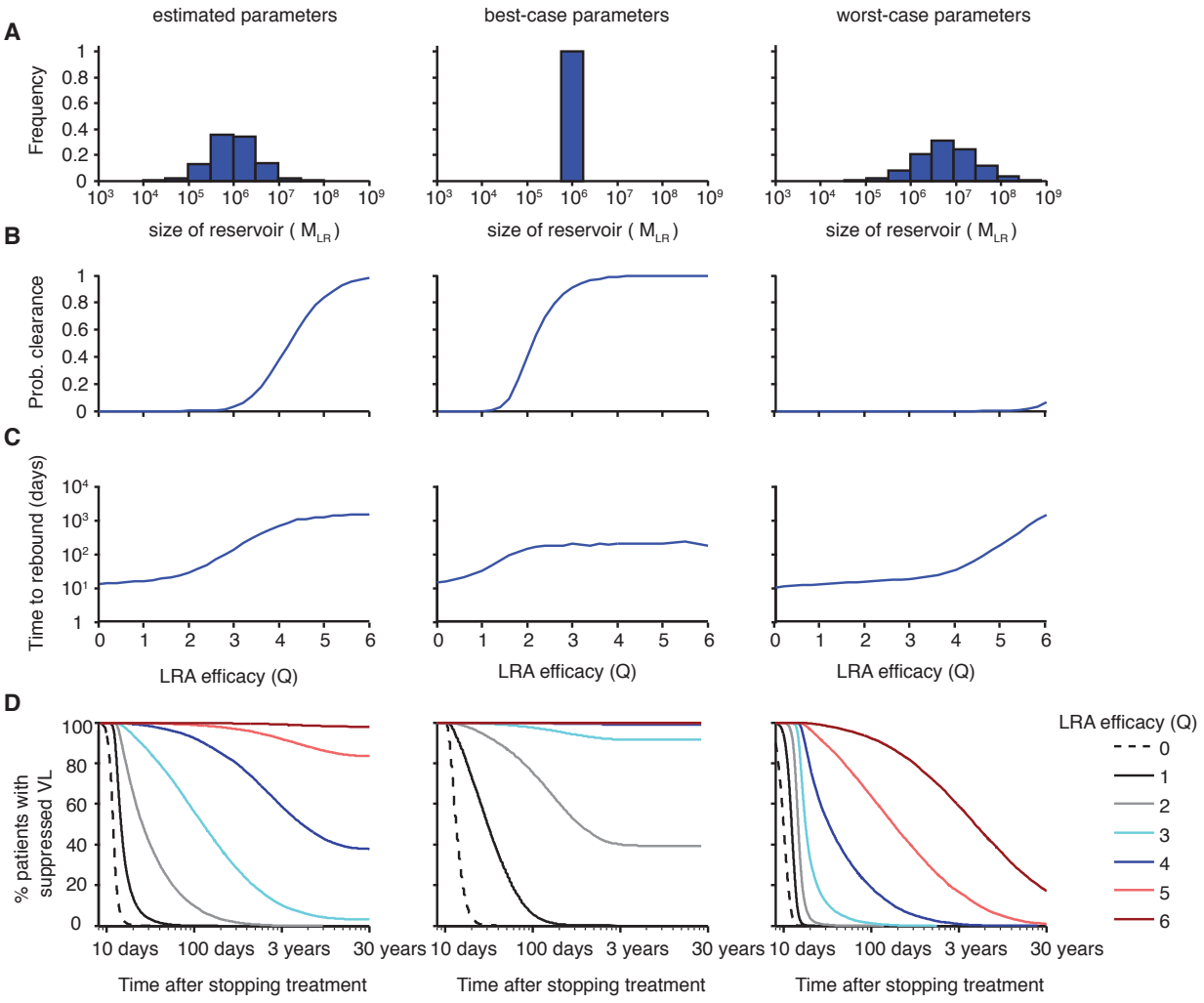

Figure 6.8: Clearance probabilities and rebound times after LRA predicted from model for alternate parameter choices. i) Best-estimate parameter values shown in the main text: reservoir size is predicted by the distribution of co-culture results (case ii), $a = 7 \times 10^{-5}$ day^{-1}, $d_z = 4.3 \times 10^{-4}$ day^{-1} (half-life of 44 months), $R_0 = 2$. ii) Best-case-scenario, where reservoir size is predicted by mean co-culture results (case i), half-life is short and strong stochastic effects decrease clearance probability. Parameter values are $a = 10^{-5}$ day^{-1}, $d_z = 4 \times 10^{-3}$ day^{-1} (half-life 6 months), $R_0 = 2.2$, $\lambda = 50$, and $M_{LR} = 10^6$. This low estimate for a follows from the assumption that all cells with HIV-DNA contribue to the residual viral load observed during HAART. iii) Worst-case-scenario, when LR is large (case iii), cells reactivate frequently, are extremely long lived, and smaller stochastic effects mean most reactivating cells lead to rebound. Parameter values are $a = 7 \times 10^{-5}$ day^{-1}, $d_z = 0$ day^{-1}, $R_0 = 2$, $\lambda = 2$, median $M_{LR} \approx 7 \times 10^6$. This high estimate for a follows from the assumption that all virions in the residual viral load come from cells with virus with intact provirus. The lower limit on d_z is realized if homeostatic proliferation or other mechanisms balance reservoir decay caused by mechanisms other than reactivation. R_0 is always adjusted to ensure that the baseline rebound time following HAART interruption was constant. All results are for $10^4 - 10^6$ simulated patients.

7

Infectious disease modeling of social contagion in networks

7.1 Abstract

Many behavioral phenomena have been found to spread interpersonally through social networks, in a manner similar to infectious diseases. An important difference between social contagion and traditional infectious diseases, however, is that behavioral phenomena can be acquired by non-social mechanisms as well as through social transmission. We introduce a novel theoretical framework for studying these phenomena (the SISa model) by adapting a classic disease model to include the possibility for 'automatic' (or 'spontaneous') non-social infection. We provide an example of the use of this framework by examining the spread of obesity in the Framingham Heart Study Network. The interaction assumptions of the model are validated using longitudinal network transmission data. We find that the current rate of becoming obese is 2% per year and increases by 0.5 percentage points for each obese social contact. The rate of recovering from obesity is 4% per year, and does not depend on the number of non-obese contacts. The model predicts a long-term obesity prevalence of

approximately 42%, and can be used to evaluate the effect of different interventions on steady-state obesity. Model predictions quantitatively reproduce the actual historical time course for the prevalence of obesity. We find that since the 1970s, the rate of recovery from obesity has remained relatively constant, while the rates of both spontaneous infection and transmission have steadily increased over time. This suggests that the obesity epidemic may be driven by increasing rates of becoming obese, both spontaneously and transmissively, rather than by decreasing rates of losing weight. A key feature of the SISa model is its ability to characterize the relative importance of social transmission by quantitatively comparing rates of spontaneous versus contagious infection. It provides a theoretical framework for studying the interpersonal spread of any state that may also arise spontaneously, such as emotions, behaviors, health states, ideas or diseases with reservoirs.

7.2 Introduction

Social network effects are of great importance for understanding human behavior. People interact with a varying number of individuals and with some individuals more than others, and this affects behavior in fundamental ways. Sociologists have long studied social influence through networks, and networks now routinely appear in investigations from other fields, including economics[155], physics[362], public health[209] and scientific publishing [35, 369]. Extensive reviews of social networks analysis, including investigations of their structure and their effect on social dynamics, include Mitchell[225], Wasserman[360],Watts[362], Rogers[291], Jackson[155], and Smith[333]. Networks have also long been known to be important in many areas of biology (reviewed by [216]), including ecological food webs and the evolution of cooperation[202, 243, 252, 345]. Social networks have also been studied as determinants of health (reviewed by Smith [333]), ranging from determining the patterns of infectious disease spread [176] to the propagation of phenomena such as emotions [55, 111, 142], smoking cessation [69] , obesity [68], suicide [31], altruism[112], anti-social behavior [284], and online health forum participation [61].

These studies suggest that on top of the physical environment, the social environment can also be an important contributor to health. They have lead to suggestions that public health interventions must be designed that work with the network structure and that the network can be exploited to spread health related information[70, 333].

Within network studies, much work has focused on how information, trends, behaviors and other entities spread between the individuals in social networks. These processes are generally referred to as 'contagion'. Such suggestions of contagious dynamics and the possible relevance of network structure can be rigorously examined using mathematical models of contagious processes. These can then be used to obtain accurate measures of expected prevalences, interventional efficacy, and optimized information flow. Many previous models have been proposed to study influential interactions between individuals. Most of these have considered well-mixed populations, although more recent work has focused on network-structured populations. The most well studied are classic epidemiological models (like SIS and SIR) for the spread of microbial infectious diseases [10], including spread in network-structured populations [22, 175, 219, 363], [266], [176]. Various related processes have been used to model social influence, with important contributions including the same epidemiological models [86, 123], diffusion models [29, 45, 208, 211, 224, 291], statistical mechanics type interactions [21, 58], and threshold models[361](reviewed by Jackson [155] and Newman et al.[236]).

Each of these models, however, has one or more properties that are problematic for studying social contagion. Many do not capture the probabilistic nature of contagion, or the asymmetry inherent in traditional infectious disease (where the infected state spreads through social contagion whereas the non-infected state does not). Others only consider well-mixed populations, where everyone is influenced by everyone else, ignoring the effect of network structure. Most models inspired by epidemiology are not directly applicable to the social spread of other phenomenon, because many phenomena that spread by social contagion may also arise spontaneously. That is, it is possible to adopt a trend or behavior,

or obtain information, from an outside source, without directly 'catching' it from a contact in the network. In other words, on top of the probability of obtaining the infection from each infected contact, there is also a non-zero probability of 'automatically' obtaining the infection, independent of the local network. This 'automatic' non-social infection is not included in traditional infectious disease models. Economic models for the diffusion of innovations, based on early work by Bass [29], do take into account 'automatic' infection. Individuals move from 'susceptible' (non-adopter) to an infected (adopter) state by adopting a new product or idea, influenced by both social and non-social factors. However, these models do not allow for recovery; because the innovation adoptions are assumed to be permanent changes in behavior, individuals never move back to a susceptible state. This results in the entire population becoming adopters at equilibrium. This does not reflect the dynamics of many phenomena that spread socially, which may be repeatedly acquired and lost (for example, happiness or obesity). Through a balance of infection and recovery, a steady-state with multiple states of individuals coexisting can be reached. Finally, most previous models make assumptions about the type of interaction between individuals, the particulars of which are not usually validated with real data. Yet, long term behavior of a model and the prevention strategies it suggests can depend critically on the specifics of the interaction assumptions.

Here, we introduce a new model to study the spread of entities in a social network which has all of the important properties listed above. We then analyze its characteristics and show how it can be applied in different contexts. This model is an extension of the classical infectious disease model, combining features from other models mentioned above. It describes infections that can be contracted both spontaneously and through social (network-structured) transmission, and allows for recovery from infection. As an example, we focus on the spread of obesity in the Framingham Heart Study (FHS) network. The interaction assumptions of the model will be validated using longitudinal network transmission data. We show how we can quantitatively assess the values for the rate of

adopting a trend spontaneously versus by contagion to determine the extent to which social transmission is important. We use it to predict prevalences and intervention effectiveness (i.e. get quantitative output, not just qualitative behavior). The results of this model are very different from models with other interaction assumptions, such as the 'majority rules' models. We will show that transmissive components are often small compared to the automatic component, but may still contribute materially to prevalence levels. Lastly, we will use pair-wise approximations to generate analytic results for infections in network-structured populations, as well as presenting simulations using a real social network.

7.3 Methods

7.3.1 Classic infectious disease modeling

In the simplest infectious disease models [10], individuals are classified as occupying one of two states: 'susceptible', meaning they do not have the disease, and 'infected', meaning they do have the disease. The disease can be transmitted to a susceptible person when they come into contact with an infected person. The rate of this disease transmission from infected to susceptible is defined as β, the *transmission rate*. Once an individual is infected, they recover from the disease at a constant rate g, regardless of their contacts with susceptibles or infecteds. In one class of disease models (susceptible-infected-recovered, or SIR), recovered individuals become immune to further infection and enter a 'recovered' state. However, behaviors, trends, health states, etc, can occur many times over an individual's life, and therefore we assume infected individuals return to the susceptible state after recovering. This form of susceptible-infected-susceptible (SIS) model is used to model infectious diseases that do not confer immunity, like many STDs.

7.3.2 Application to social contagion

In the standard SIS model, infection can only be transmitted by having a contact between an infected and a susceptible individual. Social 'infections', however, can also arise due to spontaneous factors other than transmission. Therefore, we extend the SIS model by adding a term whereby uninfected individuals spontaneously (or 'automatically') become infected at a constant rate a, independent of infected contacts. A diagrammatic representation of our modified SIS model, which we will call SISa, is shown in Figure 7.1. The corresponding differential equations for a well-mixed population are described in Eq. 7.1

$$\begin{aligned} dI/dt &= \beta SI - gI + aS \\ dS/dt &= -\beta SI + gI - aS \\ I + S &= N \end{aligned} \tag{7.1}$$

where I is the number of infected individuals, S is the number of susceptible individuals, N is the population size, β is the transmission rate, g is the recovery rate, and a is the rate of spontaneous infection. This model assumes a constant population size and neglects birth and death. The SISa model is related to infectious disease models with 'imports' (migration of infecteds into the population), although here the rate of spontaneous infection is proportional to the number of susceptibles, while in import models it is a constant or proportional to the total population size.

In the infectious disease literature, a disease is said to be 'endemic' if a stable, non-zero fraction of the population is infected at steady state. If a single infected individual is introduced to a totally susceptible population, then the average number of secondary infections they cause before recovery is called the *basic reproductive ratio*, R_0. For the regular SIS model in a well-mixed population of N individuals, $R_0 = \beta N/g$. An epidemic,

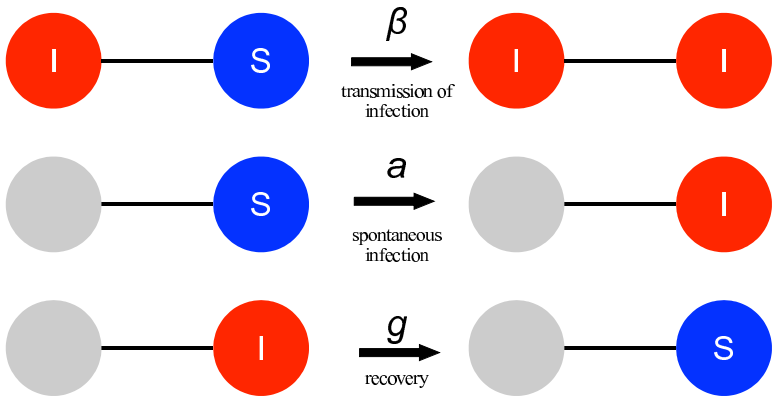

Figure 7.1: The SISa model of infection. There are three processes by which an individual's state can change. (i) An infected individual transmits infection to a susceptible contact with rate β. (ii) A susceptible individual spontaneously becomes infected at rate a, regardless of the state of their contacts. (iii) An infected individual returns to being susceptible at rate g, independent of the state of their contacts.

leading to an endemic equilibrium, only occurs for $R_0 > 1$, and hence R_0 is a fundamental quantity used to describe and compare infectious diseases. For the SISa model, an epidemic occurs for all parameter values, due to the spontaneous infection term. Thus, social behaviors that can be adopted independently of neighbors mean that there is no longer a threshold for the behavior to become prevalent in a population, and even in the absence of contagion there would be a non-zero steady state prevalence. Because of this, there is not an obvious definition for R_0 in the SISa model. The steady state fraction of infected individuals in a well-mixed population is given by Eq. 7.2.

$$\frac{I^*}{N} = \frac{1}{2}(1 - \frac{a+g}{\beta N} + \sqrt{(1 - \frac{a+g}{\beta N})^2 + \frac{4a}{\beta N}}) \tag{7.2}$$

7.3.3 Infectious diseases on networks

Traditional models of infection assume that the population is well-mixed. However, this assumption is unrealistic for many diseases, and also for the social spread of trends and behaviors. To account for the population structure, the infectious process can be

constrained to take place on a social network. An infected individual can only pass their infection on to the suspectibles to whom they are connected. Properties of the infectious process thus depend on both the epidemiological parameters and the network structure, and there are often no longer simple analytic formulas to describe the reproductive ratio or steady state level of infection. For example, a property of disease spread on networks are *spatial correlations* (in the network sense) that arise between individuals in the same state. This correlation is defined as the ratio of the observed number of connections between two types of individuals to the number of connections expected if the positioning of individuals in the network was random. Spatial correlations of like individuals can be caused by an infective process spreading within a network [175], but may also be caused by confounding environmental factors which similarly influence the behavior of connected individuals, or the formation of contacts based on similar behavior (also called homophily). For a network of N individuals with a total of E connections between them, the correlation between two states X and Y is defined by:

$$\begin{aligned} C_{XY} &= \frac{\text{observed number of X-Y edges}}{\text{expected number of X-Y edges}} \\ &= \frac{[XY]}{E * X * Y/N^2} \end{aligned} \tag{7.3}$$

The correlation between infected individuals, C_{II}, rises above one as the epidemic proceeds, due to cluster formation as infected individuals transmit to their contacts. Similarly, the correlation between infected and susceptible individuals, C_{SI}, drops below one. The deviation of these correlations from 1 increases with (i) the ratio of transmissive infection (β) to spontaneous infection (a) in our model (there are no correlations without a transmissive component), and (ii) the inter-connectivity (transitivity) of the network. As a result of these spatial correlations, diseases on networks can progress more slowly than their well-mixed counterparts, leading to lower basic reproductive ratios. However, heterogeneity in the number of contacts per individual acts to increase R_0. For two

networks with the same average degree, if one has a larger variance in degree, then R_0 will be increased. Thus, it is possible for diseases on networks to have lower (or nonexistent) thresholds for endemic epidemics.

7.3.4 Approximate pair-wise equations

There are no analytic methods to solve SIS-type dynamics on arbitrary networks without making approximations. Thus, simulations are a more accurate tool to explore theoretical disease dynamics in structured populations without making simplifying assumptions about the network structure. For scaled, well-mixed populations, the formulas given in the previous sections for R_0 and I^* are good approximations if N is replaced with n, the average contacts at a given time, while fixed networks, especially if non-uniform and highly inter-connected, can deviate from these values significantly. We can use a pair-wise approximation [99, 175, 283] to formulate the infectious process on a network structure in terms of differential equations. The fundamental variables are numbers of individuals of each type, and also the pairs of individuals, [XY] (where the edges are not directional). Because [XY]=[YX], and the total individuals and total edges is constant, the system can be reduced to three equations.

$$\begin{aligned}
[\dot{I}] &= \beta[SI] + a[S] - g[I] \\
[\dot{II}] &= 2\beta([ISI] + [SI]) + 2a[SI] - 2g[II] \\
[\dot{SI}] &= \beta([SSI] - [SI] - [ISI]) + a([SS] - [SI]) + g([II] - [SI])
\end{aligned} \tag{7.4}$$

Here [XYZ] represents the number of situations where and X individual is connected to a Y individual who in turn is connected to a Z individual. We can approximate all these triples in terms of pairs, using a moment closure approximation ([283], §7.6), which then

reduces the number of variables to three also. Then these equations can be simplified to

$$\begin{aligned}
\dot{f_I} &= \beta n f_{SI} + a - (a+g) f_I \\
\dot{f_{II}} &= 2\beta(n-1)\frac{f_{SI}^2}{1-f_I}(1-\phi+\phi\frac{f_{II}}{f_I^2}) + 2(\beta+a)f_{SI} - 2g f_{SI} \\
\dot{f_{SI}} &= \beta(n-1)\frac{f_{SI}}{1-f_I}((1-f_{II}-2f_{SI})(1-\phi+\phi\frac{f_{SI}}{f_I(1-f_I)}) - f_{SI}(1-\phi+\phi\frac{f_{II}}{f_I^2})) \\
&\quad - (\beta+a+g)f_{SI} + a(1-f_{II}-2f_{SI}) + g f_{II}
\end{aligned} \tag{7.5}$$

with

$$\begin{aligned}
f_I &= I/N \\
f_{II} &= [II]/nN \\
f_{SI} &= [SI]/nN
\end{aligned} \tag{7.6}$$

where n is the number of contacts each individual has and ϕ is the transitivity of the network (the ratio of triangles to triples). Having a simplified set of equations is very useful for understanding contagion dynamics in structured populations. Integrating equations is much faster than running simulations on large networks, and from them analytic results can be derived which allows determination of parameter dependence. These equations assume that the local neighborhood for each individual is identical, that is, everyone has the same number of contacts (n) and the same ϕ. They thus take into account the effects of fixed network structure but not heterogeneities between individuals. In the Supplementary Information (§7.6) we have included the extension of these equations to include heterogeneities. These equations can be used to easily simulate disease spread and get expected steady state prevalences and correlations, which are very useful approximations and give insight into parameter dependence. Later, we will compare these equations to results from full simulations on realistic networks. When $\phi = 0$ (which is

approximately the case for most random graphs) we can get a closed-form solution for the prevalence at steady state:

$$I^* = \frac{1}{2}(1 - \frac{a+g}{\beta n C^*_{SI}} + \sqrt{(1 - \frac{a+g}{\beta n C^*_{SI}})^2 + \frac{4a}{\beta n C^*_{SI}}}) \tag{7.7}$$

$$C^*_{SI} = \frac{(1 - J(a+g)}{J\beta n(1 - Jg)} \tag{7.8}$$

$$0 = ((a+g)^2 - g\beta n(n-1) + \beta n a)J^2 + (\beta n(n-1) + (n-2)(a+g))J - (n-1) \tag{7.9}$$

The result of a network structure is that the number of partnerships between susceptible and infected individuals quickly becomes less than if random, and so $C_{SI} < 1$. We can compare Eq. 7.7 to the well mixed result (Eq. 7.2), and see that the effect of the network is to lower the effective transmission rate by a factor of C_{SI}, and hence lower the prevalence, due to these correlations that build up locally. The larger β is compared to a, the more network effects are important. If infection is mostly automatic (when $\beta/a \to 0$), the network no longer matters. Equation 7.7 actually holds generally (for any homogeneous network and any ϕ value), while Equations 7.8 and 7.9 are only applicable with ϕ=0.

Analyzing the n-regular pair-wise equations allows us to get analytic results and determine how and under what conditions network structure affects the spread of behaviors which are both spontaneously acquired and spread interpersonally. Although simple closed-form solutions do not exist when ϕ is non-zero, these equations can easily be integrated or numerically solved to get solutions. These equations ignore heterogeneities in the number of edges for different individuals, which can facilitate spread under some conditions (see supplement §7.6 for extension). Full stochastic simulations on large networks can be carried out to determine how and when the results differ.

7.4 Results

7.4.1 Calibrating model with FHS Network data

The SISa model provides a formal way for assessing the social contagion of trends and behaviors that may be repeatedly caught and recovered from. Using data from the Framingham Heart Study (FHS)[90] we tested the validity of this model and estimated transmission parameters for various health related behaviors, though the focus here is on obesity as an example. To both demonstrate that obesity can display infectious-disease-like dynamics, and to estimate values for the model parameter a, β, and g, we use dynamic information about transitions between states based on our multiple time points of data. For data points separated by time intervals (Δt) smaller than the average time between transitions, the transition probabilities can be linearized. The probability of a transition from susceptible to infected after a time Δt can be given by $P(S \to I, \Delta t) \sim (a + \beta n_I)\Delta t$, and the probability of transition from infected to susceptible after time Δt, by $P(I \to S, \Delta t) \sim g\Delta t$. It is necessary for the time between measurements to not be comparable to or greater than the average lifetime of a state to keep the probability of double transitions within a time interval low.

This epidemiological approach to social contagion has important differences from other models which look at correlations in present and past states of connected individuals. Here, similar to others [9, 68, 69, 111] we look at how contacts influence the transitions between states, which better captures the nature of contagion. Since we use pre-existing social ties, we do not see effects from selection bias in choosing friends with similar states. Additionally, time invariant confounding events that lead to concurrent changes in connected individuals will not show up as contagion effects in this model.

The dataset we use is a subset of individuals from the Framingham Heart Study [90]. This study was initiated in 1948 in Framingham, Massachusetts and has continued enrolling subjects through the present. We examined individuals in the Offspring Cohort,

enrolled starting in 1971. Subjects come to a central facility at regular intervals (approximately every 4 years) for medical examination and collection of other survey data. Body mass index (BMI) was measured at each exam, and obesity was defined as BMI ≥ 30 [59]. All other, lower, weights, which include underweight, normal range weight and over-weight, were classified as 'not obese'. In additional to information on mental and physical health, subjects were asked to name at least one close friend at each exam, and were also connected to all first-order relatives, as well as coworkers and residential neighbors. For each subject, the following social connection data is available: (i) each other person to whom they were connected, (ii) the dates of initiation and termination of that relationship, (iii) the type of relationship (neighbour, coworker, first-degree relative, or friend), and (v) the geographic distance between the two subjects. The social network for each exam was constructed by creating a network matrix G, where $G_{ijk} = 1$ if subject i nominated subject j as a connection before or during the time that subject i was administered exam k. All relationship types are mutual except for friendships, which are self-nominated, such that $G_{ijk} \neq G_{jik}$ is possible for friendships.

To study the transmission of obesity, we examine changes in BMI between sequential exams. Seven exams were administered to the Offspring Cohort between 1971 to 2001, with network data collected for each. We examine transitions occurring between each exam. The average fraction of the network that was classified as obese increased between these seven exams, suggesting the transmission process is not yet at steady state (Exam 1: 14% obese; Exam 7: 29% obese). Each set of exams were closely and consistently spaced ($\Delta t = 7.9 \pm 0.5$ year (exam 1), 3 ± 1 year (exam 7)). In general when modeling an infectious process, the rates of infection and recovery are assumed to be constant over time, with the prevalence changing as the infectious process begins and finally reaches equilibrium or is eliminated. When examining the spread of obesity using longitudinal data on transitions between exams, we can actually test this assumption and detect changes in the rates themselves.

A given state X is considered infectious if having more contacts in state X makes you more likely to switch to state X. That is, a positive relationship between the number of contacts in state X and the probability to transition from state Y to state X indicates that state X is infectious with respect to state Y. Therefore, to test whether a given state X is infectious with respect to another state Y, we perform an ordinary least squares (OLS) linear regression as follows. Each subject in state Y in exam N is coded as either having transitioned to state X (transition=1) or not (transition=0) in exam N+1. We then regress this binary transition variable for each subject against the number of contacts in state X that subject had during exam N. A significant positive correlation indicates that having more friends in state X at the earlier exam makes you more likely to switch to state X in the later exam. If state X is infectious (a significant positive correlation exists), then the value of β can be calculated from the slope of the regression line, and the value of a can be calculated from the intercept. If state X is not infectious (no significant correlation exists), then the value of g can be calculated from the intercept. Δt was taken as the average time between examinations, which varied between exams from 3 to 8 years. Using logistic regression as opposed to OLS regression gives very similar results, as the datapoint line is within the linear range of the logistic model.

The structure of the Framingham Heart Study social network varies over the course of time, ranging from 7500 individuals with an average of 5.3 connections each at the first exam, to 3500 individuals with 2.8 connections on average at the seventh exam. Summary statistics are presented in the supplement (Table 7.2). These changes in population size and average degree occur because individuals may die or drop out of the study but new individuals are not added. The network is approximately Poisson distributed (see Figure 7.2), although with some subjects having no connections. The transitivity ϕ is consistent over time at approximately 0.64. While neighbors were included as contacts in the study, like Fowler and Christakis[68] we find no significant trends when including neighbors, and so did not include these contacts. For friendships, we only consider the

contacts of an individual to be those other individuals whom they nominated (other relationships are all mutual), and so the network is directional.

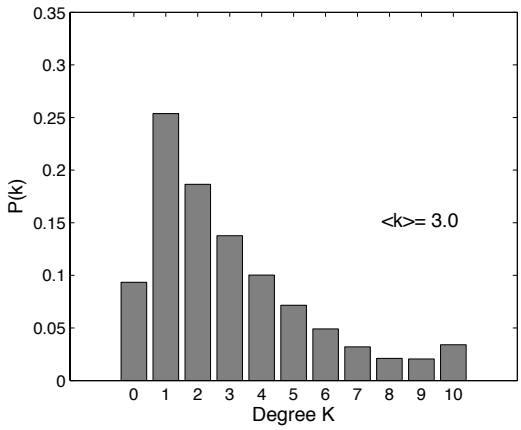

Figure 7.2: The degree distribution of the Framingham Heart Study social network at the most recent exam (7) considered in this study. Connections include friends, family and coworkers. The average degree is around k=3 and the transitivity is ϕ=0.64 (the ratio of triangles to triples).

The results of infectiousness analysis for the spread of obesity between exams 4 and 5 are shown in Figure 7.3 as an example. Consistent with the SISa model formulation, we find a significant positive correlation between the probability of transitioning from 'not obese' to 'obese' and the number of 'obese' contacts (Figure 7.3A, coeff=0.016, p=0.0001), and no significant relationship between the transition from 'obese' to 'not obese' and the number of 'not obese' contacts (Figure 7.3D, coeff=0.006, p=0.15). Additionally we find no significant relationship between the probability of transitioning from 'not obese' to obese and the number of 'not obese' contacts (Figure 7.3B, coeff=-0.0005, p=0.75) , or the probability of transitioning from 'obese' to 'not obese' and the number of obese contacts (Figure 7.3C, coeff=-0.002, p=0.85). The same analysis was repeated for each interval between sequential exams and very similar results were found. The full results from the regression analysis are presented in the supplement (Table S2). This suggests that obesity can indeed be modeled as an infectious process in the SISa framework, with 'not obese' susceptibles becoming 'obese' infecteds, and transmitting obesity to other susceptibles. The parameters for the SISa model can be calculated from the transition probabilities

mentioned earlier, by dividing slope and intercept values by Δt, the average time between exams. These values are reported for each exam in Figure 7.4, and the values at the latest exam intereval are summarized in Table 7.1. For most recent exam, the transmission rate, β, is found to be 0.0050 /year. The spontaneous transmission parameter a is found to be 0.019 /year. The recovery parameter g is found to be 0.043 /year. From these SISa model parameters, other values of interest can be calculated. The 'average lifetime' of a state is the average length of time and individual spends in this state before recovering, which was found to be 24 years for this time period. The 'influence' of a state is the cumulative probability that the infection will be passed from an infected to a susceptible connection before the infected individual recovers, and is observed here to be 13%. The 'cycle length' is the average length of time between spontaneous infections, and is 53 years. The basic reproductive ratio is approximately 0.35, which implies that without spontaneous appearance, the obesity epidemic would not be self-sustaining based on transmission alone. However this calculation is an approximation since uses the formula for a population that is well-mixed but only effectively contacting a fraction of the total population at each time (n contacts), so does not factor in fixed network structure (there is no analytic formula for this situation). We observed a correlation in the positioning of obese and non-obese individuals of C_{II}=1.3 and C_{SI}=0.9.

Since these rates were measured for 6 different inter-exam transitions over 30 years, we can look at how the value of these rates changes over time. Figure 7.4 shows the measured automatic infection (a), transmission (β), and recovery rates (g) for each exam interval. Error bars are 95% confidence intervals on measurements from analyses like Figure 7.3. While the rate of recovery (g) has remained relatively constant since the 1970s, the rate of spontaneous infection (a) has steadily increased over time. The transmission rate, β, also appears to have increased over time. These trends were tested using weighted regression (to include the different errors for each measurement) and found to be significant for a and β but constant for g. For the rest of the study we used the time-averaged value of g,

Table 7.1: Parameter estimates for obesity between exams 6 and 7 (1995-2001) using the SISa model framework. The 'average lifetime' of a state is the average length of time an individual spends in this state before recovering. The 'influence' of a state is the cumulative probability that the infection will be passed from an infected to a susceptible connection before the infected individual recovers. The 'cycle length' is the average length of time between spontaneous infections. The basic reproductive ratio is calculated by setting $a = 0$. However this calculation is an approximation since it does not factor in fixed network structure. Since $R_0 < 1$, the obesity epidemic would not be self-sustaining based on transmission alone.

Parameter	Description	Value
a	rate of spontaneous infection	0.019/yr
g	rate of recovery	0.043/yr
β	rate of transmission through contact	0.0050 /yr
1/a	cycle	53 years
1/g	lifetime	24 years
$1 - e^{\frac{-\beta n}{g}}$	influence	0.13
$R_o = \beta n/g$	basic reproductive ratio	0.35

$g = 0.035$. This suggests that the obesity epidemic may be driven by increasing rates of becoming obese, both spontaneously and transmissively, but not by decreasing rates of losing weight.

We also found that both happiness and depression fit the SISa model, both being contagious from a neutral emotional state[142] , that smoking cessation, though not smoking itself, also fit, and that both alcohol consumption and abstinence were contagious from the opposite state (data not shown). For all of the above cases, we tested if the transition probability depended instead on the *fraction* of contacts in a state, instead of the *number*, and found no significant dependence. We also tested for dependence on other personal attributes such as age, sex and education, and found no dependence in most cases. For obesity, the transition probability from not obese to obese decreased slightly with age (coeff=-0.0012, p=0.04). Our results show that many models of social influence make assumptions about interpersonal interactions that are not supported by this longitudinal data. One of these assumptions is the 'majority rules' interaction, which assumes that people will be most likely to switch to the state most of their contacts are in[21]. Here, transitions depend on the number of contacts, and only certain states (those we class as

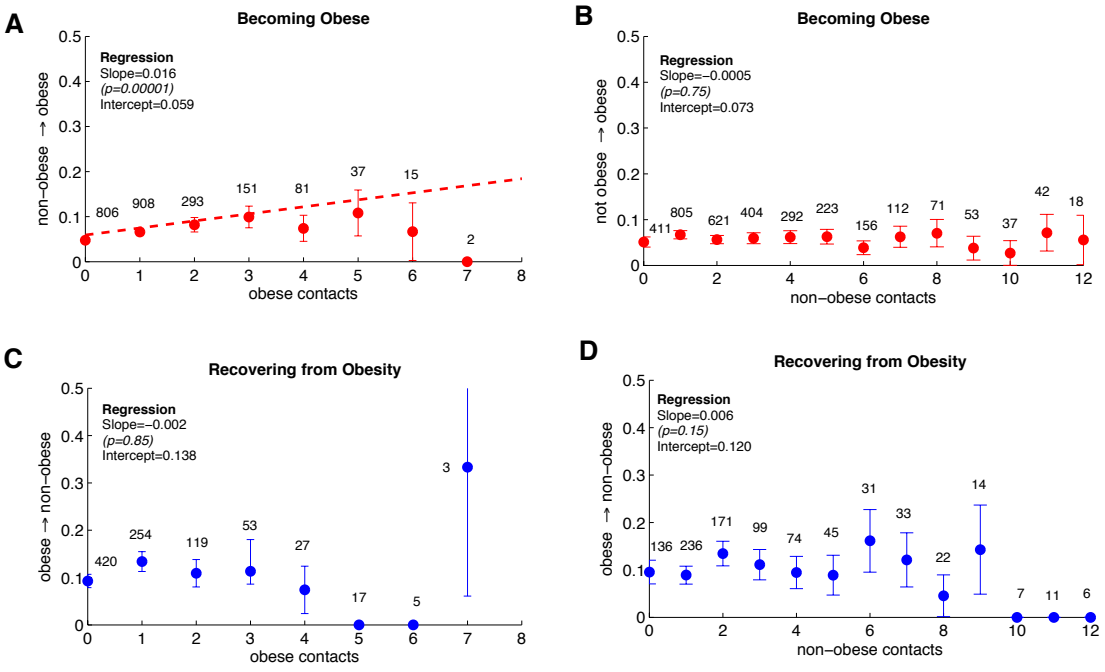

Figure 7.3: Evidence for disease-like spread of obesity. Obesity behaves like a disease agent, infecting those in a susceptible 'not obese' state. The probability of transitioning from 'not obese' to 'obese' increases in the number of 'obese' contacts (A), and doesn't depend on the number of 'not obese' contacts (B). Conversely, the probability of recovering to the 'not obese' state does not depend on the number of 'not obese' contacts (D) or the 'obese' contacts (C)). Labels above points on plot are the number of observations averaged into that data point, and error bars are the standard error of the proportion.

'infectious') actually influence transitions (in other words, contagion is only in one direction). This has significant effects on the predictions for epidemic progression. For example, 'majority rules' models predict 100 % infected at steady state, and that weight loss behavior spreads and so an effective intervention is to 'pin' certain individuals at low weights. Also, many models assume that the probability of transitioning to a state is zero if no contacts are in that state, but these results show that there is a constant probability of spontaneously becoming 'infected'. Finally, using this framework, we can get rates for transitions, and hence have an idea for the time-course of the progression, not just the final outcome.

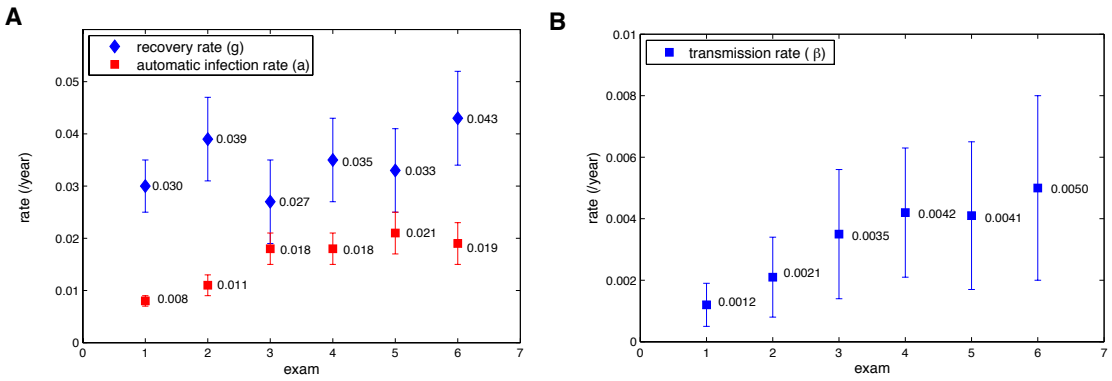

Figure 7.4: Change in observed parameters over time. Parameter measurements for obesity from each set of consecutive exams. Data point at exam N represents the value for the transition from exam N to N+1. Error bars are 95% confidence intervals on measurements from regression of transition probability versus number of contacts of a certain type. (A) Contact-independent rates. The rate of recovery (g) appears to be constant within the margins of error throughout the study while the rate of automatic infection (a) appears to increase between exams 1 and 3, then stay constant. (B) The contact-dependent transmission rate (β) appears to increase over time.

7.4.2 Case study: Modeling the obesity epidemic

In this section, we will use the SISa model to make predictions and evaluate interventions for the obesity epidemic, using the parameters observed in the FHS data. For simplicity and generality, we will keep the parameters a and β constant at the values observed for the most recent exams, and use the time-averaged value of g. Since we are mostly interested in predicting future trends, and the parameters seem to have relatively constant values over the final decade, this simplification should not affect these predictions. We also keep the network fixed at the structure observed at Exam 6, except when we compare to historic data. While the simplified pair-wise equations we present are designed for symmetrical networks, they can be approximately adapted to directional networks by letting n represent the average out-degree (average number of influential contacts) instead of the total number of contacts. In the Framingham data, greater than 90% of contacts are symmetrical, and so there is little error in this approximation. For hypothetical networks were the contacts formed by out-degree and in-degree are very different sets of individuals, deviations are expected. Figure 7.5 shows the results of both the n-regular pair-wise equations and a full

simulation on the FHS network for the spread of the obesity epidemic. The parameters used were those measured from FHS as discussed earlier. One of the important properties of the SISa model is that it always leads to a stable coexistance of both infected and susceptible individuals, with infecteds becoming 100% prevalent only in the limit as a or β approaches infinity. This is very different from statistical-physics-based interaction models where the population always 'coarsens' to everyone in a single state [21] . These results show that for the parameters measured for obesity, the pair-wise equations are not significantly different from the full simulations for predicting prevalence, and hence provide a good substitute. The reason is that the spontaneous rate (a) is significantly larger than the transmissive component (β). For larger values of β/a, there is a noticeable difference (shown in the next section).

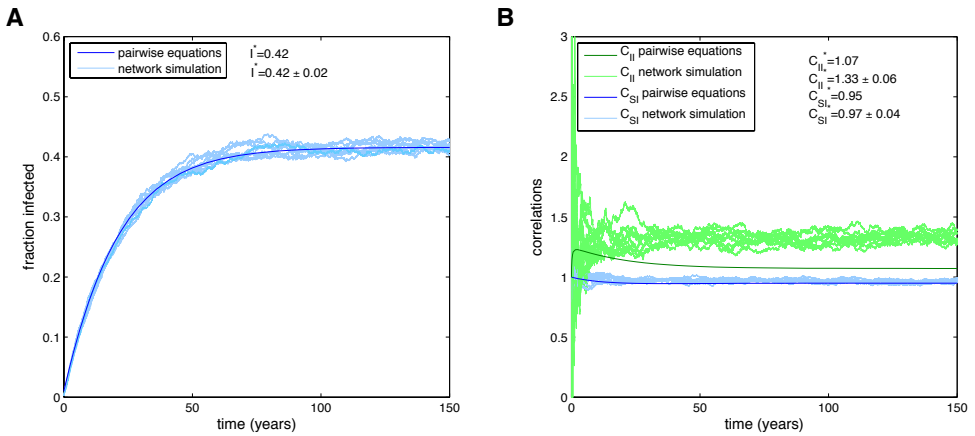

Figure 7.5: Simulations of obesity epidemic using SISa model. Time series of an epidemic on the Framingham Heart Study network, using full simulations (light blue) or the n-regular pair-wise equations (dark blue). Parameters used are those measured for the obesity epidemic: $a = 0.019, \beta = 0.0050, g = 0.035, \phi = 0.64, n = 3.0$. In the SISa model there is a co-existance of susceptible and infected individuals at steady state. For these parameters there is a good agreement with simulations and the pair-wise equations for the fraction infected (A), but the equations predict less correlations (B), due to the neglect of heterogeneities in the number of contacts.

This model predicts that, assuming the rates do not further change over time, the steady state proportion of obese individuals will be 42 %. While not great, this is a much more optimistic estimate than 100 % [21]. However, all of the parameters observed in this

study have an error associated with them, and so there is some uncertainty in this prediction. Figure 7.4 shows the ranges of the 95% confidence intervals for these values. We can estimate the uncertainty in this prediction by using first the values of these parameters, within the range of one standard deviation, that would give the highest prevalence $(a + \delta a, g - \delta g, \beta + \delta\beta)$ and then those that would give the lowest $(a - \delta a, g + \delta g, \beta - \delta\beta)$. We used g=0.05, a=0.015 and β=0.002 to get the minimum and g=0.03, a=0.023 and β=0.008 to get the maximum. These simulations suggest the confidence interval for the expected prevalence can be approximated as 25% to 54%. This model also allows us to estimate the time-course of the epidemic, and suggests it would take around 40 more years for the obesity prevalence to be within 1% of this maximum value. At the first time point in our data (1970), we measured the rates to be a=0.008, g=0.03 and β=0.001, and the prevalence to be 14 %. These parameters would have led to a steady state prevalence of 24 %, which suggests that the rates of becoming obese must have originally been much lower than this.

We can also compare historical data on the obesity prevalence (from both national studies [59]and the FHS data) to the predicted time course shown here. To generate the model prediction, we simulated an epidemic with the pair-wise equations but allowed the rate values and network parameters to change as measured from the data (see Figure 7.4 and Table 7.2). We kept g constant at the average value observed, 0.035, and varied a and β as observed. The value for parameter a measured for the transition between exam N and $N + 1$ (a_N) was used in the simulation for times (years) between the average examination dates of exams N and $N + 1$, and then increased to a_{N+1} for the next time interval. The same was done for β. For times before the earliest data points in FHS for which we have measured rate constants(pre 1970), we assumed the epidemic was at a steady state of 14%. This could be achieved, for example, with $a = 0.0057$ and $\beta = 0$. Figure 7.6 shows that there is a good match in the time course of the model with reality after 1970, with similar rates of increase in the prevalence.

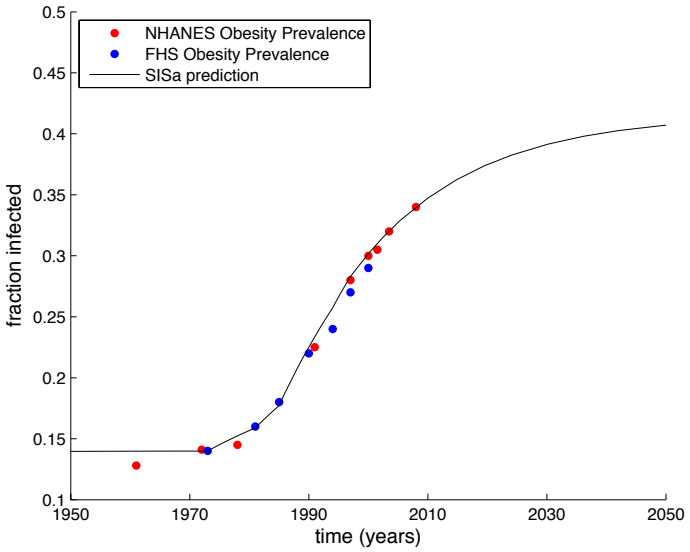

Figure 7.6: Comparing SISa model timecourse to historical data. A comparison of historical data on the prevalence of obesity in the Framingham Heart Study (blue dots) and the National Health and Nutrition Examination Survey (red dots) with the timeseries predicted from the SISa model with time-varying parameters. For the simulation, we allowed the parameters a and β to vary as observed in Figure 7.4, but kept g constant at its average value. Before 1970 (when our measurements started), the prevalence of obesity was assumed to be stable at 14%. The model and the data both show very similar rates of increase, with a slow post-1970 increase, followed by a rapid increase, and then increasing more slowly. The SISa model predicts the prevalence of obesity will increase slowly to a peak at 42%.

We can use the pair-wise equations to see how the steady state prevalence depends on various parameters, which is especially useful to see how interventions that aim to change a certain parameter may affect the prevalence. Figure 7.7 shows these results. For the parameter values for obesity, although a is quite large, β is still important. If β changes from 0 to 0.005, the expected steady state changes from around 0.35 to 0.42. However, much larger changes can be realized by decreasing a or increasing g. For the obesity parameters, completely removing the contagious component is only expected to change the steady state prevalence by around 7 %. However, changing the spontaneous infection term can have much larger effects. While a 50% change in β will result in only a 3% decrease in I, cutting a in half will reduce the prevalence by 15%. However, a similar absolute decrease of 0.005 would also lead to a 7% difference. The efficiency of changing one parameter

versus the other can be looked directly at dI/dx for various parameters, which will be shown in the next section.

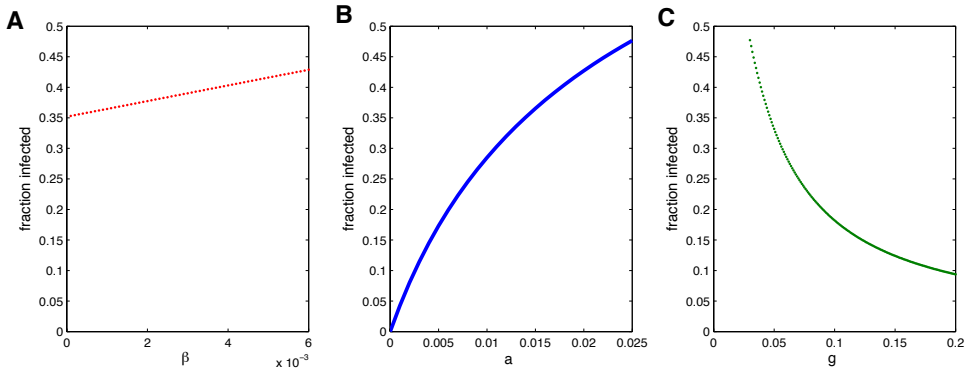

Figure 7.7: Fraction infected versus SISa model parameters. Dependance of the equilibrium fraction infected on obesity interventions which act to change the rates of infection (transmission (A) and 'automatic' infection(B)) or recovery (C). When not varying, parameters are $a = 0.019, \beta = 0.0050, g = 0.035, \phi = 0.64, n = 3.0$

7.4.3 General properties of SISa model

In this section we will examine the more general properties of 'infections' following SISa model dynamics. While Figure 7.5 showed excellent agreement between the pair-wise equations and full simulations for the time dynamics, this is not true for all parameter regimes. When β is larger and a is smaller (as shown in Figure 7.8), and the network is strongly heterogeneous (as the Framingham network is), the pair-wise model deviates more. The reason is that heterogeneous network effects become more important for larger β, and the pair-wise approximations are best for homogeneous networks. The extension of the pair-wise equations to heterogeneous networks is described in the supplement (§7.6).

We can use the pair-wise equations to see how the steady state prevalence depends on various parameters, which is especially useful to see how interventions that aim to change a certain parameter may affect the prevalence. Figure 7.9 shows how the steady state changes with the rate of transmission, β. The blue line ($a = 0$) shows what would happen in a classical epidemic, with no spontaneous infection. When β is below a certain value

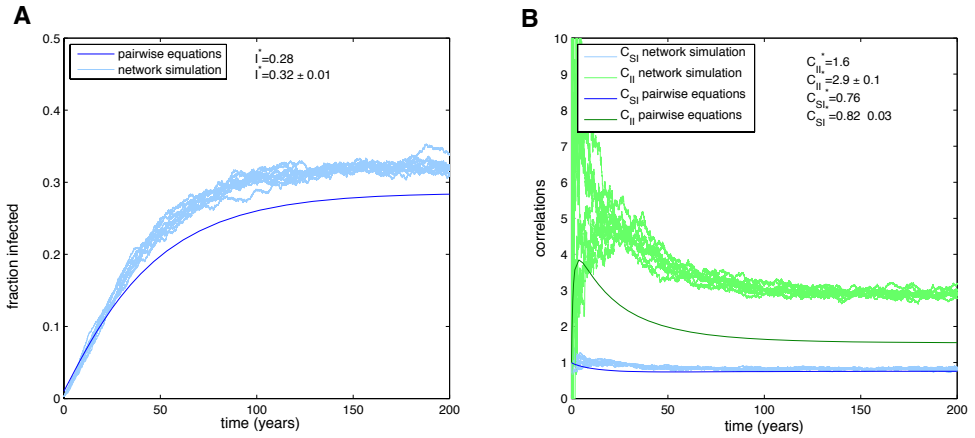

Figure 7.8: Pairwise equations diverge from simulations when transmission is higher. Time series of an epidemic on the Framingham Heart Study network, using full simulations (light blue) or the n-regular pair-wise equations (dark blue). When the ratio of β/a is larger than that observed for the spread of obesity, the pair-wise equations diverge more from the full simulations, both for the fraction infected (A) and the correlations (B). $a = 0.005, \beta = 0.02, g = 0.0045, \phi = 0.64, n = 3.0$

($R_o > 1$), the infection does not spread. The fraction infected increases rapidly with β in this regime. As soon as we add $a > 0$, this thresholding behavior disappears. When $a > 0$ the steady state is less sensitive to β. The red line ($a = 0.02$) shows the approximate parameter values for obesity. Here although a is quite large, β is still important. As with classical infectious disease models [175], disease spread on a network leads to decreased C_{SI}, the spatial correlation between infected and susceptible individuals, and increase C_{II} and C_{SS}, the correlation between pairs of infected individuals and pairs of susceptible individuals, respectively. If we look at C_{II} , we can see that we expect there to be some correlations of infected people at some β/a values, but not all. So while seeing spatial correlation may hint there is a inductive process, it is definitely not necessary. You can have an infectious process without seeing correlations, just like you can see correlations without it being caused by the dynamics of influence. Spatial correlation is much higher when a is small.

Figure 7.10 shows the dependence on the rate of spontaneous infection, a. The more spontaneous infection, the more infected. When β is larger (red line), increasing a has less

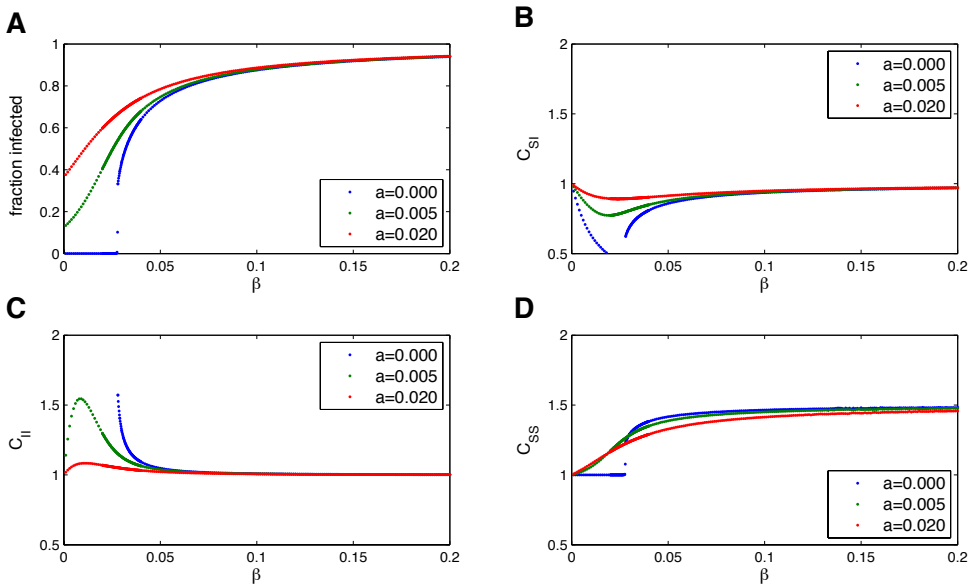

Figure 7.9: Dependance of the equilibrium fraction infected (A) and correlations (C_{SI}:(B), C_{II}:(C), C_{SS}:(D)) on the rate of transmission, β. When $a > 0$, expected in most social infections, there is no longer a threshold ($R_o > 1$) needed for the infection to invade the population. The network causes infected individuals to cluster $C_{II} > 1$ away from susceptible individuals $C_{SI} < 1$, and this is more pronounced for larger β/a and lower fraction infected. Parameters are $g = 0.035, \phi = 0.64, n = 3.0$

effect. The green line is for the parameters measured for obesity. We can use these graphs to compare the effects of various interventions which may reduce the rate of infection. In Figure 7.9 (vs β), we can see the expected decrease in the prevalence of the infection for a given decrease in β. Changing β has more effect when a is small. The rate of recovery from an infection is g, and in the obesity case, represents the rate at which obese people lose weight and transition to normal BMI values, in probability per year. Higher rates of recovery lead to lower fraction infected (Fig. 7.11). One possible intervention is to increase the rate of recovery. For low recovery values, this has a large effect on I, but for g around 0.04 (the value for obesity), only small changes in I result from changing g.

In general, the spatial correlations (C_{II}) are negatively correlated with the fraction infected (I); more correlations are observed when a disease is not too infectious. If the spatial correlations were fixed to be a certain value (for example obese people cluster

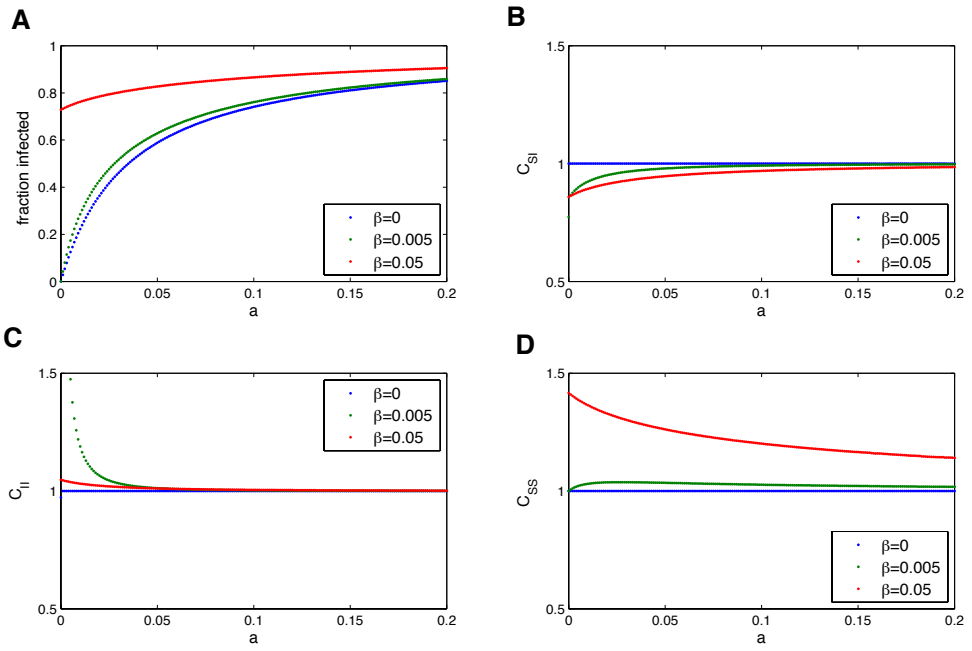

Figure 7.10: Dependance of the equilibrium fraction infected (A) and correlations (C_{SI}:(B), C_{II}:(C), C_{SS}:(D)) on the rate of automatic infection, a. Parameters are $g = 0.035, \phi = 0.64, n = 3.0$

together due to selection bias in friendships or confounding factors), then this would actually serve to slow infection. Since we do not observe contagion of losing weight, it does not seem like it would be beneficial to have an intervention which broke up obese clusters.

The most direct way to compare various parameters for spread, and therefore interventions that reduce one of the parameters, is to look directly at dI/dx for various parameters (I is the steady state fraction infected, x is the parameter of interest. Figure 7.12 shows that for most parameter regimes, it is always best to increase the recovery rate, g, as a method to reduce the fraction infected, I. However, for low a and low β , it is best to decrease the spontaneous infection term a, and for a window of intermediate β, it is best to decrease the transmissive component β. The third plot shows the results for the a value measured for obesity, and because β is low here we are in a regime where it decreasing β has the most effect, so this is the best intervention.

Many analytic models of network phenomenon assume the transitivity, ϕ, is zero,

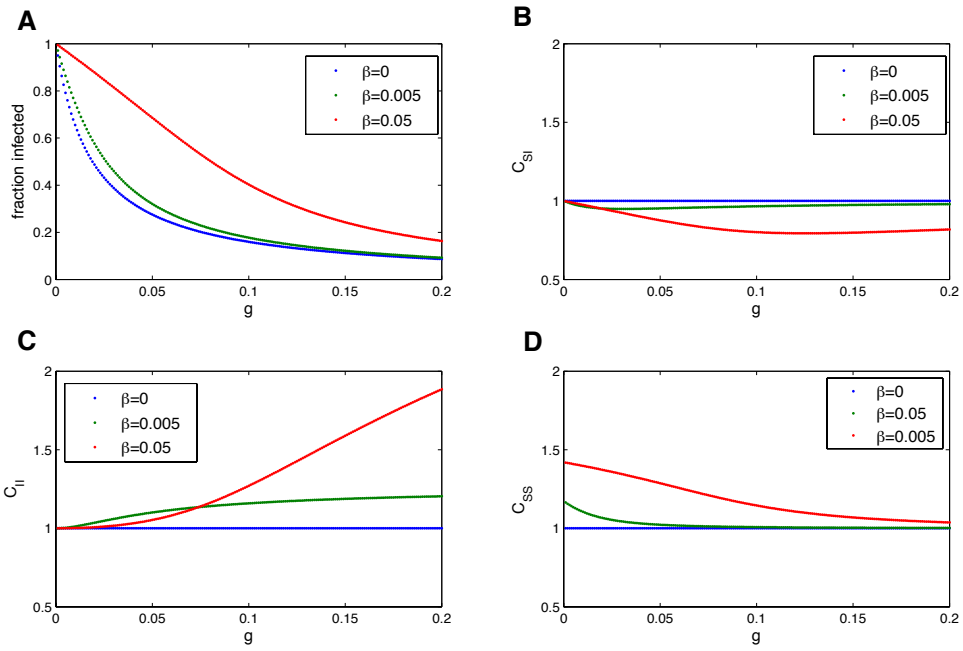

Figure 7.11: Dependance of the equilibrium fraction infected(A) and correlations (C_{SI}:(B), C_{II}:(C), C_{SS}:(D)) on the rate of recovery from infection, g. Parameters are $a = 0.019, \phi = 0.64, n = 3.0$

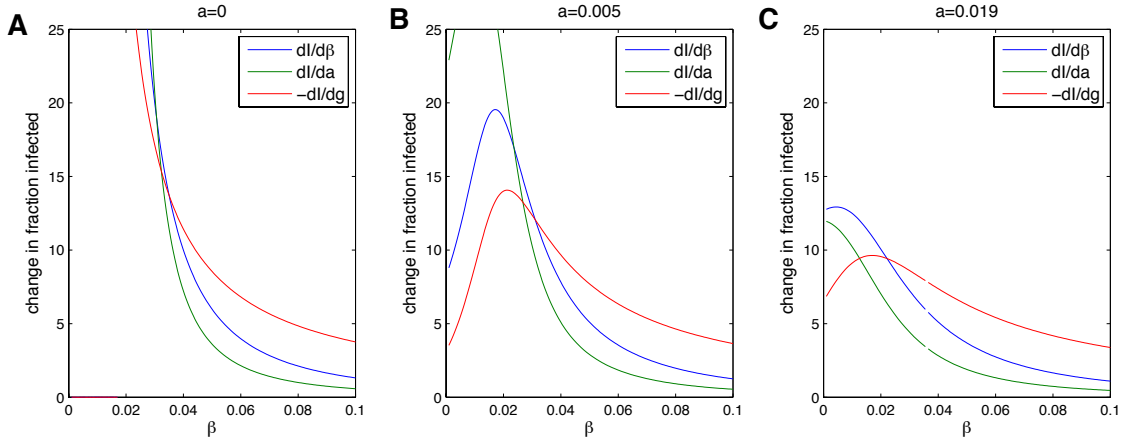

Figure 7.12: Determining the best parameter to target in an intervention. This graph compares interventions which act to change different parameters of infection (transmission (A), 'automatic' infection (B), recovery (C)). Shown is the rate of change of the fraction infected at equilibrium with respect to a change in various parameters of infection. The y axis labels represent the absolute change in the percent infected for a change of 0.01 in one of the parameters. Changing a is better for small β and changing g is best for larger β. For intermediate β, changing β is best. Parameters are $g = 0.035, \phi = 0, n = 3.0$

meaning there are no triangles in the network. This is done to get the analytic expression presented here (Eq. 7.2), which is not necessary to numerically integrate the pair-wise equations, as presented in the results above. In the FHS network, we observed that ϕ is 0.64, suggesting human social networks are quite transitive. We want to examine the importance of ϕ in predicting the fraction infected. For the observed βn value, the effect of ϕ is negligible, as shown in Figure 7.13. The reason is that the dominant effect here is the spontaneous infection, which does not depend on the network structure. This justifies ignoring ϕ for infections that have only low infectivity terms. However, for large βn values (the equivalent of $R_0 \sim 2$ is shown in Figure 7.14) ϕ has a more pronounced effect. While for a purely infectious process (blue line), at high ϕ, a disease can die out, even for $R_0 > 1$, when $a > 0$, this doesn't occur, but ϕ still slightly reduces the spread. It also results in more observed spatial correlation of infected individuals. Overall, there is very little effect of ϕ in the SISa model.

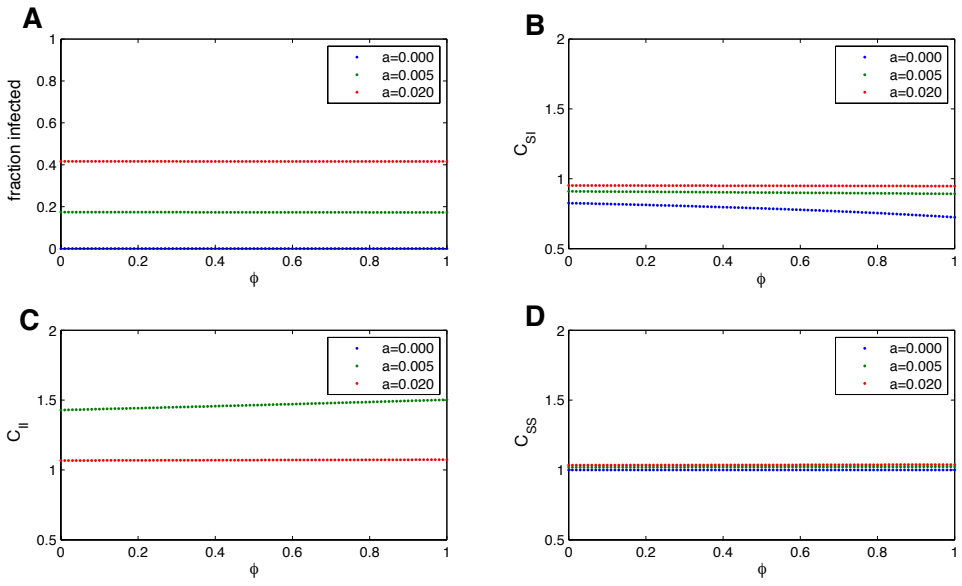

Figure 7.13: The dependence of the equilibrium fraction infected(A) and correlations (C_{SI}:(B), C_{II}:(C), C_{SS}:(D)) measured from the pair-wise equations on the network transitivity, ϕ. For the parameters measured for the transmission of obesity, shown here, there is no strong dependence on ϕ. Hence for studying the obesity epidemic it is justified to ignore ϕ to simplify calculations. Parameters are $\beta = 0.0050, g = 0.035, n = 3.0$

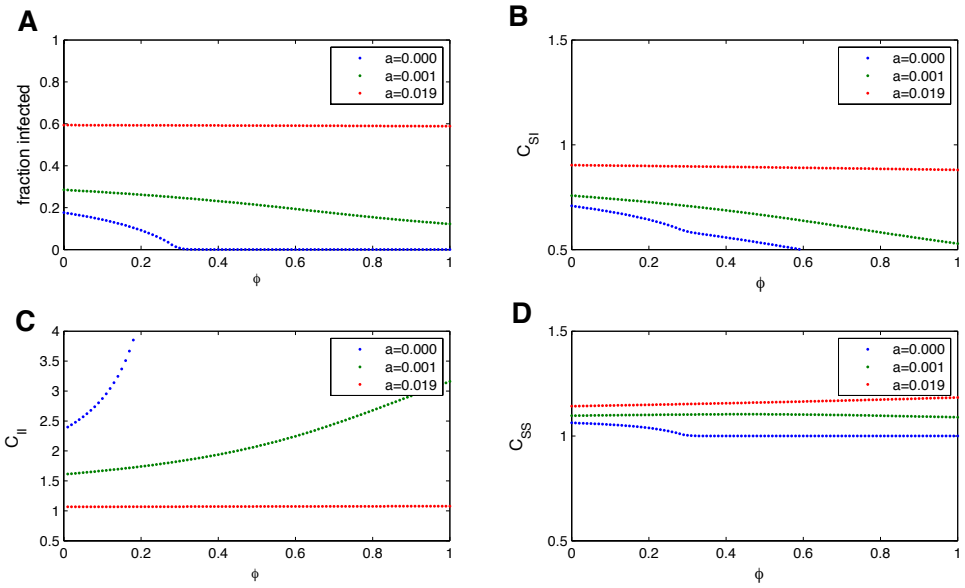

Figure 7.14: The dependence of the equilibrium fraction infected (A) and correlations (C_{SI}:(B), C_{II}:(C), C_{SS}:(D)) measured from the pair-wise equations on the network transitivity, ϕ. For larger β/a, ϕ slightly decreases the fraction infected by leading to more spatial correlation of infected individuals. Parameters are $\beta = 0.02, g = 0.035, n = 3.0$

We've already discussed how changes in parameters of infection affect the steady state prevalence, and we can consider this an analysis of different types of public health interventions that change rates of recovery, infection or network structure. In previous analysis of the obesity epidemic done by Bahr et al[21] they suggest a strategy of 'pinning' groups of people to stay in a non-obese state, similar to vaccinating against an microbial disease, as a method to remove the 'infection' from the population. However, in the Bahr model this intervention works (if enough people are 'pinned') because becoming non-obese is also contagious, which we don't find in this analysis. In the classical infectious disease setting, vaccinating can lower R_o below the threshold for disease invasion, but in the SISa model there is no threshold, and so neither mechanism makes this an effective strategy in the SISa model. Two other possible intervention strategies come out of this model. Firstly, from Eq. 7.7 we can see that the fraction infected decreases with C_{SI}, the correlation of suceptible and infected people. If an intervention actively reduced this number, by isolating

or clustering infected people, this could reduce the prevalence. Secondly, the fraction infected could be reduced if it were possible to make the 'susceptible' state also contagious through contacts.

7.5 Discussion

The SISa model offers a framework for quantitatively analyzing and predicting the public health affects of socially contagious phenomenon. Using a longitudinally measured health outcome and social network data, the SISa model can be used to determine the dynamics of a health trend in terms of rates of acquisition, recovery and inter-personal transmission. From these rates, the relative importance of social contagion can be determined, and changes in prevalence over time can be predicted. The framework can also be used to examine how these rates themselves change over time, helping to understand the mechanisms behind drastic changes in disease prevalence, such as in the obesity epidemic current effecting the United States. Finally, understanding the dynamics of a health behavior using the SISa model allows us to evaluate the benefits of various interventions, especially those that may work within social networks.

The prevalence of obesity in the Framingham Heart Study cohort has increased from 14% in the 1970s to 30% in 2000, and continues to increase. We find that the most recent rate of becoming obese is 2%per year and increases by 0.5% for each obese social contact. The rate of recovering from obesity is 4% per year, and does not depend on the number of non-obese contacts. These results show that obesity has an infectious character: obesity can be acquired through social contagion as well as through non-social factors. Examining over 30 years of data, we find that these rates have changed throughout the course of the study, with the rate of becoming obese through mechanisms other than social contagion increasing approximately twofold since 1970, and the rate of transmission increasing approximately fourfold. The rate of recovery, however, has changed little. These results suggest that social norms are changing the propensity for becoming obese by non-social

mechanisms, and also magnifying the affect that obese individuals have on their non-obese contacts. It is possible that while causing changes in prevalence, these rates may also be responding to changing prevalences (i.e. more obese people leads to increased social acceptability of obesity, which leads to higher rate of becoming obese), creating a positive feedback mechanism and a continuously increasing obese fraction of the population. It has been suggested that changing social norms that stigmatized smoking may have lead to it s decline[182], and just the opposite may be true for obesity [63].

Using the SISa model with these parameter values estimated for obesity, we can make predictions about the future of the obesity epidemic and the important factors controlling it. Our models suggest that if the most recent rates stay constant, the population will stabilize at 42% obese. However, it is very likely that the rates of obesity infection may continue to increase if successful interventions are not conducted. Our results show that while the rate of automatic development of obesity appears to have leveled off in the past decade, the rate of transmission has been steadily increasing.

This model allows us to can predict how much spatial correlation is expected from a purely infectious process, and compare this to what is observed in the data, which could be influenced by confounding factors and selection bias in choosing friends. A coefficient of 1 indicates that arrangement of infected nodes is random, while higher values are indicative of spatial correlations. We observed a correlation coefficient for obese individuals of 1.30, which was quite close to what was predicted from epidemic simulations (1.33). This suggests that infection alone is sufficient for explaining the observed correlations, and there may not be much selection bias or confounding factors in effect. We also show that network transitivity is not predicted to have a strong affect on prevalences when there is an automatic component to infection. However, our model also shows that contrary to popular belief, a contagious process on a network does not always result in clustering of infected individuals . This is especially true if there is a large automatic infection term, which is likely with many trends and behaviors.

The SISa approach allows us to compare the effectiveness of different classes of intervention. For the parameter range observed, we find that decreasing the rate of transmission β is the most effective intervention (largest decrease in prevalence per unit decrease in rate), although decreasing the automatic infection a is almost as effective. More generally, while we find that gaining weight is contagious, we do not find that losing weight is contagious. Thus it does not seem to be beneficial to 'break-up' clusters of obese individuals or 'pin' the weight of certain people in these clusters. Our results actually suggest that clusters of obese people serve to slow the spread of obesity by reducing social contagion to non-obese others outside of the clusters. Another possible intervention would involve somehow facilitating the social spread of becoming non-obese (losing weight), creating a bi-directional transmissive process.

One possible limitation of this study is the incompleteness of the social network dataset used. Because the Framingham Heart Study was not designed as a study of social networks, no attempt was made to capture all of a person's important social contacts. Many close friends of a person could be missing (usually only one friend per person was recorded) and family and coworkers who play only a small part in one s actual social network may have been counted. However, even if under-sampling of real-world contacts did occur in the FHS Network, it does not change our results qualitatively: our data clearly show that rates of becoming obese increase with the number of 'infected' contacts (i.e. is contagious) while the rate of 'recovery' to a non-obese state does not depend on contacts. However, under-sampling could quantitatively effect our measurement of the rate constants. If a constant number of contacts for each person were missed, our estimate of the y intercept of the transition graphs would be shifted up from its true value, and the actual a would be smaller than the a we measured. If a constant fraction of contacts for each person were missed, then our estimate of the x axis would be compressed from its true value and the slope would be increased, so then the actual value of β would be smaller than the β we measured. While it is likely that the FHS network underestimates the total

number of contacts, the relationship to the number of 'influential' contacts is unclear. In this sense, the observed value of the transmission rates, β, are network dependent. Additionally, network connections may be weighted differently according to their ability to transmit behaviors. Longitudinal studies designed specifically with the intent of measuring social networks and health, which carefully define contacts, such as by amount of time spent together per day, influence, etc, are an important area for future research.

It has recently been suggested that certain, particular types of latent homophily, in which an unobservable trait influences both which friends one chooses and current and future behavior, may be impossible to distinguish from contagion in observational studies and hence may bias estimates of contagion and homophily [314]. The circumstances under which this is likely to be a serious source of bias (e.g., whether people, empirically, behave in these sorts of ways), and what (if anything) might be done about it (absent experimental data of the kind that some new networks studies are providing [112]) merits further study. Observational data invariably pose problems for causal inference, and require one set of assumptions or another to analyze; the plausibility of these assumptions (even of standard ones that are widely used) warrants constant review.

The SISa model as presented here assumes that all individuals have the same probability of changing state (though not everyone will actually change state within their lifetime). It is clearly possible, however, that there is heterogeneity between individuals in these rates. We do not have sufficient data on obesity in the Framingham dataset to explore this issue, which would require observing numerous transitions between states for each individual. Exploring individual differences in acquisition rate empirically is a very interesting topic for future research, as is extending the theoretical framework we introduce to take into account individual differences.

The results we have presented here reiterate an important general principle of network processes: networks tend to magnify whatever they are seeded with, but they must be seeded with something. The increase in obesity is not purely a network-diffusion

phenomenon. Automatic infection serves to start and continuously seed the epidemic. Here we show that the dominant process in the increasing prevalence of obesity is contact-independent weight gain; however, the rate of interpersonal transmission contribute significantly to the overall prevalence and appears to be increasing steadily over time. Thus consideration of social transmission and network effects is an important issue for health and policy professionals.

7.6 Supplementary Information

7.6.1 Deriving pairwise network equations for heterogeneous networks

In the main text, the pairwise equations were derived assuming all individuals had the same number of contacts. This allowed us to reduce the dynamics to three differential equations (after applying a moment closure approximation) tracking the changes in the number of pairs of the form [AB] . Now we relax the assumption of homogeneity, and track pairs for each class of individuals, where classes are defined by the total number of contacts an individual has. This analysis follows that presented in Eames and Keeling, 2002 [99].

Table 7.2: notation used in pairwise equations for heterogeneous networks

Term	Description
a	rate of spontaneous infection
g	rate of recovery
β	rate of transmission through contact
$[n]$	# of individuals with n contacts
$[nm]$	# of pairs of individuals with n and m contacts
$[A]$	# of A individuals
$[A^n]^*$	# of A individuals with n contacts
$[A^nB^m]$	# of edges between an A^n and a B^m individual
$[A^nB]^* = \sum_m [A^nB^m]$	# of B contacts of all A^n's
$[A^nB^mC^q]$	# of triples with B^m having both A^n and C^q as contacts

Table 7.2 summarizes the types of variables tracked with this approach. After describing some variables in terms of others, only those that are starred (*) remain, for a

total of $3k$ equations, where k is the maximum number of contacts of any individual in the network. Whenever there is a sum, it is over all possible values for the number of contacts an individual has, i.e $\sum_n$ implies $\sum_{n=0}^{k}$. Note that while in the main text we wrote equations for the fraction of individuals in various classes, here we have left the equations for the absolute numbers, for simplicity of notation.

$$\begin{aligned}
\frac{d}{dt}[I^n] &= \beta[S^n I] + a[S^n] - g[I^n] \\
\frac{d}{dt}[I^n I] &= \sum_m \frac{d}{dt}[I^n I^m] \\
&= \beta(\sum_{m,q}([I^n S^m I^q] + [I^q S^n I^m]) + [S^n I] + [I^n S]) + a([S^n I] + [I^n S]) - 2g[I^n I] \\
\frac{d}{dt}[S^n I] &= \sum_m \frac{d}{dt}[S^n I^m] \\
&= \beta(\sum_{m,q}([S^n S^m I^q] - [I^q S^n I^m]) - [S^n I]) + a([S^n S] - [S^n I]) + g([I^n I] - [S^n I])
\end{aligned} \tag{7.10}$$

Many variables on the right hand side of these equations can be simplified until only $3k$ variables remain (equal to the number of equations). Firstly, triples can be reduced to pairs using the moment closure approximation [283]:

$$[A^n B^m C^q] = \frac{(m-1)}{m}\frac{[A^n B^m][B^m C^p]}{[B^m]}(1 - \phi + \phi C_{A^n C^q}) \tag{7.11}$$

$$C_{A^n C^q} = \frac{[n][q]}{[nq]}\frac{[A^n C^q]}{[A^n][C^q]} \tag{7.12}$$

$$\tag{7.13}$$

We still assume there is one ϕ that describes the whole population. We could have ϕ_{nmq}, though this would be unnecessarily complicated for most applications. Furthermore, we can approximate pairs of the type $[A^n B^m]$ in terms of the smaller set of pairs of the

type $[A^n B]$ using:

$$[A^n B^m] = \frac{[A^n B][B^m A]}{[AB]} \frac{[nm] \sum_q q[q]}{nm[n][m]} \tag{7.14}$$

Finally, since all individuals are either infected or susceptible, we can use:

$$\begin{aligned} [I^n S] &= n[I^n] - [I^n I] \\ [S^n S] &= n[S^n] - [S^n I] \\ [I] &= \sum_n [I^n] \\ [S] &= N - [I] \end{aligned} \tag{7.15}$$

This results in $3k$ equations and variables. If we want to find the spatial correlation discussed in the paper, we can use:

$$C_{AB} = \frac{[AB]}{\sum_{n,m} \frac{[nm]}{[n][m]} [A^n][B^m]} \tag{7.16}$$

7.7 Acknowledgments

We thank Laurie Meneades for assistance with the Framingham Heart Study Network database. This work was supported by the National Institute on Aging grant P01 AG031093, the John Templeton Foundation, the Bill and Melinda Gates Foundation, the National Science Foundation/National Institutes of Health joint program in mathematical biology (National Institutes of Health Grant R01GM078986), and graduate fellowships from the National Science Foundation and the Canadian Natural Sciences and Engineering Research Council. NHLBI's Framingham Heart Study is supported by contract number N01-HC-25195. The funders had no role in study design, data collection and analysis,

decision to publish, or preparation of the manuscript.

7.8 Manuscript Information

7.8.1 Previously published as

This manuscript appeared in [143]:

A. L. Hill, D. G. Rand, M. A. Nowak, and N. A. Christakis. Infectious disease modeling of social contagion in networks. *PLoS Comput Biol*, 6(11):e1000968, Nov. 2010. doi: 10.1371/journal.pcbi.1000968. URL http://dx.doi.org/10.1371/journal.pcbi.1000968

7.8.2 The author's contribution

Analyzed the model and the data: ALH. Wrote the paper: ALH DGR. Conceived and designed the mathematical model and analysis: ALH DGR MAN NAC.

8

Emotions as infectious diseases in a large social network: the SISa model

8.1 Abstract

Human populations are arranged in social networks that determine interactions and influence the spread of diseases, behaviours, and ideas. Here, we evaluate the spread of long-term emotional states across a social network. We introduce a novel form of the classical SIS disease model which includes the possibility for 'automatic' or 'spontaneous' infection, in addition to disease transmission (the SISa model). Using this framework and data from the Framingham Heart Study, we provide formal evidence that positive and negative emotional states behave like infectious diseases spreading across social networks over long periods of time. The probability of becoming content is increased by 0.02 per year for each content contact, and the probability of becoming discontent is increased by 0.04 per year per discontent contact. Our mathematical formalism allows us to derive various quantities from the data, such as the average lifetime of a contentment 'infection' (10 years) or discontentment 'infection' (5 years). Our results give insight into the

transmissive nature of positive and negative emotional states. Determining to what extent particular emotions or behaviours are infectious is a promising direction for further research with important implications for social science, epidemiology, and health policy. Our model provides a theoretical framework for studying the interpersonal spread of any state that may also arise spontaneously, such as emotions, behaviours, health states, ideas or diseases with reservoirs.

8.2 Introduction

Social network effects are of great importance for understanding human behaviour. People interact with different numbers of individuals and with some individuals more than others, and this affects behaviour in fundamental ways. Investigations from diverse fields, including sociology, economics, physics, mathematics, and public health, have studied social networks, both to understand their structure and their affect on social dynamics. Economic behaviour, such as purchasing decisions [194], employment prospects [56, 215], bankruptcy [351], investment [77] and productivity[258] have been shown to be influenced by network contacts (reviewed in Jackson [156]). Other behaviours such as college GPA [301] and crime [122, 138] have been related to peer effects. Recently, social networks have been studied as determinants of health (reviewed by Smith [333]), ranging from determining the patterns of infectious disease spread [176] to the propogation of behaviours such as smoking cessation [69] , obesity [68] and suicidal ideation [31]. Networks also play an important role in evolutionary biology, where population structure determining interactions can facilitate the evolution of cooperative behaviour [115, 245, 252, 344, 345].

Human emotions are strongly influenced by social contacts. 'Emotional contagion' [136] is known to occur over short times scales between people in frequent close contact, such as families [192], roommates [151] and teammates [27], and even occurs in experimental situations [112]. Positive and negative moods also spread during workplace interactions such as cooperation [27], negotiation[183] and successful leadership [48]. The

spread of positive mood is a common technique in interpersonal relations, and the 'service with a smile' technique is a well-known example [277]. Depressive moods and symptoms have been found to be contagious both by media and by personal contact with strangers or acquaintances [161]. Over longer time scales, clinically relevant depressive states can also spread between social contacts [349]. Unlike most of these previous studies, in the present work we demonstrate the interpersonal spread of long-lasting emotional states over protracted time-scales.

Recently, Fowler and Christakis [111] have studied the properties of happiness in relation to a network of social contacts, extracted from the Framingham Heart Study [90]. They observe correlations in happiness between individuals that are connected in a social network. If your friends are happy, then you are more likely to be happy in the future. This correlation, they suggest, is caused in part by an inductive effect of happiness spreading from person to person. Thus, happiness could be thought of as a form of social infection. Here, we evaluate this conceptual approach to emotional transmission in a mathematically rigourous way, by formally modelling the spread of positive and negative emotions using theoretical tools from epidemiology.

Mathematical models for the spread of microbial infections help us to understand and predict the spread of disease [10]. Such models have also been used to explore the spread of non-microbial infections, such as rumors [86] or computer viruses [266]. Studying the dynamics of epidemiological models on social networks is currently an active area of research. Many models have been developed to study how the structure of networks affects disease spread [176]. These models have been used to understand contagious diseases where the network describes contacts in geographical proximity (for example SARS [222], Foot-and-mouth disease [109]), or for studying sexually transmitted diseases where the network consists of sexual partnerships [99].

Here we introduce a novel approach for studying the spread of emotions in a social network. We can think of emotions at three levels: 'moods','states' or 'traits'. These levels

have increasing duration and permanence, and differ in terms of the extent to which they are deeply characteristic of the individual, and therefore the extent to which they are mutable or immutable. We will use the word 'long-term emotional states' to describe the phenomena of interest to us here, lying in between fleeting moods and permanent traits (like personality traits). We use the terms *content* and *discontent* for these phenomena that have been characterized, in prior work, as akin to happiness and depression, with validated scales. We modify a classical infectious disease model to represent the spread of emotions, to account for the fact that emotions can by contracted both spontaneously and through transmission. We then use this model to ask whether emotional states in the Framingham Heart Study dataset [90] do indeed act like infectious diseases. For an emotional state such as content to fit the classical definition of an infectious disease, (i) the probability of becoming content must depend on the number of content contacts (and not on the number of non-content contacts), and (ii) the probability of switching from content back to neutral ('recovering' from content) should be independent of any properties of social contacts. The particular structure of the Framingham Heart Study dataset, with a social network, reliable emotional evaluation, and longitudinal follow-up, allows application of our model to the spread of content and discontent over long time scales. We find that both content and discontent behave like infectious diseases. The data allow us to then estimate values for model parameters, and to calculate derived quantities which give insight into the dynamics of emotional contagion.

8.3 Methods

8.3.1 Basic infectious disease model

In the simplest infectious disease models [10], individuals are classified as occupying one of two states: 'susceptible', meaning they do not have the disease, and 'infected', meaning they do have the disease. The disease can be transmitted to a susceptible person when

they come into contact with an infected person. The rate of this disease transmission from infected to susceptible is defined as β, the *transmission rate*. Once an individual is infected, she recovers from the disease at a constant rate g, regardless of her contact with susceptible or infected others. In one class of disease models (susceptible-infected-recovered, or SIR), recovered individuals become immune to further infection and enter a 'recovered' state. However, an emotion can occur many times over an individual's life, and therefore we use assume infected individuals return to the susceptible state after recovering. This form of susceptible-infected-susceptible (SIS) model is used to model infectious diseases that do not confer immunity, such as many sexually transmitted diseases.

In the standard SIS model, infection can only be transmitted by having a contact between an infected and a susceptible individual. Emotional 'infections', however, can also arise due to spontaneous factors other than transmission. Therefore, we extend the SIS model by adding a term whereby uninfected individuals spontaneously (or 'automatically') become infected at a constant rate a, independent of infected contacts. A diagrammatic representation of our modified SIS model, which we will call SISa, is shown in Figure 8.1. The corresponding differential equations for a well-mixed population are described in Eq. 8.1. When the population is not well-mixed but instead constrained on a social network, the transmission rate for each individual depends on the number of infected contacts (n_I) instead of the total number of infected individuals (I).

$$\begin{aligned} dS/dt &= -\beta SI + gI - aS \\ dI/dt &= \beta SI - gI + aS \\ I + S &= N \end{aligned} \tag{8.1}$$

where S is the number of susceptible individuals, I is the number of infected individuals β is the transmission rate, g is the recovery rate, and a is the rate of spontaneous infection. This model assumes a constant population size, neglecting birth and death.

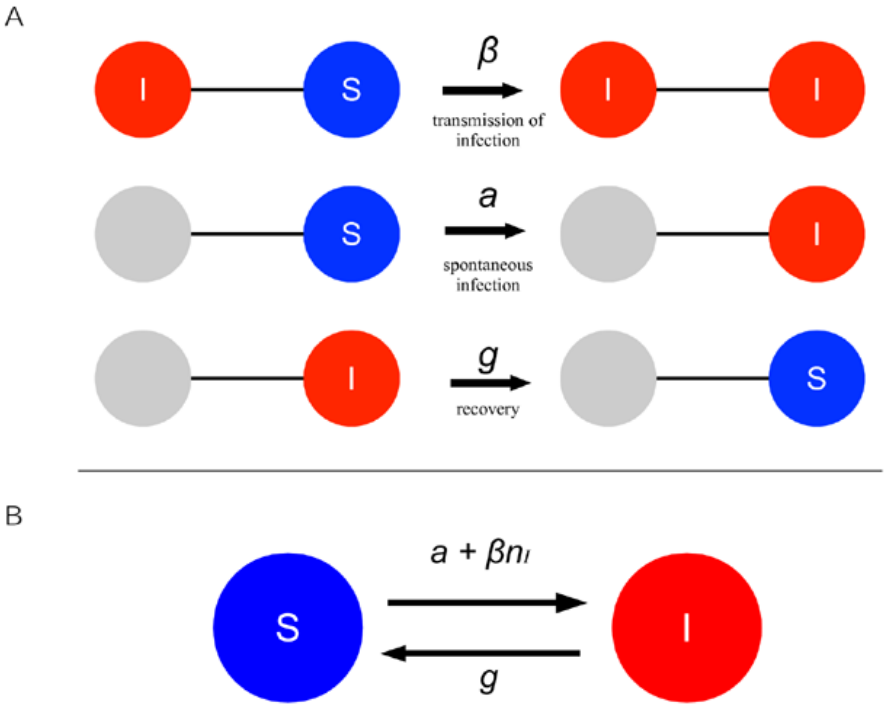

Figure 8.1: The SISa model of infection. A) There are three processes by which an individual's state can change. (i) An infected individual transmits infection to a susceptible contact with rate β. (ii) A susceptible individual spontaneously ('automatically') becomes infected at rate a, regardless of the state of her contacts. (iii) An infected individual returns to being susceptible at rate g, independent of the state of her contacts. B) The rates of movement for an individual between the susceptible and infected states. n_I is the number of infected contacts.

8.3.2 Parameter estimation

The classical definition of an infectious disease in the SIS/SIR context is that (i) the probability of an individual transitioning from susceptible to infected is an increasing function of the number of infected contacts, while (ii) the probability of a transition from infected to susceptible (i.e. recovery) is independent of the number or state of contacts. Exposure to infected individuals makes you more likely to become sick, but once you are infected you recover at a constant rate regardless of contacts. In addition to infectious contagion, the SISa model has an additional spontaneous mode of acquiring disease. To both test that a behavior displays infectious-disease-like dynamics, and to estimate values for the model parameters a, β, and g, we can use dynamic information about transitions

between states based on multiple time points in longitudinal data. For data points separated by time intervals (Δt) smaller than the average time between transitions, the transition probabilities can be linearized. The probability of a transition from susceptible to infected after a time Δt can be given by $P(S \to I, \Delta t) \sim (a + \beta n_I)\Delta t$, and the probability of transition from infected to susceptible after time Δt, by $P(I \to S, \Delta t) \sim g\Delta t$. It is necessary for the time between measurements to not be comparable to or greater than the average lifetime of a state to keep the probability of double transitions within a time interval low.

8.3.3 Dataset

In this study, we evaluate the assumption that emotions behave like infectious agents. We use data from the Framingham Heart Study [90] and the framework discussed above to test whether content and discontent fit the dynamics of infectious diseases. The Framingham study was initiated in 1948 in Framingham, Massachusetts and has continued enrolling subjects through the present. Subjects were examined at regular intervals of approximately three years. They were administered a psycho-social exam called the CES-D, which allowed us to classify each individual as *content*, *discontent* or *neutral*. We used the well-defined cut-off of a score of 16 on the full CES-D scale to classify subjects as *discontent*. This measure has previously been called 'depression', though it is not specific to clinical depression and represents general distress or depressive symptoms [299]. *Content* was defined as a score of 12 on the positively worded questions of the CES-D, and is the same subscale used by others and called 'positive affect', 'well-being' or 'happiness' [111, 229, 256, 276]. The terms 'content', 'discontent' and 'emotional state' as used in this paper represent long-term states reflecting general life satisfaction, as opposed to short-lived moods evinced in response to stimuli. Additionally, social networks were constructed for each subject based on recorded information on friends, family, coworkers and residential neighbours. For details, see the Electronic Supplementary Material (ESM).

We hypothesize that a neutral emotional state may act like a susceptible state, and that content and discontent act like 'infected' states (Fig. 8.1). We validate this classification using the data analysis presented below. Note that we exclude the possibility of *coinfection* by both content and discontent simultaneously, as this doubly infected state very rarely appears in the data (ESM Fig. S1). However, *superinfection* may be possible: individuals could potentially move directly between being content and discontent without passing through neutral. The data is used to validate the model assumptions and estimate values for the parameters β, a and g. These parameters are then used to calculate derived quantities of interest, such as the average lifetime of an emotional infection, the probability an infected person passes the infection to a given contact sometime during the course of her infection, and the average frequency with which infections arise spontaneously. Additionally, agent based simulations are used to compare model dynamics and clustering with the observational data.

8.3.4 Measuring transmission of emotions

To study the transmission of emotions, we examine changes in emotional state between the two sequential exams of the Framingham Heart Study in which the CES-D was administered (Exams 6 and 7). The average fraction of the network that was classified as content or discontent was very similar between the two exams, suggesting the transmission process is at steady state (Exam 6: 65% content, 9% discontent; Exam 7: 62% content, 9% discontent). Additionally, these exams were closely and consistently spaced ($\Delta t = 3 \pm 1$year). We include only subjects who answered all questions on the CES-D in both exams.

Subjects were initially classified as first as either 'content' or 'not content', and then separately as 'discontent' or 'not discontent'. Individuals who are neither 'content' nor 'discontent' are classified as 'neutral'. As expected, very few people who are classified as 'content' are also classified as 'discontent' (less than 1/1000). Thus we have three possible

emotional states. A diagram of the distribution of subjects between emotional states in included in the Electronic Supplementary Material (Fig. S1).

A given state x is considered infectious if having more contacts in state x makes you more likely to switch to state x. That is, a positive relationship between the number of contacts in state x and the probability to transition from state y to state x indicates that state x is infectious with respect to state y. Therefore, to test whether a given state x is infectious with respect to another state y, we perform an ordinary least squares (OLS) linear regression as follows. Each subject in state y in exam 6 is coded as either having transitioned to state x (transition=1) or not (transition=0) in exam 7. We then regress this binary transition variable for each subject against that subject's number of contacts in state x during exam 6. A significant positive correlation indicates that having more friends in state x at the earlier exam makes you more likely to switch to state x in the later exam. If state x is infectious (a significant positive correlation exists), then the value of β can be calculated from the slope of the regression line, and the value of a can be calculated from the intercept. If state x is not infectious (no significant correlation exists), then the value of g can be calculated from the intercept. Δt was taken as the average time between examinations, which was 2.5 years. Using logistic regression as opposed to OLS regression gives very similar results, as the datapoint line is within the linear range of the logistic model.

It is important for our analysis that subjects do not change emotional states rapidly (days or weeks), but instead on the timescale of years or longer. While the CES-D asks subjects to evaluate feelings in the last week, it is known to be a reliable measure of long-term emotions, as opposed to short-lived moods evinced in response to stimuli. Several studies have shown CES-D scale scores to be stable for up to 12 months, with high intra-individual test-retest correlations [281, 290]. Furthermore, we find a strong positive correlation between each subject's emotional state in the two measurement periods (r=0.47). This suggests that emotional states are not fluctuating on the timescale of weeks

or months, but rather on the timescale at which we are measuring: if they were changing faster than 3-5 years, then a subject s state in Exam 6 would not be strongly predictive of her state in Exam 7. Note that this correlation is also confirmed by a more detailed analysis [111]. Thus, there is strong evidence that the emotions we are measuring change only on the time scale we are measuring, as opposed to fluctuating much more rapidly.

Our epidemiological approach to social contagion has important differences from other models which look at correlations in present and past states of connected individuals [68, 69, 111]. Here, we look at how contacts influence the transitions between states, which better captures the nature of contagion. Since we use pre-existing social ties, we do not see effects from selection bias in choosing friends with similar emotional states. Additionally, confounding events that lead to concurrent changes in connected individuals will not show up as contagion effects in this model.

8.4 Results

In the Framingham Heart Study network, individuals may be connected to neighbours, coworkers, first-degree relatives and self-nominated friends. An individual s degree is the number of contacts that individual has to other people in the network. Restricting to only individuals who had been administered the CES-D at both exam 6 and 7, and their connections that existing at exam 6, gives a population of size N=1880, with average degree 3.1. The network is approximately Poisson distributed, with a long tail, although with some subjects having no connections. It has been previously shown found that family and friends living more than 2 miles away are not significantly associated with emotional influence [111], suggesting that face-to-face contact is important for transmission. Thus we restrict our analysis to connections involving only friends and relatives living closer than 2 miles away, next-door or same address neighbours and coworkers. With these further constraints, the degree of the network was reduced to 1.25 ± 1.35.

The results of the infectiousness analysis for the spread of content and discontent

between exams 6 and 7 are shown in Figure 8.2. Consistent with the SISa model formulation, we find a significant positive correlation between the probability of transitioning from neutral to content and the number of content contacts (Figure 8.2A, coeff=0.052, p=0.024), and no significant relationship between the transition from content to neutral and the number of neutral contacts (Figure 8.2B, coeff=-0.011, p=0.59). Additionally we find no significant relationship between the probability of transitioning from neutral to content and the number of neutral contacts (coeff=0.48, p=0.10), or the probability of transitioning from content to neutral and the number of content contacts (coeff=0.22, p=0.98). This suggests that content can indeed be modelled as an infectious process in the SISa framework, with neutral susceptibles more likely to become content infecteds with each content contact they have. The parameters for the SISa model can be calculated from the transition probabilities using equations mentioned previously, by dividing slope and intercept values by Δt, the average time between exams. The transmission rate, β, is found to be 0.02 /year. The spontaneous infection parameter a is found to be 0.18 /year. The recovery parameter g is found to be 0.088 /year. These results are dependent on restricting analysis to contacts who had exams separated by less that three and a half years (75%). For longer times it becomes increasingly likely that more than one transition has been made between exams.

We now repeat this analysis for discontent. We find that discontent can be also described in the SISa framework as a contagious emotion with neutral as the susceptible state. The probability of transitioning from neutral to discontent is positively correlated with the number of discontent contacts (Figure 8.2C, coeff=0.097, p=0.027), and the probability of transitioning from discontent back to neutral is independent of the number of neutral contacts (Figure 8.2D, coeff=0.032, p=0.56). Additionally we find no significant relationship between the probability of transitioning from neutral to discontent and the number of neutral contacts (coeff=0.11, p=0.75), or the probability of transitioning from discontent to neutral and the number of discontent contacts (coeff=0.002, p=0.99). The

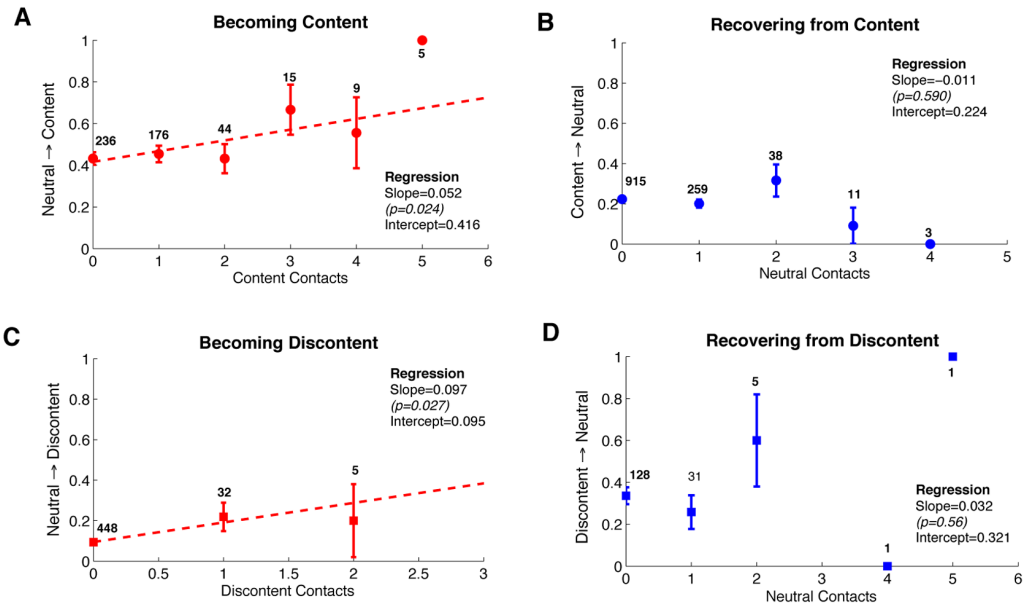

Figure 8.2: Both content and discontent behave like disease agents, infecting those in a susceptible neutral emotional state. The probability of transitioning from neutral to content increases in the number of content contacts (A), and the probability of transitioning from neutral to discontent increases in the number of discontent contacts (C). Conversely, the probability of recovering to the neutral state does not depend on the number of neutral contacts for either emotion (B,D). Error bars represent the standard error of the mean, and labels are the number of individuals averaged for each data point. We also find no significant dependence of these transitions on age, sex or education (A: age, coeff=0.0014, p=0.52; education, coeff=0.0024, p=0.81; sex, coeff=-0.0074, p=0.87. B: age, coeff=0.0016, p=0.21; education, coeff=-0.0095, p=0.08; sex, coeff=0.0109, p=0.64. C: age, coeff=0.0001, p=0.93; education, coeff=0.0008, p=0.90; sex, coeff=0.0485, p=0.08. D: age, coeff=-0.0006, p=0.88; education, coeff=-0.0165, p=0.35; sex, coeff=-0.024, p=0.77).

model parameters are $\beta = 0.04$ /year, $a = 0.040$ /year, $g = 0.13$ /year . Interestingly, the rate of transmission though a contact is similar for both content and discontent, while the rate of spontaneous infection is much larger for content and the rate of recovery is larger for discontent.

We also include for the possibility of direct transitions between content and discontent ('superinfection'), which are sometimes observed. We calculate the rate of direct transitions from content to discontent to be $s_{cd} = (0.009 \pm 0.003)$ /year and the rate from discontent to content to be $s_{dc} = (0.07 \pm 0.02)$ /year. See ESM for details. The estimated rates of all transitions are visualized in Figure 8.3.

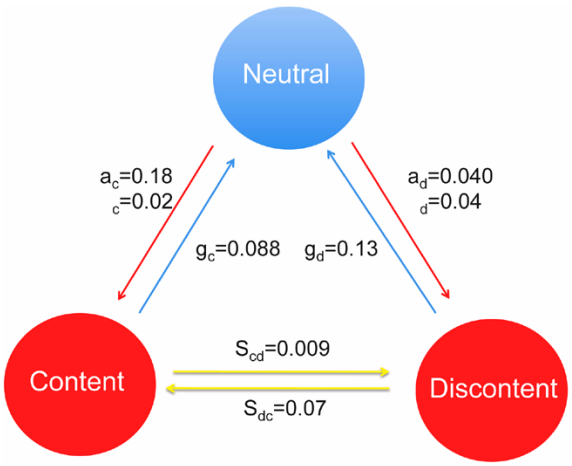

Figure 8.3: Parameter estimates for content and discontent using the SISa model framework. From these results, derived from Figure 8.2, we show that content and discontent are infectious emotions that can be 'caught' by neutral (susceptible) individuals from content or discontent (infected) contacts. There is also some 'superinfection' present: direct transitions between content and discontent. $a_c(a_d)$=rate of spontaneously becoming content (discontent), $g_c(g_d)$=rate of recovery from content (discontent), $\beta_c(\beta_d)$=transmission rate of content (discontent), $s_{cd}(s_{dc})$=rate of spontaneous superinfection from content to discontent (discontent to content)

From the SISa model parameter estimates, various quantities of interest can be calculated. The average lifetime of an emotional state is the average length of time an individual spends in this state before recovering. For both content and discontent, 'recovering' usually means going to the neutral state (g_c or g_d), but also includes the possibility of transitioning directly to the other 'infected state' (s_{cd} or s_{dc}). The total recovery rate (g_T) is the sum of both these rates. The average lifetime of a contentment infection is 10.1 years, and for discontentment it is 5.0 years. Thus the average contentment infection appears to last twice as long as the average discontentment episode. The 'influence' of an emotion is the cumulative probability that the infection will be passed from an infected to a susceptible connection before the infected individual recovers. This is calculated as $1 - e^{-r/g_T} \simeq r/g_T$. For both content and discontent, this value is 0.18. The 'cycle length' is the average length of time between spontaneous infections, and is 5.6 years for content and 25 years for discontent. This suggests that that an individual may spontaneously become content many times throughout life.

In the regular SIS or SIR models, the average number of secondary infections caused before recovery is called the *basic reproductive ratio*, R_0. An epidemic only occurs for $R_0 > 1$. In the SISa model, there is no thresholding behavior as seen in traditional models, because of the spontaneous infection term. Even if there are no individuals initially infected and no contagion (β=0), spontaneous infection will nonetheless lead to a non-zero steady state level of infected. In the absence of spontaneous infection, the effective R_o can be estimated as $\beta n/g$, where n is the average degree. For content, R_0 is 0.28 and for discontent it is 0.39. Since for both R_o is less than one, self-sustained epidemics of either emotion could not be sustained if people did not become spontaneously infected.

We also perform further analysis to examine differences in local network structure for individuals in different emotional states. Content individuals have on average 1.26 connections to other people in the data, neutral individuals 1.37 connections, and discontent individuals 0.97 connections. The smaller number of connections among discontent individuals suggests isolation, which could be contributing to or secondary to depressive symptoms. We can also ask whether people in a given state tend to cluster. Clustering is a measure of the spatial correlation (in the network sense) between individuals in the same emotional state. Clustering is defined as the ratio of the observed number of connections between two types of individuals to the number of connections expected if the positioning of individuals in the network was random. Clustering of like individuals can be caused by an infective process spreading within a network [175], but may also be caused by confounding environmental factors influencing behaviour, or selection of contacts based on similar behaviour. In a purely infectious process on a network, the average correlation between two infected individuals will be greater than one, and the average correlation between an infected and a susceptible individual will be less than one. To compare observed clustering to that expected from a pure infection, we perform agent based simulations of SISa epidemics on networks with the FHS network topology and calculate the predicted clustering (Table 8.1). For content, there is good

agreement between observed and predicted clustering, suggesting that the inductive spread of content can explain the observed clustering of content individuals. For discontent, however, there is less clustering in the data then predicted by the infectious disease simulations. Thus discontent people are more isolated in the network then predicted by the infectious model, which is consistent with the reduced average degree observed above. This could be explained by a tendency for depression to cause people to interact less with others, or for social isolation to lead to depression [32].

Table 8.1: Network structure dependance on emotional states, and comparison with epidemic simulations. Discontent individuals have a significantly lower number of contacts (degree) than others. C_{xy} is the clustering between individuals of type x and y. c=content, d=discontent, n=neutral. The clustering of like individuals that arises from an infectious process can explain the clustering of content individuals, but discontent individuals are less clustered than expected for the transmission rate.

	Content	Discontent	Neutral
average degree	1.26	0.97	1.37
observed clustering	C_{cc}=1.04 C_{cn}=0.91	C_{dd}= 1.07 C_{dn}=0.77	- -
simulated clustering	C_{cc}=1.09 C_{cn}=0.95	C_{dd}=1.92 C_{dn}= 1.0	- -

8.5 Discussion

Here we have shown that long-term emotional states can spread between socially connected individuals. The transmission rate for content is found to be $r = 0.02$ /year, and the spontaneous infection parameter is found to be $a = 0.18$ /year, thus each content contact increases the probability of becoming content by 11%/year. For discontent, the rate of spontaneous infection is $a = 0.040$ and the rate of transmission is $\beta = 0.04$, so each discontent contact makes an individual 100%/year more likely to become discontent. The average lifetime of a contentment 'infection' is measured to be 10 years, and a discontentment 'infection', 5 years. We have introduced a novel framework for formalising social contagion derived from the study of infectious diseases, which can be used to study

the spread of emotions or other social phenomena. This infectious disease approach has several advantages over methods which examine correlations in behaviours of connected individuals. Our method controls for selection bias in choosing contacts with similar behaviour, as well as confounding environmental factors synchronously affecting contacts. Moreover, we find no dependence of the probability of changing emotional state on age, sex, or education, which have been found in previous studies of content and discontent to affect the propensity for emotions and confound the correlations between contacts [11, 111]. This lack of dependence when we focus on transitions suggests that our approach is more robust to variation across individuals than previous methods.

Much of the appeal of our approach is the significance of our results despite the great simplicity of the model used, and the assumptions made about the dataset. Determining the various transition rates for the model requires the implicit assumption that all individuals are identical in their susceptibility to various emotional states. These rates therefore represent ensemble averages over the population. In reality, individuals are likely to differ in their predispositions to various emotional states.

The ability to observe transmission of emotional states over long time frames requires some particular properties of the Framingham Heart Study. These include large sample sizes, longitudinal follow-up, extensive information on social contacts and various relationships, closely and consistently spaces exams, and reliable measures of emotions and behavioural states. This study was not designed to study social networks or mental health, and so there are some drawbacks that could be improved upon in more specifically designed projects. For example, we only examine changes between two time points, which give us stationary values for the rates of transmission, although it is plausible that these rates themselves change over time. Future work exploring the dynamic spread of emotions with higher resolution data collection is called for. This may also allow for more complex and perhaps realistic models, such as modeling emotions as continuous variables rather than discrete states, with transmission depending on the severity of infection.

One possible limitation of this study is the social network dataset used. We have also assumed that the social network collected through the Framingham Heart Study is the same as the contact network for the spread of emotions, which is almost certainly not true given the sparseness of the Framingham network. Because the Framingham Heart Study was not designed as a study of social networks, no attempt was made to capture all of a persons important contacts. Many close friends of a person could be missing (usually only one was recorded) and family and coworkers who aren't part of ones actual social network may have been counted. Even if undersampling of real-world contacts did occur, it does not change our results qualitatively: our data clearly show that rates of becoming "content" or "discontent" increase with the number of "infected" contacts (i.e. are contagious) while the rates of "recovery" to a "neutral" state do not depend on contacts. However, it could change the measured rate constants. If we missed a constant number of contacts for each person, the intercept of the transition graphs would be shifted to the right, then the actual a would be smaller than the a we measured. If we missed a constant fraction of contacts for each person, then the x axis would be compressed and the slope would be increased, so then the actual value of β would be smaller than the β we measured. However, while it is likely that the Framingham network underestimates the total number of contacts, the relationship to the number of 'influential' contacts is unclear. In this sense, the observed value of the transmission rates, β, are network dependent. Additionally, network connections may be weighted differently according to their ability to transmit emotions. It would be ideal to design longitudinal study with the intent of measuring social networks and health and carefully define contacts, such as by amount of time spent together per day, influence, etc.

A CES-D score of greater than 16 (which we defined as 'discontent') can occur with major depression (94% specific) as well as alcohol or drug dependence, anxiety, dysthymia, or bipolar disorder. Thus it is a measure of depressive symptoms or general distress and not necessarily clinical depression [281, 299]. The 10-year prevalence of all affective

disorders is close to 30% [11] which suggests that a large portion of the population is susceptible to depressive symptoms. This fact is consistent with our ensemble treatment, and with the observed cycle length for discontent of 25 years. Treating discontent as a spontaneously acquired or transmitted infection has one major drawback: it assumes that the probability of becoming discontent is independent of an individual's history of depressive episodes. In reality, depression is known to be a recurrent condition, with relative risk increasing with history of illness [12]. It has been found that 72 % of people with major or minor depression experience recurrent episodes [179]. No comparable data exists for the CES-D measurement of content, which is less routinely used. Relevant data for comparison will likely become available as the study of 'positive psychology', and especially its relation to health [276], becomes more widespread. There have been no studies to our knowledge which examine the lifetime or cycle of discontent or content in the general population, as defined by the CES-D.

Our study provides evidence for a transmissive component to the dynamics of the emotions of content and discontent. However, this dataset does not give insight into the mechanism of infection. It is possible that displayed emotions are directly contagious (via mimicry, pheromones, etc), or that emotions spread indirectly, for example by sharing some type of good fortune. While short-term emotional states have been suggested as a mechanism for systemically coordinating body functions to react in the most favourable way to an environmental stimulus, and as a means of 'quick-and-dirty' communication of this stimulus to others [201], it is not obvious how this argument extends to the contagion of long-term emotional states. The observed fact that 'catching' content and discontent depends on social contacts, while 'recovering' to a neutral state does not, suggests that infection involves a process similar to teaching a life skill that can then persist without a constant stimulus. The mechanisms behind the transmission of long-term emotional states merit further study.

We have formally demonstrated that emotions can be thought of as infectious diseases

spreading across social networks. We have introduced a novel form of mathematical infectious disease model for describing the spread of emotions which has advantages over previous methods. We have validated this model by studying content and discontent propagating across a large social network. Our results give insight into the transmissive nature of positive and negative emotions, and our model provides a theoretical framework for studying the spread of other emotions, as well as a wide range of other social phenomena. Determining to what extent particular emotions or behaviours are infectious is a promising direction for further research with important implications for social science, epidemiology, and health policy.

8.6 Supplemental Information

8.6.1 Framingham Heart Study Dataset

In this study, we evaluate the assumption that emotions behave like infectious agents. We use data from the Framingham Heart Study [90] and the framework discussed above to test whether positive and negative emotions fit the dynamics of an infectious disease. The Framingham study was initiated in 1948 in Framingham, Massachusetts and has continued enrolling subjects through the present. We examined individuals in the Offspring Cohort, enrolled starting in 1971. Subjects come to a central facility at regular intervals (approximately every 3 years) for medical examination and collection of other survey data. In additional to information on mental and physical health, subjects were asked to name at least one close friend at each exam, and were also connected to all first-order relatives, coworkers, and residential neighbours.

For each subject, the following social connection data is available: (i) each other person to whom they were connected, (ii) the dates of initiation and termination of that relationship, (iii) the type of relationship (neighbour, coworker, first-degree relative, or friend), and (v) the geographic distance between the two subjects. The social network for

each exam was constructed by creating a network matrix G, where $G_{ijk} = 1$ if subject i nominated subject j as a connection before or during the time that subject i was administered exam k. All relationship types are mutual except for friendships, which are self-nominated, such that $G_{ijk} \neq G_{jik}$ is possible for friendships.

Individuals in the Framingham Heart Study were administered a widely validated psycho-social exam called the CES-D (The Center for Epidemiologic Studies Depression Scale, [281]) at exams 6 and 7 (administered on average in 1997 and 2000). The full version of this survey style exam is commonly used to classify depressive symptoms [281, 299, 309] and a subscale which comprises a distinct factor [164, 276, 282, 318, 347] has also been validated as a measure of positive affect [229, 256, 276]. Similar measures of positive affect using subjective surveys have been shown to be highly correlated with objective measures of well-being [257]. We have chosen to call this positive state measured by the CES-D *content*, though it has been called 'happiness' by others. It is also related to optimism and self-esteem. The negative emotion measured by the full CES-D scale is generally called 'depression', though as described in [299], this measure is generally agreed to represent a long-term emotional state of depressive symptomology that is distinct from (and less severe than) the mental illness state of clinical depression. To prevent confusion, we have called this measure *discontent* throughout the paper.

A content score and a discontent score were calculated for each subject from the raw responses to 20 multiple choice questions from the CES-D. The questions asked subjects to judge the frequency with which they experienced a particular feeling or behaviour, with available answers being 0=(rarely or none of the time, <1 day per week), 1=(some or a little of the time, 1-2 days per week), 2=(occasionally or a moderate amount of the time, 3-4 days per week) and 3=(most of the time, 5-7 days per week). Subjects are classified as *content* if they scored the maximum value of 3 on each of four particular questions related to positive feelings. Summing the answers to the 16 CES-D questions related to negative feelings and adding inverted answers to the 4 positive questions, subjects are classified as

discontent if they have a total score greater than 16 (out of a possible 60). Individuals who are neither content nor discontent are classified as *neutral*. The distribution of emotional states among our subjects is shown in Figure S1A. We find that less than 1 out of every 1000 subjects are both content and discontent, validating our classification of emotions into the three states content, discontent and neutral. Figure S2B shows the number of people who made each transition between the two examinations.

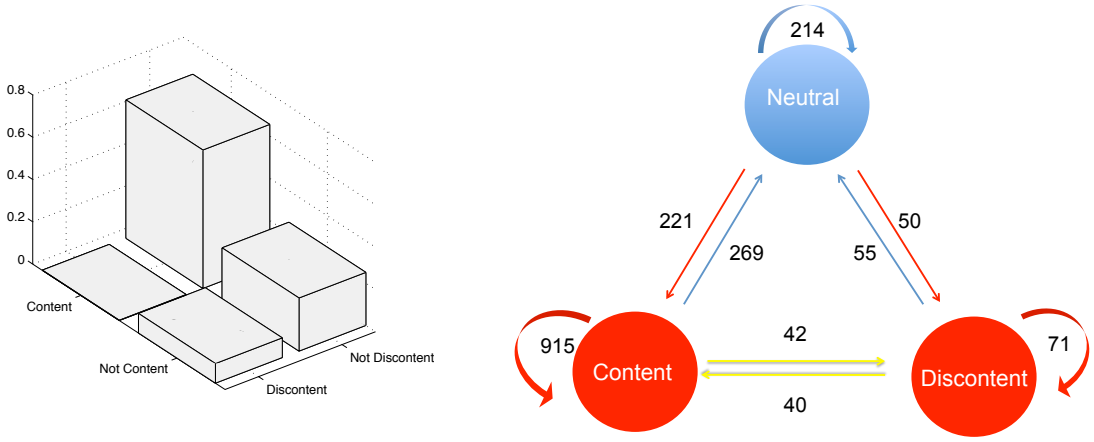

Figure 8.4: Figure S1. A) The distribution of subjects between four emotional states measured by the CES-D. Subjects were classified as first as either 'content' or 'not content', and then separately as 'discontent' or 'not discontent'. Individuals who are neither 'content' nor 'discontent' are classified as 'neutral'. As expected, very few people who are classified as 'content' are also classified as 'discontent', while those that are 'not content' may be 'discontent' or 'not discontent'. Fraction content=0.63, discontent=0.09, neutral=0.28. B) Each circle represents an emotional state, and the arrows and numbers display the number of transitions that occurred between each state.

8.6.2 Super-infection: Direct transitions between content and discontent infected states

Figure S1B shows that direct transitions between the content and discontent states are sometimes observed. There are two possibles explanations for these transitions. Firstly, because exams are only every 3 years, it is possible that some of these individuals actually moved through the neutral state, and thus made two transitions between observations (ie content to neutral to discontent). The second explanation is that these individuals actually

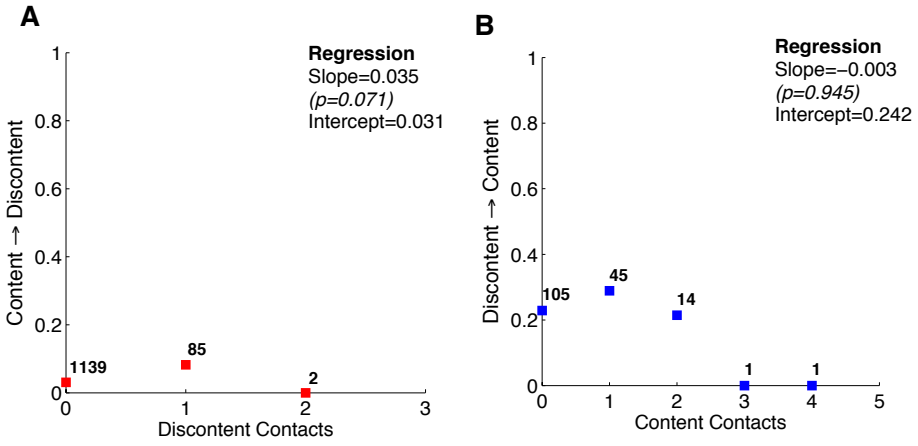

Figure S2. Observed rates of direct transitions between content and discontent and vice versa. We see no significant dependance on the number of infected contacts for these direct transitions.

moved directly between these states via 'super-infection'. We can predict how often we would expect double transitions to occur within the 3 year window, based on the estimates for each individual transition. These predictions are lower than the observed number of direct transitions. Thus the difference between the observed and expected can be interpreted as the rate of actual direct transitions. This is explained in detail below. The estimated rates of all transitions are visualized in Figure 3 in the main text.

For a Markov process, if an event occurs at a rate a, then the probability that this event has occurred after a time Δt is $1 - e^{-a\Delta t}$. If two events occur at rates a_1 and a_2, and must occur in that sequential order, then in a time period Δt the probability that both occur is :

$$\int_0^{\Delta t} a_1(1 - e^{-a_2(\Delta t - t)})\, dt = a_1\Delta t - \frac{a_1}{a_2}(1 - e^{-a_2\Delta t}) \tag{8.2}$$

From this expression we can calculate the expected rate of double transitions between content and discontent (going through the neutral state) in a single time period between exams.

For content → discontent, the two transitions that must occur are : content to neutral ($a_1 = g_c$) and neutral to discontent ($a_2 = a_d + \beta_d n_d$). There values are:

- $g_c = 0.088 \pm 0.006$ /year
- $a_d = 0.040 \pm 0.006$ /year
- $\beta_d = 0.04 \pm 0.02$ /year

For discontent $\rightarrow$ content, the two transitions that must occur are : discontent to neutral ($a_1 = g_d$) and neutral to content ($a_2 = a_c + \beta_c n_c$). There values are:

- $g_d = 0.13 \pm 0.02$ /year
- $a_c = 0.18 \pm 0.01$ /year
- $\beta_c = 0.02 \pm 0.01$ /year

Using Equation 8.2, the expected rate of double transitions are (with standard deviations included):

- content to discontent: $c_{expected} = (0.004 \pm 0.001) + (0.004 \pm 0.001) * n_d$ /year
- discontent to content: $c_{expected} = (0.025 \pm 0.004) + (0.003 \pm 0.002) * n_c$ /year

Observed double transition, from Figure S2:

- content to discontent: $c_{observed} = (0.013 \pm 0.002) + (0.014 \pm 0.019) * n_d$ /year
- discontent to content: $c_{observed} = (0.097 \pm 0.016) + (-0.0013 \pm 0.043) * n_c$ /year

Note that the contact dependent terms for the double transition are observed to be non-significant, and also expected to be overlapping with zero due to the margins of error on the calculated rates. We hence ignore them for the reported rates of double transitions. The rate of direct bypass transitions is the extra number of transitions that cannot be accounted for by double transitions. This is found by subtracting the expected rates ($c_{expected}$) from the observed rates ($c_{observed}$)

Rate of direct bypass transition:

- content to discontent: $s_{cd} = (0.009 \pm 0.003)$ /year
- discontent to content: $s_{dc} = (0.07 \pm 0.02)$ /year

It is interesting to note that in Figure S1B, the number of individuals transitioning directly from content to discontent is very similar to number transitioning from discontent to content. The same is true of the transitions between content and neutral, and between discontent and neutral. Thus the system is in *detailed balance*, suggesting a unique subset of the population may be responsible for the direct transitions between content and discontent. For example, it could be those suffering from bipolar disease, who represent about 1% of the population and switch between manic and discontent episodes on the order of months.

8.7 Acknowledgments

This work was supported by the National Institute on Aging grant P01 AG031093, the John Templeton Foundation, the Bill and Melinda Gates Foundation, the National Science Foundation/National Institutes of Health joint program in mathematical biology (National Institutes of Health Grant R01GM078986), and graduate fellowships from the National Science Foundation and the Canadian Natural Sciences and Engineering Research Council. NHLBI's Framingham Heart Study is supported by contract number N01-HC-25195. We thank Laurie Meneades for assistance with the database and Erez Leiberman, Michael Manapat, JB Michel, Dan Gilbert, Matt Killingsworth, and Niels Rosenquist for helpful discussions throughout this study.

8.8 Manuscript Information

8.8.1 Previously published as

This manuscript appeared in [142]:

A. L. Hill, D. G. Rand, M. A. Nowak, and N. A. Christakis. Emotions as infectious diseases in a large social network: the SISa model. *Proceedings of the Royal Society B: Biological Sciences*, 277(1701):3827 –3835, Dec. 2010. doi: 10.1098/rspb.2010.1217. URL http://rspb.royalsocietypublishing.org/content/277/1701/3827.abstract

*the first two authors contributed equally to this work

8.8.2 The author's contribution

The first two authors contributed equally to this work. Analyzed the data: ALH. Wrote the paper: ALH DGR. Designed the model and analysis: ALH DGR. Conceived of the project: DGR MAN NAC.

References

1. J. Abate, G. L. Choudhury, and W. Whitt. An introduction to numerical transform inversion and its application to probability models. *Computational Probability*, pages 257–323, 1999.

2. A. B. Abecasis, P. Lemey, N. Vidal, T. de Oliveira, M. Peeters, R. Camacho, B. Shapiro, A. Rambaut, and A.-M. Vandamme. Recombination confounds the early evolutionary history of human immunodeficiency virus type 1: Subtype g is a circulating recombinant form. *Journal of Virology*, 81(16):8543 –8551, Aug. 2007. doi: 10.1128/JVI.00463-07. URL http://jvi.asm.org/content/81/16/8543.abstract.

3. M. E. Abram, A. L. Ferris, W. Shao, W. G. Alvord, and S. H. Hughes. Nature, position, and frequency of mutations made in a single cycle of HIV-1 replication. *J. Virol.*, 84:9864–9878, Oct. 2010. doi: 10.1128/JVI.00915-10. URL http://jvi.asm.org/cgi/content/abstract/84/19/9864.

4. G. Achaz, S. Palmer, M. Kearney, F. Maldarelli, J. W. Mellors, J. M. Coffin, and J. Wakeley. A robust measure of HIV-1 population turnover within chronically infected individuals. *Mol. Biol. Evol.*, 21(10):1902–1912, 2004.

5. J. B. Alimonti, T. B. Ball, and K. R. Fowke. Mechanisms of CD4+ t lymphocyte cell death in human immunodeficiency virus infection and AIDS. *J Gen Virol*, 84(7): 1649–1661, July 2003. doi: 10.1099/vir.0.19110-0. URL http://vir.sgmjournals.org/cgi/content/abstract/84/7/1649.

6. H. K. Allen, J. Donato, H. H. Wang, K. A. Cloud-Hansen, J. Davies, and J. Handelsman. Call of the wild: antibiotic resistance genes in natural environments. *Nat Rev Micro*, 8(4):251–259, Apr. 2010. ISSN 1740-1526. doi: 10.1038/nrmicro2312. URL http://dx.doi.org/10.1038/nrmicro2312.

7. T. M. Allen, M. Altfeld, S. C. Geer, E. T. Kalife, C. Moore, K. M. O'Sullivan, I. DeSouza, M. E. Feeney, R. L. Eldridge, E. L. Maier, D. E. Kaufmann, M. P. Lahaie, L. Reyor, G. Tanzi, M. N. Johnston, C. Brander, R. Draenert, J. K. Rockstroh, H. Jessen, E. S. Rosenberg, S. A. Mallal, and B. D. Walker. Selective escape from CD8+ t-cell responses represents a major driving force of human immunodeficiency virus type 1 (HIV-1) sequence diversity and reveals constraints on HIV-1 evolution. *Journal of Virology*, 79(21):13239 –13249, Nov. 2005. doi: 10.1128/JVI.79.21.13239-13249.2005. URL http://jvi.asm.org/content/79/21/13239.abstract.

8. C. L. Althaus and R. J. De Boer. Dynamics of immune escape during HIV/SIV infection. *PLoS Comput Biol*, 4(7):e1000103, July 2008. doi: 10.1371:journal.pcbi.1000103. URL http://dx.plos.org/10.1371:journal.pcbi.1000103.

9. A. Anagnostopoulos, R. Kumar, and M. Mahdian. Influence and correlation in social networks. In *Proceeding of the 14th ACM SIGKDD International Conference on Knowledge Discovery and Data Mining*, page 7–15, 2008.

10. R. M. Anderson and R. M. May. *Infectious diseases of humans: dynamics and control*. Oxford University Press, USA, 1991.

11. J. Angst. Epidemiology of depression. *Psychopharmacology*, 106:71–74, 1992. doi: 10.1007/BF02246240.

12. J. Angst, A. Gamma, R. Sellaro, P. W. Lavori, and H. Zhang. Recurrence of bipolar disorders and major depression. *European archives of psychiatry and clinical neuroscience*, 253(5):236–240, 2003. doi: 10.1007/s00406-003-0437-2.

13. S. Aral and D. Walker. Identifying influential and susceptible members of social networks. *Science*, 337(6092):337–341, July 2012. ISSN 0036-8075, 1095-9203. doi: 10.1126/science.1215842. URL http://www.sciencemag.org/content/337/6092/337.

14. N. M. Archin, A. Espeseth, D. Parker, M. Cheema, D. Hazuda, and D. M. Margolis. Expression of latent HIV induced by the potent HDAC inhibitor suberoylanilide hydroxamic acid. *AIDS Research and Human Retroviruses*, 25(2):207–212, Feb. 2009. ISSN 0889-2229, 1931-8405. doi: 10.1089/aid.2008.0191. URL http://online.liebertpub.com/doi/abs/10.1089/aid.2008.0191.

15. N. M. Archin, M. Cheema, D. Parker, A. Wiegand, R. J. Bosch, J. M. Coffin, J. Eron, M. Cohen, and D. M. Margolis. Antiretroviral intensification and valproic acid lack sustained effect on residual HIV-1 viremia or resting CD4+ cell infection. *PLoS ONE*, 5(2):e9390, Feb. 2010. doi: 10.1371/journal.pone.0009390. URL http://dx.doi.org/10.1371/journal.pone.0009390.

16. N. M. Archin, A. L. Liberty, A. D. Kashuba, S. K. Choudhary, J. D. Kuruc, A. M. Crooks, D. C. Parker, E. M. Anderson, M. F. Kearney, M. C. Strain, D. D. Richman, M. G. Hudgens, R. J. Bosch, J. M. Coffin, J. J. Eron, D. J. Hazuda, and D. M. Margolis. Administration of vorinostat disrupts HIV-1 latency in patients on antiretroviral therapy. *Nature*, 487(7408):482–485, July 2012. ISSN 0028-0836. doi: 10.1038/nature11286. URL http://www.nature.com/nature/journal/v487/n7408/full/nature11286.html.

17. N. M. Archin, N. K. Vaidya, J. D. Kuruc, A. L. Liberty, A. Wiegand, M. F. Kearney, M. S. Cohen, J. M. Coffin, R. J. Bosch, C. L. Gay, J. J. Eron, D. M. Margolis, and A. S. Perelson. Immediate antiviral therapy appears to restrict resting CD4+ cell HIV-1 infection without accelerating the decay of latent infection. *Proceedings of the National Academy of Sciences of the United States of America*, 109(24):9523–9528, June 2012. ISSN 1091-6490. doi: 10.1073/pnas.1120248109. PMID: 22645358.

18. K. K. Ari n, G. Vanham, and E. J. Arts. Is HIV-1 evolving to a less virulent form in humans? *Nature Reviews Microbiology*, 5(2):141–151, 2007. URL

file:///Users/Ali/Documents/MN/HIVarticles/HIV.Data/PDF/HIVevolvinglessvirulent07-2153608193/HIVevolvinglessvirulent07.pdf.

19. J. R. Arribas, A. Horban, J. Gerstoft, G. Fätkenheuer, M. Nelson, N. Clumeck, F. Pulido, A. Hill, Y. van Delft, T. Stark, and C. Moecklinghoff. The MONET trial: darunavir/ritonavir with or without nucleoside analogues, for patients with HIV RNA below 50 copies/ml. *AIDS*, 24(2):223–230, 2010. ISSN 1473-5571. doi: 10.1097/QAD.0b013e3283348944. URL http://www.ncbi.nlm.nih.gov/pubmed/20010070.

20. B. Asquith. The evolutionary selective advantage of HIV-1 escape variants and the contribution of escape to the HLA-Associated risk of AIDS progression. *PLoS ONE*, 3 (10):e3486, Oct. 2008. doi: 10.1371/journal.pone.0003486. URL http://dx.doi.org/10.1371/journal.pone.0003486.

21. D. B. Bahr, R. C. Browning, H. R. Wyatt, and J. O. Hill. Exploiting social networks to mitigate the obesity epidemic. *Obesity*, 17(4):723–728, Jan. 2009. ISSN 1930-7381. URL http://dx.doi.org/10.1038/oby.2008.615.

22. F. Ball, D. Mollison, and G. Scalia-Tomba. Epidemics with two levels of mixing. *The Annals of Applied Probability*, 7(1):46–89, 1997.

23. D. R. Bangsberg, A. R. Moss, and S. G. Deeks. Paradoxes of adherence and drug resistance to HIV antiretroviral therapy. *J. Antimicrob. Chemother.*, 53(5):696 –699, 2004. doi: 10.1093/jac/dkh162.

24. D. R. Bangsberg, E. P. Acosta, R. Gupta, D. Guzman, E. D. Riley, P. R. Harrigan, N. Parkin, and S. G. Deeks. Adherence-resistance relationships for protease and non-nucleoside reverse transcriptase inhibitors explained by virological fitness. *AIDS*, 20(2):223–231, 2006. ISSN 0269-9370. doi: 10.1097/01.aids.0000199825.34241.49. URL http://www.ncbi.nlm.nih.gov/pubmed/16511415.

25. D. R. Bangsberg, D. L. Kroetz, and S. G. Deeks. Adherence-resistance relationships to combination HIV antiretroviral therapy. *Current HIV/AIDS Reports*, 4(2):65–72, May 2007. ISSN 1548-3568. URL http://www.ncbi.nlm.nih.gov/pubmed/17547827. PMID: 17547827.

26. D. H. Barouch. Challenges in the development of an HIV-1 vaccine. *Nature*, 455 (7213):613–619, 2008. URL file:///Users/Ali/Documents/MN/HIVarticles/HIV.Data/PDF/nature07352-0056501249/nature07352.pdf.

27. S. G. Barsade. The ripple effect: Emotional contagion and its influence on group behavior. *Administrative Science Quarterly*, pages 644–675, 2002.

28. I. Bartha, P. Simon, and V. M ller. Has HIV evolved to induce immune pathogenesis? *Trends in Immunology*, 29(7):322–328, July 2008. ISSN 1471-4906. doi: 10.1016/j.it.2008.04.005. URL http://www.sciencedirect.com/science/article/pii/S1471490608001269.

29. F. M. Bass. A new product growth for model consumer durables. *Management Science*, 15(5):215–227, Jan. 1969. ISSN 00251909. URL http://www.jstor.org/stable/2628128.

30. R. Batorsky, M. F. Kearney, S. E. Palmer, F. Maldarelli, I. M. Rouzine, and J. M. Coffin. Estimate of effective recombination rate and average selection coefficient for HIV in chronic infection. *Proceedings of the National Academy of Sciences*, 108(14): 5661–5666, Apr. 2011. ISSN 0027-8424, 1091-6490. doi: 10.1073/pnas.1102036108. URL http://www.pnas.org/content/108/14/5661.abstract?ijkey=e34aae298f6644694bac9406838a44b5e8692ad1&keytype2=tf_ipsecsha.

31. P. S. Bearman and J. Moody. Suicide and friendships among american adolescents. *American Journal of Public Health*, 94(11):89–95, 2004.

32. A. T. Beck and B. A. Alford. *Depression: Causes and Treatment*. University of Pennsylvania Press, 2009. ISBN 0812219643, 9780812219647.

33. N. Beerenwinkel, B. Schmidt, H. Walter, R. Kaiser, T. Lengauer, D. Hoffmann, K. Korn, and J. Selbig. Diversity and complexity of HIV-1 drug resistance: A bioinformatics approach to predicting phenotype from genotype. *Proceedings of the National Academy of Sciences*, 99(12):8271 –8276, June 2002. doi: 10.1073/pnas.112177799. URL http://www.pnas.org/content/99/12/8271.abstract.

34. N. Beerenwinkel, T. Lengauer, M. Daumer, R. Kaiser, H. Walter, K. Korn, D. Hoffmann, and J. Selbig. Methods for optimizing antiviral combination therapies. *Bioinformatics*, 19(Suppl 1):i16, 2003.

35. C. T. Bergstrom, J. D. West, and M. A. Wiseman. The eigenfactor metrics. *Journal of Neuroscience*, 28(45):11433, 2008.

36. B. Best, P. Koopmans, S. Letendre, E. Capparelli, S. Rossi, D. Clifford, A. Collier, B. Gelman, G. Mbeo, J. McCutchan, et al. Efavirenz concentrations in CSF exceed IC50 for wild-type HIV. *J. Antimicrob. Chemother.*, 66(2):354, 2011.

37. A. Biancotto, J.-C. Grivel, F. Gondois-Rey, L. Bettendroffer, R. Vigne, S. Brown, L. B. Margolis, and I. Hirsch. Dual role of prostratin in inhibition of infection and reactivation of human immunodeficiency virus from latency in primary blood lymphocytes and lymphoid tissue. *Journal of Virology*, 78(19):10507–10515, Oct. 2004. ISSN 0022-538X, 1098-5514. doi: 10.1128/JVI.78.19.10507-10515.2004. URL http://jvi.asm.org/content/78/19/10507.

38. J. Blankson, D. Persaud, and R. Siliciano. The challenge of viral reservoirs in HIV-1 infection. *Annual Review of Medicine*, 53(1):557 593, 2002.

39. J. N. Blankson. The study of elite controllers: a pure academic exercise or a potential pathway to an HIV-1 vaccine? *Current Opinion in HIV and AIDS*, 6(3):147–150, May 2011. ISSN 1746-6318. doi: 10.1097/COH.0b013e3283457868. URL http://www.ncbi.nlm.nih.gov/pubmed/21399493. PMID: 21399493.

40. J. N. Blankson, J. D. Siliciano, and R. F. Siliciano. The Effect of early treatment on the latent reservoir of HIV-1. *Journal of Infectious Diseases*, 191(9):1394–1396, May 2005.

41. C. I. Bliss. The toxicity of poisons applied jointly. *Ann. Appl. Biol.*, 26(3):585–615, Aug. 1939. ISSN 1744-7348. doi: 10.1111/j.1744-7348.1939.tb06990.x. URL http://onlinelibrary.wiley.com/doi/10.1111/j.1744-7348.1939.tb06990.x/abstract.

42. S. Blower, E. Bodine, J. Kahn, and W. McFarland. The antiretroviral rollout and drug-resistant HIV in africa: insights from empirical data and theoretical models. *AIDS (London, England)*, 19(1):1–14, Jan. 2005. ISSN 0269-9370. URL http://www.ncbi.nlm.nih.gov/pubmed/15627028. PMID: 15627028.

43. S. M. Blower, H. B. Gershengorn, and R. M. Grant. A tale of two futures: HIV and antiretroviral therapy in san francisco. *Science*, 287(5453):650–654, Jan. 2000. ISSN 0036-8075, 1095-9203. doi: 10.1126/science.287.5453.650. URL http://www.sciencemag.org/content/287/5453/650.

44. M. C. Boerlijst, S. Bonhoeffer, and M. A. Nowak. Viral quasi-species and recombination. *Proceedings of the Royal Society B: Biological Sciences*, 263: 1577–1584, 1996.

45. J. D. Bohlmann, R. J. Calantone, and M. Zhao. The effects of market network heterogeneity on innovation diffusion: An Agent-Based modeling approach. *Journal of Product Innovation Management*, 27(5):741–760, 2010. doi: 10.1111/j.1540-5885.2010.00748.x. URL http://dx.doi.org/10.1111/j.1540-5885.2010.00748.x.

46. V. F. Boltz, Y. Zheng, S. Lockman, F. Hong, E. K. Halvas, J. McIntyre, J. S. Currier, M. C. Chibowa, C. Kanyama, A. Nair, W. Owino-Ong'or, M. Hughes, J. M. Coffin, and J. W. Mellors. Role of low-frequency HIV-1 variants in failure of nevirapine-containing antiviral therapy in women previously exposed to single-dose nevirapine. *Proc. Natl. Acad. Sci. USA*, 108(2):9202–9207, 2011.

47. S. Bonhoeffer and M. A. Nowak. Pre-existence and emergence of drug resistance in HIV-1 infection. *Proc. R. Soc. B*, 264(1382):631–637, 1997.

48. J. E. Bono and R. Ilies. Charisma, positive emotions and mood contagion. *The Leadership Quarterly*, 17(4):317–334, 2006. doi: 10.1016/j.leaqua.2006.04.008.

49. C. Boutwell, M. Rolland, J. Herbeck, J. Mullins, and T. Allen. Viral evolution and escape during acute HIV?1 infection. *The Journal of Infectious Diseases*, 202(S2): S309–S314, Oct. 2010. ISSN 0022-1899, 1537-6613. doi: 10.1086/655653. URL http://ukpmc.ac.uk/abstract/MED/20846038.

50. M. T. Bretscher, C. L. Althaus, V. M ller, and S. Bonhoeffer. Recombination in HIV and the evolution of drug resistance: for better or for worse? *BioEssays*, 26(2): 180–188, Feb. 2004. ISSN 0265-9247. doi: 10.1002/bies.10386. URL http://onlinelibrary.wiley.com/doi/10.1002/bies.10386/abstract.

51. T. Britton. Stochastic epidemic models: A survey. *Mathematical Biosciences*, 225(1): 24–35, May 2010. ISSN 0025-5564. doi: 10.1016/j.mbs.2010.01.006. URL http://www.sciencedirect.com/science/article/pii/S0025556410000143.

52. A. Brown. Analysis of HIV-1 env gene sequences reveals evidence for a low effective number in the viral population. *Proceedings of the National Academy of Sciences*, 94 (5):1862, 1997.

53. Z. L. Brumme, M. John, J. M. Carlson, C. J. Brumme, D. Chan, M. A. Brockman, L. C. Swenson, I. Tao, S. Szeto, P. Rosato, J. Sela, C. M. Kadie, N. Frahm, C. Brander, D. W. Haas, S. A. Riddler, R. Haubrich, B. D. Walker, P. R. Harrigan, D. Heckerman, and S. Mallal. HLA-Associated immune escape pathways in HIV-1 subtype b gag, pol and nef proteins. *PLoS ONE*, 4(8):e6687, 2009. doi: 10.1371/journal.pone.0006687. URL http://dx.doi.org/10.1371/journal.pone.0006687.

54. J. J. Bull, R. Sanju n, and C. O. Wilke. Theory of lethal mutagenesis for viruses. *Journal of Virology*, 81(6):2930 –2939, Mar. 2007. doi: 10.1128/JVI.01624-06. URL http://jvi.asm.org/content/81/6/2930.abstract.

55. J. T. Cacioppo, J. H. Fowler, and N. A. Christakis. Alone in the crowd: The structure and spread of loneliness in a large social network. *Journal of Personality and Social Psychology*, 97(6):977–991, Dec. 2009. URL http://papers.ssrn.com/sol3/papers.cfm?abstract_id=1319108.

56. A. Calvo-Armengol and M. O. Jackson. The effects of social networks on employment and inequality. *American Economic Review*, 94(3):426–454, 2004. doi: 10.1257/0002828041464542. URL http://www.atypon-link.com/AEAP/doi/abs/10.1257/0002828041464542.

57. J. M. Carlson, Z. L. Brumme, C. M. Rousseau, C. J. Brumme, P. Matthews, C. Kadie, J. I. Mullins, B. D. Walker, P. R. Harrigan, P. J. R. Goulder, and D. Heckerman. Phylogenetic dependency networks: Inferring patterns of CTL escape and codon covariation in HIV-1 gag. *PLoS Comput Biol*, 4(11):e1000225, Nov. 2008. doi: 10.1371:journal.pcbi.1000225. URL http://dx.doi.org/10.1371:journal.pcbi.1000225.

58. C. Castellano, S. Fortunato, and V. Loreto. Statistical physics of social dynamics. *Reviews of Modern Physics*, 81(2):591, May 2009. doi: 10.1103/RevModPhys.81.591. URL http://link.aps.org/doi/10.1103/RevModPhys.81.591.

59. CDC. NHANES-National health and nutrition examination survey homepage. http://www.cdc.gov/nchs/nhanes.htm, 2009. URL http://www.cdc.gov/nchs/nhanes.htm.

60. CDC. HIV surveillance — united states, 1981–2008. *Morbidity and Mortality Weekly Report*, 60(21):689–693, June 2011. URL http://www.cdc.gov/mmwr/preview/mmwrhtml/mm6021a2.htm.

61. D. Centola. The spread of behavior in an online social network experiment. *Science*, 329(5996):1194, 2010.

62. J. J. Chang and M. Altfeld. Innate immune activation in primary HIV?1 infection. *The Journal of Infectious Diseases*, 202(S2):S297–S301, Oct. 2010. doi: 10.1086/655657. URL http://dx.doi.org/10.1086/655657.

63. V. W. Chang and N. A. Christakis. Medical modelling of obesity: A transition from action to experience in a 20th century american medical textbook. *Sociology of Health & Illness*, 24(2):151–177, 2002.

64. S. H. Cheeseman, D. Havlir, M. M. McLaughlin, T. C. Greenough, J. L. Sullivan, D. Hall, S. E. Hattox, S. A. Spector, D. S. Stein, and M. Myers. Phase I/II evaluation of nevirapine alone and in combination with zidovudine for infection with human immunodeficiency virus. *J. Acquir. Immune Defic. Syndr.*, 8(2):141–151, Feb. 1995. ISSN 1077-9450. URL http://www.ncbi.nlm.nih.gov/pubmed/7530585. PMID: 7530585.

65. Y.-L. Chiu and W. C. Greene. The APOBEC3 cytidine deaminases: An innate defensive network opposing exogenous retroviruses and endogenous retroelements. *Annual Review of Immunology*, 26(1):317–353, Apr. 2008. ISSN 0732-0582, 1545-3278. doi: 10.1146/annurev.immunol.26.021607.090350. URL http://www.annualreviews.org/doi/abs/10.1146/annurev.immunol.26.021607.090350.

66. T.-C. Chou. Derivation and properties of Michaelis-Menten type and hill type equations for reference ligands. *J. Theor. Biol.*, 59(2):253–276, 1976. ISSN 0022-5193. doi: 16/0022-5193(76)90169-7. URL http://www.sciencedirect.com/science/article/pii/0022519376901697.

67. S. K. Choudhary and D. M. Margolis. Curing HIV: pharmacologic approaches to target HIV-1 latency. *Annual Review of Pharmacology and Toxicology*, 51(1):397–418, 2011. doi: 10.1146/annurev-pharmtox-010510-100237. URL http://www.annualreviews.org/doi/abs/10.1146/annurev-pharmtox-010510-100237. PMID: 21210747.

68. N. A. Christakis and J. H. Fowler. The spread of obesity in a large social network over 32 years. *New England Journal of Medicine*, 357(4):370, 2007.

69. N. A. Christakis and J. H. Fowler. The collective dynamics of smoking in a large social network. *New England Journal of Medicine*, 358(21):2249, 2008.

70. N. A. Christakis and J. H. Fowler. *Connected: The Suprising Power of Our Social Networks and How They Shape Our Lives*. Little Brown & Co., 2009.

71. T. W. Chun, D. Finzi, J. Margolick, K. Chadwick, D. Schwartz, and R. F. Siliciano. In vivo fate of HIV-1-infected t cells: quantitative analysis of the transition to stable latency. *Nature medicine*, 1(12):1284–1290, Dec. 1995. ISSN 1078-8956. PMID: 7489410.

72. T. W. Chun, L. Carruth, D. Finzi, X. Shen, J. A. DiGiuseppe, H. Taylor, M. Hermankova, K. Chadwick, J. Margolick, T. C. Quinn, et al. Quantification of latent tissue reservoirs and total body viral load in HIV-1 infection. *Nature*, 387 (6629):183–188, 1997. ISSN 0028-0836.

73. T. W. Chun, L. Stuyver, S. B. Mizell, L. A. Ehler, J. A. Mican, M. Baseler, A. L. Lloyd, M. A. Nowak, and A. S. Fauci. Presence of an inducible HIV-1 latent reservoir during highly active antiretroviral therapy. *Proceedings of the National Academy of Sciences of the United States of America*, 94(24):13193–13197, Nov. 1997. ISSN 0027-8424. PMID: 9371822.

74. T. W. Chun, D. Engel, M. M. Berrey, T. Shea, L. Corey, and A. S. Fauci. Early establishment of a pool of latently infected, resting CD4(+) t cells during primary HIV-1 infection. *Proceedings of the National Academy of Sciences of the United States of America*, 95(15):8869–8873, July 1998. ISSN 0027-8424. PMID: 9671771.

75. Y. Chung and C. An . Comparing two bayesian methods for gene Tree/Species tree reconstruction: Simulations with incomplete lineage sorting and horizontal gene transfer. *Systematic Biology*, 60(3):261, 2011.

76. A. Cillo. Only a small fraction of HIV-1 proviruses in resting CD4+ t cells can be induced to produce virions ex vivo with anti-CD3/CD28 or vorinostat. In *20th Conference on Retroviruses and Opportunistic Infections*, Atlanta, 2013.

77. L. Cohen, A. Frazzini, and C. Malloy. The small world of investing: Board connections and mutual fund returns. *Journal of Political Economy*, 116(5):951–979, Oct. 2008. doi: 10.1086/592415. URL http://dx.doi.org/10.1086/592415.

78. M. L. Cohen. Epidemiology of drug resistance: Implications for a Post Antimicrobial era. *Science*, 257(5073):1050 –1055, 1992. doi: 10.1126/science.257.5073.1050. URL http://www.sciencemag.org/content/257/5073/1050.abstract.

79. T. Cohen and M. Murray. Modeling epidemics of multidrug-resistant m. tuberculosis of heterogeneous fitness. *Nat Med*, 10(10):1117–1121, Oct. 2004. ISSN 1078-8956. doi: 10.1038/nm1110. URL http://dx.doi.org/10.1038/nm1110.

80. J. H. Condra. Resistance to HIV protease inhibitors. *Haemophilia*, 4:610–615, 1998.

81. J. M. Conway and D. Coombs. A stochastic model of latently infected cell reactivation and viral blip generation in treated HIV patients. *PLoS Computational Biology*, 7(4):e1002033, Apr. 2011.

82. S. Crotty, C. Cameron, and R. Andino. Ribavirin's antiviral mechanism of action: lethal mutagenesis? *Journal of Molecular Medicine (Berlin, Germany)*, 80(2):86–95, Feb. 2002. ISSN 0946-2716. doi: 10.1007/s00109-001-0308-0. URL http://www.ncbi.nlm.nih.gov/pubmed/11907645. PMID: 11907645.

83. S. Crowe, T. Zhu, and W. Muller. The contribution of monocyte infection and trafficking to viral persistence, and maintenance of the viral reservoir in HIV infection. *Journal of leukocyte biology*, 74(5):635 641, 2003.

84. N. W. Cummins and A. D. Badley. Mechanisms of HIV-associated lymphocyte apoptosis: 2010. *Cell Death and Dis*, 1:e99, Nov. 2010. URL http://dx.doi.org/10.1038/cddis.2010.77.

85. D. G. Cvitkovitch, Y.-H. Li, and R. P. Ellen. Quorum sensing and biofilm formation in streptococcal infections. *Journal of Clinical Investigation*, 112(11):1626–1632, Dec. 2003. ISSN 0021-9738. doi: 10.1172/JCI20430. URL http://www.jci.org/articles/view/20430.

86. D. J. Daley and D. G. Kendall. Epidemics and rumours. *Nature*, 204:1118, 1964. doi: 10.1038/2041118a0.

87. E. Dam, R. Quercia, B. Glass, D. Descamps, O. Launay, X. Duval, H. Kr usslich, A. J. Hance, F. Clavel, and A. . S. Group. Gag mutations strongly contribute to HIV-1 resistance to protease inhibitors in highly Drug-Experienced patients besides compensating for fitness loss. *PLoS Pathog*, 5(3):e1000345, Mar. 2009. doi: 10.1371/journal.ppat.1000345. URL UR-http://dx.doi.org/10.1371/journal.ppat.1000345,http://dx.doi.org/10.1371/journal.ppat.1000345.

88. R. T. Davey, Jr., N. Bhat, C. Yoder, T.-W. Chun, J. A. Metcalf, R. Dewar, V. Natarajan, R. A. Lempicki, J. W. Adelsberger, K. D. Miller, J. A. Kovacs, M. A. Polis, R. E. Walker, J. Falloon, H. Masur, D. Gee, M. Baseler, D. S. Dimitrov, A. S. Fauci, and H. C. Lane. HIV-1 and t cell dynamics after interruption of highly active antiretroviral therapy (HAART) in patients with a history of sustained viral suppression. *Proc. Natl. Acad. Sci. USA*, 96(26):15109–15114, 1999.

89. R. T. Davey, Jr., N. Bhat, C. Yoder, T.-W. Chun, J. A. Metcalf, R. Dewar, V. Natarajan, R. A. Lempicki, J. W. Adelsberger, K. D. Miller, J. A. Kovacs, M. A. Polis, R. E. Walker, J. Falloon, H. Masur, D. Gee, M. Baseler, D. S. Dimitrov, A. S. Fauci, and H. C. Lane. HIV-1 and T cell dynamics after interruption of highly active antiretroviral therapy (haart) in patients with a history of sustained viral suppression. *Proc. Natl. Acad. Sci. USA*, 96(26):15109–15114, 1999.

90. T. R. Dawber. *The Framingham study: the epidemiology of atherosclerotic disease*. Harvard University Press, Cambridge, 1980.

91. R. J. De Boer, R. M. Ribeiro, and A. S. Perelson. Current estimates for HIV-1 production imply rapid viral clearance in lymphoid tissues. *PLoS Comput. Biol.*, 6(9): e1000906, 2010. doi: 10.1371/journal.pcbi.1000906. URL http://dx.doi.org/10.1371/journal.pcbi.1000906.

92. S. G. Deeks and B. D. Walker. Human immunodeficiency virus controllers: mechanisms of durable virus control in the absence of antiretroviral therapy.

Immunity, 27(3):406–416, 2007. URL file:///Users/Ali/Documents/MN/HIVarticles/HIV.Data/PDF/Walker07-mechanismsofelitecontrol-4032631553/Walker07-mechanismsofelitecontrol.pdf.

93. J. B. Dinoso, S. Y. Kim, A. M. Wiegand, S. E. Palmer, S. J. Gange, L. Cranmer, A. O'Shea, M. Callender, A. Spivak, T. Brennan, et al. Treatment intensification does not reduce residual HIV-1 viremia in patients on highly active antiretroviral therapy. *Proc. Natl. Acad. Sci. USA*, 106(23):9403, 2009.

94. N. M. Dixit and A. S. Perelson. HIV dynamics with multiple infections of target cells. *Proceedings of the National Academy of Sciences of the United States of America*, 102 (23):8198–8203, June 2005. ISSN 0027-8424, 1091-6490. doi: 10.1073/pnas.0407498102. URL http://www.pnas.org/content/102/23/8198.abstract.

95. P. S. Dodds and D. J. Watts. Universal behavior in a generalized model of contagion. *Physical review letters*, 92(21):218701, 2004.

96. K. Drlica. The mutant selection window and antimicrobial resistance. *J. Antimicrob. Chemother.*, 52(1):11–17, 2003. doi: 10.1093/jac/dkg269. URL http://jac.oxfordjournals.org/content/52/1/11.abstract.

97. K. Drlica and X. Zhao. Mutant selection window hypothesis updated. *Clin. Infect. Dis.*, 44(5):681 –688, 2007. doi: 10.1086/511642. URL http://cid.oxfordjournals.org/content/44/5/681.abstract.

98. C. M. Durand, J. N. Blankson, and R. F. Siliciano. Developing strategies for HIV-1 eradication. *Trends in Immunology*, 33(11):554–562, 2012. ISSN 1471-4906. doi: 10.1016/j.it.2012.07.001. URL http://www.sciencedirect.com/science/article/pii/S1471490612001123.

99. K. T. D. Eames and M. J. Keeling. Modeling dynamic and network heterogeneities in the spread of sexually transmitted diseases. *Proc Natl Acad Sci USA*, 99(20): 13330–13335, Oct. 2002. doi: 10.1073/pnas.202244299. URL http://www.pnas.org/content/99/20/13330.abstract.

100. B. Edlin, J. Tokars, M. Grieco, J. Crawford, J. Williams, E. Sordillo, K. Ong, J. Kilburn, S. Dooley, K. Castro, et al. An outbreak of multidrug-resistant tuberculosis among hospitalized patients with the acquired immunodeficiency syndrome. *New England Journal of Medicine*, 326(23):1514 1521, 1992.

101. S. Edwards. Is a new and general theory of molecular systematics emerging? *Evolution*, 63(1):1 19, 2009.

102. A. Ed n, D. Fuchs, L. Hagberg, S. Nilsson, S. Spudich, B. Svennerholm, R. Price, and M. Gissl n. HIV-1 viral escape in cerebrospinal fluid of subjects on suppressive antiretroviral treatment. *Journal of Infectious Diseases*, 202(12):1819, 2010.

103. M. Eigen. Error catastrophe and antiviral strategy. *Proceedings of the National Academy of Sciences of the United States of America*, 99(21):13374 –13376, Oct. 2002. doi: 10.1073/pnas.212514799. URL http://www.pnas.org/content/99/21/13374.short.

104. S. Eriksson, E. H. Graf, V. Dahl, M. C. Strain, S. A. Yukl, E. S. Lysenko, R. J. Bosch, J. Lai, S. Chioma, F. Emad, M. Abdel-Mohsen, R. Hoh, F. Hecht, P. Hunt, M. Somsouk, J. Wong, R. Johnston, R. F. Siliciano, D. D. Richman, U. O'Doherty, S. Palmer, S. G. Deeks, and J. D. Siliciano. Comparative analysis of measures of viral reservoirs in HIV-1 eradication studies. *PLoS Pathog*, 9(2):e1003174, Feb. 2013. doi: 10.1371/journal.ppat.1003174. URL http://dx.doi.org/10.1371/journal.ppat.1003174.

105. J. D. Estes, S. N. Gordon, M. Zeng, A. M. Chahroudi, R. M. Dunham, S. I. Staprans, C. S. Reilly, G. Silvestri, and A. T. Haase. Early resolution of acute immune activation and induction of PD-1 in SIV-Infected sooty mangabeys distinguishes nonpathogenic from pathogenic infection in rhesus macaques. *The Journal of Immunology*, 180(10):6798 –6807, May 2008.

106. W. J. Ewens. The stochastic theory. In *Mathematical Population Genetics: Theoretical Introduction*, pages 27–28. Springer, 2004. ISBN 9780387201917.

107. A. S. Fauci. Infectious diseases: Considerations for the 21st century. *Clinical Infectious Diseases*, 32(5):675 –685, Mar. 2001. doi: 10.1086/319235. URL http://cid.oxfordjournals.org/content/32/5/675.abstract.

108. J. Fellay, K. V. Shianna, A. Telenti, and D. B. Goldstein. Host genetics and HIV-1: the final phase? *PLoS Pathog*, 6(10):e1001033, Oct. 2010. doi: 10.1371/journal.ppat.1001033. URL UR-http://dx.doi.org/10.1371/journal.ppat.1001033,http://dx.doi.org/10.1371/journal.ppat.1001033.

109. N. M. Ferguson, C. A. Donnelly, and R. M. Anderson. The Foot-and-Mouth epidemic in great britain: Pattern of spread and impact of interventions. *Science*, 292(5519): 1155–1160, May 2001. doi: 10.1126/science.1061020. URL http://www.sciencemag.org/cgi/content/abstract/292/5519/1155.

110. D. Finzi, M. Hermankova, T. Pierson, L. M. Carruth, C. Buck, R. E. Chaisson, T. C. Quinn, K. Chadwick, J. Margolick, R. Brookmeyer, J. Gallant, M. Markowitz, D. D. Ho, D. D. Richman, and R. F. Siliciano. Identification of a reservoir for HIV-1 in patients on highly active antiretroviral therapy. *Science*, 278(5341):1295 –1300, Nov. 1997. doi: 10.1126/science.278.5341.1295. URL http://www.sciencemag.org/content/278/5341/1295.abstract.

111. J. H. Fowler and N. A. Christakis. Dynamic spread of happiness in a large social network: longitudinal analysis over 20 years in the framingham heart study. *British Medical Journal*, 337(dec04 2):a2338, 2008. doi: 10.1136/bmj.a2338.

112. J. H. Fowler and N. A. Christakis. Cooperative behaviour cascades in human social networks. *Proc Natl Acad Sci USA*, 107(12):5334–8, 2010.

113. S. D. Frost, M. Nijhuis, R. Schuurman, C. A. Boucher, and A. J. Leigh Brown. Evolution of lamivudine resistance in human immunodeficiency virus type 1-infected individuals: the relative roles of drift and selection. *J. Virol.*, 74(14):6262–6268, 2000.

114. H. R. Fryer, A. Scherer, A. Oxenius, R. Phillips, and A. R. McLean. No evidence for competition between cytotoxic t-lymphocyte responses in HIV-1 infection. *Proceedings of the Royal Society B: Biological Sciences*, Sept. 2009. ISSN 0962-8452. doi: 10.1098/rspb.2009.1232.

115. F. Fu, X. Chen, L. Liu, and L. Wang. Social dilemmas in an online social network: The structure and evolution of cooperation. *Physics Letters A*, 371(1-2):58–64, Nov. 2007. ISSN 0375-9601. doi: 10.1016/j.physleta.2007.05.116. URL http://www.sciencedirect.com/science/article/B6TVM-4NYJ0N2-3/2/7f522f8310f8b80f1f58c693adaa96aa.

116. G. A. Funk, M. Fischer, B. Joos, M. Opravil, H. F. Günthard, B. Ledergerber, and S. Bonhoeffer. Quantification of in vivo replicative capacity of HIV-1 in different compartments of infected cells. *J. Acquir. Immune Defic. Syndr.*, 26(5):397–404, 2001.

117. S. Funk, M. Salath , and V. A. A. Jansen. Modelling the influence of human behaviour on the spread of infectious diseases: a review. *Journal of The Royal Society Interface*, 7(50):1247 –1256, 2010. doi: 10.1098/rsif.2010.0142. URL http://rsif.royalsocietypublishing.org/content/7/50/1247.abstract.

118. A. P. Galvani. The role of mutation accumulation in HIV progression. *Proceedings of the Royal Society B: Biological Sciences*, 272(1574):1851 –1858, 2005. doi: 10.1098/rspb.2005.3083. URL http://rspb.royalsocietypublishing.org/content/272/1574/1851.abstract.

119. S. Gandon, M. J. Mackinnon, S. Nee, and A. F. Read. Imperfect vaccines and the evolution of pathogen virulence. *Nature*, 414(6865):751–756, Dec. 2001. ISSN 0028-0836. doi: 10.1038/414751a. URL http://dx.doi.org/10.1038/414751a.

120. E. M. Gardner, S. Sharma, G. Peng, K. H. Hullsiek, W. J. Burman, R. D. Macarthur, M. Chesney, E. E. Telzak, G. Friedland, and S. B. Mannheimer. Differential adherence to combination antiretroviral therapy is associated with virological failure with resistance. *AIDS*, 22(1):75–82, 2008. ISSN 1473-5571. doi: 10.1097/QAD.0b013e3282f366ff. URL http://www.ncbi.nlm.nih.gov/pubmed/18090394.

121. E. M. Gardner, W. J. Burman, J. F. Steiner, P. L. Anderson, and D. R. Bangsberg. Antiretroviral medication adherence and the development of class-specific antiretroviral resistance. *AIDS*, 23(9):1035–1046, 2009. ISSN 1473-5571. doi: 10.1097/QAD.0b013e32832ba8ec.

122. E. L. Glaeser, B. Sacerdote, and J. A. Scheinkman. Crime and social interactions. *The Quarterly Journal of Economics*, 111(2):507–548, 1996. ISSN 00335533. doi: 10.2307/2946686. URL http://www.jstor.org/stable/2946686.

123. W. Goffman and V. A. Newill. Generalization of epidemic theory: An applicaiton to the transmission of ideas. *Nature*, 204:225–228, 1964.

124. P. J. R. Goulder and D. I. Watkins. HIV and SIV CTL escape: implications for vaccine design. *Nat Rev Immunol*, 4(8):630–640, 2004. ISSN 1474-1733. doi: 10.1038/nri1417. URL http://dx.doi.org/10.1038/nri1417.

125. P. J. R. Goulder and D. I. Watkins. Impact of MHC class i diversity on immune control of immunodeficiency virus replication. *Nat Rev Immunol*, 8(8):619–630, 2008. ISSN 1474-1733. doi: 10.1038/nri2357. URL http://dx.doi.org/10.1038/nri2357.

126. R. M. Granich, C. F. Gilks, C. Dye, K. M. De Cock, and B. G. Williams. Universal voluntary HIV testing with immediate antiretroviral therapy as a strategy for elimination of HIV transmission: a mathematical model. *The Lancet*, 373(9657): 48–57, Mar. 2009. ISSN 0140-6736. doi: 10.1016/S0140-6736(08)61697-9. URL http://www.sciencedirect.com/science/article/pii/S0140673608616979.

127. F. Groot, S. Welsch, and Q. Sattentau. Efficient HIV-1 transmission from macrophages to t cells across transient virological synapses. *Blood*, 111(9):4660, 2008.

128. E. Gullberg, S. Cao, O. G. Berg, C. Ilbäck, L. Sandegren, D. Hughes, and D. I. Andersson. Selection of resistant bacteria at very low antibiotic concentrations. *PLoS Pathog.*, 7(7):e1002158, 2011. doi: 10.1371/journal.ppat.1002158. URL http://dx.doi.org/10.1371/journal.ppat.1002158.

129. R. K. Gupta, A. Hill, A. W. Sawyer, A. Cozzi-Lepri, V. von Wyl, S. Yerly, V. D. Lima, H. F. Günthard, C. Gilks, and D. Pillay. Virological monitoring and resistance to first-line highly active antiretroviral therapy in adults infected with HIV-1 treated under who guidelines: a systematic review and meta-analysis. *Lancet Infect. Dis.*, 9: 409–417, 2009.

130. R. K. GUPTA, A. KOHLI, A. L. McCORMICK, G. J. TOWERS, D. PILLAY, and C. M. PARRY. Full length HIV-1 gag determines protease inhibitor susceptibility within in vitro assays. *AIDS (London, England)*, 24(11):1651–1655, July 2010. ISSN 0269-9370. PMID: 20597164 PMCID: 2923069.

131. A. Handel, R. R. Regoes, and R. Antia. The role of compensatory mutations in the emergence of drug resistance. *PLoS Comput Biol*, 2(10):e137, Oct. 2006. doi: 10.1371/journal.pcbi.0020137. URL UR-http://dx.plos.org/10.1371/journal.pcbi.0020137,http://dx.plos.org/10.1371/journal.pcbi.0020137.

132. P. R. Harrigan, R. S. Hogg, W. W. Y. Dong, B. Yip, B. Wynhoven, J. Woodward, C. J. Brumme, Z. L. Brumme, T. Mo, C. S. Alexander, and J. S. G. Montaner.

Predictors of HIV drug-resistance mutations in a large antiretroviral-naive cohort initiating triple antiretroviral therapy. *J. Infect. Dis.*, 191(3):339–347, 2005. ISSN 0022-1899. doi: 10.1086/427192. URL http://www.ncbi.nlm.nih.gov/pubmed/15633092.

133. R. S. Harris, K. N. Bishop, A. M. Sheehy, H. M. Craig, S. K. Petersen-Mahrt, I. N. Watt, M. S. Neuberger, and M. H. Malim. DNA deamination mediates innate immunity to retroviral infection. *Cell*, 113(6):803–809, June 2003. ISSN 0092-8674. URL http://www.ncbi.nlm.nih.gov/pubmed/12809610. PMID: 12809610.

134. L. Harrison, H. Castro, P. Cane, D. Pillay, C. Booth, A. Phillips, A. M. Geretti, and D. Dunn. The effect of transmitted HIV-1 drug resistance on pre-therapy viral load. *AIDS*, 24(12):1917–1922, July 2010. ISSN 0269-9370. doi: 10.1097/QAD.0b013e32833c1d93. URL http://journals.lww.com/aidsonline/Abstract/2010/07310/The_effect_of_transmitted_HIV_1_drug_resistance_on.13.aspx.

135. D. L. Hartl and A. G. Clark. *Principles of Population Genetics*. Sinauer Associates, 2007. ISBN 9780878933082.

136. E. Hatfield, J. T. Cacioppo, and R. L. Rapson. *Emotional contagion*. Cambridge university press, 1994.

137. D. V. Havlir, N. S. Hellmann, C. J. Petropoulos, J. M. Whitcomb, A. C. Collier, M. S. Hirsch, P. Tebas, J.-P. Sommadossi, and D. D. Richman. Drug susceptibility in HIV infection after viral rebound in patients receiving Indinavir-Containing regimens. *J. Am. Med. Ass.*, 283(2):229 –234, 2000. doi: 10.1001/jama.283.2.229.

138. D. L. Haynie. Delinquent peers revisited: Does network structure matter? *American Journal of Sociology*, 106(4):1013–1057, Jan. 2001. doi: 10.1086/320298. URL http://dx.doi.org/10.1086/320298.

139. J. L. Heeney, A. G. Dalgleish, and R. A. Weiss. Origins of HIV and the evolution of resistance to AIDS. *Science*, 313(5786):462 –466, July 2006. doi: 10.1126/science.1123016. URL http://www.sciencemag.org/content/313/5786/462.abstract.

140. T. J. Henrich, Z. Hu, J. Z. Li, G. Sciaranghella, M. P. Busch, S. M. Keating, S. Gallien, N. H. Lin, F. F. Giguel, L. Lavoie, V. T. Ho, P. Armand, R. J. Soiffer, M. Sagar, A. S. Lacasce, and D. R. Kuritzkes. Long-Term Reduction in Peripheral Blood HIV-1 Reservoirs Following Reduced-Intensity Conditioning Allogeneic Stem Cell Transplantation. *Journal of Infectious Diseases*, Mar. 2013.

141. J. T. Herbeck, V. M ller, B. S. Maust, B. Ledergerber, C. Torti, S. Di Giambenedetto, L. Gras, H. F. G nthard, L. P. Jacobson, J. I. Mullins, and G. S. Gottlieb. Is the virulence of HIV changing? a meta-analysis of trends in prognostic markers of HIV disease progression and transmission. *AIDS*, 26(2):193–205, Jan. 2012. ISSN 0269-9370. doi: 10.1097/QAD.0b013e32834db418. URL

http://journals.lww.com/aidsonline/Abstract/2012/01140/Is_the_virulence_of_HIV_changing__A_meta_analysis.9.aspx.

142. A. L. Hill, D. G. Rand, M. A. Nowak, and N. A. Christakis. Emotions as infectious diseases in a large social network: the SISa model. *Proceedings of the Royal Society B: Biological Sciences*, 277(1701):3827 –3835, Dec. 2010. doi: 10.1098/rspb.2010.1217. URL http://rspb.royalsocietypublishing.org/content/277/1701/3827.abstract.

143. A. L. Hill, D. G. Rand, M. A. Nowak, and N. A. Christakis. Infectious disease modeling of social contagion in networks. *PLoS Comput Biol*, 6(11):e1000968, Nov. 2010. doi: 10.1371/journal.pcbi.1000968. URL http://dx.doi.org/10.1371/journal.pcbi.1000968.

144. A. L. Hill, D. I. S. Rosenbloom, and M. A. Nowak. Evolutionary dynamics of HIV at multiple spatial and temporal scales. *Journal of Molecular Medicine*, 90(5):543–561, May 2012. ISSN 0946-2716. doi: 10.1007/s00109-012-0892-1. URL http://www.springerlink.com/content/l4511r1091r86672/abstract/.

145. M. Hirsch, F. Brun-Vézinet, R. D'Aquila, S. Hammer, V. Johnson, D. Kuritzkes, C. Loveday, J. Mellors, B. Clotet, B. Conway, et al. Antiretroviral drug resistance testing in adult HIV-1 infection: recommendations of an International AIDS Society–USA panel. *J. Am. Med. Ass.*, 283:2417–2426, 2000.

146. Y.-C. Ho, L. Shan, J. Wang, N. Hosmane, J. N. Blankson, and R. Siliciano. Characterization of non--induced HIV--1 proviruses dampens the hope for HIV--1 eradication. Atlanta, GA, 2013.

147. R. D. Hockett, J. M. Kilby, C. A. Derdeyn, M. S. Saag, M. Sillers, K. Squires, S. Chiz, M. A. Nowak, G. M. Shaw, and R. P. Bucy. Constant mean viral copy number per infected cell in tissues regardless of high, low, or undetectable plasma HIV RNA. *J. Exp. Med.*, 189(10):1545 –1554, 1999. doi: 10.1084/jem.189.10.1545. URL http://jem.rupress.org/content/189/10/1545.abstract.

148. C. J. Hoffmann, S. Charalambous, J. Sim, J. Ledwaba, G. Schwikkard, R. E. Chaisson, K. L. Fielding, G. J. Churchyard, L. Morris, and A. D. Grant. Viremia, resuppression, and time to resistance in human immunodeficiency virus (HIV) subtype c during first-line antiretroviral therapy in south africa. *Clin. Infect. Dis.*, 49: 1928–1935, 2009.

149. E. C. Holmes. Evolutionary history and phylogeography of human viruses. *Annual Review of Microbiology*, 62(1):307–328, Oct. 2008. ISSN 0066-4227, 1545-3251. doi: 10.1146/annurev.micro.62.081307.162912. URL http://www.annualreviews.org/doi/abs/10.1146/annurev.micro.62.081307.162912.

150. E. C. Holmes. *Evolution and Emergence of RNA Viruses*. Oxford University Press, USA, 2009.

151. M. J. Howes, J. E. Hokanson, and D. A. Loewenstein. Induction of depressive affect after prolonged exposure to a mildly depressed individual. *Journal of Personality and Social Psychology*, 49(4):1110–1113, 1985.

152. G. Hütter, D. Nowak, M. Mossner, S. Ganepola, A. Müßig, K. Allers, T. Schneider, J. Hofmann, C. Kücherer, O. Blau, I. W. Blau, W. K. Hofmann, and E. Thiel. Long-term control of HIV by CCR5 Delta32/Delta32 stem-cell transplantation. *N. Engl. J. Med.*, 360(7):692–698, Feb. 2009.

153. S. Hu , R. J. Gifford, D. Dunn, E. Fernhill, and D. Pillay. Demonstration of sustained drug-resistant human immunodeficiency virus type 1 lineages circulating among treatment-na ve individuals. *Journal of Virology*, 83(6):2645–2654, Mar. 2009. ISSN 0022-538X. doi: 10.1128/JVI.01556-08. PMID: 19158238 PMCID: 2648277.

154. J. P. A. Ioannidis, D. V. Havlir, P. Tebas, M. S. Hirsch, A. C. Collier, and D. D. Richman. Dynamics of HIV-1 viral load rebound among patients with previous suppression of viral replication. *AIDS*, 14:1481–1488, 2000.

155. M. O. Jackson. *Social and Economic Networks*. Princeton University Press, 2008. ISBN 9780691134406.

156. M. O. Jackson. Networks and economic behavior. *Annual Review of Economics*, 1(1), 2009. doi: 10.1146/annurev.economics.050708.143238. URL http://arjournals.annualreviews.org/doi/abs/10.1146/annurev.economics.050708.143238.

157. J. A. Jacquez, C. P. Simon, J. Koopman, L. Sattenspiel, and T. Perry. Modeling and analyzing HIV transmission: the effect of contact patterns. *Mathematical Biosciences*, 92(2):119–199, Dec. 1988. ISSN 0025-5564. doi: 10.1016/0025-5564(88)90031-4. URL http://www.sciencedirect.com/science/article/pii/0025556488900314.

158. J. Jansson, D. P. Wilson, A. Carr, K. Petoumenos, and M. A. Boyd. Currently available medications in resource-rich settings may not be sufficient for lifelong treatment of HIV. *AIDS (London, England)*, Dec. 2012. ISSN 1473-5571. doi: 10.1097/QAD.0b013e32835e163d. PMID: 23276809.

159. B. L. Jilek, M. Zarr, M. E. Sampah, S. A. Rabi, C. K. Bullen, J. Lai, L. Shen, and R. F. Siliciano. A quantitative basis for antiretroviral therapy for HIV-1 infection. *Nat Med*, 18(3):446–451, Feb. 2012. ISSN 1078-8956. doi: 10.1038/nm.2649. URL http://www.nature.com/nm/journal/v18/n3/full/nm.2649.html.

160. W. E. Johnson and R. C. Desrosiers. Viral persistence: HIV's strategies of immune system evasion. *Annual Review of Medicine*, 53(1):499–518, Feb. 2002. ISSN 0066-4219, 1545-326X. doi: 10.1146/annurev.med.53.082901.104053. URL http://www.annualreviews.org/doi/abs/10.1146/annurev.med.53.082901.104053.

161. T. E. Joiner and J. Katz. Contagion of depressive symptoms and mood: Meta-analytic review and explanations from cognitive, behavioral, and interpersonal viewpoints. *Clinical Psychology: Science and Practice*, 6(2):149–164, 1999. doi: 10.1093/clipsy.6.2.149.

162. C. Jolly, K. Kashefi, M. Hollinshead, and Q. Sattentau. HIV-1 cell to cell transfer across an env-induced, actin-dependent synapse. *The Journal of Experimental Medicine*, 199(2):283, 2004.

163. L. Josefsson, M. S. King, B. Makitalo, J. Br nnstr m, W. Shao, F. Maldarelli, M. F. Kearney, W.-S. Hu, J. Chen, H. Gaines, J. W. Mellors, J. Albert, J. M. Coffin, and S. E. Palmer. Majority of CD4+ t cells from peripheral blood of HIV-1 infected individuals contain only one HIV DNA molecule. *Proceedings of the National Academy of Sciences*, 108(27):11199–11204, July 2011. ISSN 0027-8424, 1091-6490. doi: 10.1073/pnas.1107729108. URL http://www.pnas.org/content/108/27/11199.long.

164. S. Joseph and C. A. Lewis. Factor analysis of the center for epidemiological Studies-Depression scale. *Psychological reports*, 76:40–40, 1995.

165. G. Jourdain, T. A. Wagner, N. Ngo-Giang-Huong, W. Sirirungsi, V. Klinbuayaem, F. Fregonese, I. Nantasen, M. Techapornroong, G. Halue, A. Nilmanat, P. Wittayapraparat, V. Chalermpolprapa, P. Pathipvanich, P. Yuthavisuthi, L. M. Frenkel, M. Lallemant, and P. S. Group. Association between detection of HIV-1 DNA resistance mutations by a sensitive assay at initiation of antiretroviral therapy and virologic failure. *Clin. Infect. Dis.*, 50:1397–1404, 2010.

166. A. Jung, R. Maier, J.-P. Vartanian, G. Bocharov, V. Jung, U. Fischer, E. Meese, S. Wain-Hobson, and A. Meyerhans. Recombination: Multiply infected spleen cells in HIV patients. *Nature*, 418(6894):144, July 2002. ISSN 0028-0836. doi: 10.1038/418144a. URL http://dx.doi.org/10.1038/418144a.

167. C. Kamp, C. O. Wilke, C. Adami, and S. Bornholdt. Viral evolution under the pressure of an adaptive immune system: Optimal mutation rates for viral escape. *Complexity*, 8(2):28–33, Nov. 2002. ISSN 1099-0526. doi: 10.1002/cplx.10067. URL http://onlinelibrary.wiley.com/doi/10.1002/cplx.10067/abstract.

168. E. L. Kaplan and P. Meier. Nonparametric estimation from incomplete observations. *J. Amer. Statist. Assoc.*, 53(282):457–481, 1958. ISSN 0162-1459. doi: 10.2307/2281868. URL http://www.jstor.org/stable/2281868.

169. S. Karlin and H. E. Taylor. *A First Course in Stochastic Processes*. Academic Press, San Diego, Apr. 1975.

170. H. Kastrissios, J. Su rez, D. Katzenstein, P. Girard, L. Sheiner, and T. Blaschke. Characterizing patterns of drug-taking behavior with a multiple drug regimen in an AIDS clinical trial. *AIDS*, 12(17):2295, 1998.

171. A. Katzourakis, M. Tristem, O. G. Pybus, and R. J. Gifford. Discovery and analysis of the first endogenous lentivirus. *Proceedings of the National Academy of Sciences*, 104(15):6261 –6265, Apr. 2007. doi: 10.1073/pnas.0700471104. URL http://www.pnas.org/content/104/15/6261.abstract.

172. Y. Kawashima, K. Pfafferott, J. Frater, P. Matthews, R. Payne, M. Addo, H. Gatanaga, M. Fujiwara, A. Hachiya, H. Koizumi, N. Kuse, S. Oka, A. Duda, A. Prendergast, H. Crawford, A. Leslie, Z. Brumme, C. Brumme, T. Allen, C. Brander, R. Kaslow, J. Tang, E. Hunter, S. Allen, J. Mulenga, S. Branch, T. Roach, M. John, S. Mallal, A. Ogwu, R. Shapiro, J. G. Prado, S. Fidler, J. Weber, O. G. Pybus, P. Klenerman, T. Ndung/'u, R. Phillips, D. Heckerman, P. R. Harrigan, B. D. Walker, M. Takiguchi, and P. Goulder. Adaptation of HIV-1 to human leukocyte antigen class i. *Nature*, 458(7238):641–645, Apr. 2009. ISSN 0028-0836. doi: 10.1038/nature07746. URL http://dx.doi.org/10.1038/nature07746.

173. B. F. Keele, F. Van Heuverswyn, Y. Li, E. Bailes, J. Takehisa, M. L. Santiago, F. Bibollet-Ruche, Y. Chen, L. V. Wain, F. Liegeois, S. Loul, E. M. Ngole, Y. Bienvenue, E. Delaporte, J. F. Y. Brookfield, P. M. Sharp, G. M. Shaw, M. Peeters, and B. H. Hahn. Chimpanzee reservoirs of pandemic and nonpandemic HIV-1. *Science*, 313:523 –526, July 2006. doi: 10.1126/science.1126531. URL http://www.sciencemag.org/content/313/5786/523.abstract.

174. B. F. Keele, E. E. Giorgi, J. F. Salazar-Gonzalez, J. M. Decker, K. T. Pham, M. G. Salazar, C. Sun, T. Grayson, S. Wang, H. Li, X. Wei, C. Jiang, J. L. Kirchherr, F. Gao, J. A. Anderson, L.-H. Ping, R. Swanstrom, G. D. Tomaras, W. A. Blattner, P. A. Goepfert, J. M. Kilby, M. S. Saag, E. L. Delwart, M. P. Busch, M. S. Cohen, D. C. Montefiori, B. F. Haynes, B. Gaschen, G. S. Athreya, H. Y. Lee, N. Wood, C. Seoighe, A. S. Perelson, T. Bhattacharya, B. T. Korber, B. H. Hahn, and G. M. Shaw. Identification and characterization of transmitted and early founder virus envelopes in primary HIV-1 infection. *Proceedings of the National Academy of Sciences of the United States of America*, 105(21):7552 7557, May 2008. doi: 10.1073/pnas.0802203105. URL http://www.pubmedcentral.nih.gov/articlerender.fcgi?artid=2387184. PMC2387184.

175. M. J. Keeling. The effects of local spatial structure on epidemiological invasions. *Proc R Soc B*, 266(1421):859–867, Apr. 1999. ISSN 09628452. doi: 10.2307/51194. URL http://www.jstor.org/stable/51194.

176. M. J. Keeling and K. T. D. Eames. Networks and epidemic models. *Journal of the Royal Society Interface*, 2(4):295, 2005. doi: 10.1098/ rsif.2005.0051.

177. D. J. Kempf, M. S. King, B. Bernstein, P. Cernohous, E. Bauer, J. Moseley, K. Gu, A. Hsu, S. Brun, and E. Sun. Incidence of resistance in a double-blind study comparing lopinavir/ritonavir plus stavudine and lamivudine to nelfinavir plus stavudine and lamivudine. *J. Infect. Dis.*, 189:51–60, 2004.

178. T. B. Kepler and A. S. Perelson. Drug concentration heterogeneity facilitates the evolution of drug resistance. *Proc. Natl. Acad. Sci. USA*, 95(20):11514 –11519, 1998. doi: 10.1073/pnas.95.20.11514. URL http://www.pnas.org/content/95/20/11514.abstract.

179. R. C. Kessler, S. Zhao, D. G. Blazer, and M. Swartz. Prevalence, correlates, and course of minor depression and major depression in the national comorbidity survey. *Journal of Affective Disorders*, 45(1-2):19–30, Aug. 1997. ISSN 0165-0327. doi: 10.1016/S0165-0327(97)00056-6. URL http://www.sciencedirect.com/science/article/B6T2X-430GMHT-3/2/c1cc45dde93f8ebd22400ad8c251aa95.

180. P. Kiepiela, A. Leslie, I. Honeyborne, D. Ramduth, C. Thobakgale, S. Chetty, P. Rathnavalu, C. Moore, K. Pfafferott, L. Hilton, et al. Dominant influence of HLA-B in mediating the potential co-evolution of HIV and HLA. *Nature*, 432(7018): 769 775, 2004.

181. H. Kim and A. S. Perelson. Viral and latent reservoir persistence in HIV-1-Infected patients on therapy. *PLoS Comput Biol*, 2(10):e135, Oct. 2006. doi: 10.1371/journal.pcbi.0020135. URL http://dx.plos.org/10.1371/journal.pcbi.0020135.

182. S. Kim and J. Shanahan. Stigmatizing smokers: Public sentiment toward cigarette smoking and its relationship to smoking behaviors. *Journal of Health Communication: International Perspectives*, 8(4):343, 2003. ISSN 1081-0730. doi: 10.1080/10810730305723. URL http://www.informaworld.com/10.1080/10810730305723.

183. G. A. V. Kleef, C. K. W. D. Dreu, and A. S. R. Manstead. The interpersonal effects of anger and happiness on negotiation behavior and outcomes. *Journal of Personality and Social Psychology*, 86:57–76, 2004.

184. B. Korber and S. Gnanakaran. Converging on an HIV vaccine. *Science*, 333(6049): 1589–1590, Sept. 2011. ISSN 0036-8075, 1095-9203. doi: 10.1126/science.1211919. URL http://www.sciencemag.org/content/333/6049/1589.full.

185. A. Kosmrlj, E. L. Read, Y. Qi, T. M. Allen, M. Altfeld, S. G. Deeks, F. Pereyra, M. Carrington, B. D. Walker, and A. K. Chakraborty. Effects of thymic selection of the t-cell repertoire on HLA class[thinsp]I-associated control of HIV infection. *Nature*, 465(7296):350–354, May 2010. ISSN 0028-0836. doi: 10.1038/nature08997. URL http://dx.doi.org/10.1038/nature08997.

186. R. A. Koup, B. S. Graham, and D. C. Douek. The quest for a t cell-based immune correlate of protection against HIV: a story of trials and errors. *Nat Rev Immunol*, 11 (1):65–70, Jan. 2011. ISSN 1474-1733. doi: 10.1038/nri2890. URL http://dx.doi.org/10.1038/nri2890.

187. R. D. Kouyos, C. L. Althaus, and S. Bonhoeffer. Stochastic or deterministic: what is the effective population size of HIV-1? *Trends Microbiol.*, 14(12):507–511, 2006.

188. R. D. Kouyos, C. L. Althaus, and S. Bonhoeffer. Stochastic or deterministic: what is the effective population size of HIV-1? *Trends in Microbiology*, 14(12):507–511, Dec. 2006. ISSN 0966-842X. doi: 16/j.tim.2006.10.001. URL http://www.sciencedirect.com/science/article/pii/S0966842X06002332.

189. R. D. Kouyos, V. von Wyl, T. Hinkley, C. J. Petropoulos, M. Haddad, J. M. Whitcomb, J. B ni, S. Yerly, C. Cellerai, T. Klimkait, H. F. G nthard, S. Bonhoeffer, and the Swiss HIV Cohort Study. Assessing predicted HIV-1 replicative capacity in a clinical setting. *PLoS Pathog*, 7:e1002321, Nov. 2011. doi: 10.1371/journal.ppat.1002321. URL UR-http://dx.doi.org/10.1371/journal.ppat.1002321,http://dx.doi.org/10.1371/journal.ppat.1002321.

190. O. Krakovska and L. M. Wahl. Costs versus benefits: best possible and best practical treatment regimens for HIV. *J. Math. Biol.*, 54:385–406, 2007.

191. C. Kuiken, B. Foley, T. Leitner, C. Apetrei, B. Hahn, I. Mizrachi, J. Mullins, A. Rambaut, S. Wolinsky, and B. Korber, editors. *HIV Sequence Compendium 2010*. Theoretical Biology and Biophysics Group, Los Alamos National Laboratory, NM, 2010.

192. R. W. Larson and D. M. Almeida. Emotional transmission in the daily lives of families: A new paradigm for studying family process. *Journal of Marriage and the Family*, 61(1):5–20, 1999. ISSN 00222445. doi: 10.2307/353879. URL http://www.jstor.org/stable/353879.

193. G. Lawyer, A. Altmann, A. Thielen, M. Zazzi, A. S nnerborg, and T. Lengauer. HIV-1 mutational pathways under multidrug therapy. *AIDS Research and Therapy*, 8: 26, 2011. ISSN 1742-6405. doi: 10.1186/1742-6405-8-26. URL http://www.ncbi.nlm.nih.gov/pubmed/21794106. PMID: 21794106.

194. P. F. Lazarsfeld and E. Katz. *Personal influence: the part played by people in the flow of mass communications*. Free Press, 1955.

195. D. Lecossier, F. Bouchonnet, F. Clavel, and A. J. Hance. Hypermutation of HIV-1 DNA in the absence of the vif protein. *Science*, 300(5622):1112, 2003.

196. H. Y. Lee, A. S. Perelson, S.-C. Park, and T. Leitner. Dynamic correlation between intrahost HIV-1 quasispecies evolution and disease progression. *PLoS Comput Biol*, 4 (12):e1000240, Dec. 2008. doi: 10.1371:journal.pcbi.1000240. URL http://dx.doi.org/10.1371:journal.pcbi.1000240.

197. C. Lehmann, M. D umer, I. Boussaad, T. Sing, N. Beerenwinkel, T. Lengauer, N. Schmeisser, C. Wyen, G. F tkenheuer, and R. Kaiser. Stable coreceptor usage of HIV in patients with ongoing treatment failure on HAART. *Journal of Clinical Virology*, 37(4):300–304, Dec. 2006. ISSN 1386-6532. doi: 10.1016/j.jcv.2006.08.008. URL http://www.sciencedirect.com/science/article/pii/S1386653206003039.

198. A. J. Leslie, K. J. Pfafferott, P. Chetty, R. Draenert, M. M. Addo, M. Feeney, Y. Tang, E. C. Holmes, T. Allen, and J. G. Prado. HIV evolution: CTL escape mutation and reversion after transmission. *Nature Medicine*, 10:282–289, 2004.

199. D. N. Levy, G. M. Aldrovandi, O. Kutsch, and G. M. Shaw. Dynamics of HIV-1 recombination in its natural target cells. *Proceedings of the National Academy of Sciences*, 101(12):4204–4209, 2004. URL file:///Users/Ali/Documents/MN/HIVarticles/HIV.Data/PDF/PNAS-2004-Levy-4204-9-0492697857/PNAS-2004-Levy-4204-9.pdf.

200. J. A. Levy. HIV pathogenesis: 25 years of progress and persistent challenges. *AIDS (London, England)*, 23(2):147–160, Jan. 2009. ISSN 1473-5571. doi: 10.1097/QAD.0b013e3283217f9f. URL http://www.ncbi.nlm.nih.gov/pubmed/19098484. PMID: 19098484.

201. M. Lewis and J. M. Haviland-Jones. *Handbook of emotions*. The Guilford Press, 2 edition, 2004. ISBN 1593850298, 9781593850296.

202. E. Lieberman, C. Hauert, and M. A. Nowak. Evolutionary dynamics on graphs. *Nature*, 433(7023):312–316, 2005.

203. J. D. Lifson, J. L. Rossio, M. Piatak, T. Parks, L. Li, R. Kiser, V. Coalter, B. Fisher, B. M. Flynn, and S. Czajak. Role of CD8+ lymphocytes in control of simian immunodeficiency virus infection and resistance to rechallenge after transient early antiretroviral treatment. *Journal of Virology*, 75(21):10187–10199, 2001.

204. V. D. Lima, R. Harrigan, M. Murray, D. M. Moore, E. Wood, R. S. Hogg, and J. S. Montaner. Differential impact of adherence on long-term treatment response among naive HIV-infected individuals. *AIDS*, 22:2371–2380, 2008.

205. S. J. Little, A. R. McLean, C. A. Spina, D. D. Richman, and D. V. Havlir. Viral dynamics of acute HIV-1 infection. *J. Exp. Med.*, 190(6):841 –850, 1999. doi: 10.1084/jem.190.6.841. URL http://jem.rupress.org/content/190/6/841.abstract.

206. S. J. Little, S. D. W. Frost, J. K. Wong, D. M. Smith, S. L. K. Pond, C. C. Ignacio, N. T. Parkin, C. J. Petropoulos, and D. D. Richman. Persistence of transmitted drug resistance among subjects with primary human immunodeficiency virus infection. *Journal of Virology*, 82(11):5510 –5518, June 2008. doi: 10.1128/JVI.02579-07. URL http://jvi.asm.org/content/82/11/5510.abstract.

207. H. Liu, L. G. Miller, C. E. Golin, R. D. Hays, T. Wu, N. S. Wenger, and A. H. Kaplan. Repeated measures analyses of dose timing of antiretroviral medication and its relationship to HIV virologic outcomes. *Stat. Med.*, 26(5):991–1007, 2007. ISSN 1097-0258. doi: 10.1002/sim.2592. URL http://dx.doi.org/10.1002/sim.2592.

208. D. Lopez-Pintado. Diffusion in complex social networks. *Games and Economic Behavior*, 62(2):573–590, 2007.

209. D. A. Luke and J. K. Harris. Network analysis in public health: History, methods, and applications. *Annual Review of Public Health*, 28(1):69–93, 2007. ISSN 0163-7525. doi: 10.1146/annurev.publhealth.28.021406.144132. URL http://arjournals.annualreviews.org/doi/abs/10.1146/annurev.publhealth.28.021406.144132.

210. F. Maggiolo, M. Airoldi, H. D. Kleinloog, A. Callegaro, V. Ravasio, C. Arici, E. Bombana, and F. Suter. Effect of adherence to HAART on virologic outcome and on the selection of resistance-conferring mutations in NNRTI- or PI-treated patients. *HIV Clin. Trials*, 8(5):282–292, 2007. ISSN 1528-4336. doi: 10.1310/hct0805-282. URL http://www.ncbi.nlm.nih.gov/pubmed/17956829.

211. V. Mahajan and R. A. Peterson. *Models for innovation diffusion*. Sage Publications, Inc, 1985.

212. L. M. Mansky and H. M. Temin. Lower in vivo mutation rate of human immunodeficiency virus type 1 than that predicted from the fidelity of purified reverse transcriptase. *J. Virol.*, 69(8):5087–5094, 1995. ISSN 0022-538X.

213. N. Margot, B. Lu, A. Cheng, and M. Miller. Resistance development over 144 weeks in treatment-naive patients receiving tenofovir disoproxil fumarate or stavudine with lamivudine and efavirenz in study 903*. *HIV medicine*, 7(7):442 450, 2006.

214. M. Markowitz, M. Louie, A. Hurley, E. Sun, M. Di Mascio, A. S. Perelson, and D. D. Ho. A novel antiviral intervention results in more accurate assessment of human immunodeficiency virus type 1 replication dynamics and T-Cell decay in vivo. *J. Virol.*, 77(8):5037–5038, 2003. ISSN 0022-538X. doi: 10.1128/JVI.77.8.5037-5038.2003.

215. D. Marmaros and B. Sacerdote. Peer and social networks in job search. *European Economic Review*, 46(4-5):870–879, 2002. doi: 10.1016/S0014-2921(01)00221-5. URL http://www.sciencedirect.com/science?_ob=ArticleURL&_udi=B6V64-44W9NTM-1&_user=10&_rdoc=1&_fmt=&_orig=search&_sort=d&view=c&_acct=C000050221&_version=1&_urlVersion=0&_userid=10&md5=3a2028ee953c794412fa8e3c667e9313.

216. R. M. May. Network structure and the biology of populations. *Trends in Ecology & Evolution*, 21(7):394–399, 2006.

217. R. M. May and R. M. Anderson. Epidemiology and genetics in the coevolution of parasites and hosts. *Proceedings of the Royal Society of London. Series B. Biological Sciences*, 219(1216):281–313, Oct. 1983. ISSN 0962-8452, 1471-2954. doi: 10.1098/rspb.1983.0075. URL http://rspb.royalsocietypublishing.org/content/219/1216/281.

218. R. M. May and R. M. Anderson. Transmission dynamics of HIV infection. *Nature*, 326(6109):137–142, Mar. 1987. ISSN 0028-0836. doi: 10.1038/326137a0. URL http://www.ncbi.nlm.nih.gov/pubmed/3821890. PMID: 3821890.

219. R. M. May and A. L. Lloyd. Infection dynamics on scale-free networks. *Phys Rev E*, 64:066112, 2001. doi: 10.1103/PhysRevE.64.066112.

220. R. M. May and M. A. Nowak. Coinfection and the evolution of parasite virulence. *Proceedings of the Royal Society B: Biological Sciences*, 261:209–215, Aug. 1995. ISSN

0962-8452. doi: 10.1098/rspb.1995.0138. URL http://www.ncbi.nlm.nih.gov/pubmed/7568274. PMID: 7568274.

221. R. Mehla, S. Bivalkar-Mehla, R. Zhang, I. Handy, H. Albrecht, S. Giri, P. Nagarkatti, M. Nagarkatti, and A. Chauhan. Bryostatin modulates latent HIV-1 infection via PKC and AMPK signaling but inhibits acute infection in a receptor independent manner. *PloS one*, 5(6):e11160, 2010. ISSN 1932-6203. doi: 10.1371/journal.pone.0011160. PMID: 20585398.

222. L. A. Meyers, B. Pourbohloul, M. E. J. Newman, D. M. Skowronski, and R. C. Brunham. Network theory and SARS: predicting outbreak diversity. *Journal of theoretical biology*, 232(1):71–81, 2005. doi: 10.1016/j.jtbi.2004.07.026.

223. J.-B. Michel, P. J. Yeh, R. Chait, R. C. Moellering, and R. Kishony. Drug interactions modulate the potential for evolution of resistance. *Proc. Natl. Acad. Sci. USA*, 105: 14918–14923, 2008. URL http://adsabs.harvard.edu/abs/2008PNAS..10514918M.

224. D. F. Midgley, P. D. Morrison, and J. H. Roberts. The effect of network structure in industrial diffusion processes. *Research Policy*, 21(6):533–552, 1992.

225. J. C. Mitchell. *The concept and use of social networks*. Bobbs-Merrill, 1969.

226. T. Miura, M. A. Brockman, Z. L. Brumme, C. J. Brumme, F. Pereyra, A. Trocha, B. L. Block, A. Schneidewind, T. M. Allen, and D. Heckerman. HLA associated alterations in replication capacity of chimeric NL4-3 viruses encoding gag-protease from HIV-1 elite controllers. *Journal of Virology*, 83(1):140–149, 2008. doi: 10.1128/?JVI.01471-08.

227. T. Miura, C. J. Brumme, M. A. Brockman, Z. L. Brumme, F. Pereyra, B. L. Block, A. Trocha, M. John, S. Mallal, and P. R. Harrigan. HLA associated viral mutations are common in human immunodeficiency virus type 1 elite controllers. *Journal of Virology*, 83(7):3407–12, 2009. URL file:///Users/Ali/Documents/MN/HIVarticles/HIV.Data/PDF/3407-0461197569/3407.pdf.

228. S. Moir, T.-W. Chun, and A. S. Fauci. Pathogenic mechanisms of HIV disease. *Annual Review of Pathology*, 6:223–248, Feb. 2011. ISSN 1553-4014. doi: 10.1146/annurev-pathol-011110-130254. URL http://www.ncbi.nlm.nih.gov/pubmed/21034222. PMID: 21034222.

229. J. T. Moskowitz. Positive affect predicts lower risk of AIDS mortality. *Psychosom Med*, 65(4):620–626, July 2003. doi: 10.1097/01.PSY.0000073873.74829.23. URL http://www.psychosomaticmedicine.org/cgi/content/abstract/65/4/620.

230. R. Mostowy, R. D. Kouyos, D. Fouchet, and S. Bonhoeffer. The role of recombination for the coevolutionary dynamics of HIV and the immune response. *PLoS ONE*, 6(2): e16052, Feb. 2011. doi: 10.1371/journal.pone.0016052. URL http://dx.doi.org/10.1371/journal.pone.0016052.

231. J. M. Murabito. Family breast cancer history and mammography: Framingham offspring study. *American Journal of Epidemiology*, 154(10):916–923, Nov. 2001. ISSN 00029262. doi: 10.1093/aje/154.10.916.

232. V. M ller, C. Fraser, and J. T. Herbeck. A strong case for viral genetic factors in HIV virulence. *Viruses*, 3(3):204–216, Mar. 2011. ISSN 1999-4915. doi: 10.3390/v3030204. URL http://www.mdpi.com/1999-4915/3/3/204/.

233. L. M Gonigle, J. Shen, and S. Otto. Mutating away from your enemies: The evolution of mutation rate in a host parasite system. *Theoretical Population Biology*, 75: 301–311, June 2009. ISSN 0040-5809. doi: 10.1016/j.tpb.2009.03.003. URL http://www.sciencedirect.com/science/article/pii/S004058090900029X.

234. U. Nations. Millenium development goals report. http://mdgs.un.org/unsd/mdg/Default.aspx, 2010. URL http://mdgs.un.org/unsd/mdg/Default.aspx.

235. R. A. Neher and T. Leitner. Recombination rate and selection strength in HIV intra-patient evolution. *PLoS Comput. Biol.*, 6(1):e1000660, 2010.

236. M. Newman, A. Barabasi, and D. J. Watts. *The Structure and Dynamics of Networks:*. Princeton University Press, 1 edition, Apr. 2006. ISBN 0691113572.

237. B. E. Nichols, C. A. B. Boucher, J. H. v. Dijk, P. E. Thuma, J. L. Nouwen, R. Baltussen, J. v. d. Wijgert, P. M. A. Sloot, and D. A. M. C. v. d. Vijver. Cost-effectiveness of pre-exposure prophylaxis (PrEP) in preventing HIV-1 infections in rural zambia: A modeling study. *PLOS ONE*, 8(3):e59549, Mar. 2013. ISSN 1932-6203. doi: 10.1371/journal.pone.0059549. URL http://www.plosone.org/article/info:doi/10.1371/journal.pone.0059549.

238. M. Nijhuis, N. M. van Maarseveen, S. Lastere, P. Schipper, E. Coakley, B. Glass, M. Rovenska, D. de Jong, C. Chappey, I. W. Goedegebuure, G. Heilek-Snyder, D. Dulude, N. Cammack, L. Brakier-Gingras, J. Konvalinka, N. Parkin, H. Kr usslich, F. Brun-Vezinet, and C. A. B. Boucher. A novel substrate-based HIV-1 protease inhibitor drug resistance mechanism. *PLoS Med*, 4(1):e36, Jan. 2007. doi: 10.1371/journal.pmed.0040036. URL UR-http://dx.doi.org/10.1371/journal.pmed.0040036,http://dx.doi.org/10.1371/journal.pmed.0040036.

239. A. Noe, J. Plum, and C. Verhofstede. The latent HIV-1 reservoir in patients undergoing HAART: an archive of pre-HAART drug resistance. *J. Antimicrob. Chemother.*, 55:410–412, 2005.

240. A. Novick and L. Szilard. Virus strains of identical phenotype but different genotype. *Science*, 113(2924):34–35, Jan. 1951. ISSN 0036-8075. URL http://www.jstor.org/stable/1678580. ArticleType: research-article / Full publication date: Jan. 12, 1951 / Copyright © 1951 American Association for the Advancement of Science.

241. M. A. Nowak. What is a quasispecies? *Trends in Ecology & Evolution*, 7(4):118–121, Apr. 1992. ISSN 0169-5347. doi: 10.1016/0169-5347(92)90145-2. URL http://www.sciencedirect.com/science/article/pii/0169534792901452.

242. M. A. Nowak. *Evolutionary Dynamics: Exploring the Equations of Life*. Belknap Press of Harvard University Press, Sept. 2006. ISBN 0674023382.

243. M. A. Nowak. Five rules for the evolution of cooperation. *Science*, 314(5805):1560, 2006.

244. M. A. Nowak and R. M. May. Mathematical biology of HIV infections: antigenic variation and diversity threshold. *Math. Biosci*, 106(1):1–21, 1991.

245. M. A. Nowak and R. M. May. Evolutionary games and spatial chaos. *Nature*, 359 (6398):826–829, Oct. 1992. doi: 10.1038/359826a0. URL http://dx.doi.org/10.1038/359826a0.

246. M. A. Nowak and R. M. May. Superinfection and the evolution of parasite virulence. *Proceedings of the Royal Society B: Biological Sciences*, pages 81–89, 1994.

247. M. A. Nowak and R. M. C. May. *Virus dynamics: mathematical principles of immunology and virology*. Oxford University Press, USA, 2000.

248. M. A. Nowak, R. M. Anderson, A. R. McLean, T. F. Wolfs, J. Goudsmit, and R. M. May. Antigenic diversity thresholds and the development of AIDS. *Science*, 254 (5034):963–969, 1991.

249. M. A. Nowak, R. M. Anderson, A. R. McLean, T. F. W. Wolfs, J. Goudsmit, and R. M. May. Antigenic diversity thresholds and the development of AIDS. *Science*, 254:963–969, 1991.

250. M. A. Nowak, R. M. May, R. E. Phillips, S. Rowland-Jones, D. G. Lalloo, S. McAdam, P. Klenerman, B. K ppe, K. Sigmund, and C. R. M. Bangham. Antigenic oscillations and shifting immunodominance in HIV-1 infections. *Nature*, 375:606–611, 1995.

251. K. A. O'Connell, T. P. Brennan, J. R. Bailey, S. C. Ray, R. F. Siliciano, and J. N. Blankson. Control of HIV-1 in elite suppressors despite ongoing replication and evolution in plasma virus. *J. Virol.*, pages JVI.00548–10, May 2010. doi: 10.1128/JVI.00548-10. URL http://jvi.asm.org/cgi/content/abstract/JVI.00548-10v1.

252. H. Ohtsuki, C. Hauert, E. Lieberman, and M. A. Nowak. A simple rule for the evolution of cooperation on graphs and social networks. *Nature*, 441:502–505, 2006. doi: 10.1038/nature04605.

253. P. on Antiretroviral Guidelines for Adults and Adolescents. *Guidelines for the use of antiretroviral agents in HIV-1-infected adults and adolescents*. U.S. Department of Health and Human Services, 2011. URL http://aidsinfo.nih.gov/contentfiles/AdultandAdolescentGL.pdf.

254. J. U. N. P. on HIV/AIDS. UNAIDS report on the global AIDS. http://www.unaids.org, 2012. URL http://www.unaids.org.

255. J. U. N. P. on HIV/AIDS and W. H. Organization. AIDS epidemic update. http://www.who.int/hiv/data/en/, 2009. URL http://www.who.int/hiv/data/en/.

256. G. V. Ostir, K. S. Markides, S. A. Black, and J. S. Goodwin. Emotional well-being predicts subsequent functional independence and survival. *Journal of the American Geriatrics Society*, 48(5):473–478, May 2000. ISSN 0002-8614. URL http://www.ncbi.nlm.nih.gov/pubmed/10811538. PMID: 10811538.

257. A. J. Oswald and S. Wu. Objective confirmation of subjective measures of human Well-Being: evidence from the U.S.A. *Science*, 327(5965):576–579, Jan. 2010. doi: 10.1126/science.1180606. URL http://www.sciencemag.org/cgi/content/abstract/327/5965/576.

258. A. J. Oswald, E. Proto, and D. Sgroi. Happiness and productivity. *IZA Discussion Paper no. 4645, Institute for the Study of Laor (IZA), Bonn*, Dec. 2009.

259. F. J. Palella, K. M. Delaney, A. C. Moorman, M. O. Loveless, J. Fuhrer, G. A. Satten, D. J. Aschman, and S. D. Holmberg. Declining morbidity and mortality among patients with advanced human immunodeficiency virus infection. HIV outpatient study investigators. *N. Engl. J. Med.*, 338:853 860, 1998.

260. F. J. Palella, K. M. Delaney, A. C. Moorman, M. O. Loveless, J. Fuhrer, G. A. Satten, D. J. Aschman, and S. D. Holmberg. Declining morbidity and mortality among patients with advanced human immunodeficiency virus infection. HIV Outpatient Study Investigators. *N. Engl. J. Med.*, 338:853–860, 1998.

261. G. Pantaleo and R. A. Koup. Correlates of immune protection in HIV-1 infection: what we know, what we don't know, what we should know. *Nature Medicine*, 10: 806–810, 2004. URL file:///Users/Ali/Documents/MN/HIVarticles/HIV.Data/PDF/nm0804-806-4066228737/nm0804-806.pdf.

262. R. Paredes, C. M. Lalama, H. J. Ribaudo, B. R. Schackman, C. Shikuma, F. Giguel, W. A. Meyer III, V. A. Johnson, S. A. Fiscus, R. T. D'Aquilla, R. M. Gulick, D. R. Kuritzkes, and A. A. S. Team. Pre-existing minority drug-resistant HIV-1 variants, adherence, and risk of antiretroviral treatment failure. *J. Infect. Dis.*, 201:662–671, 2010.

263. J.-J. Parienti, M. Das-Douglas, V. Massari, D. Guzman, S. G. Deeks, R. Verdon, and D. R. Bangsberg. Not all missed doses are the same: sustained NNRTI treatment interruptions predict HIV rebound at low-to-moderate adherence levels. *PloS One*, 3 (7):e2783, 2008. ISSN 1932-6203. doi: 10.1371/journal.pone.0002783. URL http://www.ncbi.nlm.nih.gov/pubmed/18665246.

264. J.-J. Parienti, K. Ragland, F. Lucht, A. de la Blanchardiére, S. Dargére, Y. Yazdanpanah, J.-J. Dutheil, P. Perré, R. Verdon, and D. R. Bangsberg. Average

adherence to boosted protease inhibitor therapy, rather than the pattern of missed doses, as a predictor of HIV RNA replication. *Clin. Infect. Dis.*, 50(8):1192–1197, 2010. ISSN 1537-6591. doi: 10.1086/651419. URL http://www.ncbi.nlm.nih.gov/pubmed/20210643.

265. C. M. Parry, A. Kohli, C. J. Boinett, G. J. Towers, A. L. McCormick, and D. Pillay. Gag determinants of fitness and drug susceptibility in protease Inhibitor-Resistant human immunodeficiency virus type 1. *J. Virol.*, 83(18):9094–9101, Sept. 2009. ISSN 0022-538X, 1098-5514. doi: 10.1128/JVI.02356-08. URL http://jvi.asm.org/content/83/18/9094.

266. R. Pastor-Satorras and A. Vespignani. Epidemic spreading in scale-free networks. *Physical Review Letters*, 86(14):3200–3203, 2001. doi: 10.1103/PhysRevLett.86.3200.

267. P. S. Pennings. Standing genetic variation and the evolution of drug resistance in HIV. *PLoS Comput Biol*, 8(6):e1002527, June 2012. doi: 10.1371/journal.pcbi.1002527. URL http://dx.doi.org/10.1371/journal.pcbi.1002527.

268. P. S. Pennings. Standing genetic variation and the evolution of drug resistance in HIV. *PLoS Comput Biol*, 8(6):e1002527, June 2012. doi: 10.1371/journal.pcbi.1002527. URL http://dx.doi.org/10.1371/journal.pcbi.1002527.

269. A. S. Perelson, P. Essunger, Y. Cao, M. Vesanen, A. Hurley, K. Saksela, M. Markowitz, and D. D. Ho. Decay characteristics of HIV-1-infected compartments during combination therapy. *Nature*, 387(6629):188–191, May 1997. doi: 10.1038/387188a0. URL http://dx.doi.org/10.1038/387188a0.

270. I. Perez-Valero and J. R. Arribas. Protease inhibitor monotherapy. *Curr. Opin. Infect. Dis.*, 24:7–11, 2011.

271. D. Persaud, P. E. Palumbo, C. Ziemniak, M. D. Hughes, C. G. Alvero, K. Luzuriaga, R. Yogev, E. V. Capparelli, and E. G. Chadwick. Dynamics of the resting CD4(+) T-cell latent HIV reservoir in infants initiating HAART less than 6 months of age. *AIDS (London, England)*, 26(12):1483–1490, July 2012.

272. A. N. Phillips. Reduction of HIV concentration during acute infection: independence from a specific immune response. *Science*, 271(5248):497, 1996.

273. R. E. Phillips, S. Rowland-Jones, D. F. Nixon, F. M. Gotch, J. P. Edwards, A. O. Ogunlesi, J. G. Elvin, J. A. Rothbard, C. R. M. Bangham, C. R. Rizza, and A. J. McMichael. Human immunodeficiency virus genetic variation that can escape cytotoxic t cell recognition. *Nature*, 354(6353):453–459, Dec. 1991. doi: 10.1038/354453a0. URL http://dx.doi.org/10.1038/354453a0.

274. G. B. Pier. On the greatly exaggerated reports of the death of infectious diseases. *Clinical Infectious Diseases*, 47(8):1113 –1114, Oct. 2008. doi: 10.1086/592123. URL http://cid.oxfordjournals.org/content/47/8/1113.short.

275. M. Pingen, M. Nijhuis, J. A. de Bruijn, C. A. B. Boucher, and A. M. J. Wensing. Evolutionary pathways of transmitted drug-resistant HIV-1. *The Journal of Antimicrobial Chemotherapy*, Apr. 2011. ISSN 1460-2091. doi: 10.1093/jac/dkr157. URL v. PMID: 21502281.

276. S. D. Pressman and S. Cohen. Does positive affect influence health? *Psychological Bulletin*, 131(6):925, 2005.

277. S. D. Pugh. Service with a smile: Emotional contagion in the service encounter. *Academy of Management Journal*, pages 1018–1027, 2001.

278. F. Pulido, J. Arribas, A. Hill, and C. Moecklinghoff. No evidence for evolution of genotypic resistance after three years of treatment with darunavir/ritonavir, with or without nucleoside analogues. *AIDS Res. Hum. Retroviruses*, Mar. 2012. ISSN 1931-8405. doi: 10.1089/AID.2011.0256. URL http://www.ncbi.nlm.nih.gov/pubmed/22380531. PMID: 22380531.

279. H. Putter, S. H. Heisterkamp, J. M. A. Lange, and F. de Wolf. A Bayesian approach to parameter estimation in HIV dynamical models. *Statist. Med.*, 21(15):2199–2214, 2002.

280. M. Pérez, A. G. de Vinuesa, G. Sanchez-Duffhues, N. Marquez, M. L. Bellido, M. A. Muñoz-Fernandez, S. Moreno, T. P. Castor, M. A. Calzado, and E. Muñoz. Bryostatin-1 synergizes with histone deacetylase inhibitors to reactivate HIV-1 from latency. *Current HIV research*, 8(6):418–429, Sept. 2010. ISSN 1873-4251. PMID: 20636281.

281. L. S. Radloff. The CES-D scale: A self-report depression scale for research in the general population. *Applied psychological measurement*, 1(3):385, 1977. doi: 10.1177/014662167700100306.

282. L. S. Radloff and L. Teri. Use of the center for epidemiological Studies-Depression scale with older adults. *Clinical Gerontologist*, 5(1):119–136, 1986. ISSN 0731-7115. doi: 10.1300/J018v05n01_06. URL http://psycnet.apa.org/?fa=main.doiLanding&uid=1988-34649-001.

283. D. A. Rand. Correlation equations and pair approximations for spatial ecologies. In *Advanced ecological theory: principles and applications*, page 100. Wiley-Blackwell, 1999.

284. D. G. Rand, I. V. Armao, J. Joseph, M. Nakamaru, and H. Ohtsuki. Anti-social punishment can prevent the co-evolution of punishment and cooperation. *Journal of Theoretical Biology*, 264(4):624–632, 2010.

285. R. R. Regoes and S. Bonhoeffer. The HIV coreceptor switch: a population dynamical perspective. *Trends in Microbiology*, 13(6):269–277, June 2005. ISSN 0966-842X. doi: 10.1016/j.tim.2005.04.005. URL http://www.ncbi.nlm.nih.gov/pubmed/15936659. PMID: 15936659.

286. R. R. Regoes, D. Wodarz, and M. A. Nowak. Virus dynamics: the effect of target cell limitation and immune responses on virus evolution. *Journal of theoretical biology*, 191(4):451–462, 1998.

287. R. M. Ribeiro. In vivo dynamics of t cell activation, proliferation, and death in HIV-1 infection: Why are CD4+ but not CD8+ t cells depleted? *Proceedings of the National Academy of Sciences*, 99(24):15572–15577, Nov. 2002. ISSN 00278424. doi: 10.1073/pnas.242358099. URL http://www.ncbi.nlm.nih.gov/pmc/articles/PMC137758/.

288. R. M. Ribeiro, S. Bonhoeffer, and M. A. Nowak. The frequency of resistant mutant virus before antiviral therapy. *AIDS*, 12(5):461, 1998.

289. R. M. Ribeiro, L. Qin, L. L. Chavez, D. Li, S. G. Self, and A. S. Perelson. Estimation of the initial viral growth rate and basic reproductive number during acute HIV-1 infection. *J. Virol.*, 84(12):6096 –6102, June 2010. doi: 10.1128/JVI.00127-10. URL http://jvi.asm.org/content/84/12/6096.abstract.

290. R. E. Roberts. Reliability of the CES-D scale in different ethnic contexts. *Psychiatry Research*, 2(2):125–134, May 1980. ISSN 0165-1781. doi: 10.1016/0165-1781(80)90069-4. URL http://www.sciencedirect.com/science/article/B6TBV-45XSR26-1/2/b42468adfe0d32a95566d5e6e33aa07a.

291. D. E. M. Rogers. *Diffusion of Innovations, 5th Edition*. Simon and Schuster, 2003. ISBN 9780743258234.

292. L. Rong and A. S. Perelson. Modeling latently infected cell activation: Viral and latent reservoir persistence, and viral blips in HIV-infected patients on potent therapy. *PLoS Comput Biol*, 5(10):e1000533, Oct. 2009. doi: 10.1371/journal.pcbi.1000533. URL http://dx.doi.org/10.1371/journal.pcbi.1000533.

293. L. Rong and A. S. Perelson. Modeling HIV persistence, the latent reservoir, and viral blips. *Journal of Theoretical Biology*, June 2009. ISSN 1095-8541. doi: 10.1016/j.jtbi.2009.06.011. URL http://www.ncbi.nlm.nih.gov/pubmed/19539630. PMID: 19539630.

294. L. Rong, Z. Feng, and A. S. Perelson. Emergence of HIV-1 drug resistance during antiretroviral treatment. *Bull. Math. Biol.*, 69(6):2027–2060, 2007. ISSN 0092-8240. doi: 10.1007/s11538-007-9203-3. URL http://www.springerlink.com/content/k1g437k2m71q2pk6/.

295. L. Rong, H. Dahari, R. M. Ribeiro, and A. S. Perelson. Rapid emergence of protease inhibitor resistance in hepatitis c virus. *Science Translational Medicine*, 2(30):30ra32, 2010.

296. D. I. S. Rosenbloom, A. L. Hill, S. A. Rabi, R. F. Siliciano, and M. A. Nowak. Antiretroviral dynamics determines HIV evolution and predicts therapy outcome. *Nature Medicine*, 18(9):1378–1385, 2012. ISSN 1078-8956. doi: 10.1038/nm.2892. URL http://www.nature.com/nm/journal/v18/n9/full/nm.2892.html.

297. I. Rouzine and J. Coffin. Linkage disequilibrium test implies a large effective population number for HIV in vivo. *Proceedings of the National Academy of Sciences*, 96(19):10758, 1999.

298. L. Ruiz, J. Martinez-Picado, J. Romeu, R. Paredes, M. K. Zayat, S. Marfil, E. Negredo, G. Sirera, C. Tural, and B. Clotet. Structured treatment interruption in chronically HIV-1 infected patients after long-term viral suppression. *AIDS*, 14(4): 397, 2000. ISSN 0269-9370.

299. A. J. Rush. *Handbook of psychiatric measures*. Amer Psychiatric Pub Inc, 2007.

300. K. Ruxrungtham, R. J. Pedro, G. H. Latiff, F. Conradie, P. Domingo, S. Lupo, W. Pumpradit, J. H. Vingerhoets, M. Peeters, I. Peeters, T. N. Kakuda, G. De Smedt, and B. Woodfall. Impact of reverse transcriptase resistance on the efficacy of TMC125 (etravirine) with two nucleoside reverse transcriptase inhibitors in protease inhibitor-na ve, nonnucleoside reverse transcriptase inhibitor-experienced patients: study TMC125-C227. *HIV Medicine*, 9(10):883–896, 2008. ISSN 1468-1293. doi: 10.1111/j.1468-1293.2008.00644.x. URL http://onlinelibrary.wiley.com/doi/10.1111/j.1468-1293.2008.00644.x/full.

301. B. Sacerdote. Peer effects with random assignment: Results for dartmouth roommates. *Quarterly Journal of Economics*, 116(2):681–704, May 2001. doi: 10.1162/00335530151144131. URL http://dx.doi.org/10.1162/00335530151144131.

302. M. Salath and S. Bonhoeffer. The effect of opinion clustering on disease outbreaks. *Journal of The Royal Society Interface*, 5(29):1505, 2008.

303. M. Salath and S. Khandelwal. Assessing vaccination sentiments with online social media: Implications for infectious disease dynamics and control. *PLoS Comput Biol*, 7:e1002199, Oct. 2011. doi: 10.1371/journal.pcbi.1002199. URL http://dx.doi.org/10.1371/journal.pcbi.1002199.

304. M. E. S. Sampah, L. Shen, B. L. Jilek, and R. F. Siliciano. Dose-response curve slope is a missing dimension in the analysis of HIV-1 drug resistance. *Proc. Natl Acad. Sci. USA*, 108(18):7613–7618, May 2011. ISSN 1091-6490. doi: 10.1073/pnas.1018360108. URL http://www.ncbi.nlm.nih.gov/pubmed/21502494. PMID: 21502494.

305. M. L. Santiago, F. Range, B. F. Keele, Y. Li, E. Bailes, F. Bibollet-Ruche, C. Fruteau, R. No , M. Peeters, J. F. Y. Brookfield, G. M. Shaw, P. M. Sharp, and B. H. Hahn. Simian immunodeficiency virus infection in free-ranging sooty mangabeys (cercocebus atys atys) from the ta forest, c te d'Ivoire: implications for the origin of epidemic human immunodeficiency virus type 2. *Journal of Virology*, 79 (19):12515 –12527, Oct. 2005. doi: 10.1128/JVI.79.19.12515-12527.2005. URL http://jvi.asm.org/content/79/19/12515.abstract.

306. D. Schenzle. A model for AIDS pathogenesis. *Statistics in Medicine*, 13(19?20): 2067–2079, Oct. 1994. ISSN 1097-0258. doi: 10.1002/sim.4780131916. URL http://onlinelibrary.wiley.com/doi/10.1002/sim.4780131916/abstract.

307. J. E. Schmitz, M. J. Kuroda, S. Santra, V. G. Sasseville, M. A. Simon, M. A. Lifton, P. Racz, K. Tenner-Racz, M. Dalesandro, B. J. Scallon, J. Ghrayeb, M. A. Forman, D. C. Montefiori, E. P. Rieber, N. L. Letvin, and K. A. Reimann. Control of viremia in simian immunodeficiency virus infection by CD8+ lymphocytes. *Science*, 283 (5403):857 –860, Feb. 1999. doi: 10.1126/science.283.5403.857. URL http://www.sciencemag.org/content/283/5403/857.abstract.

308. G. Schnell, R. W. Price, R. Swanstrom, and S. Spudich. Compartmentalization and clonal amplification of HIV-1 variants in the cerebrospinal fluid during primary infection. *J. Virol.*, 84:2395–2407, 2010.

309. M. Schroevers, R. Sanderman, E. van Sonderen, and A. Ranchor. The evaluation of the center for epidemiologic studies depression (CES-D) scale: Depressed and positive affect in cancer patients and healthy reference subjects. *Quality of Life Research*, 9 (9):1015–1029, Nov. 2000. doi: 10.1023/A:1016673003237. URL http://dx.doi.org/10.1023/A:1016673003237.

310. P. Schulz zur Wiesch, J. Engelstadter, and S. Bonhoeffer. Compensation of fitness costs and reversibility of antibiotic resistance mutations. *Antimicrobial Agents and Chemotherapy*, 54(5):2085–2095, Feb. 2010. ISSN 0066-4804. doi: 10.1128/AAC.01460-09. URL https://www-ncbi-nlm-nih-gov/pmc/articles/PMC2863634/.

311. A. Sedaghat, R. F. Siliciano, and C. O. Wilke. Low-level HIV-1 replication and the dynamics of the resting CD4+ t cell reservoir for HIV-1 in the setting of HAART. *BMC Inf. Dis.*, 8(1):2, 2008. ISSN 1471-2334. doi: 10.1186/1471-2334-8-2. URL http://www.biomedcentral.com/1471-2334/8/2.

312. A. R. Sedaghat, J. B. Dinoso, L. Shen, C. O. Wilke, and R. F. Siliciano. Decay dynamics of HIV-1 depend on the inhibited stages of the viral life cycle. *Proc. Natl. Acad. Sci. USA*, 105(12):4832, 2008.

313. R. Sergeev, C. Colijn, M. Murray, and T. Cohen. Modeling the dynamic relationship between HIV and the risk of drug-resistant tuberculosis. *Science Translational Medicine*, 4(135):135ra67, May 2012. ISSN 1946-6234. doi: 10.1126/scitranslmed.3003815. URL http://www.ncbi.nlm.nih.gov/pmc/articles/PMC3387814/. PMID: 22623743 PMCID: PMC3387814.

314. C. R. Shalizi and A. C. Thomas. Homophily and contagion are generically confounded in observational social network studies. *1004.4704*, Apr. 2010. URL http://arxiv.org/abs/1004.4704.

315. L. Shan, K. Deng, N. S. Shroff, C. M. Durand, S. A. Rabi, H.-C. Yang, H. Zhang, J. B. Margolick, J. N. Blankson, and R. F. Siliciano. Stimulation of HIV-1-Specific cytolytic t lymphocytes facilitates elimination of latent viral reservoir after virus reactivation. *Immunity*, 36(3):491–501, Mar. 2012. ISSN 1074-7613. doi: 10.1016/j.immuni.2012.01.014. URL http://www.cell.com/immunity/abstract/S1074-7613(12)00084-2.

316. L. Shan et al. *In prep.*, 2013.

317. R. Shankarappa, J. B. Margolick, S. J. Gange, A. G. Rodrigo, D. Upchurch, H. Farzadegan, P. Gupta, C. R. Rinaldo, G. H. Learn, and X. He. Consistent viral evolutionary changes associated with the progression of human immunodeficiency virus type 1 infection. *J. Virol.*, 73(12):10489–10502, 1999.

318. T. J. Sheehan, J. Fifield, S. Reisine, and H. Tennen. The measurement structure of the center for epidemiologic studies depression scale. *Journal of Personality Assessment*, 64(3):507–521, 1995.

319. L. Shen, S. Peterson, A. R. Sedaghat, M. A. McMahon, M. Callender, H. Zhang, Y. Zhou, E. Pitt, K. S. Anderson, E. P. Acosta, et al. Dose-response curve slope sets class-specific limits on inhibitory potential of anti-HIV drugs. *Nat. Med.*, 14(7): 762–766, 2008.

320. L. Shen, S. A. Rabi, and R. F. Siliciano. A novel method for determining the inhibitory potential of anti-HIV drugs. *Trends in Pharmacological Sciences*, 30(12): 610–616, Dec. 2009. ISSN 1873-3735. doi: 10.1016/j.tips.2009.09.003. URL http://www.ncbi.nlm.nih.gov/pubmed/19837466. PMID: 19837466.

321. L. Shen, S. A. Rabi, A. R. Sedaghat, L. Shan, J. Lai, S. Xing, and R. F. Siliciano. A critical subset model provides a conceptual basis for the high antiviral activity of major HIV drugs. *Sci. Transl. Med.*, 3(91):91ra63, 2011. doi: 10.1126/scitranslmed.3002304. URL http://stm.sciencemag.org/content/3/91/91ra63.abstract.

322. H. Sheppard, C. Celum, N. Michael, S. O'Brien, M. Dean, M. Carrington, D. Dondero, and S. Buchbinder. HIV-1 infection in individuals with the CCR5-[Delta] 32/[delta] 32 genotype: acquisition of syncytium-inducing virus at seroconversion. *JAIDS Journal of Acquired Immune Deficiency Syndromes*, 29(3):307, 2002.

323. G. Shirreff, L. Pellis, O. Laeyendecker, and C. Fraser. Transmission selects for HIV-1 strains of intermediate virulence: A modelling approach. *PLoS Comput Biol*, 7: e1002185, Oct. 2011. doi: 10.1371/journal.pcbi.1002185. URL http://dx.doi.org/10.1371/journal.pcbi.1002185.

324. A. Sigal, J. T. Kim, A. B. Balazs, E. Dekel, A. Mayo, R. Mili, and D. Baltimore. Cell-to-cell spread of HIV permits ongoing replication despite antiretroviral therapy. *Nature*, 477:95–98, 2011. doi: 10.1038/nature10347. URL http://www.nature.com/nature/journal/v477/n7362/full/nature10347.html.

325. J. D. Siliciano and R. F. Siliciano. Enhanced culture assay for detection and quantitation of latently infected, resting CD4+ t-cells carrying replication-competent virus in HIV-1-infected individuals. *Methods in molecular biology (Clifton, N.J.)*, 304: 3–15, 2005. ISSN 1064-3745. doi: 10.1385/1-59259-907-9:003. PMID: 16061962.

326. J. D. Siliciano and R. F. Siliciano. The latent reservoir for HIV-1 in resting CD4+ t cells: a barrier to cure. *Current Opinion in HIV and AIDS*, 1(2):121–128, Mar. 2006. ISSN 1746-6318. doi: 10.1097/01.COH.0000209582.82328.b8. URL http://www.ncbi.nlm.nih.gov/pubmed/19372795. PMID: 19372795.

327. J. D. Siliciano, J. Kajdas, D. Finzi, T. C. Quinn, K. Chadwick, J. B. Margolick, C. Kovacs, S. J. Gange, and R. F. Siliciano. Long-term follow-up studies confirm the stability of the latent reservoir for HIV-1 in resting CD4+ t cells. *Nat Med*, 9(6): 727–728, June 2003. ISSN 1078-8956. doi: 10.1038/nm880. URL http://dx.doi.org/10.1038/nm880.

328. J. D. Siliciano, J. Lai, M. Callender, E. Pitt, H. Zhang, J. B. Margolick, J. E. Gallant, J. Cofrancesco, R. D. Moore, S. J. Gange, and R. F. Siliciano. Stability of the latent reservoir for HIV-1 in patients receiving valproic acid. *Journal of Infectious Diseases*, 195(6):833–836, Mar. 2007. ISSN 0022-1899, 1537-6613. doi: 10.1086/511823. URL http://jid.oxfordjournals.org/content/195/6/833.

329. G. Silvestri, D. L. Sodora, R. A. Koup, M. Paiardini, S. P. O'Neil, H. M. McClure, S. I. Staprans, and M. B. Feinberg. Nonpathogenic SIV infection of sooty mangabeys is characterized by limited bystander immunopathology despite chronic high-level viremia. *Immunity*, 18(3):441–452, Mar. 2003. ISSN 1074-7613. URL http://www.ncbi.nlm.nih.gov/pubmed/12648460. PMID: 12648460.

330. B. B. Simen, J. F. Simons, K. H. Hullsiek, R. M. Novak, R. D. Macarthur, J. D. Baxter, C. Huang, C. Lubeski, G. S. Turenchalk, M. S. Braverman, B. Desany, J. M. Rothberg, M. Egholm, and M. J. Kozal. Low-abundance drug-resistant viral variants in chronically HIV-infected, antiretroviral treatment-naive patients significantly impact treatment outcomes. *J. Infect. Dis.*, 199:693–701, 2009.

331. V. Simon, D. D. Ho, and Q. Abdool Karim. HIV/AIDS epidemiology, pathogenesis, prevention, and treatment. *The Lancet*, 368:489–504, Aug. 2006. ISSN 0140-6736. doi: 10.1016/S0140-6736(06)69157-5. URL http://www.sciencedirect.com/science/article/pii/S0140673606691575.

332. T. Smit, B. Brew, W. Tourtellotte, S. Morgello, B. Gelman, and N. Saksena. Independent evolution of human immunodeficiency virus (HIV) drug resistance mutations in diverse areas of the brain in HIV-infected patients, with and without dementia, on antiretroviral treatment. *Journal of virology*, 78(18):10133, 2004.

333. K. P. Smith and N. A. Christakis. Social networks and health. *Annual Review of Sociology*, 34:405–429, July 2008. doi: 10.1146/annurev.soc.34.040507.134601.

334. R. J. Smith. Adherence to antiretroviral HIV drugs: how many doses can you miss before resistance emerges? *Proc. R. Soc. B*, 273(1586):617–624, 2006. doi: 10.1098/rspb.2005.3352. URL http://rspb.royalsocietypublishing.org/content/273/1586/617.abstract.

335. R. J. Smith?, J. T. Okano, J. S. Kahn, E. N. Bodine, and S. Blower. Evolutionary dynamics of complex networks of HIV drug-resistant strains: The case of san francisco. *Science*, page science.1180556, Jan. 2010. doi: 10.1126/science.1180556. URL http://www.sciencemag.org/cgi/content/abstract/science.1180556v1.

336. J. D. d. Sousa, V. M ller, P. Lemey, and A.-M. Vandamme. High GUD incidence in the early 20th century created a particularly permissive time window for the origin and initial spread of epidemic HIV strains. *PLoS ONE*, 5(4):e9936, Apr. 2010. doi: 10.1371/journal.pone.0009936. URL UR-http://dx.doi.org/10.1371/journal.pone.0009936,http://dx.doi.org/10.1371/journal.pone.0009936.

337. B. Spellberg. Dr. william h. stewart: Mistaken or maligned? *Clinical Infectious Diseases*, 47(2):294, July 2008. doi: 10.1086/589579. URL http://cid.oxfordjournals.org/content/47/2/294.1.short.

338. S. Stearns. Life-history tactics: a review of the ideas. *Quarterly review of biology*, page 3 47, 1976.

339. S. Stearns. The evolution of life history traits: a critique of the theory and a review of the data. *Annual Review of Ecology and Systematics*, 8:145 171, 1977.

340. S. C. Stearns and J. C. Koella. *Evolution in Health and Disease*. Oxford University Press, USA, 2 edition, Jan. 2008. ISBN 0199207461.

341. M. C. Strain, S. J. Little, E. S. Daar, D. V. Havlir, H. F. Günthard, R. Y. Lam, O. A. Daly, J. Nguyen, C. C. Ignacio, C. A. Spina, D. D. Richman, and J. K. Wong. Effect of treatment, during primary infection, on establishment and clearance of cellular reservoirs of HIV-1. *Journal of Infectious Diseases*, 191(9):1410–1418, May 2005.

342. V. Supervie, J. G. Garc a-Lerma, W. Heneine, and S. Blower. HIV, transmitted drug resistance, and the paradox of preexposure prophylaxis. *Proceedings of the National Academy of Sciences*, 107(27):12381–12386, July 2010. doi: 10.1073/pnas.1006061107.

343. B. Taiwo, L. Zheng, S. Gallien, R. M. Matining, D. R. Kuritzkes, C. C. Wilson, B. I. Berzins, E. P. Acosta, B. Bastow, P. S. Kim, and J. Eron, Joseph J. Efficacy of a nucleoside-sparing regimen of darunavir/ritonavir plus raltegravir in treatment-naive HIV-1-infected patients (ACTG a5262). *AIDS*, 25(17):2113–2122, Nov. 2011. ISSN 1473-5571. doi: 10.1097/QAD.0b013e32834bbaa9. URL http://www.ncbi.nlm.nih.gov/pubmed/21857490. PMID: 21857490.

344. C. E. Tarnita, T. Antal, H. Ohtsuki, and M. A. Nowak. Evolutionary dynamics in set structured population. *Proc Natl Acad Sci USA*, 106(21):8601, 2009. doi: 10.1073/pnas.0903019106. In Press.

345. C. E. Tarnita, H. Ohtsuki, T. Antal, F. Fu, and M. A. Nowak. Strategy selection in structured populations. *Journal of Theoretical Biology*, 259:570–581, 2009. doi: 10.1016/j.jtbi.2009.03.035.

346. M. Thomson and R. N jera. Molecular epidemiology of HIV-1 variants in the global AIDS pandemic: an update. *AIDS Rev*, 7(4):210 224, 2005.

347. J. A. Thorson and F. C. Powell. The CES-D: four or five factors? *Bulletin of the Psychonomic Society*, 31(6):577–578, 1993.

348. W. R. Trevathan, E. O. Smith, and J. McKenna. *Evolutionary Medicine and Health: New Perspectives*. Oxford University Press, USA, 1 edition, Nov. 2007. ISBN 0195307062.

349. K. Ueno. The effects of friendship networks on adolescent depressive symptoms. *Social Science Research*, 34(3):484–510, 2005. doi: 10.1016/j.ssresearch.2004.03.002.

350. J. Ugander, L. Backstrom, C. Marlow, and J. Kleinberg. Structural diversity in social contagion. *Proceedings of the National Academy of Sciences*, 109(16):5962–5966, Apr. 2012. ISSN 0027-8424, 1091-6490. doi: 10.1073/pnas.1116502109. URL http://www.pnas.org/content/109/16/5962.

351. B. Uzzi. The sources and consequences of embeddedness for the economic performance of organizations: The network effect. *American Sociological Review*, 61 (4):674–698, 1996. ISSN 00031224. doi: 10.2307/2096399. URL http://www.jstor.org/stable/2096399.

352. V. Valen. A new evolutionary law. *Evolutionary Theory*, 1(1):1–30, 1973. doi: 10.1038/344864a0.

353. T. W. Valente. Network interventions. *Science (New York, N.Y.)*, 337(6090):49–53, July 2012. ISSN 1095-9203. doi: 10.1126/science.1217330. URL http://www.ncbi.nlm.nih.gov/pubmed/22767921. PMID: 22767921.

354. D. van de Vijver, A. M. J. Wensing, and C. A. B. Boucher. The epidemiology of transmission of drug resistant HIV-1. In T. Leitner, editor, *HIV Sequence Compendium 2007*, pages 17–36. Theoretical Biology and Biophysics Group, Los Alamaos National Laboratory, 2007.

355. A. C. van der Kuyl and M. Cornelissen. Identifying HIV-1 dual infections. *Retrovirology*, 4(1):67, Sept. 2007. ISSN 1742-4690. doi: 10.1186/1742-4690-4-67. URL http://www.biomedcentral.com/1742-4690/4/67.

356. G. van Marle, M. J. Gill, D. Kolodka, L. McManus, T. Grant, and D. L. Church. Compartmentalization of the gut viral reservoir in HIV-1 infected patients. *Retrovirology*, 4:87, 2007.

357. G. F. Vanhove, J. M. Schapiro, M. A. Winters, T. C. Merigan, and T. F. Blaschke. Patient compliance and drug failure in protease inhibitor monotherapy. *J. Am. Med. Ass*, 276(24):1955–1956, 1996. ISSN 0098-7484, 1538-3598. doi: 10.1001/jama.1996.03540240033024. URL http://jama.ama-assn.org/content/276/24/1955.

358. L. M. Wahl and M. A. Nowak. Adherence and drug resistance: predictions for therapy outcome. *Proc. R. Soc. B*, 267(1445):835 –843, 2000. doi: 10.1098/rspb.2000.1079. URL http://rspb.royalsocietypublishing.org/content/267/1445/835.abstract.

359. C. Walker, D. Moody, D. Stites, and J. Levy. CD8+ lymphocytes can control HIV infection in vitro by suppressing virus replication. *Science*, 234(4783):1563 –1566, Dec. 1986. doi: 10.1126/science.2431484. URL http://www.sciencemag.org/content/234/4783/1563.abstract.

360. S. Wasserman and K. Faust. *Social network analysis: methods and applications*. Cambridge University Press, 1994. ISBN 9780521387071.

361. D. J. Watts. A simple model of global cascades on random networks. *Proc Natl Acad Sci USA*, 99(9):5766–5771, Apr. 2002. doi: 10.1073/pnas.082090499. URL http://www.pnas.org/content/99/9/5766.abstract.

362. D. J. Watts. The "New" science of networks. *Annual Review of Sociology*, 30(1): 243–270, Aug. 2004. ISSN 0360-0572. doi: 10.1146/annurev.soc.30.020404.104342.

363. D. J. Watts and S. H. Strogatz. Collective dynamics of 'small-world' networks. *Nature*, 393(6684):440 442, 1998.

364. X. Wei, S. K. Ghosh, M. E. Taylor, V. A. Johnson, E. A. Emini, P. Deutsch, J. D. Lifson, S. Bonhoeffer, M. A. Nowak, and B. H. Hahn. Viral dynamics in human immunodeficiency virus type 1 infection. *Nature*, 373(6510):117–122, 1995.

365. X. Wei, J. M. Decker, S. Wang, H. Hui, J. C. Kappes, X. Wu, J. F. Salazar-Gonzalez, M. G. Salazar, J. M. Kilby, and M. S. Saag. Antibody neutralization and escape by HIV-1. *Nature*, 422(6929):307–312, 2003.

366. A. D. Weinberger, A. S. Perelson, R. M. Ribeiro, and L. S. Weinberger. Accelerated immunodeficiency by anti-CCR5 treatment in HIV infection. *PLoS Comput Biol*, 5 (8):e1000467, 2009. doi: 10.1371/journal.pcbi.1000467. URL http://dx.doi.org/10.1371/journal.pcbi.1000467.

367. J. O. Wertheim and S. L. Kosakovsky Pond. Purifying selection can obscure the ancient age of viral lineages. *Molecular Biology and Evolution*, 28(12):3355–3365, Dec. 2011. ISSN 1537-1719. doi: 10.1093/molbev/msr170. URL http://www.ncbi.nlm.nih.gov/pubmed/21705379. PMID: 21705379.

368. J. O. Wertheim and M. Worobey. Dating the age of the SIV lineages that gave rise to HIV-1 and HIV-2. *PLoS Comput Biol*, 5(5):e1000377, May 2009. doi: 10.1371/journal.pcbi.1000377. URL UR-http://dx.doi.org/10.1371/journal.pcbi.1000377,http://dx.doi.org/10.1371/journal.pcbi.1000377.

369. J. D. West, T. Bergstrom, and C. T. Bergstrom. The eigenfactor metrics: A network approach to assessing scholarly journals. *College and Research Libraries*, In Press, 2010.

370. C. O. Wilke and I. S. Novella. Phenotypic mixing and hiding may contribute to memory in viral quasispecies. *BMC Microbiology*, 3:11, June 2003. ISSN 1471-2180. doi: 10.1186/1471-2180-3-11. URL http://www.ncbi.nlm.nih.gov/pubmed/12795816. PMID: 12795816.

371. L. Wittkop, H. F. G nthard, F. de Wolf, D. Dunn, A. Cozzi-Lepri, A. de Luca, C. K cherer, N. Obel, V. von Wyl, B. Masquelier, C. Stephan, C. Torti, A. Antinori, F. Garc a, A. Judd, K. Porter, R. Thi baut, H. Castro, A. I. van Sighem, C. Colin, J. Kjaer, J. D. Lundgren, R. Paredes, A. Pozniak, B. Clotet, A. Phillips, D. Pillay, and G. Ch ne. Effect of transmitted drug resistance on virological and immunological response to initial combination antiretroviral therapy for HIV (EuroCoord-CHAIN joint project): a european multicohort study. *The Lancet Infectious Diseases*, 11(5): 363–371, May 2011. ISSN 1473-3099. doi: 10.1016/S1473-3099(11)70032-9. URL http://www.sciencedirect.com/science/article/pii/S1473309911700329.

372. D. Wodarz and D. N. Levy. Effect of multiple infection of cells on the evolutionary dynamics of HIV in vivo: implications for host adaptation mechanisms. *Experimental Biology and Medicine*, 236:926 –937, 2011. doi: 10.1258/ebm.2011.011062. URL http://ebm.rsmjournals.com/content/236/8/926.abstract.

373. D. Wodarz, K. M. Page, R. A. Arnaout, A. R. Thomsen, J. D. Lifson, and M. A. Nowak. A new theory of cytotoxic t-lymphocyte memory: implications for HIV treatment. *Philosophical Transactions of the Royal Society B: Biological Sciences*, 355 (1395):329–343, 2000.

374. N. D. Wolfe, W. M. Switzer, J. K. Carr, V. B. Bhullar, V. Shanmugam, U. Tamoufe, A. T. Prosser, J. N. Torimiro, A. Wright, E. Mpoudi-Ngole, F. E. McCutchan, D. L. Birx, T. M. Folks, D. S. Burke, and W. Heneine. Naturally acquired simian retrovirus infections in central african hunters. *The Lancet*, 363(9413):932–937, Mar. 2004. ISSN 0140-6736. doi: 10.1016/S0140-6736(04)15787-5. URL http://www.sciencedirect.com/science/article/pii/S0140673604157875.

375. J. K. Wong, M. Hezareh, H. F. Günthard, D. V. Havlir, C. C. Ignacio, C. A. Spina, and D. D. Richman. Recovery of replication-competent HIV despite prolonged suppression of plasma viremia. *Science*, 278(5341):1291–1295, Nov. 1997. ISSN 0036-8075, 1095-9203. doi: 10.1126/science.278.5341.1291. URL http://www.sciencemag.org/content/278/5341/1291.

376. M. Worobey, M. Gemmel, D. E. Teuwen, T. Haselkorn, K. Kunstman, M. Bunce, J.-J. Muyembe, J.-M. M. Kabongo, R. M. Kalengayi, E. Van Marck, M. T. P. Gilbert, and S. M. Wolinsky. Direct evidence of extensive diversity of HIV-1 in kinshasa by 1960. *Nature*, 455(7213):661–664, Oct. 2008. ISSN 0028-0836. doi: 10.1038/nature07390. URL http://dx.doi.org/10.1038/nature07390.

377. M. Worobey, P. Telfer, S. Souqui re, M. Hunter, C. A. Coleman, M. J. Metzger, P. Reed, M. Makuwa, G. Hearn, S. Honarvar, P. Roques, C. Apetrei, M. Kazanji, and P. A. Marx. Island biogeography reveals the deep history of SIV. *Science*, 329(5998): 1487–1487, Sept. 2010. ISSN 0036-8075, 1095-9203. doi: 10.1126/science.1193550. URL http://www.sciencemag.org/content/329/5998/1487.full.

378. J. K. Wright, Z. L. Brumme, J. M. Carlson, D. Heckerman, C. M. Kadie, C. J. Brumme, B. Wang, E. Losina, T. Miura, F. Chonco, M. van der Stok, Z. Mncube, K. Bishop, P. J. R. Goulder, B. D. Walker, M. A. Brockman, and T. Ndung'u. Gag-protease-mediated replication capacity in HIV-1 subtype c chronic infection: Associations with HLA type and clinical parameters. *Journal of Virology*, 84(20): 10820–10831, Aug. 2010. ISSN 1098-5514. doi: 10.1128/JVI.01084-10. PMID: 20702636.

379. H. Wu, Y. Huang, E. P. Acosta, S. L. Rosenkranz, D. R. Kuritzkes, J. J. Eron, A. S. Perelson, and J. G. Gerber. Modeling long-term HIV dynamics and antiretroviral response: effects of drug potency, pharmacokinetics, adherence, and drug resistance. *J. Acquir. Immune Defic. Syndr.*, 39(3):272–283, 2005. ISSN 1525–4135. URL http://www.ncbi.nlm.nih.gov/pubmed/15980686.

380. S. Xing, C. K. Bullen, N. S. Shroff, L. Shan, H.-C. Yang, J. L. Manucci, S. Bhat, H. Zhang, J. B. Margolick, T. C. Quinn, D. M. Margolis, J. D. Siliciano, and R. F. Siliciano. Disulfiram reactivates latent HIV-1 in a bcl-2-transduced primary CD4+ t cell model without inducing global t cell activation. *Journal of Virology*, 85(12): 6060–6064, June 2011. ISSN 0022-538X, 1098-5514. doi: 10.1128/JVI.02033-10. URL http://jvi.asm.org/content/85/12/6060.

381. S. Xing, S. Bhat, N. S. Shroff, H. Zhang, J. A. Lopez, J. B. Margolick, J. O. Liu, and R. F. Siliciano. Novel structurally related compounds reactivate latent HIV-1 in a bcl-2-transduced primary CD4+ t cell model without inducing global t cell activation. *Journal of Antimicrobial Chemotherapy*, 67(2):398–403, Feb. 2012. ISSN 0305-7453. doi: 10.1093/jac/dkr496. URL http://www.ncbi.nlm.nih.gov/pmc/articles/PMC3254198/. PMID: 22160146 PMCID: PMC3254198.

382. A. Yates, J. Stark, N. Klein, R. Antia, and R. Callard. Understanding the slow depletion of memory CD4+ t cells in HIV infection. *PLoS Med*, 4(5):e177, May 2007. doi: 10.1371/journal.pmed.0040177. URL http://dx.doi.org/10.1371/journal.pmed.0040177.

383. X. Zhao and K. Drlica. Restricting the selection of Antibiotic-Resistant mutant bacteria: Measurement and potential use of the mutant selection window. *J. Infect. Dis.*, 185(4):561–565, 2002. doi: 10.1086/338571. URL http://jid.oxfordjournals.org/content/185/4/561.abstract.

384. P. A. zur Wiesch, R. Kouyos, J. Engelst dter, R. R. Regoes, and S. Bonhoeffer. Population biological principles of drug-resistance evolution in infectious diseases. *The Lancet Infectious Diseases*, 11(3):236–247, Mar. 2011. ISSN 1473-3099. doi: 10.1016/S1473-3099(10)70264-4. URL http://www.sciencedirect.com/science/article/pii/S1473309910702644.

385. S. vila R os, G. Reyes-Ter n, and E. Espinosa. Cornering HIV: taking advantage of interactions between selective pressures. *Medical Hypotheses*, 69(2):422–431, 2007. ISSN 0306-9877. doi: 10.1016/j.mehy.2006.12.012. URL http://www.sciencedirect.com/science/article/pii/S0306987706009145.

Colophon

This thesis was typeset using LaTeX, originally developed by Leslie Lamport and based on Donald Knuth's TeX. A template, which can be used to format a PhD thesis with this look and feel, has been released under the permissive MIT (X11) license, and can be found online at github.com/suchow/ or from the author at suchow@post.harvard.edu.